Characterisation of the *in vitro* effects of Asiatic acid in Glioblastoma

by

Flourina Thakor

A thesis submitted in partial fulfilment for the requirements for the degree of Doctor of Philosophy at the University of Central Lancashire

April 2016

STUDENT DECLARATION FORM

Concurrent registration for two or more academic awards

I declare that while registered as a candidate for the research degree, I have not been a registered candidate or enrolled student for another award of the University or other academic or professional institution

Material submitted for another award

I declare that no material contained in the thesis has been used in any other submission for an academic award and is solely my own work

Signature of Candidate 

Type of Award **Doctor of Philosophy**

School **Pharmacy and Biomedical Sciences**

ABSTRACT

Glioma arises from glial cells in the brain and is a common intracranial neoplasm of the central nervous system. Standard treatment is surgery followed by radiation and chemotherapy, however, the prognosis remains poor. Presence of the blood brain barrier (BBB) poses a significant challenge to drug delivery due to the tight junctions between adjacent endothelial cells. However, studies have confirmed that integrity of the tight junctions in the BBB is compromised in primary and metastatic brain tumours.

It is a known fact that tumour masses are hypoxic and oxygen consumption in a tumour is erratic. A drop in the partial pressure of oxygen changes gene expression mediated by the activation of hypoxia inducible factor (HIF). HIF system plays an important role in tumour growth by controlling the transcription of genes responsible for cell proliferation, angiogenesis and energy metabolism.

Asiatic acid is a herbal extract of the plant *Centella asiatica*. Asiatic acid has been shown to possess anti-cancer activity, in addition, it also aids wound healing, collagen synthesis and can cross the BBB.

Results from this study showed that asiatic acid reduced cell viability in comparison to the chemotherapeutic drug-cisplatin, under hypoxia. Apoptosis was observed under hypoxia following asiatic acid treatment, however, no significant effects on cell proliferation or reactive oxygen species generation were observed.

Taken together, these results suggest that asiatic acid is a potent inducer of cell apoptosis under hypoxia and mainly acts via downregulation of Bcl-2, intracellular calcium increase and mitochondrial stress.

Asiatic acid is a hydrophobic compound and thus creates a challenge for its delivery to tumours. In addition to studying the effects of asiatic acid under hypoxia in this study, we have also aimed at designing a vehicular system for the delivery of asiatic acid into tumours. Biodegradable nanoparticles formulated with poly-ε-caprolactone (PCL) were prepared to investigate sustained, localised delivery of asiatic acid. Monodisperse blank and asiatic acid-loaded nanoparticles, that were stable for 60 days were prepared and ranged between 133 ± 1.8nm to 152.5 ± 2.7nm and 134.4 ± 1.5nm to 150.2 ± 1.2nm in size, respectively. The asiatic acid-loaded nanoparticles had a drug loading efficiency of 28 ± 1.2% and no release of the drug in phosphate buffered saline at pH 7.4 following 24 hour incubation. Although nanoparticle internalisation was observed with the coumarin-6 loaded nanoparticles, *in vitro* studies did not show any significant effects on cell viability of SVGp12 or U87-MG cell lines. The lack of the particular lipase in mammals leads to a slow degradation of PCL by hydrolysis and can take up to 4 years for complete degradation.

Thus, we established that asiatic acid induces apoptosis in glioblastoma cells *in vitro* and also under hypoxia. However, asiatic acid-loaded nanoparticles showed no differences in cell viability due to the lack of lipase in the cells.

Contents

List of Figures

List of Tables

ACKNOWLEDGEMENTS

I would like to take this opportunity to express my gratitude towards all those people who gave me constant and undeterred support, making it possible for me to reach this stage. Firstly, I wish to thank my grandfather Mr. Suresh Thakor for allowing this wonderful opportunity and his constant support. He has stood by me like a pillar of strength always encouraging me perform better than before and this task would not have been possible without him.

I would like to thank my parents, Rajshree and Kumar Thakor, and my grandfather Ram Kumar Shoora, for their strength, support and faith in me. Their constant emotional and mental support has helped me strive through all the hurdles I have faced. I also wish to acknowledge my brother Heeraka Thakor and my dear cousin Puneet Choudhary for being patient with me in my testing times. I wish to express my gratitude towards my supervisors Dr. Gail Welsby, Dr. Philip Welsby and Dr. Ka-Wai Wan for their patience, concern and constant encouragement. Their dedication, enthusiasm and hard work will inspire me through my future. I am also grateful to Tamar Garcias and Jim at the JB Firth analytical department, and Dr. Julie Burrows for providing me with the necessary training on the equipment, being around for troubleshooting and all other help they have offered. I wish to express my deepest gratitude to Viviana Petinou for all the help and support she has offered me as friend and a laboratory partner. Lastly, I want to say thank you to all my friends, here and abroad, for their constant encouragement.

The successful completion of this undertaking would not have been possible without the support and assistance of all these people.

ABBREVIAITIONS

AA	Asiatic acid
ADP	Adenosine diphosphate
AJ	Adherens junctions
AMT	Adsorptive mediated transcytosis
ARNT	Aryl hydrocarbon nuclear translocator
ATP	Adenosine triphosphate
AU	Arbitrary units
B/Akt	Protein kinase B, also known as Akt
BBB	Blood brain barrier
Bcl	B-cell lymphoma
BCRP	Breast cancer resistance proteins
BL	Basal lamina
Ca^{2+}	Calcium ion
CAD	COOH-terminal transactivation domain
CaD	Caspase-activated DNase
CAIX	Carbonic anhydrase IX
Cdc	Cell division cycle
Cdk	Cyclin dependent kinase
CFDA-SE	Carboxyfluorescein diacetate succinimidyl ester
c-FLIP	Cellular FLICE (FADD-like IL-1β-converting enzyme)-inhibitory protein
CGI	CpG islands
Cis	Cisplatin
CKI	Cyclin-dependent kinase inhibitors
CNS	Central nervous system
CTL	$CD8^+$ cytotoxic T lymphocyte
CTR1	High affinity copper transporter
Ctrl	Control
DIABLO	Direct IAP Binding protein with Low pI
DISC	Death inducing signalling complex
DNA	Deoxyribonucleic acid
EC_{50}	Half maximal effective concentration

EGFR	Epidermal growth factor receptor
ER	Endoplasmic reticulum
FADD	Fas-associated death domain
$FADH_2$	Reduced flavin adenine dinucleotide
FasL	Fas Ligand
FasR	Fas Receptor
Fe^{2+}	Iron with an oxidation number of +2
Fe^{3+}	Iron with an oxidation number of +3
FIH	Factor inhibiting hypoxia
FSC	Forward-angle light scatter
GBM	Glioblastoma multiforme
H^+	Hydrogen ion
HER	Human epidermal growth factor receptor
HIF	Hypoxia inducible factor
HPLC	High Pressure Liquid Chromatography
HtrA2	Omi/high temperature requirement protein A
IAP	Inhibitor of apoptosis proteins
ICaD	Inhibitor of Caspase Activated DNAse
IgG	Immunoglobulin G
INF	Interferon
JAM	Junctional adhesion molecules
LDH	Lactate dehydrogenase
LOH	Loss of heterozygosity
MAPK	Mitogen-activated protein kinase
MCE	Mixed cellulose esters
MDR	Multi-drug resistance
MGMT	Methylguanine-DNA methyltransferase
mTOR	Mammalian/mechanistic target of rapamycin
NAD^+	Oxidised nicotinamide adenine dinucleotide
NADPH	Nicotinamide adenine dinucleotide phosphate
NADH	Reduced nicotinamide adenine dinucleotide
NF-κB	Nuclear transcription factor kappa B
NK	Natural killer cells
NPs	Nanoparticles

ODDD	Oxygen-dependant degradation domain
PBS	Phosphate buffered saline
PCL	Poly-ε-caprolactone
PDGFR	Platelet-derived growth factor receptor
PDH	Pyruvate dehydrogenase
PDI	Polydispersity index
PEG	Polyethylene glycol
P-gp	P-glycoprotein
PHD	Proline hydroxylase enzymes
PI3K	Phosphatidyl-inositol 3'- kinase
pO_2	Partial pressure of O_2
PS	Phosphatidyl serine
PTEN	Phosphatase and tensin homolog
PVDF	Polyvinylidene difluoride
Rb	Retinoblastoma protein
RIP	Receptor-interacting protein
RING finger protein	Really Interesting New Gene
RMT	Receptor mediated transcytosis
RNA	Ribonucleic acid
ROS	Reactive oxygen species
RT	Radiotherapy
SB	Stereotactic brachytherapy
Smac	Second mitochondria-derived activator of caspases
SSC	Side-angle light scatter
TCA cycle	Tricarboxylic acid cycle
TJ	Tight junction
TKI	Tyrosine kinase inhibitors
TMZ	Temozolomide
TNF	Tumour necrosis factor
TNFR	Tumour necrosis factor receptor
TRADD	TNF receptor-associated death domain
VEGFR	Vascular endothelial growth factor receptor
VHL	von Hippel-Lindau tumour suppressor gene
WHO	World health organisation

ZO	Zona occludins

CHAPTER 1

INTRODUCTION

1.1 Glioma

Glioma, a common intracranial neoplasm of the central nervous system, is a highly malignant brain tumour having poor prognosis due to the associated neovascularisation (Skog et al., 2008). Glioma arises from the glial cells in the brain which include astrocytes, oligodendrocytes and ependymal cells that support and nourish the brain (Jia et al., 2012; Toyooka et al., 2008). The World Health Organisation (WHO) scheme for the grading of gliomas is the classification of the tumours on their hypothesised line of differentiation and by the features they display whether of ependymal cell, astrocyte or oligodendrocyte origin. They are graded on a scale of I-IV depending upon the degree of malignancy (Table 1.1; Maher et al. 2001).

Table 1.1: WHO grading system for gliomas and their incidence rate

Tumour grade	Characteristics	Incidence
I (Pilocytic Astrocytoma)	Low proliferative potential, possibility of cure after surgery	~2% of all gliomas
II (Diffuse Astrocytoma)	Infiltrative, low proliferative potential, may recur and progress to higher grades of malignancy	10-15% of astrocytic tumours
III (Anaplastic Astrocytoma)	Infiltrative and proliferative, histological evidence of malignancy	30% of astrocytic tumours
IV (Glioblastoma)	Highly infiltrative and proliferative, histological evidence of malignancy, mitotically active, prone to necrosis, associated with rapid preoperative and postoperative disease progression and fatal outcome	70% of astrocytic tumours

Adapted from: Brain tumour staging, American Society of Clinical Oncology, reviewed, June 2013 and Chalmers, 2011

1.1.1 Glioblastoma Multiforme

Glioblastoma multiforme (GBM) is the most aggressive and malignant form of glioma. GBM may be a primary neoplasm of the brain or develop from a low-grade astrocytoma or an oligodendroglioma. It accounts for 12-15% of all intracranial tumours (Bruce & Harris, 2011). GBM arises from the genetic and epigenetic alterations in the normally functioning astroglial cells (Fig. 1.1), and many other genetic and cytogenetic chromosomal alterations have been described as playing a role in the onset of the tumour (Haque & Ray, 2011).

GBM may be classed as a primary or secondary tumour with the primary type accounting for 95% of the GBM cases; most associated with adults over 50 years of age. Secondary GBM, accounting for 5% of the total GBM cases, is seen in younger patients of less than 45 years of age, typically developing from a low-grade astrocytoma or an anaplastic astrocytoma with the time scale ranging from 1-10 years for its development (Ohgaki and Kleihues, 2013)

1.1.2 Genetic Pathways Leading to GBM

The development of glioma may be *de novo* or through the progression from a low grade or anaplastic astrocytoma (Kleihues and Ohgaki, 1999). Several genetic alterations have been identified in the malignant transformation of astrocytes; however, the understanding of the sequence and types of gene alterations remains incomplete. The existence of prominent mutations in the components of the cell cycle and the apoptotic pathways in glioma along with dysregulation of growth, survival and migration suggests the likelihood of these targets to be important in glial development (Maher et al., 2001).

Comprehensive genetic screens of GBM have shown that genetic loss is scattered across the entire genome, affecting nearly all chromosomes at frequencies

ranging from 2% to 80%. Particularly common regions of loss include areas on 1p, 6q, 9p, 10p, 10q, 13q, 14q, 15q, 17p, 18q, 19q, 22q, and Y (Kanu et al., 2009). Loss of heterozygosity (LOH) on chromosome 10q is the most common genetic alteration for primary (complete loss) and secondary GBM (partial loss), occurring in 60-90% of GBM cases. However, several other LOH studies have shown three distinct loci to be deleted, 10p14–p15, and 10q23–24, distal to 10q25. The mutation is specific for GBM and rarely found in other tumour grades (Bruce & Harris, 2011; Kanu et al., 2009). At lower frequencies, allelic losses on 1p (31%) and 7q (9-12%) have also been seen in GBM (Kanu et al., 2009). The tumour suppressor gene *PTEN* (phosphatase and tensin homolog) on chromosome 10q23.3 encodes the protein tyrosine phosphatase, which turns off signalling pathways. A mutation of this gene leads to loss of PTEN activity giving rise to activation of cell cycle signalling pathways (Bruce & Harris, 2011).

Genetic alterations at the genomic level, amplifying the gene expression are demonstrated in GBM however, these are less frequent in comparison to loss of gene expression. The gain of gene expression occurs in the form of duplication of entire chromosomes, intra-chromosomal amplification of specific alleles, extra-chromosomal amplification often in the form of double minutes, and activating mutations (Kanu et al., 2009). The most common oncogenomic event is amplification of epidermal growth factor receptor gene (*EGFR*). The *EGFR* gene on chromosome 7, which controls cell proliferation, is amplified in GBM along with the presence of truncated isoforms of the receptor which result due to the deletion of exons 2-7 from the extracellular domain (Bruce & Harris, 2011; Kanu et al. 2009; Kleihues & Ohgaki 1999; Lang et al. 1994). EGFR is a 170kDa receptor tyrosine kinase member of the ErbB family consisting of four distinct receptors: HER1/EGFR (HER-human epidermal growth factor receptor), HER2, HER3 and HER4. It is formed of three major domains: the extracellular domain, the transmembrane domain and the cytoplasmatic domain, which harbors the tyrosine

kinase activity. Phosphorylation of the tyrosine kinase domain activates several signaling pathways, such as the phosphatidyl-inositol 3-kinase (PI3K), Akt (protein kinase B), mTOR (mechanistic target of rapamycin, encoded by *MTOR* gene), and Ras/mitogen-activated protein kinase (MAPK); resulting in the activation of several biological processes such as cell proliferation, angiogenesis, migration, survival and differentiation (Minniti et al., 2009; Normanno et al., 2006). The mutant *EGFR* thus confers enhanced tumourigenicity on human glioblastoma cells by increasing proliferation and reducing apoptosis (Kleihues and Ohgaki, 1999). *EGFR* amplification has been identified as a genetic hallmark of cancer cells including GBM (Hanahan and Weinberg, 2011b; Ohgaki et al., 2004).

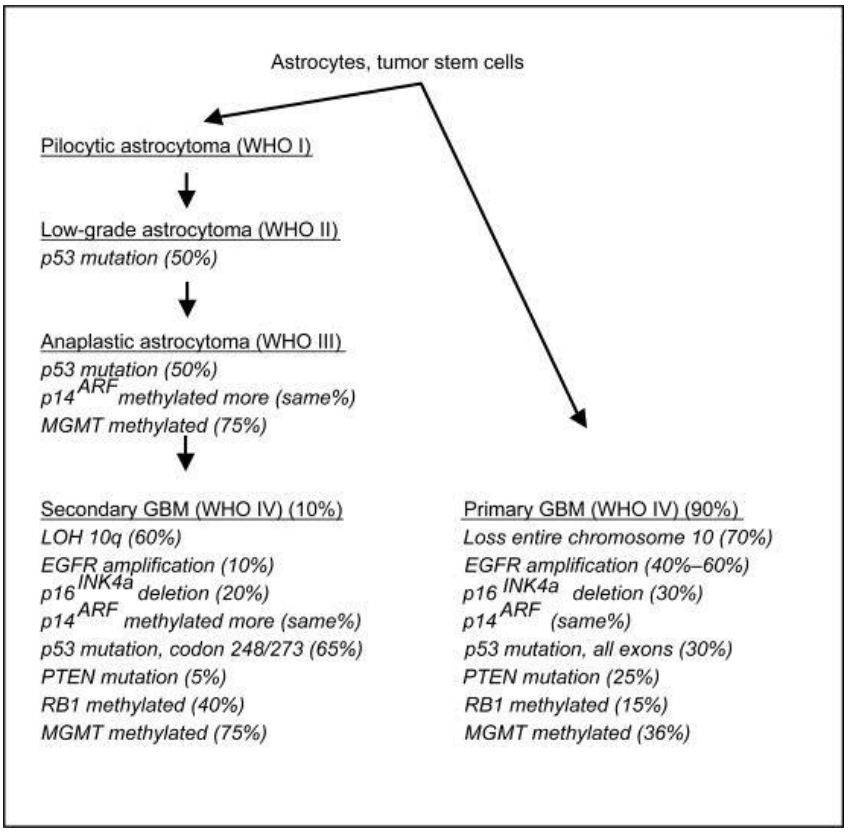

Figure 1.1: Genetic alterations involved in the progression and initiation of primary and secondary GBM

The onset of GBM involves several genetic alterations such as p53 mutation, loss of heterozygosity and EGFR amplification. Different genetic alterations are involved at different grades of tumour. Source Ohgaki et al., 2004.

Genetic alterations such as amplification or deletion represent direct glioma-inducing events; other alterations directly affect gliomagenesis by DNA instability. The overall mutation rate in somatic human cells is approximately 1.4×10^{10} nucleotides per cell division. This low spontaneous mutation rate in normal cells cannot be accountable for the large mutation rate observed in GBM (Ohgaki et al., 2004). Gliomagenesis involves errors in DNA replication and repair, chromosomal segregation, and alteration of signalling cascades not directly attributed to genomic mutations such as Ras and c-Myc (Hanahan and Weinberg, 2011b). The collection of these genetic and cellular alterations gives rise to a tumour cell phenotype, described as a mutator phenotype. DNA repair mechanisms are central to this mutator phenotype (Loeb, 2001). However, in GBM, at least four major DNA repair pathways may go askew. This includes nucleotide excision repair, base excision repair, mismatch repair, and direct reversal of lesions in recombination. The DNA repair enzyme O^6-methylguanine-DNA methyltransferase (MGMT) offers resistance towards alkylating agents where it specifically removes promutagenic alkyl groups from the O^6-position of guanine in DNA, thus protecting cells from carcinogenesis. Loss of MGMT expression is caused due to methylation of promoter CpG islands (CGI) which has been observed in secondary (75%) and primary (36%) GBMs; where ~60% are located in CGIs (Deaton et al., 2011; Hegi et al., 2005). The majority of the low-grade gliomas with *MGMT* methylation contain a mutation in the tumour suppressor gene *p53*. The *p53* gene encodes a protein that plays an important role in several cellular processes, including the cell cycle, response to DNA damage, apoptosis, cell differentiation, and neovascularisation (Bobustuc et al., 2010; Furnari et al., 2007; Ohgaki et al., 2004). p53 protein functions as a stress-inducible switch to turn on alternative pathways to G_1 arrest of the cell cycle or apoptosis (Furnari et al., 2007; Kleihues and Ohgaki, 1999). The *p53* gene has been observed to be altered or deleted in approximately 25-40% of GBMs,

more commonly in the secondary subtypes (Bruce & Harris, 2011; Kanu et al, 2009; Lang et al, 1994).

1.2 Symptoms and Treatment

The most common symptoms of glioma include headaches, fits and seizures. Other symptoms include aphasia, paresthesia, hemiparesis, and problems with the eye. Thus these are not considered very seriously by the patient, making the diagnosis of glioma very difficult. However, the initial clinical presentation is variable and depends on tumour localisation and size (Preusser et al., 2011). Glioma is often identified at the end stage when the tumour progresses to GBM. High grade glioma patients may show symptoms such as epilepsy, cognitive dysfunction and a high intra-cranial pressure (Preusser et al., 2011; Stupp et al., 2009; Verhoeff et al., 2009).

Patients with high-grade glioma have a poor prognosis and cannot be cured despite a multimodality treatment with surgery, radiation and chemotherapy. The median survival ranges from <1 to 5 years depending on tumour grade, cytogenetic analysis, age and performance status at the time of diagnosis (Preusser et al., 2011). The primary objective of surgery is to remove as much of the tumour mass as possible without disturbing the neurological function (Bruce & Harris, 2011). However, high grade tumours have infiltrating cells making entire tumour removal very difficult (Kleihues and Ohgaki, 1999). Surgery can improve patient prognosis but the small amount of tumour that may be left behind after surgery may lead to a relapse (Jallo & Ramachandran, 2012). Radiation (RT) and chemotherapy on the other hand are non-invasive but have many adverse side effects and reduce the overall immunity of the patient, making the cells and tissue more prone to other infections (Chamberlain et al., 1998).

1.2.1 Cisplatin

Cisplatin (cis-diamminedichloroplatinum or CDDP), is a potent chemotherapeutic drug widely used for cancer treatment. The discovery of cisplatin in the 1960's has sparked a huge interest in the potential of platinum-II and other metal containing compounds in the treatment of different types of cancer (Frezza et al., 2010). The clinical use of cisplatin includes the treatment of sarcomas, ovarian and cervical cancer, cancers of the bone, soft tissue and blood; and paediatric solid tumours. Patients have thus obtained better prognosis. Cisplatin was first applied to a cancer patient in 1971 and became available for clinical use in 1978 as Platinol® (Bristol-Myers Squibb) in Canada and thereafter in the United States, followed by the rest of the world (Lebwohl and Canetta, 1998).

The clinical use of cisplatin is very limited due its dose-dependent toxicity on normal tissue and cellular resistance (Florea and Büsselberg, 2011; Frezza et al., 2010; Tezcan et al., 2013). Some of the side-effects of cisplatin include nausea and vomiting, other cell damaging effects such as a drop in the blood cell count, platelet production in the bone marrow and immunosuppression. More specific side effects include nephrotoxicity, neurotoxicity and loss of hearing (Florea and Büsselberg, 2011; Momekov et al., 2006; Ramesh and Brian Reeves, 2002; Sheleg et al., 2002). Cisplatin is often used in combination with other drugs, so as to produce a synergistic effect and thus reduce the side-effect profile of the drug (Desoize and Madoulet, 2002; Momekov et al., 2006; Mori et al., 2003).

The main mechanism of action of cisplatin is *via* DNA intercalation following a spontaneous aquation reaction which involves the sequential replacement of the cis-chloro ligands of cisplatin with water molecules. Cisplatin enters cells by passive diffusion and induces its cytotoxicity mainly by forming DNA-protein; and DNA-DNA

inter-strand and intra-strand cross-links. The platinum ion of cisplatin forms bi-functional intra-strand crosslinks with the DNA at the N^7 purine base. Cisplatin thus induces a kink in DNA structure and is a critical lesion allowing biomolecular recognition of the cell (Baruah et al., 2002; Florea and Büsselberg, 2011; Lanjwani et al., 2006; Siddik, 2003; Wang and Lippard, 2005). The physical distortion of the inter-strand platinum crosslinks facilitates the binding of various proteins (e.g. TATA box-binding protein and high-mobility group box protein 1) to the recognised damaged DNA inducing apoptosis and changes in the cell cycle (Wang and Lippard, 2005).

Upon entering cells, cisplatin binds to intracellular thiols- metallothionein and glutathione, in turn reducing the amount of cisplatin available to bind to DNA. However, a continued exposure to cisplatin escalates the amount of cellular thiols which increases the cell's resistance to cisplatin (Hagrman et al., 2003; Komatsu et al., 2000). In mouse cells and yeast, cisplatin resistance has been shown to be due to a mutation or deletion of the *CTR1* gene (encodes for a high affinity copper transporter), which results in increased cisplatin resistance and reduction of cellular platinum levels due to overexpression of a multidrug resistance protein MRP2 or a copper-transporting P-type ATPase ATP7B. Also, the exporter protein- ATP-binding cassette protein subfamily C2 has been shown to play a role in cisplatin resistance by promoting its efflux from cells (Holzer et al., 2004; Ishida et al., 2002). Other mechanisms of cellular resistance of cisplatin include increased repair of DNA adducts, reduction in cisplatin accumulation by changing influx/efflux profile and the failure of apoptotic pathways (Mamenta et al., 1994; Miyashita et al., 2003; Nakayama et al., 2002; Siddik, 2003).

However, the absorption of cisplatin into the perifocal tumour is hindered by the presence of the blood brain barrier. The use of cisplatin as a chemotherapy drug is restricted due its high molecular weight (300Da) (Sheleg et al., 2002).

1.2.2 Temozolomide

More recently, radiotherapy and concomitant temozolomide (TMZ) followed by adjuvant TMZ has become the standard of care for patients with glioblastoma since the European and Canadian randomized trial was published in 2005 (Mineo et al., 2007; Stupp et al., 2005; Taal et al., 2008). TMZ is a second-generation imidazotetrazine derivative, exerting its cytotoxic effects by the methylation of specific DNA sites, with the methylation of the O^6 position of guanine bases in the DNA considered to be the most critical (Sheleg et al., 2002). The median survival rate was increased when RT and chemotherapy were combined versus chemotherapy alone (16 months versus 11 months) (Mineo et al., 2007). The cytotoxic effects of TMZ are associated with intracellular levels of MGMT. The high levels of MGMT in tumour tissue cause the resistance of tumour cells to TMZ. Epigenetic silencing of *MGMT* by promoter methylation is directly associated with improved survival in patients treated with TMZ (Minniti et al., 2009).

1.2.3 Other Treatments

Interstitial brachytherapy with iodine (I-125), another component of standard therapy, has been used as an adjuvant treatment for malignant brain tumours (Zhang et al., 2012). While the primary radionucleotide for brachytherapy is iodine, a more recent move is taking place towards permanent low-activity implants from the temporary high-activity implants (McDermott et al., 1998; Zhang et al., 2012). This technique is used to treat small (<4 cm), radiographically well-defined lesions with a single high-dose fraction of ionizing radiation in stereotactically directed narrow beams, thus providing an added improvement to the survival outcome to patient with glioma. Stereotactic brachytherapy (SB), a spatially precise stereotactic implantation technique, is used in patients with supratentorial tumours that do not involve the corpus callosum, brain stem, thalamus, intraventricular or ependymal surfaces, and are well defined, unifocal

tumours of 1-4cm in diameter. SB accurately places an inflating balloon catheter containing radioactive isotopes or interstitial diffusion-based drug delivery systems within the brain tumour, without producing cytotoxic effects on normal brain structures (Pelloski and Gilbert, 2007; Schwarz et al., 2012; Zhang et al., 2012).

Carmustine, a 1,3-bis(2-chloroethyl)-1-nitrosourea (BCNU®) is a nitrosourea and a chemotherapeutic drug approved by the Food and Drug Administration for use in the treatment of GBM (Reithmeier et al., 2010; Westphal et al., 2003). Nitrosoureas are DNA alkylating agents characterised by high lipophilicity permitting blood-brain barrier penetration. Nitrosoureas such as carmustine, lomustine or nimustine were commonly used in the first line of treatment for GBM prior to 1999 (Weller et al., 2013). Intracavitary carmustine wafers are recommended as part of first-line therapy for patients with an intraoperative diagnosis of high-grade glioma whose tumours are suitable for >90% resection (Wang et al., 2002). Neurosurgical clinics in the USA use carmustine wafers (Gliadel®) in interstitial chemotherapy for incurable relapses of malignant brain gliomas. In a phase III clinical trial in the USA, the median survival of patients treated with Gliadel® was 31 weeks (27 US medical centres, 222 patients with recurrent malignant brain gliomas) (Sheleg et al., 2002).

Several aberrantly activated signalling pathways characterise GBM. Epidermal growth factor receptor (EGFR), vascular endothelial growth factor receptor (VEGFR) and platelet-derived growth factor receptor (PDGFR) are overexpressed, amplified and/or mutated, leading to uncontrolled cell proliferation, angiogenesis, migration, survival and differentiation of the glioma cells (Minniti et al., 2009; Normanno et al., 2006). Thus, several targeted inhibitors for EGFR, VEGFR and PDGFR are being developed. Recently, the use of small-molecule tyrosine kinase inhibitors (TKIs) and monoclonal antibodies against EGFR and VEGFR were evaluated in phase II clinical

trials for potential use in the treatment of GBM (Minniti et al., 2009). Pre-clinical studies involving the murine humanised monoclonal antibody cetuximab (Erbitux®, Merck & Co) have shown that EGFR inhibition leads to reduced proliferation and VEGF expression in glioma cells along with cell apoptosis (Minniti et al., 2009). Two oral, small TKI molecules, gefitinib (Iressa®, AstraZeneca) and erlotinib (Tarceva®, Osi Pharmaceuticals) were also evaluated in several phase I and phase II clinical trials in GBM patients (Minniti et al., 2009). Phase I and II studies of gefitinib and erlotinib used as single agents adjuvant to RT have shown no major improvements in survival. A modest progression free and median survival of 8.1 and 39.4 weeks respectively has been shown in phase II clinical trials consisting of 53 recurrent GBM patients (Minniti et al., 2009; Rich et al., 2004). A similar phase II trial of erlotinib has shown a median progression-free survival of only 2-3 months with a 6-25% response rate (Minniti et al., 2009; Raizer et al., 2010). New growth factor inhibitors such as lapatinib (a dual EGFR and ErbB-2 inhibitor) and canertinib (a pan-ErbB inhibitor) have shown the potential for use in the treatment of GBM. An increased suppression of tumour growth following canertinib administration was observed in athymic nude mice bearing xenografts of human SF-767 glioblastoma (Minniti et al. 2009).

Other potentially useful agents for the treatment of GBM are represented by the PDGFR, mTOR and integrin inhibitors (Minniti et al., 2009).

One of the major problems with chemotherapy is the achievement of the therapeutic drug concentration at the tumour site without causing undesirable effects on the other organs of the body. The vascular system of the tumours is highly disorganised and unpredictable thus making drug delivery into the tumour very difficult (Chawla and Amiji, 2002).

1.3 Blood Brain Barrier

The blood brain barrier (BBB) is a physiological barrier and a cellular transport system made by the complex tight junctions between adjacent endothelial cells (Risau & Wolburg 1990; Abbott & Romero 1996; Abbott 2002; Fig. 1.2).

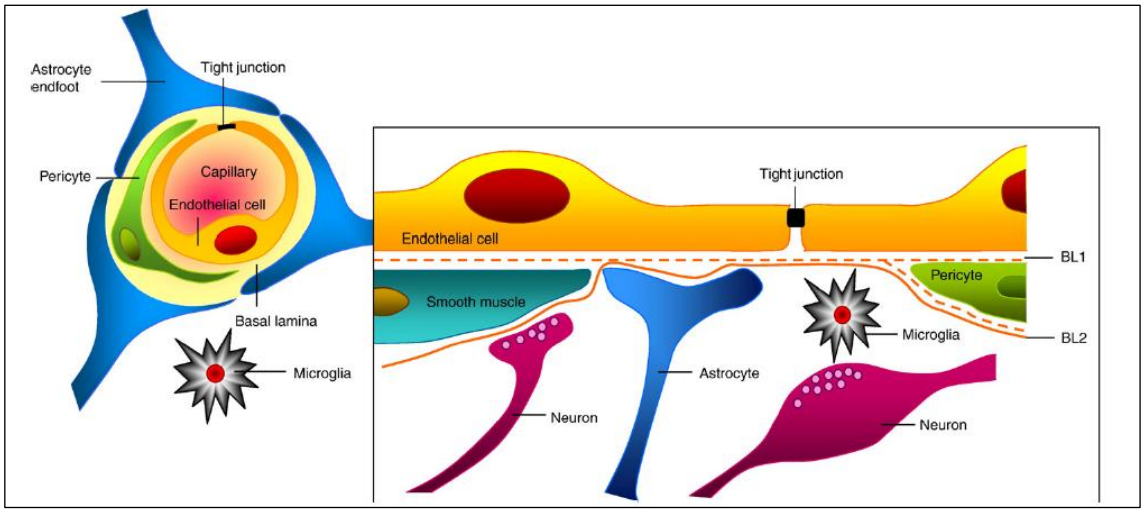

Figure 1.2: Cell associations at the blood brain barrier

The cerebral endothelial cells form TJs at their margins sealing diffusional paracellular pathway between cells. Pericytes distributed along the length of the cerebral capillaries, surrounding the endothelium, are enclosed by and contribute to the local basement membrane forming a distinct perivascular extracellular matrix. The properties and maintenance of the BBB is due to the astrocyte foot processes surrounding the capillaries.

Source: (Abbott et al., 2010)

The BBB maintains homeostasis of the central nervous system (CNS) by restricting paracellular movement of water-soluble substances from blood to the brain microenvironment (Colgan et al., 2007). Endothelial cells line the microvessels of the brain and their tight junctions force a transcellular route of the molecular traffic across the brain instead of the paracellular route (Hawkins and Davis, 2005; Wolburg and Lippoldt, 2002). These endothelial cells exhibit specialised properties such as extremely

low permeability, high transendothelial electrical resistance and low occurrence of pinocytic vesicles (Colgan et al., 2007). These cells also secrete the basal lamina, which surrounds the brain capillaries that decreases the capillary permeability. Furthermore, the capillaries of the brain are in contact with the astrocyte foot processes (astrocytes are glial cells), thus separating the capillaries from the neurons (Abbott et al., 2006).

Junctional complexes between endothelial cells include adherens junctions (AJs) and tight junctions (TJs). In AJs, cadherin proteins span the intercellular cleft and are linked into the cell cytoplasm by the scaffolding proteins alpha, beta and gamma catenin. AJs hold cells together giving the tissue structural support and are essential for formation of TJs (fig. 1.3). The disruption of AJs leads to barrier disruption (Wolburg and Lippoldt, 2002). The barrier function of the BBB is maintained by the highly regulated presence of tight junctions between adjacent cells and comprise of claudins, occludin, junctional adhesion molecules (JAM) 1-3, cingulin, 7H6 tight junction associated antigen, spectrin and zona occludens (ZO) 1, 2, 3. The ZOs link the tight junction proteins to each other and the actin cytoskeleton (Abbott et al. 2010; Colgan et al. 2007). Activation of actin is initiated by a rise in intracellular calcium, e.g., resulting from ligand binding to B2 bradykinin receptor and may change the configuration of claudins and occludin thus modifying the TJ properties (Abbott et al., 2010).

Twenty four isoforms of claudin have been described, claudin 1-24, of which claudin 3 and 5 are vital to the diffusion and high electrical resistance of the BBB (Fig. 1.3). Cytoplasmic proteins ZO-1, ZO-2, ZO-3 and cingulin link the cytoskeleton protein actin thus maintaining the structural and functional integrity of the BBB (Ballabh et al., 2004).

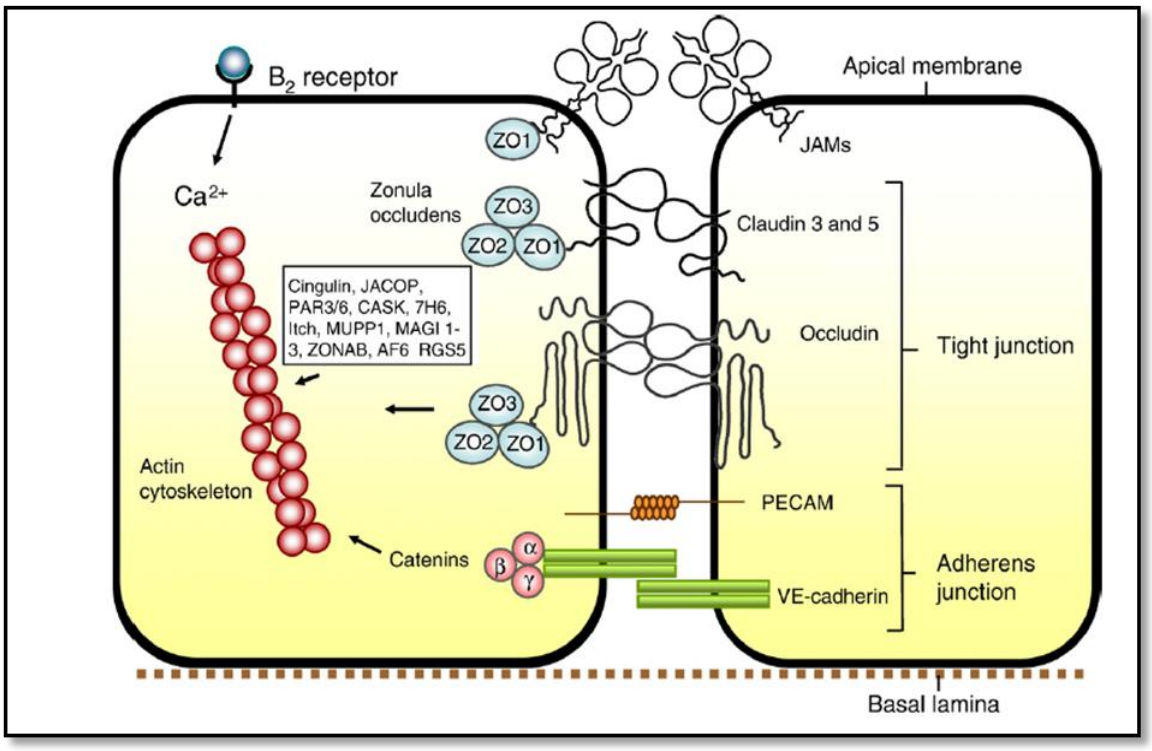

Figure 1.3: Structure of blood brain barrier tight junctions

Cadherins of the AJs provide structural integrity and cell attachment, and are necessary for the formation of TJs. Claudins associate and bind to each other across the intercellular cleft. Claudins and occludins are linked to ZO-1, 2 and 3, which are in turn linked *via* cingulin dimers to the actin/myosin cytoskeletal system within the cell. Source: Abbott et al., 2010

1.3.1 Functions of the BBB

Apart from providing a stable environment for neural function, the BBB maintains an optimum ionic composition for synaptic signalling function. The BBB helps in keeping the peripheral and central neurotransmitter pools separate, thus minimising 'cross talk' (Bernacki, *et al* 2008). Presence of macromolecules, such as albumin, prothrombin and plasminogen in the brain, activates cascades that can cause seizures, glial activation, glial cell division and scarring, and cell death (Gingrich and Traynelis, 2000; Gingrich et al., 2000). These are prevented from entering into the brain interstitial fluid by the BBB. Neurotoxic substances and xenobiotics are actively

pumped out of the brain by the ABC transporters (Dallas et al., 2006). Solute carriers allow the transport of polar nutrients such as glucose and amino acids necessary for metabolism (Zhang et al., 2002).

1.3.2 Transport across the BBB

Several potential routes for permeation across the BBB are available. These include passive diffusion, ATP-binding cassette (ABC) transporters, solute carriers, cell migration and receptor mediated (RMT) or adsorptive mediated (AMT) transcytosis.

Lipid-soluble non-polar molecules and blood gases - oxygen and carbon dioxide - can diffuse through the cell membrane passively and cross the endothelium in the BBB (Liu et al., 2004). Bases, due to their positive charge, have an advantage over acids when penetrating through the BBB. It is possibly due to the cationic nature of these molecules and an interaction with the negatively charged glycocalyx and phospholipid head groups of the outer leaflet of the cell membrane that facilitate their entry (Abbott et al., 2010). The diffusion of most polar substances through the BBB is difficult and thus all cells express a large number of solute carriers in the cell membrane (Zhang et al., 2002). These solute carriers are essential for the transport of polar nutrients such as glucose and amino acids necessary for metabolism. A wide variety of transport proteins mediating flux into and out of the brain are expressed by the BBB endothelial cells (Abbott et al., 2010).

The ABC transporters in humans are of greatest significance for efflux transport of P-glycoprotein, multidrug resistance-associated proteins, and breast cancer resistance proteins (BCRP) (Begley, 2004; Dauchy et al., 2008). These transporters also transport cholesterol and are associated with drug resistance (Dean et al., 2001). The ABC transporters intercept drugs diffusing across the cell membrane, out of the endothelial cells (Abbott et al., 2010). The major role of the ABC transporters in the BBB is to

function as active efflux pumps consuming ATP and transporting a diverse range of lipid-soluble compounds out of the brain capillary endothelium and the CNS thus removing potentially neurotoxic, endogenous or xenobiotic molecules (Dallas et al., 2006).

The main route of transcystosis of macromolecules such as proteins and peptides across the BBB is by the endocytotic mechanisms. These vesicular mechanisms involve either RMT or AMT. RMT requires specific binding of macromolecules to their receptors on the cell surface triggering an endocytotic event, whereas AMT requires a positively charged macromolecular interaction with cell surface to induce endocytosis and subsequent transcytosis (Abbott et al., 2010; Demeule et al., 2002).

1.3.3 How is the BBB Compromised in Glioma?

Studies have confirmed that the integrity of the BBB is compromised in primary and metastatic brain tumours. Alteration in the BBB architecture during the brain tumour includes compromised TJs, increase in perivascular space, presence of fenestrations in the blood capillaries and increased number and activity of pinocytic vesicles (Bart et al., 2000; Deeken & Löscher, 2007; Liebner et al 2000).

Studies have shown that in GBM, there is a selective loss of claudin-3 from the tight junctions, but not JAM, thus leading to a loss in the integrity and the functionality of the BBB (Abbott et al., 2010). Liebner and colleagues reported that claudin-1 expression was lost from nearly all microvessels in high-grade astrocytomas (Liebner et al., 2000). In contrast, claudin-5 and occludin expression were down regulated in hyperplastic vessels and ZO-1 expression was largely unaffected; suggesting the molecular structure of microvessel tight junctions is altered in high-grade astrocytomas allowing the leakage of various solutes across the BBB (Davies, 2002).

1.4 Apoptosis

Apoptosis, from the Greek word “to fall off” is a programmed cell death mechanism, first described by Kerr et al. in 1972 (Kerr et al., 1972). Apoptosis is a distinctive and an important mode of “programmed” cell death, involving genetically determined elimination of cells (Elmore, 2007). Apoptosis plays a vital role in development, and aging and in sustaining tissue homeostasis to maintain the cell populations and has been highly conserved throughout evolution (Cheung et al., 2012; Elmore, 2007; Fulda et al., 2010).

1.4.1 Morphological Changes

Apoptosis is morphologically characterised by cell shrinkage, blebbing of cell membrane, nuclear condensation, cellular fragmentation and formation of apoptotic bodies (Furuya et al., 1997; Ziegler and Groscurth, 2004).

The early stages of apoptosis involve cell shrinkage and pyknosis, which can be visualised under the light microscope (Kerr et al., 1972). Cell shrinkage results in smaller cell size, denser cytoplasm and more tightly packed cell organelles. Pyknosis results due to chromatin condensation and is a characteristic feature of apoptosis (Kroemer et al., 2009; Wong, 2011). This is followed by extensive plasma membrane blebbing (although the plasma membrane still remains intact), karyorrhexis and separation of cell fragments into apoptotic bodies also called “budding”(Elmore, 2007; Wong, 2011). Subsequently, phagocytosis by macrophages, parenchymal cells or neoplastic cells occurs, and the apoptotic bodies are degraded in the phagolysosomes (Elmore, 2007). In addition to this, during the early stages of apoptosis, externalisation of phosphatidylserine from the inner layer to the outer layer of the cell membrane occurs, thus allowing recognition of dead cells by macrophages (Johnson et al., 2000; Saraste and Pulkki, 2000; Wong, 2011). Macrophages involved in the engulfment and

digestion of apoptotic bodies are called the “tingible body macrophages” and are found in the reactive germinal centres of lymphoid follicles or sometimes in the thymic cortex (Elmore, 2007; Rahman et al., 2010). Phagocytosis occurs without any inflammation as no inflammatory cytokines are released in the process (Kurosaka et al., 2003). In addition, the apoptotic cells do not release any cellular constituents into the surrounding interstitial tissue and the rapidly occurring process prevents any tissue necrosis from occurring (Elmore, 2007).

1.4.2 Biochemical Changes

In the presence of stress stimuli such as chemotherapeutic agents, irradiation and oxidative stress, the “death signal” initiates a complex series of events, including the activation of caspases (Cheung et al., 2012; Fulda et al., 2010; Li et al., 1997).

The two main types of biochemical changes observed in apoptosis include: activation of caspases, and DNA and protein breakdown. DNA breakdown into large 50-300 kilobase pieces occurs, followed by internucleosomal cleavage of the DNA by endogenous DNases into double-stranded DNA fragments of 180 to 200 base pairs. Although a characteristic feature of apoptosis, this is not specific, as the DNA ladder is also observed in agarose gel electrophoresis of necrotic cells (Lee et al., 1997; Saraste and Pulkki, 2000).

The activation of caspases is another specific feature of apoptosis. Caspases belong to the cysteine family of proteases, where the “c” of the caspases refers to the cysteine protease family and the “aspase” refers to the enzymes property to cleave the asparatic acid residues. Activation of the caspases leads to the cleavage of many cellular proteins and breaking up of the nuclear scaffold and cytoskeleton. These biochemical changes explain in part the morphological changes, however, apoptosis can also take

place without oligonucleosomal DNA fragmentation and can be caspase-independent (Roschitzki-Voser et al., 2012; Wong, 2011).

1.4.3 Mechanism of Apoptosis

The mechanism of apoptosis is a highly complex and a sophisticated event, involving an energy-dependant cascade of molecular events. Research has shown that there are two main mechanisms of apoptosis: the intrinsic or the mitochondrial pathway and the extrinsic or the death receptor pathway (Fig. 1.4) (Chen et al., 2014; Elmore, 2007). However, evidence suggests that the two pathways are linked and the molecules from one pathway may influence the other (Elmore, 2007; Igney and Krammer, 2002). Another pathway, involving T-cell cytotoxicity and perforin-granzyme-dependent killing of the cell, also takes place in apoptotic cells. This is mediated by the granzyme B or granzyme A. All three pathways, intrinsic, extrinsic and the granzyme-B, converge down on the same execution phase, which involves the activation of caspase-3, resulting in DNA fragmentation, cellular degradation, formation of apoptotic bodies and expression of ligands for recognition by phagocytic cells (Andoniou et al., 2014; Elmore, 2007; Wong, 2011).

1.4.4 The Intrinsic Pathway

The intrinsic pathway is initiated by internal stimuli such as hypoxia, irreparable DNA damage, high cytosolic Ca^{2+}, severe oxidative stress, radiation, toxins and viral infections (Elmore, 2007; Wong, 2011).

The intrinsic pathway is the result of an increase in the mitochondrial permeability and the release of pro-apoptotic molecules such as cytochrome-c into the cytoplasm. The Bcl-2 family of proteins control and regulate the apoptotic mitochondrial events. The Bcl-2 family of proteins governs mitochondrial membrane permeability either by the pro-apoptotic (e.g., Bax, Bak, Bad, Bcl-Xs, Bid, Bik, Bim

and Hrk) or the anti-apoptotic (e.g. Bcl-2, Bcl-XL, Bcl-W, Bfl-1 and Mcl-1) proteins (Fulda et al., 2010; Wong, 2011).

The above mentioned stimuli result in the opening of the mitochondrial membrane permeability transition pore, loss of the mitochondrial transmembrane potential and release of two main groups of pro-apoptotic proteins from the intermembrane space into the cytosol (Saelens et al., 2004). The first group of proteins, cytochrome-c, Smac (secondary mitochondria-derived activator of caspase), DIABLO (direct IAP Binding protein with Low pI) and the serine protease Omi/high temperature requirement protein A (HtrA2), activate the caspase-dependant mitochondrial pathway (Elmore, 2007; Garrido et al., 2006; Guicciardi et al., 2014). Cytoplasmic release of cytochrome-c activates caspase 3 *via* the formation of a complex known as apoptosome which is made up of cytochrome c, Apaf-1 and caspase 9**.** Conversely, Smac/DIABLO and Omi/HtrA2 promote caspase activation by binding to IAP (inhibitor of apoptosis proteins), subsequently leading to the disruption in the interaction of IAPs with caspase-3 or -9 thus leading to their activation (Kroemer et al., 2007; LaCasse et al., 2008; Wong, 2011).

1.4.5 The Extrinsic Pathway

The extrinsic pathway initiates upon the binding of death ligands to the death receptor member of the tumour necrosis factor gene superfamily (TNF) and involves transmembrane receptor-mediated interactions. The best known death receptor is the TNF receptor-1 (TNFR-1) which is related to the protein Fas (CD95); their ligands are called TNF and FasL respectively (Chicheportiche et al., 1997; Elmore, 2007; Hengartner, 2001; Locksley et al., 2001; Wong, 2011). These receptors are comprised of cysteine-rich extracellular domains and have an 80 amino acid cytoplasmic domain, called the death domain, and are critical in transmitting death signal from the cell

surface to intracellular signalling pathways. The death domain is involved in recruiting adaptor proteins such as TNF receptor-associated death domain (TRADD) and Fas-associated death domain (FADD), and cysteine proteases such as caspase-8 (Chen et al., 2014; Schneider and Tschopp, 2000; Wong, 2011).

The FasL/FasR and the TNF/TNFR-1 are the best characterised models for the series of events that take place in the extrinsic apoptotic pathway (Elmore, 2007). Upon ligand binding to the receptor, cytoplasmic adaptor proteins are recruited which exhibit the binding of respective death domains to the receptors. The binding of FasL to FasR results in binding of the adaptor protein FADD, whereas, binding of TNF to TNFR results in binding of TRADD along with the recruitment of FADD and RIP (receptor-interacting protein) (Elmore, 2007; Suliman et al., 2001; Wajant, 2002). Dimerisation of the death effector domain takes place due to the association of FADD with procaspase-8. This results in the formation of a death inducing signalling complex (DISC), thus leading to auto-catalytic activation of procaspase-8. The activation of caspase-8 triggers the execution pathway. This type of apoptosis can be inhibited by the protein c-FLIP (cellular FLICE {FADD-like IL-1β-converting enzyme}-inhibitory protein) which binds to FADD and caspase-8, causing them to be ineffective (Elmore, 2007; Suliman et al., 2001; Wong, 2011).

1.4.6 The Perforin-Granzyme Pathway

Natural killer (NK) cells and $CD8^+$ cytotoxic T lymphocytes (CTL) are the most important hosts of the immune system. These cells exert their effects by two distinct mechanisms, one involves the synthesis and release of soluble mediators such as INF-γ, TNF-α and interleukins, while the other involves direct cell lysis and induction of apoptosis in target cells (Pardo et al., 2004). T-cell mediated cytotoxicity comprises of $CD8^+$ cells that kill the antigen bearing cells *via* the extrinsic pathway involving the

FasL/FasR interaction. However, these cells can exert their effects on tumour cells and infected cells *via* a different pathway involving the secretion of transmembrane pore-forming molecule, perforin, with a subsequent exocytosis of cytoplasmic granules through the pore to induce apoptosis of the target cells (Pardo et al., 2004; Trapani and Smyth, 2002). The most important components within the granules are the serine proteases granzyme A and granzyme B (Elmore, 2007; Pardo et al., 2004).

Granzyme B cleaves proteins at the aspartate residues. It thus initiates the activation of apoptosis by direct or indirect caspase activation (caspases-3 and -8) resulting in the disruption of mitochondrial membrane integrity, by cleaving factors like ICAD (Inhibitor of Caspase Activated DNAse) or by cleaving the key structural proteins in the nuclear membrane or the cytoskeleton (Brunner, 2003; Elmore, 2007; Pardo et al., 2004). Studies have also shown that granzyme B can utilise the intrinsic mitochondrial pathway for amplification of the death signal by specific cleavage of Bid and induction of cytochrome-c release (Elmore, 2007).

The granzyme-A pathway activates another cascade leading to the caspase-independent apoptotic pathway *via* the damage of single stranded DNA (Martinvalet et al. 2005). Upon entering the cell, granzyme A activates DNA fragmentation *via* DNase NM23-H1, a tumour suppressor gene product. This DNase plays an important role in immune surveillance to prevent cancer by inducing apoptosis of tumour cells (Fan et al., 2003).

A special target of granzyme A is an endoplasmic reticulum (ER-) associated complex called the SET complex. The SET complex consists of granzyme A activated DNase NM23-H1, tumour suppressor gene pp32, and three granzyme A substrates- the nucleosome assembly protein SET, the base excision repair enzyme Ape1/Ref-1, and the DNA bending protein HMG-2. The SET complex (270-420 kDa) has an important

role in maintaining chromatin structure and DNA repair. Following a CTL attack or upon the loading of granzyme A into the cells, translocation of the SET complex into the nucleus of the cell occurs. Granzyme A cleaves the SET complex, removing the inhibition of the NM23-H1 DNase, resulting in apoptotic DNA degradation (Fan et al., 2003; Martinvalet et al., 2005).

1.4.7 Execution Pathway

The final pathway of apoptosis, wherein the activation/execution of the caspases occurs, is called the execution pathway. Execution of apoptosis occurs *via* the degradation of nuclear and cytoplasmic proteins by the activated cytoplasmic endonucleases and proteases. The main effector molecules of apoptosis are the caspases-3, -6 and -7. Activation of caspase-3 by initiator caspases-8, -9 and -10 activates the endonuclease CaD (caspase-activated DNase) (O'Brien and Kirby, 2008; Yang et al., 1998). In normal proliferating cells, CaD is complexed with ICaD (inhibitor of CaD) (Nagata, 2000). Activated caspase-3 thus cleaves ICaD to release the CaD leading to DNA degradation and chromatin condensation (O'Brien and Kirby, 2008).

The *p53* gene has an important link to apoptosis and therefore to cancer. *p53* mutation occurs in the majority of human tumours and is associated with the advancement of the tumour and patient prognosis (Lowe and Lin, 2000). Normal cellular mechanisms are controlled through a mechanism which involves *p53*. Mutations or deficiencies in *p53* lead to reduced apoptosis and therefore to tumour development. Another feature of disruption of normal cellular death programme may occur due to an increase in the Bcl-2 protein, as it promotes cell survival by blocking apoptosis (Lowe and Lin, 2000; O'Brien and Kirby, 2008).

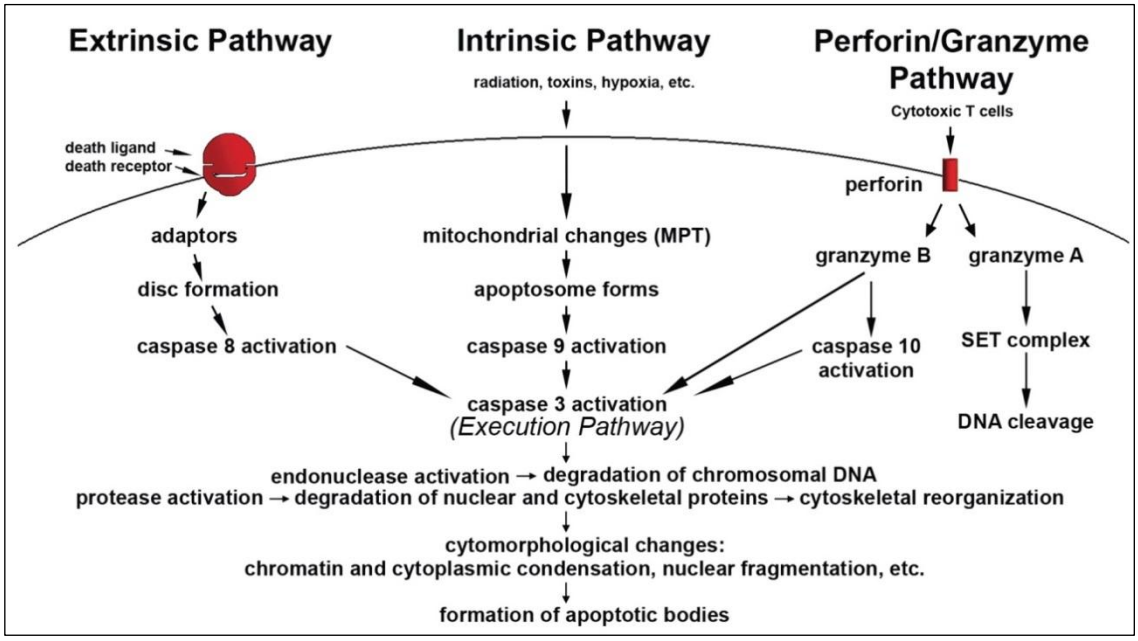

Figure 1.4: Schematic representation of the three apoptotic pathways, intrinsic, extrinsic and perforin/granzyme

All the three pathways, intrinsic, extrinsic and granzyme B, merge in the end to activate caspase-3 leading to cytoskeletal reorganisation, chromatin condensation, nuclear fragmentation and ultimately leading to formation of apoptotic bodies and cell death. Source: Biology Stack Exchange

1.5 Difference between Apoptosis and Necrosis

Necrosis is an alternative approach to cell death. Necrosis is considered to be a toxic and energy-independent process. Presence of stress stimuli such as ischemia, glutamate excitotoxicity in neurons, hypoxia, hypoglycaemia and exposure to DNA alkylating agents has been reported to trigger necrotic cell death (Fulda et al., 2010; Vanlangenakker et al., 2008). Death domain receptors such as TNFR1 and Toll-like receptors have been reported to trigger necrosis. RIP-1 (receptor-interacting protein 1), a serine/threonine kinase protein plays a crucial role in the initiation of necrosis induced by the ligand-receptor interactions. Reactive oxygen species and calcium are the main stimuli of a necrotic cell death (Vanlangenakker et al., 2008). The mechanisms of

necrosis and apoptosis differ; however, there is an overlap in the two processes. Factors that convert an on-going apoptotic process into a necrotic process include the depletion of intracellular ATP and decrease in the availability of caspases (Denecker et al., 2001; Elmore, 2007; Levin et al., 1999).

The major morphological changes that take place during necrosis include swelling of the cell, gain in cell volume due to swelling of organelles, formation of cytoplasmic vacuoles, distended endoplasmic reticulum, formation of cytoplasmic blebs, disruption of organelle membranes, swelling or rupturing of lysosymes or mitochondria and eventually, disruption of cell membrane (Kerr et al., 1972; Zong et al., 2004). The loss of cell membrane integrity leads to the release of cytoplasmic contents into the surrounding tissue, sending chemotactic signals, eventually leading to recruitment of inflammatory cells. As opposed to apoptosis, karyolysis occurs and inflammation may also occur (Denecker et al., 2001; Elmore, 2007).

1.6 Cell Proliferation and Cell Cycle Mechanism

Eukaryotic cells divide by an elaborate series of events, constituting the cell cycle, wherein the chromosome duplicates and a copy of the duplicated chromosome passes into each daughter cell. The cell cycle is a very tightly regulated process which causes an irreversible and unidirectional change in the state of the cell. The loss of this regulation leads to an uncontrolled expansion in the cell population, thus giving rise to cancer. Cell replication is controlled mainly by two consecutive phases, nuclear DNA replication and mitosis (Pinheiro and Sunkel, 2012; van den Heuvel, 2005).

Eukaryotic cell cycle can be divided into four phases: G1, S, G2 and M phase. The G1 phase is essential for the determination of the fate of the cell (the cell can

withdraw from any further proliferation and undergo differentiation in order to perform a specific task or enter into the S phase) and is the first stage of interphase. During interphase, the cell grows and there is extensive transcription and synthesis of new cellular components. Somatic cells begin by the replication of chromosome in the S (synthesis) phase. This is followed by the G2 phase where the cells undergo rapid growth and protein synthesis in order to prepare for mitosis or the M phase. Mitosis is the process of nuclear division wherein a number of activities take place in the nucleus of the cell and is concluded by the division of the mother cell into two daughter cells. This is followed by the G1 (Gap 1 or Growth) phase (Crosio et al., 2002; Pinheiro and Sunkel, 2012; Rieder, 2011; Tyson et al., 2002).

The cell cycle is controlled by a family of serine/threonine protein kinases called the cyclin-dependant kinases (Cdks) and their corresponding cyclin regulatory subunits. Different cyclin/Cdk units appear and have a specific kinase activity at different time points in the cell cycle (Table 1.2, Fig. 1.5) (Shackelford et al., 1999; Vermeulen et al., 2003). Cdks induce downstream signals and major cellular events such as chromosome condensation, DNA replication, and spindle assembly by the phosphorylation of selected proteins. The levels of Cdks during a cell cycle remain constant, as opposed to the levels of cyclins which increase and decrease thus periodically activating their respective Cdks (Tyson et al., 2002; Vermeulen et al., 2003). The regulation of the activity of Cdk is controlled by cyclin binding and cyclin-dependent kinase inhibitors (CKIs). The two main families of the CKIs include the Ink4 family and Cip/Kip family. The members of the Ink 4 family only bind to Cdk4 and 6, while the members of the Cip/Kip family bind to all Cdks (Berthet et al., 2003; Cerqueira et al., 2014).

To date, 21 Cdk encoding genes and 29 cyclin encoding genes have been identified. Amongst these, the cyclins A, B, E and D, and cyclin-dependent kinases 1, 2,

4 and 6 have been identified as the major regulators of cell cycle control (Bretones et al., 2014). The sequential activation of Cdk4 or Cdk6 followed by Cdk2, functions in early to mid-G1 phase and is important for the cell to enter into the S phase from the G0/G1 phase. While the Cdk 4 and Cdk6 associate with the D-type cyclins, the Cdk2 complexes with cyclin E during late G1 (Berthet et al., 2003; Hubbi and Semenza, 2015; Yang et al., 1997). Following the activation of the G1-phase Cdks, phosphorylation of the retinoblastoma protein (Rb) occurs allowing the accumulation of E2F transcriptional factors which consists of the genes encoding the required proteins for S phase (Bretones et al., 2014; Nevins, 2001). The Cdk1 and 2/cyclin A complex functions in the S phase whereas Cdk2/cyclin B and A complexes promote the G2/M transition (Bassermann et al., 2014; Berthet et al., 2003; Hubbi and Semenza, 2015). The cyclin B1/Cdk1 complex regulates cellular entry into mitosis and through its cytoplasmic, nuclear and centrosomal localisation, it is able to synchronise mitotic events such as nuclear envelope breakdown and centrosome separation (Wang et al., 2014). Following mitosis, Cdk7 plays an important role in cell cycle progression and RNA Polymerase II transcription as a component of the general transcription factor IIH. The catalytic subunit of Cdk7, cyclin H and a really interesting new gene (RING) finger protein, Mat1 form the CDK-activating kinase (CAK), which in turn activates the downstream Cdks by phosphorylating key threonine residues in a process known as T-loop activation (Kelso et al., 2014; Wohlbold et al., 2006).

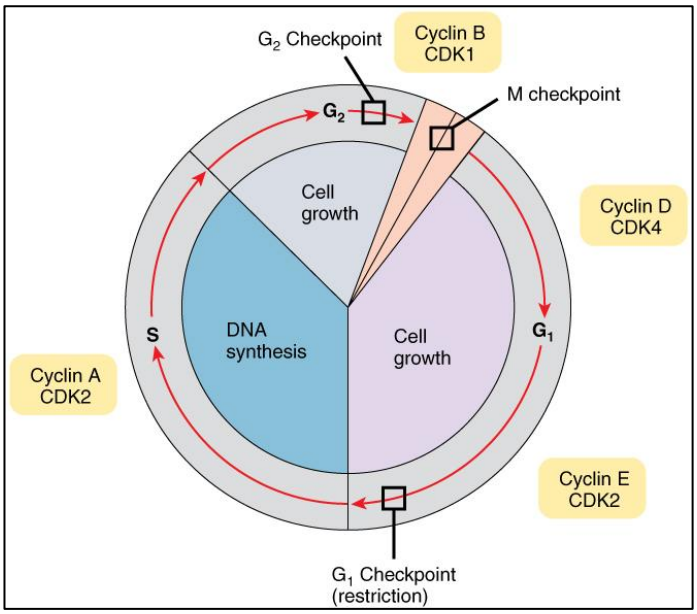

Figure 1.5: Diagrammatic representation of cyclins and cyclin dependent kinases involved in cell cycle regulation

Diagram summarises cyclins and cyclin dependent kinases that are involved in the cell cycle progression. Source: Candela Learning

Table 1.2: List of cyclin/Ckd complexes that are activated at specific time points in the cell cycle

Cdk	Cyclin	Cell cycle phase activity
Cdk 4	Cyclin D1, D2, D3	G1 phase
Cdk 6	Cyclin D1, D2, D3	G1 phase
Cdk 2	Cyclin E	G1/S phase transition
Cdk 2	Cyclin A	S phase
Cdk 1	Cyclin A	G2/M phase transition
Cdk 1	Cyclin B	Mitosis
Cdk 7	Cyclin H	CAK, all cell cycle phases

(CAK-Cdk activating kinases). (Vermeulen et al., 2003)

1.7 Oxygen Dependence

The growth, development and internal organisation of all large animals depends on the maintenance of oxygen homeostasis (Maxwell et al., 2001). However, mitochondrial respiration proves that the mitochondria are independent of oxygen presence due to the presence of high affinity cytochrome c oxidase. This gives rise to the model of "oxygen regulation", although this is more precisely explained by the "kinetic oxygen saturation" (Gnaiger, 2003). Oxygen supply to a tissue depends on the flow and oxygen content in the blood perfusing the tissue and; also upon the asymmetrical arrangement of microvessels supplying the oxygen in the surrounding region. This heterogeneity of microvasculature in tumours strongly influences the partial pressure of O_2 (pO_2) and thus the occurrence of hypoxic micro-regions. This results in the likelihood that oxygen consumption is erratic between and within tissues (Dewhirst et al., 1994).

Mammalian tissue can tolerate a wide range of oxygen tension, depending on the organ size, function and location of tissue and can thus encounter O_2 concentration ranging from 0.002-10%, with the ambient air O_2 concentration being 21% (Liu and Simon, 2004; Walmsley et al., 2005). Neutrophils, a striking example of the former, migrate in the circulation to the inflammation site and are thus required to adapt to and function in an environment with lower oxygen tension than that in the circulatory system (Walmsley et al., 2005). Also, studies dating back almost a century have demonstrated that neutrophils and macrophages depend highly on anaerobic glycolysis as a process for the production of ATP (Levene and Meyer, 1912a, 1912b). A drop in the pO_2 causes a complex change in gene expression which is mediated by the immediate activation of the hypoxia inducible factor (HIF), present in all cell types of higher eukaryotes (Liu and Simon, 2004). The HIF system has also been identified to

play an important role in the physiological challenge of achieving a balance between oxygen demand and supply (Maxwell et al., 2001).

1.7.1 The HIF System

The HIF transcriptional factor is a heterodimer comprised of alpha and beta subunits, both of which are PER-ARNT-SIM (PAS, a signal sensor) subfamily of the basic helix-loop-helix DNA binding motifs (Maxwell et al., 2001; Melillo, 2004). The β-subunit is also known as the aryl hydrocarbon receptor nuclear translocator (ARNT) and also serves as a heterodimeric partner with the aryl hydrocarbon receptor (Huang et al., 1998; Liu and Simon, 2004). In contrast to this, the α-subunit only functions as a mediator in the hypoxic response (Huang et al., 1998). From amongst the multiple isoforms of HIF, HIF-1α and HIF-2α are the best understood (Loboda et al., 2010).

HIF-1α and HIF-1β mRNA are expressed in most human and rodent tissues, while HIF-2α, HIF-3α, HIF-2β and HIF-3β show a more controlled pattern of expression. Studies have shown that HIF-1α plays a general role by signalling the presence of hypoxia to the transcriptional machinery in the cell nucleus. On the other hand, HIF-2α and HIF-3α play more specialised roles in oxygen homeostasis (Semenza et al., 2000). Although the HIF-1 and HIF-2 α subunits are highly conserved at the protein level have a similar domain structure and dimerise with HIF-1β, they have distinct tissue specific expression patterns. HIF-1α is present ubiquitously. However, the expression of HIF-2α is limited to lung, kidney, heart, small intestine and endothelium (Gordan et al., 2007; Holmquist-Mengelbier et al., 2006; Rosenberger, 2002).

1.7.2 O_2 Dependant HIF Degradation

The ARNT is constitutively expressed unlike the α-subunit levels whose stability is mediated by a region known as the oxygen-dependant degradation domain

(ODDD) (Huang et al., 1998). When the O_2 tension is high, (21% O_2), the α subunits are undetectable due to their rapid degradation by the product of the tumour suppressor gene called the von Hippel-Lindau tumour suppressor gene (VHL). This promotes HIF-1α degradation by the ubiquitin-26S proteasome pathway. HIF-1α inactivation and its capture by the VHL are dependent on the hydroxylation of two prolyl residues, Pro^{402} and Pro^{564}, in the ODDD. A further level of O_2-dependent regulation is by the hydroxylation of an asparaginyl residue in the C terminal transactivation domain (Asn^{803} of HIF-1) that prevents HIF-1α interaction with CBP/p300, a transcriptional coactivator protein. This results in the accumulation of the HIF-1α protein (Giaccia et al., 2003; Kamura et al., 2000; Liu and Simon, 2004; Semenza et al., 2000; Tanimoto and Makino, 2000).

Upon a reduction in O_2 tension to below 6%, the α subunits are stabilized and translocated into the nucleus where they dimerise with the ARNT *via* the PAS domain (Fig. 1.6). This leads to an active transcription of a wide array of genes that are critical to adapt to hypoxia (Table 1.3). Examples include VEGFR, PDGFR and plasminogen activator inhibitor-1 (Giaccia et al., 2003; Liu and Simon, 2004; Maxwell, 2003; Semenza et al., 2000).

1.7.3 Prolyl Hydroxylases

The oxygen-dependant prolyl-4-hydroxylation of HIF-1α is catalysed by three proline hydroxylase enzymes (PHD1, PHD2 and PHD3). PHDs are 2-oxoglutarate-dependant dioxygenases that hydroxylate key proline residues (Pro^{402} and Pro^{564}) in the ODDD of HIF-1α. These enzymes require molecular oxygen and iron as a co-substrate for the reaction to take place, thus the PHD also acts as an oxygen sensor. The characterisation of these enzymes has shown a reduced activity under the hypoxia "mimics" such as iron chelators, cobaltous ions and decreased oxygen availability

(Bruick and McKnight, 2001; Cioffi et al., 2003; Cockman et al., 2000; Ohh et al., 2000).

Table 1.3: List of HIF-1 targeted genes

Gene	Fucntion
Red blood cell production	Erythropoietin
Iron metabolism	Transferrin, transferrin receptor, ceruloplasmin
Cell proliferation, differentiation and viability	Cyclin G2, caspase 9, regulated in development and DNA damage responses 1 (RTP801)
Vascular architecture and tone	VEGF receptor-1, endoglin, plasminogen activator inhibitor-1, adrenomedullin, endothelin-1. Nitric oxide synthase-2, heme oxygenase-1
Matrix metabolism	Prolyl-4-hydroxylase-α1
pH regulation	Carbonic anhydrase-9
Energy metabolism	Glucose transporters 1 & 3, Glyceraldehyde phosphate dehydrogenase, pyruvate kinase M, lactate dehydrogenase A

VEGF- vascular endothelial growth factor. Maxwell, 2003; Semenza et al., 2000

Additionally, the transcriptional activity of HIF-1α is regulated by dioxygen-dependant hydroxylation of asparagine (Asn^{803}) residue in the COOH-terminal transactivation domain (CAD) of HIF-1α. This reduces the downstream transcription of HIF-1α targeted genes by inhibiting the coactivator p300. An enzyme, called the FIH (factor inhibiting hypoxia), carries out the hydroxylation of the asparagine residue in the CAD region of HIF-1α and thus plays a role in preventing the transcriptional activation role of CAD. The reaction rates of both the enzymes, PHD and FIH, are extensively influenced by the oxygen level. These enzymes thus act as oxygen sensors regulating the stability and the activity of HIF (Cioffi et al., 2003; Epstein et al., 2001; Esteban and Maxwell, 2005; Lando et al., 2002).

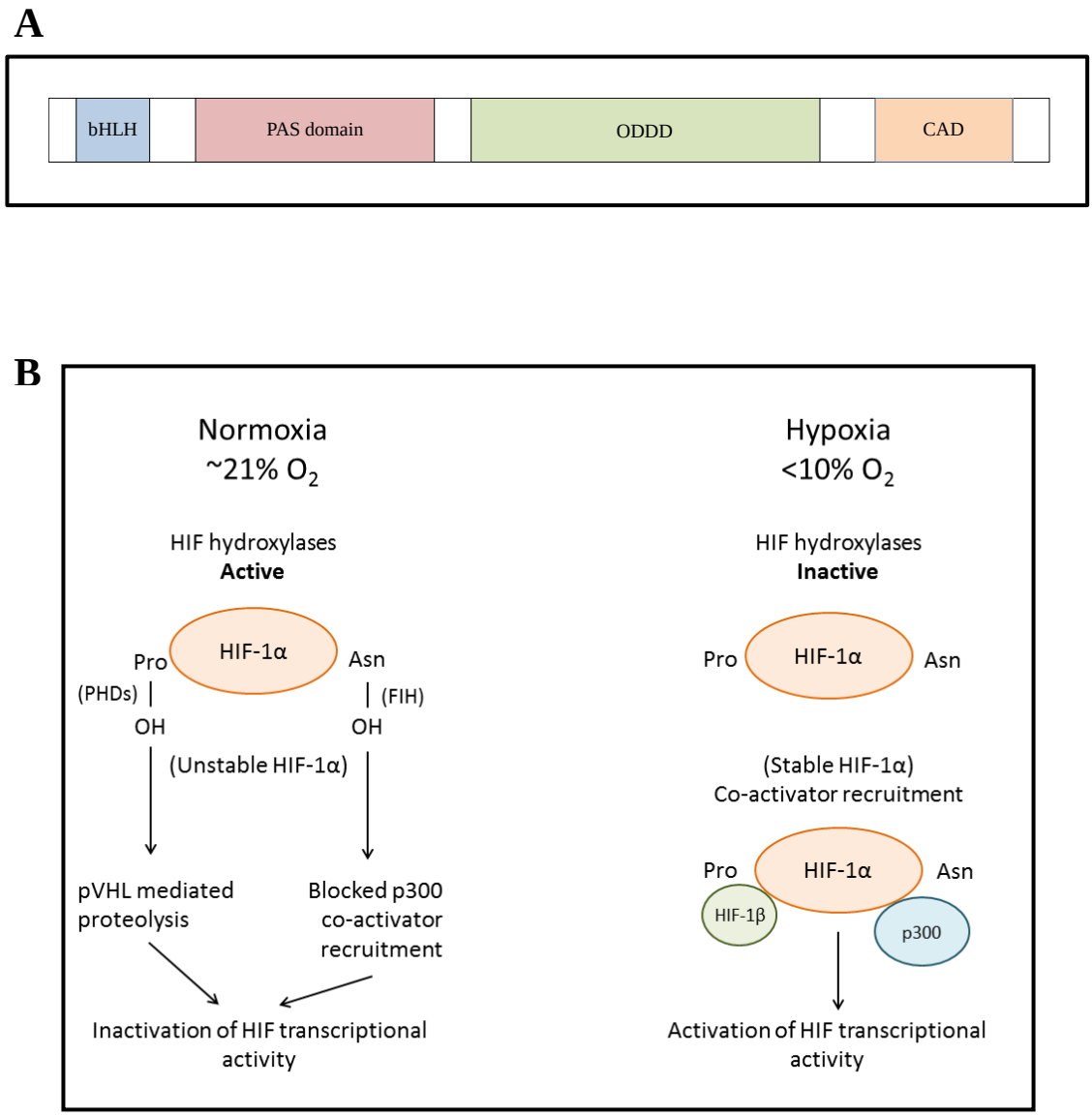

Figure 1.6: Representation of the domains and regulation of HIF-1α

(A) Diagrammatic representation of HIF-1α showing the different domains. (B) Regulation of HIF. At high levels of oxygen (normoxia), HIF-1α forms an inactive HIF-1 complex, which is unstable. This occurs due to the hydroxylation of the prolyl residue (by PHDs) and the hydroxylation of the asparagine residue (by FIH) in the ODD domain of HIF. Entrapment by the VHL gene occurs and degradation of the HIF-1α takes place by the proteasome pathway. On the other hand, at low oxygen levels (hypoxia), HIF-1α is stabilised and translocates to the nucleus leading to transcription of genes essential to adapt to hypoxia.

1.8 Reactive Oxygen Species

Reactive oxygen species (ROS) are involved in almost all biological functions. Hydroxyl radicals (•OH), superoxide anions ($O_2•^-$), singlet oxygen ($^1O_2$) and hydrogen peroxide (H_2O_2) are constantly generated in the mitochondria as a result of aerobic metabolism (Kryston et al., 2011; Matés and Sánchez-Jiménez, 2000; Song et al., 2014; Wiseman and Halliwell, 1996). Inflammatory cells, both- allergenic and non-allergenic, produce ROS (Simon et al., 2000). Persistent oxidative stress leads to destruction of the essential biomolecules such as DNA, proteins and lipids. ROS also function to form a defence mechanism against bacterial infections, thus acting as a part of defence system (Matés and Sánchez-Jiménez, 2000; Shen et al., 1996; Valko et al., 2006). Specialised enzymes in the biological system such as NADPH-oxidase, myeloperoxidase and nitric oxide synthase, generate reactive oxygen or nitrogen species in order to kill the harmful bacteria that may enter the biological systems. NADPH-oxidase is found in the plasma membrane of phagocytes and B lymphocytes, and participates in phagocytic activity by releasing superoxide radical, a primary element that ignites antibacterial defence. In this manner, ROS play a dual role in the biological system as they can be both harmful and beneficial (Matés and Sánchez-Jiménez, 2000; Valko et al., 2006; Zorov et al., 2014). ROS has been shown to be involved in intracellular signalling pathways such as inflammation, regulation of insulin production and in the activation of the hypoxia inducible factor. In this manner of cellular or molecular signalling, ROS production targets at reversible protein modifications, modulation of gene regulation and adaptive MAP kinase signalling activation (Bashan et al., 2009; Kikusato et al., 2015; Lu et al., 2015; Weidinger and Kozlov, 2015). ROS has been strongly implicated in hypoxia wherein the activation of a number of transcription factors takes place due to ROS (Kolamunne et al., 2013).

The generation of ROS is controlled by the antioxidants present in cells such as reduced glutathione, catalase, and superoxide dismutase, thereby detoxifying the ROS (Clerici et al., 1995; Kryston et al., 2011; Simon et al., 2000). Antioxidants can be classified according to their mode of action as scavenging, preventative or enzymatic. Scavenging antioxidants prevent antioxidant stress by scavenging the radicals as they form. Preventative antioxidants work mainly by sequestering transition metal ions and those formed from Fenton reactions (Fenton's reaction is where Fe^{2+} is oxidised by hydrogen peroxide to Fe^{3+}, forming a hydroxyl radical and a hydroxide ion in the process). Enzymatic antioxidants comprise of systems that function by catalysing the oxidation of other molecules (Chapple, 1997). Superoxide dismutase has been considered as the most effective intracellular enzymatic antioxidant that catalyzes the dismutation of $O2^{\bullet-}$ to O2 and to the less-reactive species H_2O_2 (McCord and Fridovich, 1969; Valko et al., 2006). Catalse is involved in converting hydrogen peroxide to water; while glutathione peroxidase is involved in reducing peroxides by forming selenoles (Se-OH) (Bauer and Zarkovic, 2015; Matés et al., 1999; Nishimoto et al., 2015; Valko et al., 2006; Yu et al., 2014).

1.8.1 Relationship between Cancer and ROS

ROS are a double-edged sword. The basal ROS level in cancer cells is higher than normal cells. This is due to the high metabolic activity of the cells and mitochondrial energetics. The hypoxic conditions of the cancerous cells lead to activation of HIF, as explained in section 1.7. Various alterations in the mitochondrial electron transfer chain lead to an increased possibility of the electron transfer to oxygen. Chronic inflammation, increased cytokine release and the activation of c-Myc protein (c-Myc is a member of the Janus kinase family, involved in cell proliferation and apoptosis) coupled with its downstream signalling proteins together lead to an increase in the ROS production in cancerous cells (Chiang et al., 2015; Tong et al., 2015; Vafa et al., 2002).

This elevated ROS level enhances cancer growth and proliferation; and is involved in tumour angiogenesis and promotes cancer cell invasion and metastasis (Chen et al., 2015; Pelicano et al., 2004).

Cellular metabolism can cause an oxidative DNA damage which has been shown to induce malignant transformation of normal cells *in vitro* (Cooke et al., 2003). ROS can cause both purine and pyrimidine base changes along with changes in the deoxyribose backbone of the DNA, single or double-stranded DNA breaks, DNA cross-links and damage to important genes and proto-oncogenes, thus giving rise to cancer (Dizdaroglu et al., 2002; Wiseman and Halliwell, 1996). The DNA damage resulting from ROS exposure can thus cause errors in replication, transcription and translation, signal induction pathways (including NF-κB, activated protein-1, phospholipase A2, mitogen activated protein kinases and c-Jun kinase) and genomic instability, all of which result in carcinogenesis. It has been well established that free-radical mediated DNA-damage occurs in cancer tissues (Cooke et al., 2003; Valko et al., 2006).

1.9 Nanoparticles

The potential to use polymeric nanoparticles (NPs) as drug delivery vehicles for anti-cancer therapeutics has recently been identified and could revolutionise the future of cancer therapy (Ma et al., 2011). Polymeric NPs prepared from natural and synthetic polymers have drawn major attention due to higher stability, versatility for industrial manufacture and opportunity for further surface nano-engineering (Shenoy et al., 2005). Nanoparticles, due to their submicron-size and increased surface to mass ratio, have unique physicochemical properties. They can be tailor-made to achieve a controlled drug release and disease specific localisation by tuning polymer characteristics and surface chemistry (Shenoy et al., 2005). The use of NPs for drug delivery is attributed to

the improved pharmacokinetic profile, decreased effective dose and increased availability associated with it. It has been established that NPs as drug carriers can preferentially be concentrated in the tumour mass by virtue of the enhanced permeation and retention (EPR) mechanism and upon deposition, can act as drug depots thus providing a continuous supply of the combined therapeutic drug compound into the tumour mass (Feng et al., 2012; Shenoy and Amiji, 2005).

Different synthetic polymers used for nanoparticle preparation include poly-lactic acid (PLA), poly-ε-caprolactone (PCL), poly(lactide-co-glycolide) (PLGA) and poly(alkyl cyanoacrylate) (PACA) while natural polymers include chitosan, alginates, gelatin and albumin (Kumari et al., 2010; Yordanov, 2012). Doxorubicin-loaded lipid-modified dextran based polymeric nano-system have shown noticeable anti-proliferative effects against multi-drug resistant osteosarcoma cell lines (Susa et al., 2009). A few drug delivery systems using nanoparticles have been approved by the FDA and are available for cancer treatment. These include pegylated liposomal doxorubicin (Doxil and Caelyx) and liposomal daunorubicin (DaunoXome). Recently, an albumin bound paclitaxel nanoparticle Abraxane was approved by the FDA for breast cancer treatment (Haley and Frenkel, 2008)

1.9.1 Enhanced Permeation and Retention Mechanism:

The lack of lymphatic drainage in solid tumours has two effects on drug delivery and retention in solid tumours. Firstly, defective lymphatic flow in solid tumours decreases the clearance of high-molecular-weight compounds from tumour interstitium (Jang et al., 2003; Maeda, 2001; Matsumura and Maeda, 1986). Secondly, this together with leaky tumour blood vessels, results in enhanced accumulation and retention of high molecular-weight compounds in solid tumours, a phenomenon recognised as the enhanced permeability and retention effect (Jang et al., 2003; Maeda, 2001).

1.9.2 Poly-ε-caprolactone:

The synthetic polymer poly-ε-caprolactone (PCL; Fig 1.7) was selected for this study due to its biocompatibility and biodegradability. It is a semi-crystalline non-toxic polymer with neutral biodegradation end-products approved by the FDA for clinical use (Cho et al., 2002; Shenoy and Amiji, 2005; Tarafder et al., 2013). The applications of PCL include suture coatings, absorbable medical devices such as intravascular stents as support to vein grafts, and as external grafting material for broken bones (Sarasam, 2001). PCL reinforced with glass fibres has been used as intramedullary fracture fixation pins and applied in tissue engineered constructs for craniofacial repair (Coombes et al., 2004). PCL is produced from crude oil and has a good resistance to water, oil, solvents and chlorine. PCL usually has a glass transition temperature of −60°C and melting point of 45°-60°C, depending on the molecular weight (Coombes et al., 2004; Gan et al., 1999). PCL is versatile in the sense that it allows modification of its physical, chemical and mechanical properties by co-polymerisation or blending with many other polymers efficiently (Dash and Konkimalla, 2012).

PCL degradation is slow thus making it suitable for use as a long term drug delivery system (Sinha et al., 2004). The degradation of PCL in the human body can be affected by molecular weight, crystallinity, environment and temperature (Coombes et al., 2004). PCL undergoes random, non-enzymatic cleavage beginning in the amorphous region and is auto-catalysed by the carbonyl end groups of the fragmented polymeric chain; water permeability of the polymer being the rate-limiting step. This is followed by enzymatic surface erosion of the polymer characterised by grooves and cracks on the surface. These fragments are then utilised in the tricarboxylic acid (TCA) cycle and phagocytosed to complete the degradation (Dash and Konkimalla, 2012). Thus, PCL nanoparticles can serve as a biocompatible drug delivery system with minimal toxicity.

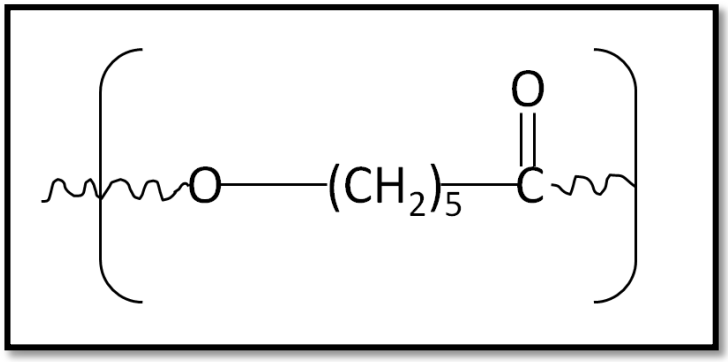

Figure 1.7: Polymeric structure of PCL

PCL is prepared by the ring opening polymerization of ε-caprolactone to polycaprolactone. Source: Kumari et al., 2010

1.10 Asiatic acid

Triterpenes are terpenes consisting of six isoprene units with a molecular formula $C_{30}H_{48}$. These are biosynthesised in plants by cyclisation of squalene (Huang et al., 2011). Triterpenes are extensively distributed in composite plants, and their biological activities have attracted abundant attention. Many triterpenoids have proven promising as antineoplastic agents (Hsu et al., 2004; Huang et al., 2011). Asiatic acid (AA), a herbal extract of the plant *Centella asiatica* (family Apiaceae) (Fig 1.8), is native to many countries such as India, Sri Lanka, Thailand, China, Indonesia and Malaysia. The extracts of *Centella asiatica* – asiatic acid, madecassic acid and the three asiaticosides, asiaticoside, asiaticoside A and asiaticoside B, have been used as a traditional herb in both Indian and Chinese medicine to treat heart disease, rheumatism, nervous disorders and bronchitis (Gohil et al., 2010; Lee et al., 2012).

Figure 1.8: Picture of the plant *Centella asiatica*

Found mostly in Asia, used as a culinary leaf and an herbal medicine. Source: (Thai beauty products)

Asiatic acid, a pentacyclic triterpenoid (Fig. 1.9), is the active constituent of the plant, showing many properties such as anti-angiogenesis, wound-healing, inhibition of collagen production at wound site, low risk of severe side-effects, anti-ulcer, anti-hepatofibric activity and inhibition of β-amyloid induced hepatotoxicity (Hsu et al., 2004; Kavitha et al., 2011; Krishnamurthy et al., 2009; Singh and Rastogi, 1969). There has been satisfactory evidence to suggest that asiatic acid can cross the blood brain barrier, and is cytotoxic to many cancer lines including the U87-MG glioblastoma cell line (Cho et al., 2006; Kavitha et al., 2011). It has also been reported that asiatic acid can be neuroprotective in a mouse model of focal ischemia and preserves BBB integrity in a post-ischemic episode (Krishnamurthy et al., 2009; Lee et al., 2014a, 2012).

Asiatic acid induces a time- and dose-dependent cell death of the U-87MG cell lines *via* both apoptosis and necrosis by activation of caspase-3 and caspase-9 (Cho, 2006). Asiatic acid also exhibits cell cycle arrest in the S-G2/M phase and apoptosis in

breast cancer cell lines MCF-7 and MDA-MB-237 (Hsu et al., 2004). Treatment with AA has been reported to induce apoptotic cell death in human hepatoma and malignant glioma cells by enhancing intracellular calcium release (Cho et al., 2006; Lee et al., 2002).

Park et al. (2005) reported that asiatic acid induced apoptosis in melanoma cells by increasing the levels of reactive oxygen species. Asiatic acid was also shown to reduce H_2O_2-related cell death, decrease intracellular free radical concentrations and regulate the metabolism of carbohydrates in diabetic rats by modulation of key regulatory enzymes (Lee et al., 2014b). Asiatic acid as well as *Centella asiatica* extract have also been shown to possess strong efficacy against rat colon cancer cells (Bunpo et al., 2005, 2004). A study by Wang et al. (2013) showed that the synthetic derivative of AA, A-3, markedly inhibited the growth of non-small cell lung cancer cell line A549 and PC9/G cells *via* downregulation of the Ras/Raf/MEK/ERK pathway and cell cycle arrest at G1/S and G2/M phases. Asiatic acid has also shown cell growth inhibition in breast cancer cell lines by inducing S-G2/M phase arrest and apoptosis (Hsu et al., 2004).

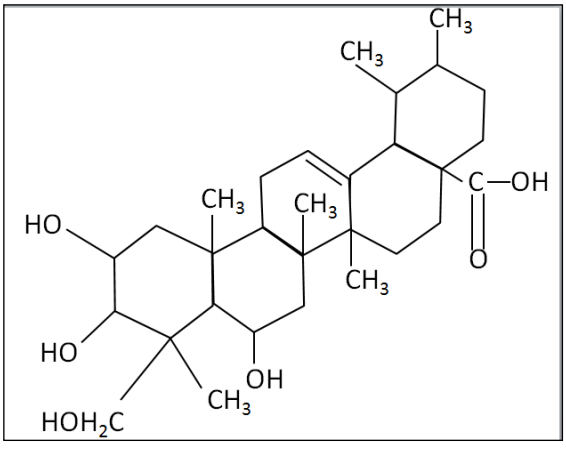

Figure 1.9: Chemical structure of asiatic acid

Asiatic acid is a pentacyclic triterpenoid, consisting of six isoprene units biosynthesised by cyclisation of squalene. Source: (Huang et al., 2011)

Asiatic acid inhibits VEGF and a significant improvement of oedema of lower limbs has been observed in previous studies (Kavitha et al., 2011). However, one major problem associated with administration of asiatic acid is its low solubility in aqueous and oil medium thus hindering dissolution causing decreased bioavailability of the drug (Zhao et al., 2010).

1.10.1 Conventional *Centella asiatica* Preparations

Centella asiatica is available in liquid or solid pharmaceutical forms for oral intake and *via* parenteral route for homeopathic use (Brendler et al., 2000).

Centellase® (Scharper, Italy), an extract prepared from *Centella asiatica* comprising madecassic acid (30%), asiatic acid (30%) and asiaticosides (40%), was available in the form of tablets (10 and 30mg), drops (10mg/ml), powder (2%) and ointment (1%). This preparation, however, is no longer found in German markets (Brinkhaus et al., 2000).

Another *Centella asiatica* extract comprising of asiaticoside (40%), asiatic acid (29-30%), madecassic acid (29-30%), and madasiatic acid (1%), called Madecassol® (La Roche, Belgium; Bilim, Greece) is currently only available in France. Madecassol was marketed in the form of an ointment or cream (1%), powder (2%) and 10mg tablets and used for accelerating cicatrisation and grafting of wounds (Brinkhaus et al., 2000; Gohil et al., 2010; Jamil et al., 2007).

Another preparation, Emdecassol® ointment, containing asiaticoside (0.4g) and a triterpenoid acid mixture (0.6g standardized to 0.29-0.3g asiatic acid, 0.29-0.3g madecassic acid and a maximum of 0.1g madiasiatic acid). However, this ointment is no longer available due to the inadequacies in the qualitative standardisation. The ointment,

when applied topically on the open wounds of rats, increased collagen synthesis and cellular proliferation at the wound site thus accelerating wound healing (Brinkhaus et al., 2000; Gohil et al., 2010; Jamil et al., 2007).

Elha-dermidyn® and Ekzevowen® ointment, complex homeopathic preparations, are indicated for the treatment of various dermatological conditions (Brinkhaus et al., 2000).

Centella asiatica extracts in a dose of 60mg once or twice a day are frequently used in modern herbal medicine (Brinkhaus et al., 2000).

1.11 Aims

The aim of this project was to study the effects of asiatic acid on glioblastoma cells *in vitro* and compare these against the widely used chemotherapeutic agent, cisplatin. Characterisation of asiatic acid induced cytotoxicity was performed using cell viability assays such as apoptosis, cell cycle analysis and cell proliferation analysis. This project also aimed at characterising a drug delivery system for asiatic acid to prepare monodispersed AA-loaded NPs less than 250nm in size having a surface charge of -10mV to -20mV in order to allow them to move across the BBB. Characterisation of these NPs included measurement of parameters such as size and surface charge, analysis of the drug loading and drug encapsulation efficiency and drug release from AA-loaded NPs using the High Pressure Liquid Chromatography (HPLC) system.

CHAPTER 2

MATERIALS and METHODS

2.1 Materials

All reagents used were of the highest grade commercially available and obtained from the following suppliers:

ATCC®

SVGp12 and U87-MG cell line

Biotium

Carboxyfluorescein diacetate succinimidyl ester (CFDA-SE)

Cell Signalling

EGF-receptor antibody, anti-rabbit IgG HRP-linked antibody

Lonza Group LTD., UK

Eagle's minimum essential medium (EMEM), sodium pyruvate, non-essential amino acids, L-glutamine, trypsin

Fisher Scientific Ltd., UK

Millex® MCE (mixed cellulose esters) sterile 33mm 0.45µm pore size syringe driven filter, Sterile PES (polyethersulfone) low protein binding 0.45µm pore size Whatman™ syringe driven filter, sterile plastic disposable syringe without needles 10mL and 20mL, acetone, methanol, acetonitrile, acetic acid, ultra-pure water, tris-HCl, glycine, ammonium pyrosulphate, sodium dodecyl sulphate, glycerol, bromophenol blue, dithiothreitol, triton X-100, HEPES buffer, sodium chloride, Amerhcam prime ECL Prime-chemilumiscent agent, 25cm cell scrapers, SimplyBlue™ SafeStain, ethylenediaminetetraacetic acid disodium salt dehydrate (EDTA), sodium fluoride, sodium deoxycholate, ponceau-S, potassium chloride, Mini-Protean Tetra Cell 10-well 4-gel system, restore western blot stripping buffer, BCA solution, acrylamide/Bis-acrylamide 30% solution (29:1), bovine serum albumin lyophilized powder ≥96%, 8-

well chambered cover glass NUNC, cell culture treated 96-well plates NUNC, cell culture treated black walled 96-well plates NUNC, cell culture treated 6-well plates NUNC, T25 and T75 cell culture flasks

GE Healthcare Life Sciences

ECL prime western blotting detection reagent

Invitrogen/Life Technologies™, UK

Foetal bovine serum, PrestoBlue®, Dead Cell Apoptosis Kit with Annexin V Alexa Fluor® 488 & Propidium Iodide, MagicMark™ XP western protein standard

Sigma Aldrich®, UK

Polycaprolactone (Mwt ~14,000), Pluronic F-68, lipase from *Pseudomonas sp.* (Type XIII, 27units/mg), polyethylene glycol (PEG), asiatic acid, cisplatin, coumarin-6, 2',7' – dichlorofluorescin diacetate (DCFDA), luperox, coumarin-6, SUPELCOSIL™ LC-18 HPLC Column

Scientific Laboratory Supplies Ltd., UK

Whatman™ Nylon membrane circles 0.45µm 90mm vacuum bench-top, protease inhibitor cocktail, phosphatase Inhibitor cocktail 2

VWR®, UK

Pluronic F-68

2.2 Cell Culture Work

2.2.1 Cell Maintenance

SVGp12 (human foetal astroglial cells) and U87-MG (human brain astroglial cell) cells were maintained in 75cm^2 flasks containing Eagles Minimum Essential Media (EMEM), supplemented with 10% foetal bovine serum (FBS), 2mM L-glutamine, 1% non-essential amino acids (NEAA) and 1mM sodium pyruvate at 37°C humidified atmosphere containing 5% CO_2. The cells were allowed to reach a maximum confluence of 80% after which the monolayer was passaged by 1x trypsinisation. Cells were pipetted gently to ensure a single cell suspension. Cells were either passaged at 1:3 into freshly prepared flasks to maintain the cell line or seeded into multi-well plates for experimental analysis.

Cells were seeded under normal conditions and allowed to adhere for a minimum of 2 hours before being transferred to 1% (1% oxygen: 5% carbon dioxide: 94% nitrogen) or 5% (5% oxygen: 5% carbon dioxide: 90% nitrogen) hypoxia using Baker Ruskinn's Invivo$_2$ 400 hypoxia workstation.

2.2.2 Growth Curves

In order to determine the rate of growth of the cell lines, growth curve measurements were performed over a period of 7 days, under normoxia and 1% hypoxia. Cells were seeded in triplicate, at a density of 20,000 cells per well in a 6-well plate. Each day, replicate wells for each cell line were trypsinised and the cell number determined using a haemocytometer and trypan blue exclusion.

2.2.3 PrestoBlue® Cell Linearity Assay

To determine a suitable working range for the cell number, a linearity assay using PrestoBlue® at different cell numbers was performed. Cells were seeded at a density of 0, 50, 100, 250, 500, 1000, 5000, 10,000 and 20,000 cells/well in a volume of

100µl/well media in 96-well plates. Cells were incubated for 24, 48 and 72 hours. Following incubation, a volume of 10µl of PrestoBlue® was added to each well and fluorescence measured after incubation for one hour.

2.2.4 Cell Viability using Cisplatin and Asiatic acid

In order to determine the EC_{50} values of cisplatin and asiatic acid, a concentration-dependent dose response curve was generated in both SVGp12 and U87-MG cell lines, under normoxia. Cells were seeded at a density of 1000 cells/well at a volume of 90µl in a 96-well plate and cultured for 24 hours before drug treatment at 10µl/well using the following drug concentrations: 0.1, 0.3, 1, 3, 10, 30, 100µM. Cell viability was measured at 24, 48 and 72 hours post treatment using PrestoBlue®. EMEM in the absence of cells was used as control. For experiments under hypoxia, cells were seeded and allowed to adhere to the plate before being transferred to hypoxia of either 1% or 5%.

2.2.5 Combination Studies

A drug combination study of cisplatin and asiatic acid was performed on the cell lines, U87-MG and SVGp12. Cells were seeded at a density of 1000 cells/well at a volume of 90µl/well in a 96-well plate. Following 24 hours of incubation, the cells were treated with cisplatin and asiatic acid at 100, 30, 10, 3, 1, 0.3, 0.1µM in triplicates in combination with 30µM asiatic acid and 2µM cisplatin, respectively. Cell viability was measured using the PrestoBlue® assay at 24, 48 and 72 hours respectively.

2.2.6 Cellular Reactive Oxygen Species Detection

A reactive oxygen species assay was performed on the SVGp12 and U87-MG cell line using a modified protocol from Abcam®. Cells were seeded at a density of 25,000cells/well in a blacked-walled 96-well plate and allowed to adhere overnight. The following day, media was discarded and cells were washed with 100µl 1X PBS. Cells

were incubated for 45 minutes in dark at 37°C following the addition of 20µM DCFDA in phenol free medium. The DCFDA solution was removed and cells were treated with 100µl/well of 2, 10 and 40µM cisplatin and 30, 50 and 70µM asiatic acid in triplicate. Non treated cells were used as control and a positive control using 50µM luperox was performed. Fluorescence was measured at an Ex/Em of 485-535nm.

2.2.7 Effect of Nanoparticle Treatment on Cell Viability

A nanoparticle dose response curve was generated to measure the effects of nanoparticles, blank and asiatic acid-loaded, on cell viability. Cells were seeded at 100cells/well in a volume of 100µl/well in 96-well plates. Blank and asiatic acid-loaded nanoparticles were prepared fresh (Section 2.6.1), under sterile conditions, prior to treatment. Following the preparation of the nanoparticles, 1ml of the nanoparticles was centrifuged at 12,600 x g to remove unbound drug. The resultant supernatant was discarded and the pellet re-suspended in 1X PBS. The nanoparticles were added to the wells at a volume of 2, 6, 10, 14, 18 and 22µl/well in triplicate. The total volume in all wells was standardised to 122µl using 1X PBS to maintain volume consistency. PrestoBlue® viability assay was performed following 24, 48, 72, 120 and 168 hours of incubation to measure cell viability. EMEM in the absence of cells, media in the presence of cells without any treatment and cells treated with 1X PBS were used as the blank, positive and vehicle control respectively.

2.3 Flow cytometric analysis

2.3.1 Apoptosis Assay using Annexin V/Alexa Fluor® 488 and Propidium Iodide

Flow cytometry with annexin V/Alexa Fluor® 488 and propidium iodide staining was used to determine early and late apoptotic cells following their treatment with blank and asiatic acid-loaded nanoparticles. SVGp12 and U87-MG cells were seeded at a

density of 100,000cells/well in 6-well plates and incubated for 24 hours prior to treatment with nanoparticles and the EC_{50} concentrations of cisplatin and asiatic acid. Cells were harvested by trypsinisation and centrifuged at 1000rpm for 5 minutes to obtain a cell pellet, following 24, 48, 72 and 120 hours of treatment. Cells were maintained at 4°C, to prevent any further apoptosis, following harvesting. Nanoparticle suspension in 1X PBS was prepared as described in Section 2.6.1 prior to addition to the cells. Treatments were 10µM cisplatin, 50µM asiatic acid and 6 & 22µl blank and asiatic acid-loaded nanoparticles. Non-treated cells and cells with 1X PBS were used as the positive control and vehicle control respectively. Cell pellets were resuspended in binding buffer consisting of 1:100 dilution of the stock concentration of annexin V (as per manufacturer's instructions) and propidium iodide at a final concentration of 5µg/ml, and incubated at room temperature for 15 minutes prior to analysis.

Flow cytometry was performed on the FACSAria (BD Bioscience, Franklin Lakes, New Jersey, USA). Relative differences in cell size were gated on the forward-angle light scatter (FSC) while the internal complexity of the cells was detected by the side-angle light scatter (SSC). Detection was performed at 488nm (blue laser) and at 407nm (violet laser) for the propidium idodide and annexin V/Alexa Fluor® 488 stains respectively. A total of 10,000 gated events were collected.

Apoptosis assay was also performed under 1% and 5% hypoxia. Cells were seeded as described above and were allowed to adhere overnight prior to transfer to hypoxia 2 hours before the addition of 10µM cisplatin and 50µM asiatic acid. Non treated cells were used as controls. Flow cytometry was performed using the Guava easyCyte™-12HT (Merck Millipore, Merck KGaA, Darmstadt, Germany) flow cytometer.

2.3.2 Cell Proliferation Assay using CFDA-SE

Cell proliferation using the carboxyfluorescein diacetate succinimidyl ester (CFDA-SE) dye was examined in both SVGp12 and U87-MG cell lines. Cells were seeded at a density of 100,000 cells/well in 6-well plates. 22 hours post seeding, the cells were treated with CFDA-SE at a final concentration of 5µM in 1xPBS and incubated for 30 minutes at 37°C in the dark. The CFDA-SE/PBS was discarded, 1.5ml of fresh media added and the plates returned to the incubator. Nanoparticle treatment, blank and asiatic acid-loaded, at 6 and 22µl and treatment with 10µM cisplatin and 30µM asiatic acid was performed 24 hours after cell seeding and the plates were incubated for 24, 48, 72 and 120 hours before harvesting the cells. Non-treated CFDA-SE stained and unstained cell controls were harvested by trypsinisation for analysis on the flow cytometer.

Cell proliferation assay was also performed under 1% and 5% hypoxia. Cells were seeded as described above and allowed to adhere overnight and transferred to hypoxia 2 hours before the addition of 10µM cisplatin and 50µM asiatic acid. Non treated cells were used as controls.

Flow cytometry was performed using the Guava easyCyte™-12HT flow cytometer. All samples were gated on the FSC versus SSC and a total of 10,000 gated events were recorded. The excitation and emission peaks for CFDA-SE are 492nm and 517nm respectively.

2.3.3 Cell Cycle Analysis

Cell cycle analysis of SVGp12 and U87-MG cell lines, under normoxia and hypoxia (1% and 5%), was performed on the Guava easyCyte™-12HT flow cytometer. Cells were seeded at a density of 100,000cells/well in 6-well plates. Cells were allowed to adhere overnight prior to treatment with 10µM cisplatin or 50µM asiatic acid.

Following incubation for 24, 48, 72 and 120 hours, cells were trypsinised, centrifuged at 1000 rpm and maintained at 4°C. The supernatant was discarded and the cell pellet re-suspended in 1X PBS containing of 250µg/ml RNase and 5µg/ml propidium iodide. Cells were stained for 30 minutes at room temperature and analysed using by flow cytometry. Detection was performed using the Guava EasyCyte™-12 HT flow cytometer at 488nm (blue laser) for propidium idodide. Dead cells and doublets were gated out and a total of 10,000 gated events were collected.

2.4 Microscopy

2.4.1 Scratch/Wound Healing Assay

An *in vitro* scratch assay on SVGp12 and U87-MG cell lines was performed. Cells were seeded at 45,000cells/well in a total volume of 0.5ml in a 24-well plate. Cells were allowed to adhere overnight and the cell monolayer was scraped in a single line using a sterile toothpick to create a scratch. Medium was replaced and cells were treated with 10µM cisplatin or 30µM asiatic acid. Cell imaging, for 18 hours, was performed on a modified Zeiss Cell Observer imaging system using a Zeiss Plan-Apo 20 x 0.8 NA air objective. Non treated cells were used as control.

2.4.2 Cellular Uptake of Nanoparticles using Microscopy

Coumarin-6 loaded blank nanoparticles were prepared as described in Section 2.6.1., immediately prior to addition to the cells. A 0.5mg/ml stock solution of coumarin-6 in acetone was prepared, following which 0.625, 1.25 and 6.25ml was added in the organic phase to give final concentrations of 0.05, 0.1 and 0.5%, respectively. 1ml of the nanoparticle suspension was centrifuged at 12,600 x g to remove unbound coumarin-6 and the resulting supernatant discarded. The pellet was re-suspended in 1ml sterile EMEM and stored at 4°C until required.

SVGp12 and U87-MG cells were plated onto 8-well chamber slides at a density of 20,000 cells per well in a volume of 200µl and allowed to adhere overnight. 22µl of coumarin-6-loaded nanoparticle suspension was added to each well and uptake into cells was recorded at 18 and 24 hours following addition. Images were captured on a modified Zeiss Cell Observer imaging system using a Zeiss Plan-Apo 20 x 0.8 NA air objective. Coumarin-6 was imaged using a GFP filter set with Ex/Em of 450-490nm and 500-550nm respectively. Analysis of the images was carried out using the Zeiss ZEN desk imaging software.

2.5 Biochemical Analysis

2.5.1 Western Blotting

Preparation of Cell Extracts

Western blot analysis for EGF-receptor was performed on SVGp12 and U87-MG cell lines. Cells were grown to 80% confluence in T25 flasks. Flasks were treated with 10µM cisplatin and 50µM asiatic acid for 24, 48 and 72 hours, under normoxia and 1% hypoxia. Cells were washed with 1X PBS, scraped, re-suspended in 250µl lysis buffer (RIPA buffer 7.8ml [7.62gm HEPES pH 7.5, 5.61 NaCl, 20% Triton X-100 32ml, 10% Sodium deoxycholate 32ml, 10% sodium dodecyl sulphate 6.4ml], 0.5M sodium fluoride 2ml, 0.5M EDTA 0.1ml, 0.1M sodium phosphate 1ml, phosphatase inhibitors 25µl, protease inhibitors 25µl, dH_2O 0.8ml) on a rotator for 1 hour at 4°C and centrifuged at 13,000 rpm for 15 minutes to get rid of any cell debris.

Protein assay was carried out using cell lysate. 10µl of cell lysate or BSA at the concentration of 1.8, 1.6, 1.4, 1.2, 1, 0.8, 0.6, 0.4, 0.2 mg/ml was added in each well of a 96-well plate, in triplicate. CuSO4:BCA (bicinchoninic acid) 1:50 solution was prepared fresh each time, 200µl added to the wells and incubated in the dark at room

temperature for 20 minutes. Absorbance was measured at an absorbance of 485nm. Protein concentration in each sample was calculated using the standard curve generated.

Immunoblotting

Proteins were separated on a 10% sodium dodecyl sulphate-polyacrylamide gel and transferred to polyvinylidene difluoride (PVDF) membranes. Semi-dry transfer using Bio-Rad Trans-Blot® SD transfer cell was performed at 15V for 20 minutes. Following transfer, membranes were blocked for 1 hour at room temperature with 5% skimmed milk in Tris-buffered saline-0.1% Tween 20 (TBS-tween). Membranes were then incubated with EGF-receptor antibody (1:1000 dilution) overnight at 4°C with gentle shaking. Membranes were washed three times with TBS-tween and twice with 1xPBS, incubated with anti-rabbit IgG, HRP-conjugated secondary antibody (1:2000 dilution) at room temperature for 1 hour and washed again in TBS-tween and 1X PBS. Immunoreactive proteins were detected by enhanced chemiluminescence using ECL reagent, Bio-Rad. Results were quantified by measuring the relative intensity compared to the non-treated controls using Bio-Rad Molecular Imager ChemiDoc™ XRS+ System with Image Lab™ Software, UK. Data was normalised to the amount of β-actin measured in the respective blots.

2.6 Nanoparticle Preparation

2.6.1 Protocol for Nanoparticle Preparation

Blank NPs were prepared by a modified solvent displacement method as described by Chawla & Amiji (2002). PCL (500mg) along with PEG (5g) was dissolved in acetone (25ml) in a sonicating bath maintained at 40°C. The aqueous phase consisted of Pluronic F-68 (150mg) dissolved in distilled water (50ml) using moderate magnetic

stirring. The organic phase was added to the aqueous phase over magnetic stirring leading to instant nanoparticle formation. Nanoparticles were centrifuged at 12,600 x g for one hour, the supernatant discarded and the pellet re-suspended in distilled water to a total volume of 20ml. Nanoparticles were filtered through 0.45µm Millex® syringe driven filter unit, 5ml of nanoparticle suspension was injected through each filter, and stored at either room temperature or 4°C. Asiatic acid-loaded nanoparticles were prepared using the same protocol 20mg of drug was dissolved in the organic phase along with PCL and PEG.

2.6.2 Other Techniques for Nanoparticle Preparation

Nanoparticles were also prepared by the solvent displacement method and were ultra-sonicated or homogenised to give an improved particle size. Ultra-sonification was carried out under ice cooling for 5 minutes at 70% amplitude in a pulse regime (1 minute sonication, 15 second pause) using a SONICS® Vibra Cell sonicator. Homogenisation under ice cooling was carried out for 20 minutes at speed 4, using the IKA® Ultra-Turrax T8 homogeniser. Weight of all the compounds remained constant; however, the amount of acetone used was 50ml. NPs were also prepared by the magnetic stirring process as mentioned in Section 2.6.1 and were stored at room temperature to obtain a direct comparison.

2.6.3 Nanoparticle Filtration Studies

Nanoparticles were prepared as described in Section 2.6.1. and filtered using sterile PES (polyethersulfone) low protein binding 0.45µm pore size Whatman™ syringe driven filter, Millex® MCE (mixed cellulose esters) sterile 33mm 0.45µm pore size syringe driven filter or Whatman™ Nylon membrane circles 0.45µm 90mm vacuum bench-top filters. A set of non-filtered samples was analysed for comparison.

2.7 Nanoparticle Characterisation

2.7.1 Size and Surface Charge Measurement

The size, surface charge and polydispersity index (PDI) of each set of nanoparticle formulations, blank and asiatic acid-loaded, was measured using the Malvern Zetasizer® Nano-ZS. The instrument was equipped with appropriate software for size and surface charge analysis. Prepared nanoparticles were measured over a period of 60 days to monitor stability. An aliquot of 1ml into a 12mm square polystyrene cuvette was used for size measurement and a disposable capillary cell containing a volume of 800µl of sample was used for performing surface charge measurements.

2.7.2 Effect of Storage Temperature on Blank-Nanoparticles

Blank nanoparticles (Section 2.6.1) were maintained at room temperature and at 4°C. Size and surface charge measurements were undertaken for a period of 60 days or until precipitation was observed. Precipitation was determined by the presence of large aggregates at the bottom of the vials the nanoparticles were stored in.

2.7.3 Maximisation of Nanoparticle Yield

To maximise nanoparticle yield, the ratio of aqueous phase to organic phase, volume of Pluronic F-68, temperature of the organic phase before addition to the aqueous phase, duration of magnetic stirring and use of filters were altered. Nanoparticle yield was measured using High Pressure Liquid Chromatography (HPLC).

2.7.4 Drug Loading Efficiency of Asiatic acid-loaded Nanoparticles

The percentage loading and the amount of drug loaded per milligram of the polymer was determined by injecting the nanoparticle suspension through the HPLC. Prior to performing drug loading studies, a calibration curve for the drug was prepared. The calibration curve of asiatic acid in methanol/water (1:1, v/v) was constructed from

the peak area ratio of asiatic acid versus 8 nominal asiatic acid concentrations (100, 50, 25, 17.5, 10, 7.5 and 5µg/ml). The reproducibility of linearity was confirmed by analysing three series of standard solutions of asiatic acid. A calibration curve for PCL was performed in a similar fashion. The calibration curve for PCL in acetonitrile was constructed from the peak area ratio of PCL versus 8 nominal PCL concentrations (200, 150, 120, 100, 80, 60 and 50µg/ml). The different concentrations used for the calibration of asiatic acid and PCL reflect the amount of asiatic acid and PCL used in the formulation.

Analytical separation of the compounds was undertaken on the instrumentation consisting of Jasco™ PU-1580 Intelligent HPLC Pump, a Jasco™ LG-1580-02 Ternary Gradient Unit and a Waters™ 486 Tunable Absorbance Detector. A SUPELCOSIL™ LC-18 (25cm x 4.6mm, 5µm) analytical column with a Phenomenex® C-18 (4 x 3mm, 5µm) guard column was used. Mobile phase consisted of methanol, acetonitrile and 0.1% acetic acid solution in the ratio of 5:65:30 (v/v/v). Flow rate was maintained at 1ml/min with the injection volume being 25µl. Column temperature was maintained at 25°C, run time was 15 minutes and detection was performed at a wavelength of 217nm. Chromatographic data were recorded and processed using Azur HPLC software version 5.0.10.0.

Asiatic acid-loaded nanoparticles were prepared as described in Section 2.6.1. nanoparticles were re-suspended in distilled water and a 500µl aliquot centrifuged at 12,600 x g for 5mins. The pellet and the supernatant were injected through the HPLC. The amount of drug recorded in the pellet provided the amount of drug that was entrapped within the nanoparticles whereas the amount recorded in the supernatant was the amount of free drug in the nanoparticle suspension. The drug loading efficiency in milligrams was calculated using the equation generated from the HPLC calibration

curve of asiatic acid. The percentage drug loading was calculated as the total amount of asiatic acid present in the formulation from the initial amount of asiatic acid added while preparing the NPs.

2.8 Drug Release Studies

2.8.1 Drug Release in PBS in the Absence and Presence of Lipase

Asiatic acid-loaded nanoparticles containing 20mg of asiatic acid were prepared as previously described (Section 2.6.1). Nanoparticles were re-suspended in 1X PBS, pH 7.4 in the absence and presence of lipase (45units/l). The suspension was maintained at a constant temperature of 37°C on a rocker kept inside an incubator. 500µl samples were collected every 1 hour for 3 hours and then at 24 hours following NP preparation. The samples were re-centrifuged at 12,600 x g for 5 min and the supernatant and pellet injected into the HPLC using the method described in Section 2.7.4. The amount of drug recorded in the supernatant represented the amount of drug released by the nanoparticles while the amount recorded in the pellet was the amount of drug encapsulated within the nanoparticles.

2.8.2 Drug Release in Cell Culture Medium

Nanoparticles were prepared as described in Section 2.6.1. and re-suspended in 20ml EMEM supplemented with 10% foetal bovine serum, 2mM L-glutamine, 1% non-essential amino acids and 1mM sodium pyruvate. NPs were maintained in a 37°C humidified atmosphere containing 5% CO_2. 500µl samples were collected every 1 hour for 3 hours and then at 24, 48 and 72 hours following nanoparticle preparation. The samples were re-centrifuged at 12,600 x g for 5 min and the supernatant was injected into the HPLC using the method described in Section 2.7.4. The amount of drug recorded in the supernatant represented the amount of drug released by the nanoparticles

while the amount recorded in the pellet was the amount of drug encapsulated within the nanoparticles.

2.8.3 Effect of pH on Drug Release from Asiatic acid-loaded Nanoparticles

Asiatic acid-loaded NPs containing 20mg asiatic acid (Section 2.6.1) were re-suspended in 1X PBS, pH 5.5. The suspension was maintained at 37°C on a rocker placed in an incubator. Sample aliquots of 500µl were collected at every 1 hour for 3 hours and then at 24 hours. Samples were centrifuged at 12,600 x g for 5mins. The pellet and the supernatant were injected through the HPLC as described in Section 2.7.4. The amount of drug recorded in the supernatant represented the amount of drug released by the nanoparticles while the amount recorded in the pellet was the amount of drug encapsulated within the nanoparticles.

2.9 Freeze-Drying of the Nanoparticles

Blank nanoparticles prepared using the protocol in Section 2.6.1 were freeze-dried in the absence and presence of 1% and 10% sucrose using a Christ® LCG freeze dryer. The equipment consisted of a small freeze-drying chamber containing a temperature-controlled stage and a vacuum pump to ensure evacuation. Prior to freeze-drying, 5ml samples, stored in a 50ml beaker, were frozen overnight at -18°C. Samples were then placed on the shelf of the freeze-dryer and main drying was performed at -20°C for 3.5 hours, 1mbar pressure. Final drying was performed at -76°C and a pressure of 0.0010mbar for 10 hours. Sample beakers, prior to freeze-drying, were sealed with parafilm and perforated using a 9 gauge needle to allow water sublimation during the freeze-drying process. Freeze-dried samples were stored in the refrigerator at 4°C until further analysis. Samples were re-hydrated using 5ml distilled water and size and

surface charge measurements were performed to record any changes in the nanoparticles after the freeze-drying process.

2.10 Visualisation of Surface Morphology using Scanning Electron Microscopy

For scanning electron microscopy (SEM) analysis of the freeze-dried nanoparticles, a random sample was mounted on an aluminium sample mount and sputter-coated with gold at 30mA for 4 min. SEM analysis was performed using an FEI Quanta 200 ESEM™, USA, scanning electron microscope at a working distance of 10mm and an accelerating voltage of 20kV.

2.11 Statistical Analysis

Statistical analysis of data was carried out using one-way and two-way ANOVA with Bonferroni's post-test as described in the GraphPad software Prism version 5.00 for Windows (GraphPad Software, San Diego California USA, www.graphpad.com). Significant differences were accepted for $p < 0.05$ and have been represented as $*p < 0.05$, $**p < 0.01$, $***p < 0.001$. . All results have been expressed as mean ± SEM.

CHAPTER 3

Effect of Asiatic acid on Cell Death

3.1 Introduction

Alterations in gene expression, including amplification or deletion, take place in glioma. The alteration of genes such as *EGFR*, *MTOR* and *VEGF* result in the activation or changes in cell growth and apoptosis (Kanu et al., 2009; Minniti et al., 2009; Normanno et al., 2006).

It is known that a wide range of oxygen tension can be tolerated by mammalian tissue, and this depends on the type, function and location of the tissue (Liu and Simon, 2004; Walmsley et al., 2005). The rate and pattern of growth of cells under different oxygen conditions causes complex changes in gene expression mediated by HIF and this also affects the mechanism of action of all drugs (Koch et al., 2003; Liu and Simon, 2004; Maxwell et al., 2001; Yao et al., 2005).

In addition, different cell types exhibit different growth durations and patterns. In this study, we chose the U87-MG cell line because it is a grade IV astrocytoma cell line. We chose SVGp12, an immortalised human foetal glial cell line, as our control. Both these cell lines are established cell lines used widely for research purposes.

The cytotoxic effects of drugs depend upon the pattern of growth of cells thus also affecting cell viability and apoptosis following drug treatments. In order to be able to correctly drug treat cells, it would be important to understand the lag, log and stationary phases of cell growth of individual cell lines. As cell growth, viability and apoptosis would be affected by hypoxia-associated genetic alterations, we also examined the effects of hypoxia on these factors.

Under any given condition, cell death either takes place *via* apoptosis or necrosis. Although apoptosis is a highly programmed mechanism; necrosis is an energy-independent process usually occurring due to stress such as hypoxia and

hypoglycaemia. The failure of many chemotherapeutic drugs is due to the inability of these drugs in inducing apoptosis (Elmore, 2007; Fulda et al., 2010; Kerr et al., 1972; Shah and Schwartz, 2001; Vanlangenakker et al., 2008). In addition to this, cell death is quite often mediated by the generation of reactive oxygen species (Cheung et al., 2012; Fulda et al., 2010; Li et al., 1997; Vanlangenakker et al., 2008). Thus, we measured the amounts of cellular reactive oxygen species generated following various drug treatments.

Objectives: We established the effects of hypoxia on cell growth, viability, generation of reactive oxygen species and mode of cell death using fluorescent dyes.

3.2 Results

3.2.1 Growth Curve

Growth curves were performed to study the growth pattern, rate of growth and identify the lag and the log phases of SVGp12 and U87-MG cells lines.

Normoxia

Both cell lines showed an increase in growth for duration of approximately 6 days following which, the cells reached a stationary phase in their growth (Fig. 3.1). The population doubling time of the two cell lines was identified to be 48 hours for SVGp12 (38,000 ± 1667) and 24 hours for the U87-MG (39,333 ± 1347) cell line. Significant differences were observed between the rate of growth of SVGp12 and U87-MG cell lines on day 5 (SVGp12 114,700 ± 2457, U87-MG 205,300 ± 1644; $p < 0.001$), day 6 (SVGp12 133,300 ± 962, U87-MG 312,700 ± 15261; $p < 0.001$) and day 7 (SVGp12 155,300 ± 839, U87-MG 367,000 ± 11259; $p < 0.001$).

1% hypoxia

Both cell lines showed an increase in growth for duration of approximately 6 days following which, the cells reached a stationary phase in their growth (Fig. 3.1). The population doubling time of the two cell lines was identified to be 60 hours for SVGp12 (40,813 ± 1299) and 36 hours for the U87-MG (39,750 ± 1721) cell line. Significant differences were observed between the rate of growth of SVGp12 and U87-MG cell lines on day 5 (SVGp12 105,400 ± 11261, U87-MG 201,000 ± 3108; $p < 0.001$), day 6 (SVGp12 129,900 ± 1431, U87-MG 309,600 ± 3877; $p < 0.001$) and day 7 (SVGp12 140,800 ± 2666, U87-MG 340,300 ± 5632; $p < 0.001$).

A significant difference in the doubling time of SVGp12 and U87-MG cell lines was observed under hypoxia ($p < 0.01$).

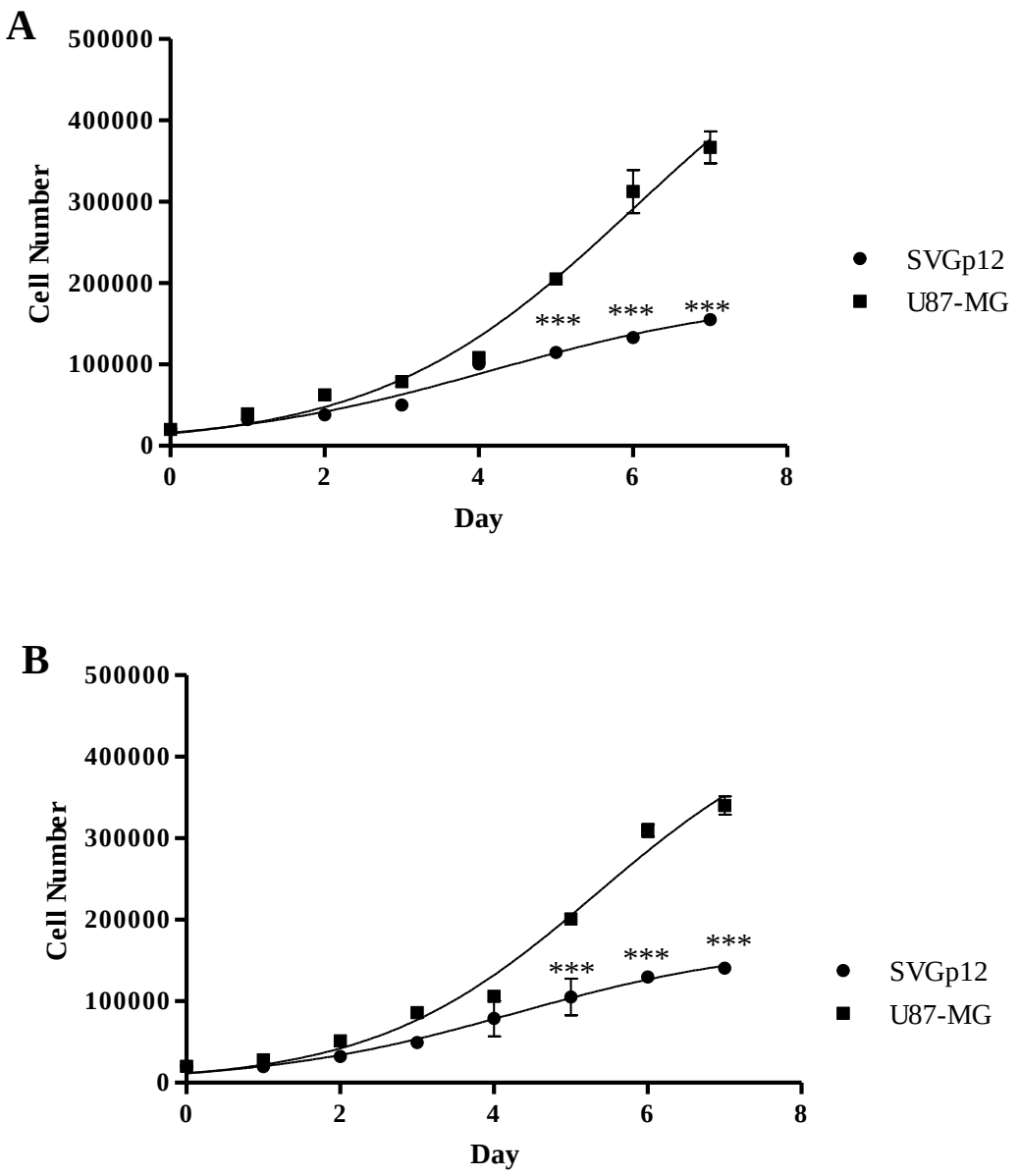

Figure 3.1: Growth curve for SVGp12 and U87-MG cell lines

Cell proliferation, for an initial seeding density of 20,000 cells/well, was determined by haemocytometer and trypan blue exclusion for a period of 7 days. Under normoxia (A), SVGp12 and U87-MG cell lines demonstrated a doubling time of 48 and 24 hours respectively. Under 1% hypoxia (B), SVGp12 and U87-MG cell lines demonstrated a doubling time of 60 and 36 hours respectively. Significant differences were observed between SVGp12 and U87-MG cells under normoxia and hypoxia on days 5, 6, and 7. Values represent mean ± S.E. for three experiments in triplicate.

3.2.2 PrestoBlue® Cell Linearity Assay

To carry out future viability studies, we decided to the dye PrestoBlue®. As this is a fluorescent dye, it was important to establish the saturation point of the dye using different cell densities.

The linearity between cell number and the associated fluorescence (Fig. 3.2) was studied using the PrestoBlue® cell viability reagent at increasing cell densities in a 96-well plate. Following an incubation of 24 hours, a linear relationship between the cell number and the fluorescence was observed in both the cell lines (R^2=0.97 for SVGp12 and R^2=0.98 for U87-MG). After 48 hours of incubation, fluorescence was linear up to 5000 cells/well (R^2=0.92 for both cell lines), following which there was saturation in the fluorescence measured. The saturation point, however, reduced to 2500 cells/well following 72 hours of incubation in both two cell lines. From the results obtained, subsequent experiments were undertaken using a cell density of 1000 cells/well in 96-well plate, for both, SVGp12 and U87-MG cell lines.

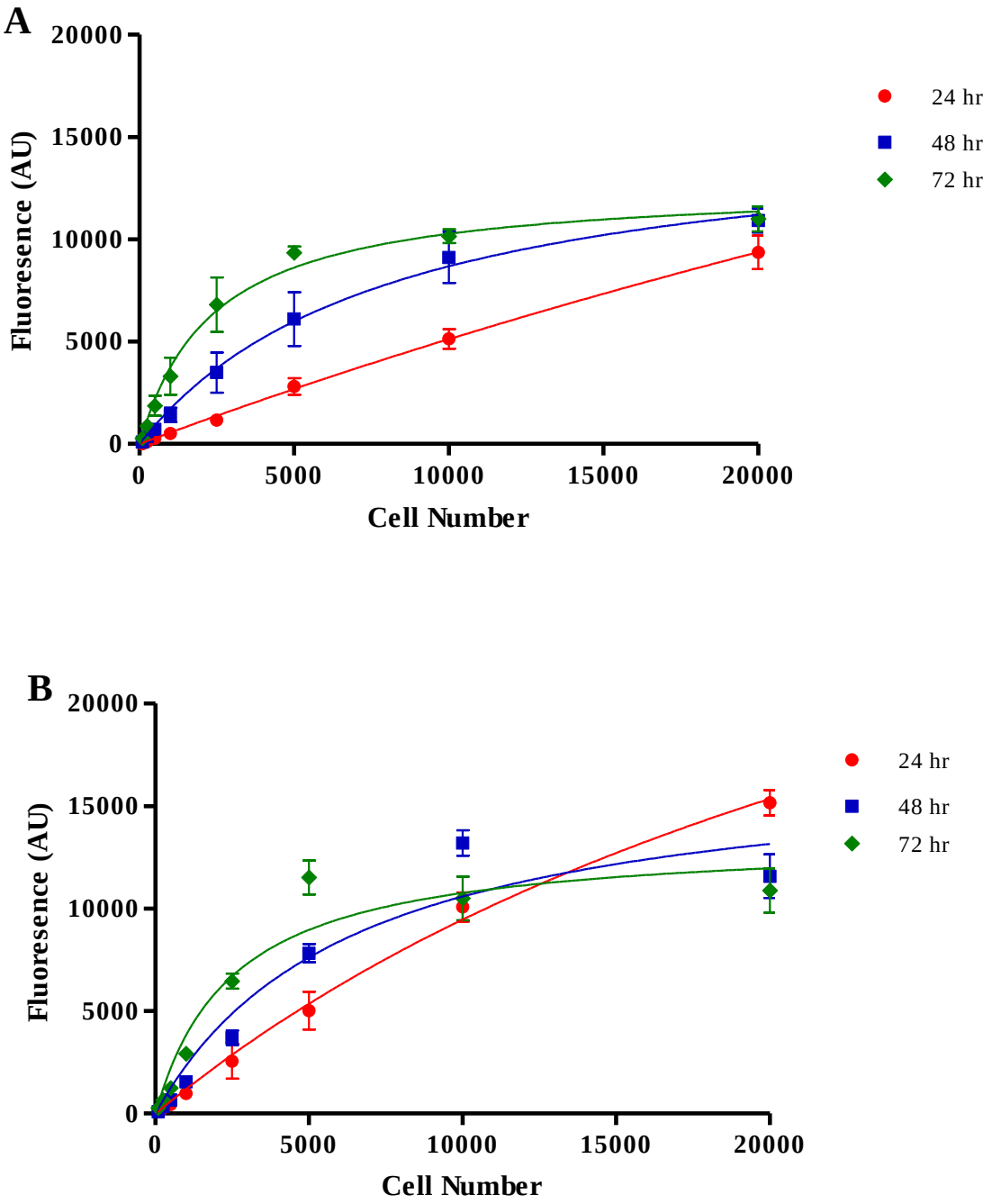

Figure 3.2: Effect of different cell concentrations on fluorescence using the PrestoBlue® reagent

A linearity assay, to establish the relationship between cell number and fluorescence in SVGp12 (A) and U87-MG (B) cell lines after 24, 48 and 72 hours of incubation, was performed using the PrestoBlue® reagent. Saturation in fluorescence was observed at 2500 cells/well for both cell lines at 72 hours. Values represent mean ± S.E. for three experiments in triplicate.

3.2.3 Effect of Cisplatin and Asiatic acid on Cell Viability

To assess the effect of cisplatin and asiatic acid on SVGp12 and U87-MG cell line viability, concentration-dependant dose response curves were performed. In addition, it was also important to establish the EC_{50} values of cisplatin and asiatic acid for further experiments and obtain a standard for direct comparison.

Normoxia

Cisplatin showed a reduction in cell viability in a time and dose dependent manner. EC_{50} values obtained for cisplatin on SVGp12 cell line were 33, 11 and 5µM at 24, 48 and 72 hours, respectively. EC_{50} values obtained for asiatic acid on SVGp12 cell line were 29, 61 and 57µM at 24, 48 and 72 hours, respectively (Fig. 3.3, Table 3.1).

EC_{50} values for U87-MG cell line following cisplatin treatment were 94, 7.3 and 4.6µM at 24, 48 and 72 hours, respectively. EC_{50} values for asiatic acid treatment on U87-MG cell line were 36, 47 and 42µM at 24, 48 and 72 hours, respectively (Fig. 3.4, Table 3.1).

Based on these results, an average EC_{50} value over the period of 72 hours, for both cell lines, was calculated and used for all further experiments. The EC_{50} value for cisplatin was calculated as 10µM and for asiatic acid was 50µM.

5% hypoxia

Under 5% hypoxia, cisplatin showed gradual decrease in the cell viability of SVGp12 cell line. EC_{50} values obtained for cisplatin on SVGp12 cell line were 159, 115 and 61µM at 24, 48 and 72 hours, respectively. It wasn't possible to fit a line of best curve through the asiatic acid treatments on the graph (Fig. 3.5, Table 3.1).

A reduction in cell viability of U87-MG cell line was observed with cisplatin (Fig. 3.6, Table 3.1). EC_{50} values for U87-MG cell line following cisplatin treatment were 11450, 210 and 131µM at 24, 48 and 72 hours, respectively. It wasn't possible to

fit a line of best curve through the asiatic acid treatments at 24 and 72 hours on the graph. EC_{50} value for asiatic acid at 48 hours, however, was calculated to be 82µM.

1% hypoxia

Under 1% hypoxia, a gradual decrease in the cell viability of SVGp12 cell line was shown by cisplatin (Fig. 3.7, Table 3.1). EC_{50} values obtained for cisplatin were 34, 22 and 11 µM at 24, 48 and 72 hours, respectively. It wasn't possible to fit a line of best curve with asiatic acid treatment at 24 hours, however, EC_{50} values at 48 and 72 hours were 109 and 105µM, respectively.

EC_{50} values obtained for cisplatin in U87-MG cell line were 123 and 232µM at 24 and 48 hours, respectively. It wasn't possible to fit a line of best curve at 72 hours for cisplatin (Fig. 3.8, Table 3.1). EC_{50} values obtained for asiatic acid were 84 and 81µM at 48 and 72 hours, respectively. It wasn't possible to fit a line of best curve at 72 hours for asiatic acid.

Table 3.1: EC_{50} values for cisplatin and asiatic acid under normoxia and hypoxia (1% and 5%)

Normoxia	Cisplatin (µM)			Asiatic acid (µM)		
	24 hours	48 hours	72 hours	24 hours	48 hours	72 hours
SVGp12	32	11	5	29	61	57
U87-MG	94	7	5	36	47	42

5% hypoxia	Cisplatin (µM)			Asiatic acid (µM)		
	24 hours	48 hours	72 hours	24 hours	48 hours	72 hours
SVGp12	159	115	61	NA	NA	NA
U87-MG	11450	210	131	NA	82	NA

1% hypoxia	Cisplatin (µM)			Asiatic acid (µM)		
	24 hours	48 hours	72 hours	24 hours	48 hours	72 hours
SVGp12	34	22	11	NA	109	105
U87-MG	123	232	NA	NA	84	83

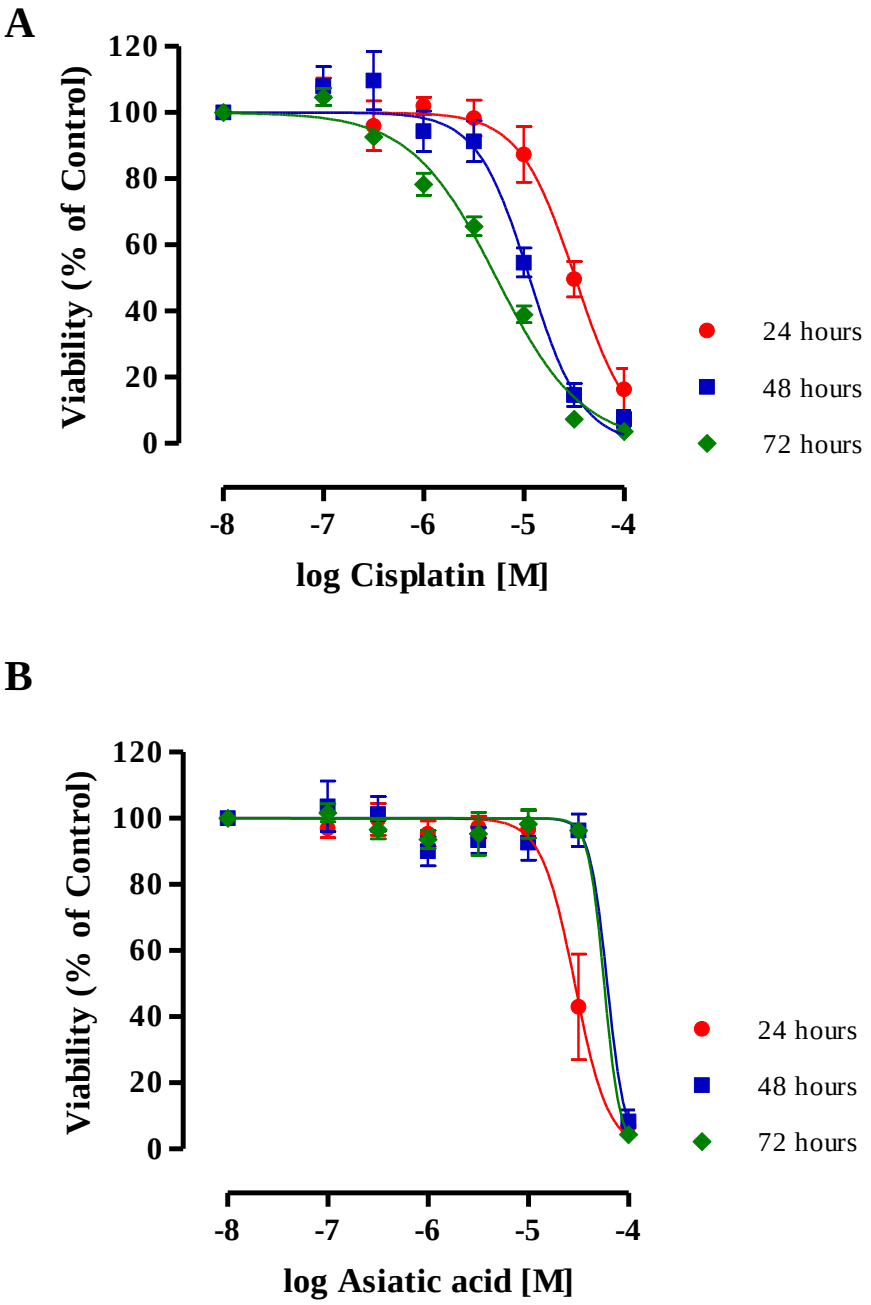

Figure 3.3: Data illustrating the effect of concentration dependent treatment of cisplatin and asiatic acid on SVGp12 cell line, under normoxia

Cell viability was performed using the PrestoBlue® reagent on SVGp12 cell line following 24, 48 and 72 hours of incubation with cisplatin (A) and asiatic acid (B). A time and concentration dependent reduction in cell viability was observed with cisplatin, asiatic acid mainly showed its effects at 100 and 30µM. Values represent mean ± S.E. for three experiments in triplicate.

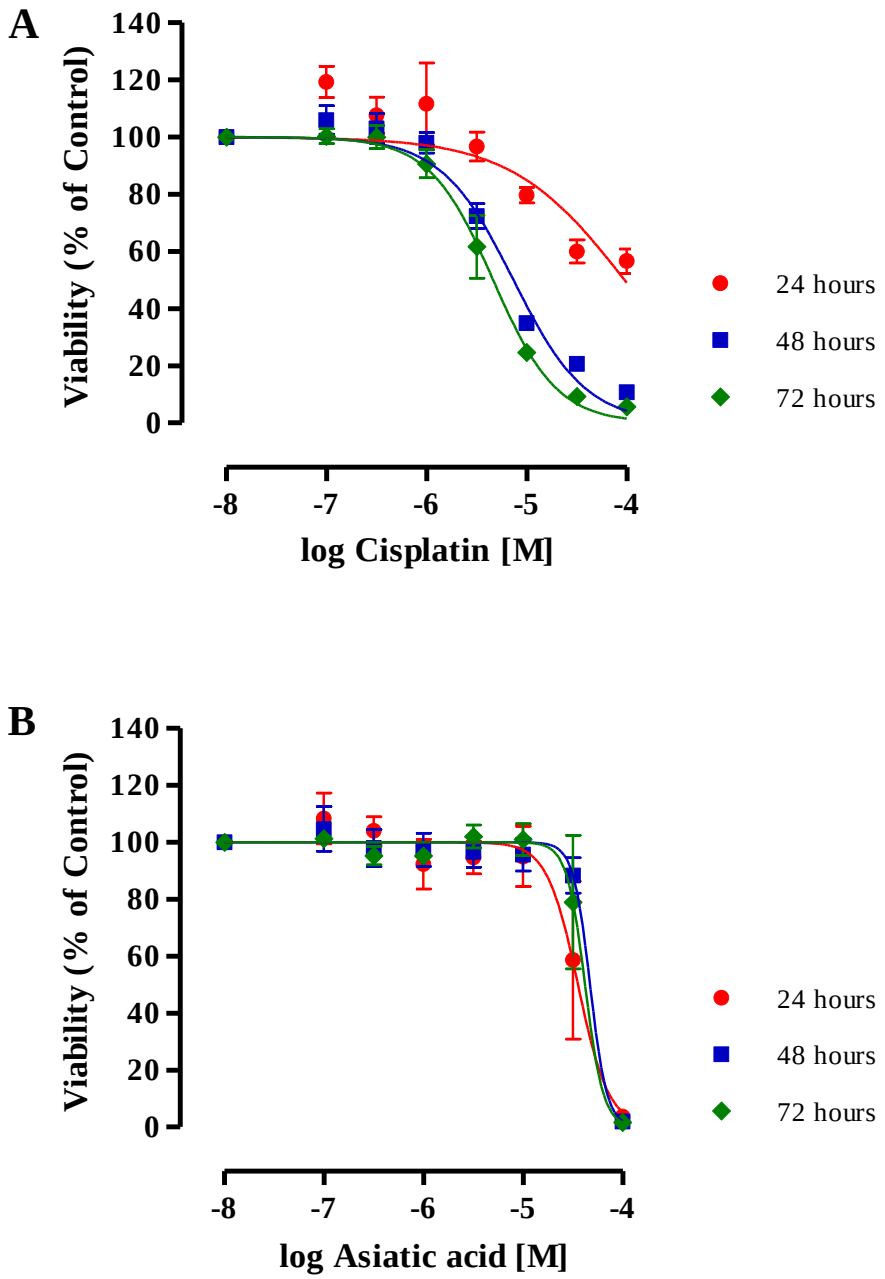

Figure 3.4: Data illustrating the effect of concentration dependent treatment of cisplatin and asiatic acid on U87-MG cell line, under normoxia

Cell viability was measured using the PrestoBlue® reagent on U87-MG cell line following 24, 48 and 72 hours of incubation with cisplatin (A) and asiatic acid (B). A time and concentration dependent reduction in cell viability was observed with cisplatin, asiatic acid mainly showed its effects at 100 and 30µM. Values represent mean ± S.E. for three experiments in triplicate.

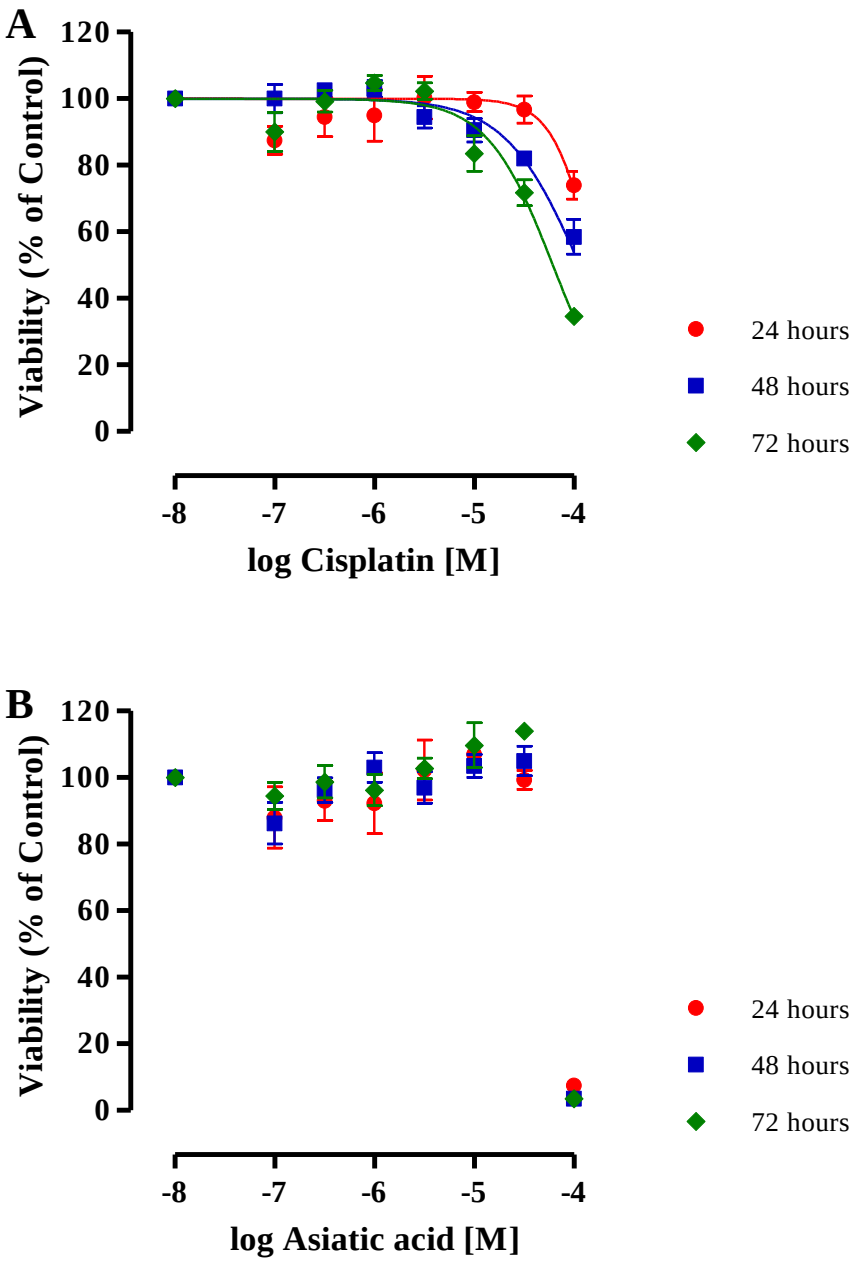

Figure 3.5: Data illustrating the effect of concentration dependent treatment of cisplatin and asiatic acid on SVGp12 cell line, under 5% hypoxia

Cell viability was performed using the PrestoBlue® reagent on SVGp12 cell line following 24, 48 and 72 hours of incubation with cisplatin (A) and asiatic acid (B).. Values represent mean ± S.E. for three experiments in triplicate.

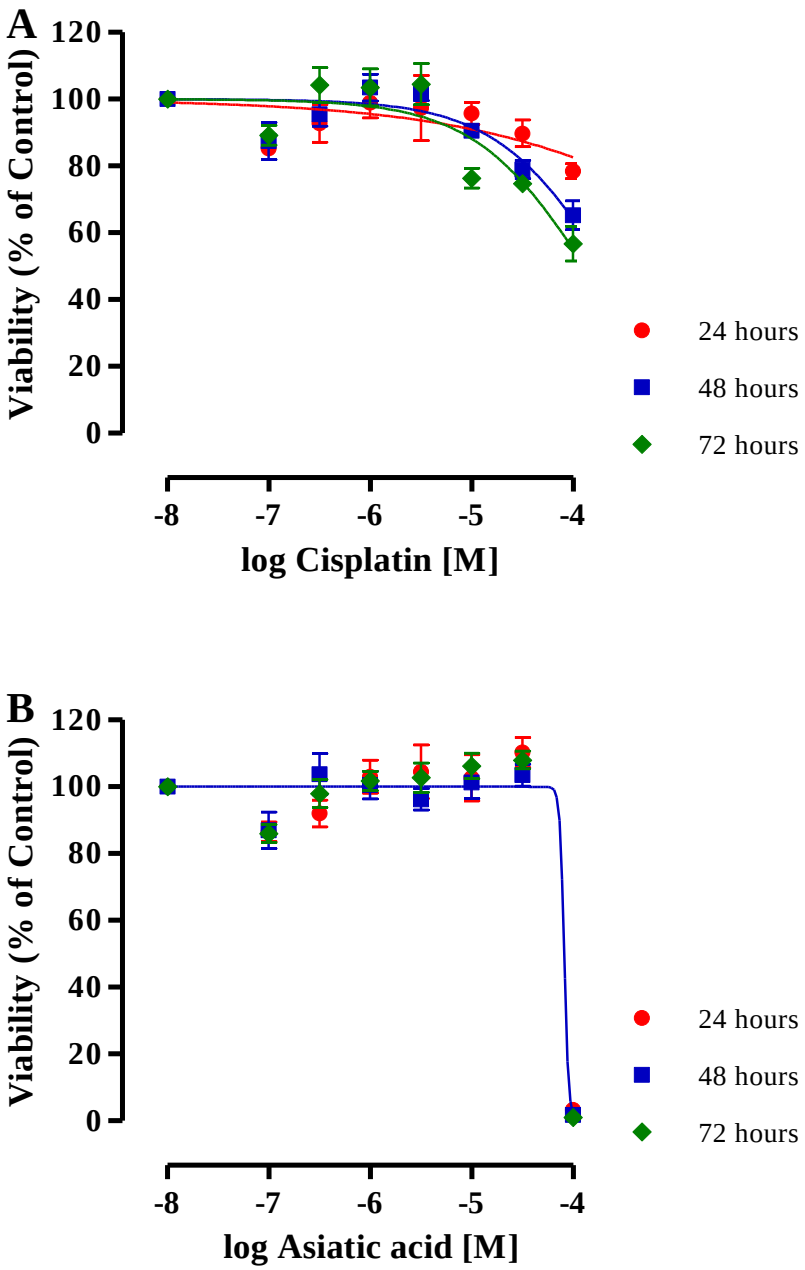

Figure 3.6: Data illustrating the effect of concentration dependent treatment of cisplatin and asiatic acid on U87-MG cell line, under 5% hypoxia

Cell viability was performed using the PrestoBlue® reagent on U87-MG cell line following 24, 48 and 72 hours of incubation with cisplatin (A) and asiatic acid (B). Values represent mean ± S.E. for three experiments in triplicate.

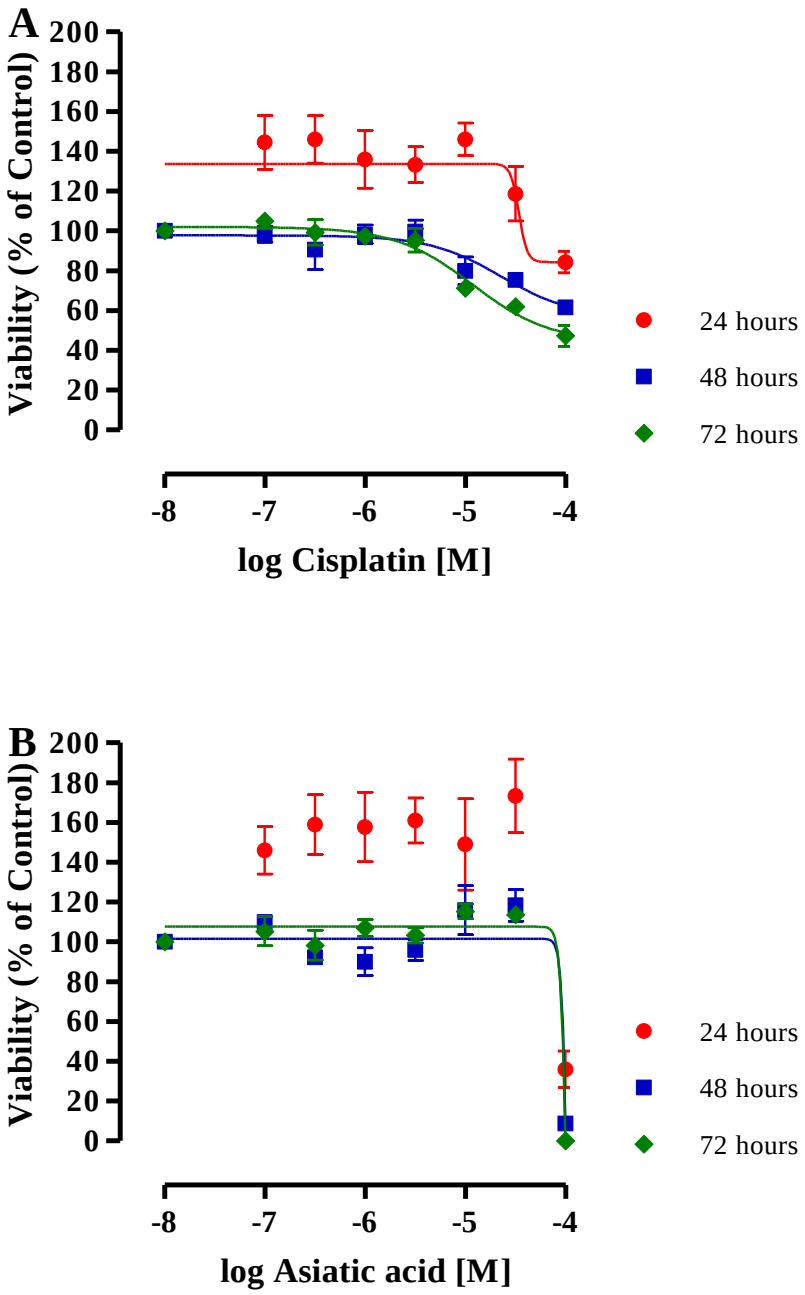

Figure 3.7: Data illustrating the effect of concentration dependent treatment of cisplatin and asiatic acid on SVGp12 cell line, under 1% hypoxia

Cell viability was performed using the PrestoBlue® reagent on SVGp12 cell line following 24, 48 and 72 hours of incubation with cisplatin (A) and asiatic acid (B). Values represent mean ± S.E. for three experiments in triplicate.

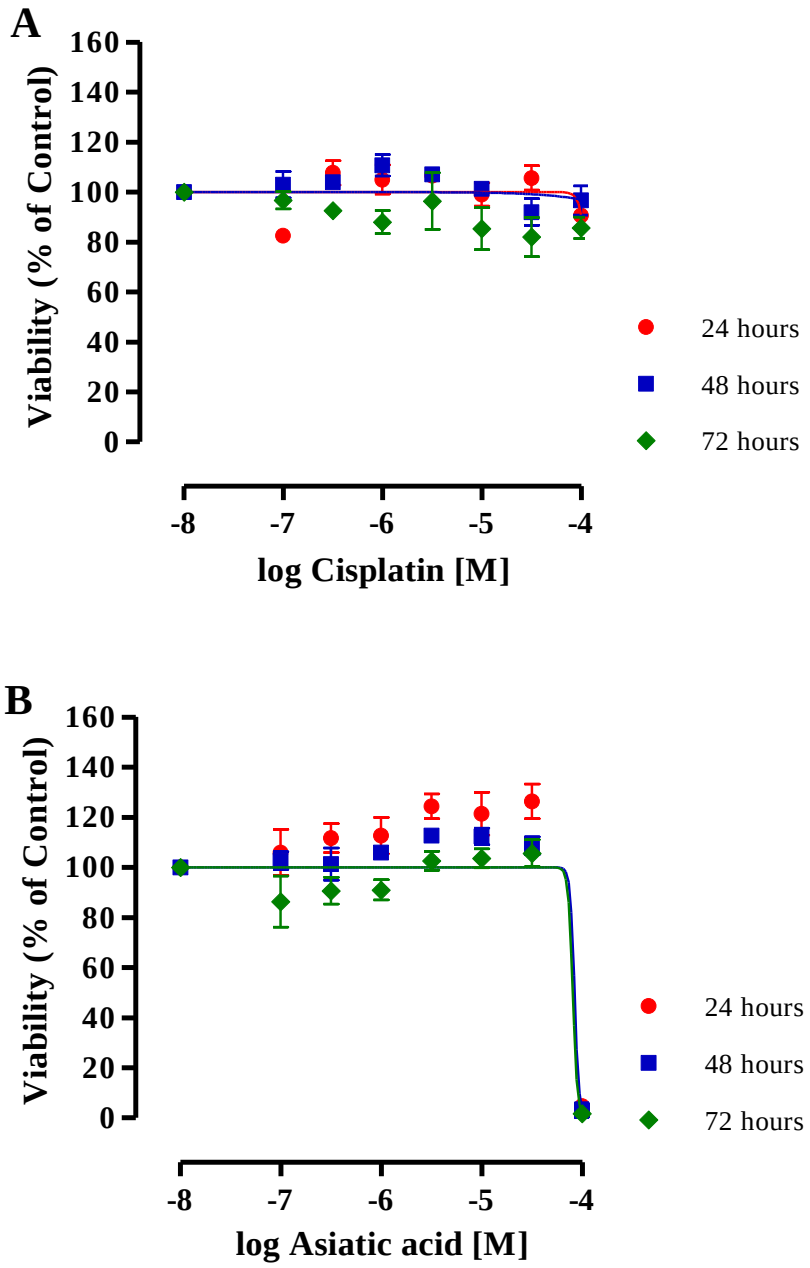

Figure 3.8: Data illustrating the effect of concentration dependent treatment of cisplatin and asiatic acid on U87-MG cell line, under 1% hypoxia

Cell viability was performed using the PrestoBlue® reagent on U87-MG cell line following 24, 48 and 72 hours of incubation with cisplatin (A) and asiatic acid (B). Values represent mean ± S.E. for three experiments in triplicate.

3.2.4 Apoptosis Assay using Annexin V/Alexa Fluor 488® and Propidium Iodide

Cell death under any condition, is mediated either by apoptosis or necrosis. To assess the relative percentage of cells that were undergoing apoptosis and necrosis following respective treatments with cisplatin and asiatic acid, an apoptosis assay was performed on the flow cytometer using fluorescent dyes Annexin V/Alexa Fluor 488® and propidium iodide staining.

Normoxia

Cisplatin and asiatic acid showed an increase in the number of apoptotic and necrotic cells over time. In the SVGp12 cell line, significant decrease was observed with cisplatin treatment at 48 hours in the early apoptotic population (control 17 ± 2.9%, cisplatin 5.8 ± 0.6%; $p < 0.05$), (Figs. 3.9 & 3.10). Following 120 hours of cisplatin treatment, significant decrease was observed in live (control 73.5 ± 0.4%, cisplatin 53.7 ± 3.3%; $p < 0.05$), significant increase in the early apoptotic (control 0.2 ± 0.05, cisplatin 19.6 ± 1.7%, $p < 0.001$), significant increase in the late apoptotic (control 0.6 ± 0.2%, cisplatin 13.8 ± 2.5%; $p < 0.001$) and significant decrease in the necrotic (control 25.7 ± 0.5%, cisplatin 12.9 ± 1.4%; $p < 0.05$) populations. Significant decrease following 24 hours of asiatic acid treatment was observed in the live (control 57.6 ± 2.4%, asiatic acid 9.7 ± 2.7%; $p < 0.001$), significant decrease in the early apoptotic (control 25.0 ± 2.1%, asiatic acid 8.3 ± 2.4%; $p < 0.001$) and significant increase in the late apoptotic (control 11.9 ± 0.4%, asiatic acid 65.7 ± 5.0%, $p < 0.001$). Significant decrease following 120 hours of asiatic acid treatment was observed in live (control 73.5 ± 0.4%, asiatic acid 49.5 ± 6.1%; $p < 0.001$), significant increase in the early apoptotic (control 0.2 ± 0.05%, asiatic acid 44.6 ± 7.2%; $p < 0.001$) and significant decrease in the necrotic (control 25.7 ± 0.5%, asiatic acid 2.7 ± 0.8%; $p < 0.001$).

In the U87-MG cell line, cisplatin treatment showed a significant decrease in the live cell population following 48 (control 95.9 ± 1.5%, cisplatin 81 ± 2.1%; $p < 0.001$) and 120 (control 95.4 ± 0.1%, cisplatin 82.7 ± 1.3%; $p < 0.001$) hours of treatment (Figs. 3.9 & 3.11). Asiatic acid showed a significant decrease following 24 hours of treatment on the live (control 92.1 ± 1.4%, asiatic acid 5.8 ± 2.1%; $p < 0.001$), significant increase in the late apoptotic (control 1.7 ± 0.5%, asiatic acid 66.0 ± 7.6%; $p < 0.001$) and significant increase in the necrotic (control 0.8 ± 0.1%, asiatic acid 13.6 ± 0.1%; $p < 0.05$) populations. Significant decrease following 120 hours of asiatic acid treatment was observed in live (control 95.4 ± 0.1%, asiatic acid 48.6 ± 3.8%; $p < 0.001$) and significant increase in the early apoptotic (control 0.3 ± 0.1%, asiatic acid 47.9 ± 5.0%; $p < 0.001$) populations.

Significant differences were also observed between SVGp12 and U87-MG cell lines. Cisplatin showed a significant difference in the live cell population following 24 (SVGp12 64.9 ± 0.9%, U87-MG 86.7 ± 0.5%; $p < 0.001$) and 48 (SVGp12 60.8 ± 2.1%, U87-MG 81.0 ± 2.12%; $p < 0.001$) hours of treatment. A significant difference was also observed in the early apoptotic population of both cell lines following 24 (SVGp12 23.8 ± 1.1%, U87-MG 8.0 ± 0.4%; $p < 0.01$) and 120 (SVGp12 19.6 ± 1.8%, U87-MG 3.8 ± 0.3%; $p < 0.001$) hours of treatment. Asiatic acid did not show any significant differences between the two cell lines.

5% hypoxia

Cisplatin did not show any significant differences in the cell populations of SVGp12 cells over the period of 72 hours (Figs. 3.12 & 3.13). Asiatic acid showed a significant reduction in the live cell population only at 24 hours (control 63.3 ±0.9%, asiatic acid 55.5 ± 0.7%; $p < 0.01$). It can be noted from the graphs that a very small fraction of cells underwent necrotic cell death (data for 72 hours, control 6.5 ± 2.1%,

cisplatin 8.1 ± 2.4%, asiatic acid 5.1 ± 1.0%) and the majority of the dead SVGp12 cells were in the early (data for 72 hours, control 27 ± 5.2%, cisplatin 26.8 ± 4.6%, asiatic acid 21.7 ± 4.1%) or late phases of apoptosis (data for 72 hours, control 22.3 ±0.7%, cisplatin 24.1 ± 0.7%, asiatic acid 26.6 ± 0.2%).

Cisplatin, again, did not show any significant differences in the cell population of U87-MG cells over the period of 72 hours. A small change was seen with the asiatic acid treatment (Figs. 3.12 % 3.13). A significant decrease was observed with 48 hours of asiatic acid treatment on the live (control 69.5 ± 4.8%, asiatic acid 53.2 ± 7.8; $p < 0.001$) and significant increase in the early apoptotic (control 11.9 ± 3.8%, asiatic acid 24.9 ± 4.9%; $p < 0.001$) populations. A significant increase was also observed in the early apoptotic population of cells following 72 hours of asiatic acid treatment (control 11.3 ± 2.1%, asiatic acid 26.5 ± 4.4%; $p < 0.01$). An overall reduction in the percentage of live cells was observed in the U87-MG cell line. It can be noted that a very small fraction of cells underwent necrotic cell death (data for 72 hours, control 3.5 ± 0.5%, cisplatin 3.1 ± 0.7%, asiatic acid 2.5 ± 0.4%) and the majority of the dead U87-MG cells were in the early (data for 72 hours, control 11.3 ± 2.1%, cisplatin 14.6 ± 2.2, asiatic acid 26.5 ± 4.4%) or late (data for 72 hours, control 26.6 ± 6.7%, cisplatin 25.8 ± 6.1%, asiatic acid 19.2 ± 2.3%) phases of apoptosis.

Between SVGp12 and U87-MG cell lines, significant differences were observed for cisplatin treatment in the live cell population at 24 hours only, (SVGp12 61.3 ± 1.4%, U87-MG 75.9 ± 1.8%; $p < 0.05$). Asiatic acid treatment did not show any significant differences in the two cell lines.

1% hypoxia

Although an increase in the apoptotic population of cells was observed upon cisplatin treatment on the SVGp12 cell line, no significant differences compared to the

control were observed until 72 hours of treatment with cisplatin (Figs. 3.14 & 3.15). Following 72 hours of treatment with cisplatin, significant decrease was observed in the live (control 30.9 ± 1.7%, cisplatin 21.9 ± 1.9%; $p < 0.01$) and late apoptotic (control 37.6 ± 1.5%, cisplatin 21.9 ± 1.9%; $p < 0.05$) populations. Asiatic acid treatment showed a significant increase in the late apoptotic population of cells following 24 (control 35.9 ± 2.3%, asiatic acid 51.6 ± 0%; $p < 0.05$) and 48 (control 40.0 ± 2.6, asiatic acid 46.8 ± 4.9%, $p < 0.05$) hours of treatment. It can be noted, from the figures, that a very small fraction of cells underwent necrotic cell death (data for 72 hours, control 8.4 ± 1.6%, cisplatin 6.1 ± 0.9%, asiatic acid 7.0 ± 1.0%) and the majority of the dead SVGp12 cells were in the early (data for 72 hours, control 23.1 ± 2.6%, cisplatin 26.7 ± 1.6%, asiatic acid 25.1 ± 1.8) or late (data for 72 hours, control 37.6 ± 1.5%, cisplatin 45.3 ± 2.5%, asiatic acid 42.8 ± 2.1%) phases of apoptosis.

Again, cisplatin showed significant differences compared to the control following 72 hours of treatment on the U87-MG cell line (Figs. 3.14 & 3.15). This difference was seen in the late apoptotic population of cells (control 37.1 ± 2.2%, cisplatin 25.2 ± 0.7%; $p < 0.05$). Significant decrease was observed with asiatic acid treatment on the U87-MG cell line following 24 hours of treatment in the live (control 50.8 ± 2.9%, asiatic acid 25.9 ± 3.3; $p < 0.001$) and significant increase in the late apoptotic (control 27.1 ± 1.1%, asiatic acid 46.7 ± 1.3%; $p < 0.001$) populations. Following 48 hours of asiatic acid treatment, a significant decrease was observed in the live cell population of U87-MG cell line (control 43.1 ± 4.6%, asiatic acid 18.9 ± 0.9; $p < 0.0.5$). Significant decrease was also observed following 72 hours of asiatic acid treatment in the live (control 45.6 ±3.8%, asiatic acid 27.1 ± 0.2%; $p < 0.001$) and significant increase in the early apoptotic (control 11.2 ± 1.3%, asiatic acid 26.6 ± 1.6%; $p < 0.01$) populations.

Significant differences were observed, at 24 hours, between the two cell lines in the live cell population of non-treated controls (SVGp12 30.4 ± 1.8%, U87-MG 50.8 ± 2.9%; $p < 0.001$). Cisplatin showed a significant difference in the live cell population of the two cell lines at 24 (SVGp12 32.3 ± 1.8%, U87-MG 52.9 ± 2.1%; $p < 0.001$), 48 (SVGp12 24.6 ± 2.6%, U87-MG 49.4 ± 3.7%; $p < 0.001$) and 72 hours (SVGp12 21.9 ± 1.9, U87-MG 52.4 ± 3.2; $p < 0.001$).

In the SVGp12 cell line under 5% hypoxia, showed a significant increase in the live (normoxia 8.1 ± 2.7%, 5% hypoxia 55.5 ± 0.7%; $p < 0.001$) and early (normoxia 8.3 ± 2.5%, 5% hypoxia 24.3 ± 3.2%; $p < 0.01$) and a significant decrease in the late apoptotic (normoxia 65.7 ± 5.0%, 5% hypoxia 16.4 ± 1.9%; $p < 0.001$) populations of cells, following 24 hours of asiatic acid treatment. Following 48 hours of asiatic acid treatment under 5% hypoxia, significant increase was observed in the live cell population of SVGp12 cells (normoxia 21.6 ± 1.1%, 5% hypoxia 59.2 ± 7.7%; $p < 0.001$). Non-treated SVGp12 cells showed significant decrease under 5% hypoxia in the live (76.0 ± 2.2%, 5% hypoxia 44.2 ± 3.9; $p < 0.001$) and a significant increase in the early apoptotic (normoxia 2.1 ± 0.6%, 5% hypoxia 27.0 ± 5.2%; $p < 0.01$) population of cells, following 72 hours of incubation. Cisplatin did not show any significant differences on SVGp12 cell line between the two conditions. Non-treated U87-MG cell line under 5% hypoxia showed a significant decrease in the live cell population at 24 (normoxia 92.1 ± 1.4%, 5% hypoxia 76.0 ± 1.6%; $p < 0.001$), 48 (normoxia 95.9 ± 1.9%, 5% hypoxia 69.5 ± 4.8%; $p < 0.001$) and 72 (normoxia 96.9 ± 0.9%, 5% hypoxia 58.6 ± 8.5; $p < 0.01$) hours. Asiatic acid treatment, under 5% hypoxia, showed a significant increase in the live cell population in U87-MG cells following 48 (normoxia 13.2 ± 4.3%, 5% hypoxia 53.2 ± 7.8%; $p < 0.001$) and 72 (normoxia 26.1 ± 4.1%, 5% hypoxia 51.8 ± 6.1%; $p < 0.001$) hours of treatment. Under 5% hypoxia, asiatic acid treatment showed a significant decrease in the early apoptotic population of cells

following 48 (normoxia 54.3 ± 6.3%, 5% hypoxia 24.9 ± 4.9%; $p < 0.001$) and 72 (normoxia 68.6 ± 4.4%, 5% hypoxia 26.5 ± 4.4%; $p < 0.001$). Cisplatin did not show any significant differences.

In the SVGp12 cell line under 1% hypoxia, a significant decrease was observed in the live cell population non-treated cells following 24 (normoxia 57.6 ± 2.4%, 1% hypoxia 30.4 ± 1.8%; $p < 0.01$), 48 (normoxia 61.6 ± 5.1%, 1% hypoxia 26.8 ± 2.1%; $p < 0.001$) and 72 (normoxia 76.0 ± 2.2%, 1% hypoxia 30.9 ± 1.7%; $p < 0.001$) hours of incubation. A significant increase was also observed in the late apoptotic population of non-treated cells at 24 (normoxia 11.9 ± 0.4%, 1% hypoxia 35.9 ± 2.3%; $p < 0.001$), 48 (normoxia 12.3 ± 2.1%, 1% hypoxia 40.0 ± 6%; $p < 0.001$) and 72 (normoxia 4.8 ± 0.9%, 1% hypoxia 37.6 ± 1.5%; $p < 0.001$) hours. Cisplatin treated cells showed a significant decrease in the live cell population following 24 (normoxia 64.9 ± 0.9%, 1% hypoxia 32.3 ± 1.8%; $p < 0.01$), 48 (normoxia 60.8 ± 2.1%, 1% hypoxia 24.6 ± 2.6%; $p < 0.01$) and 72 (normoxia 42.9 ± 1.4%, 1% hypoxia 21.9 ± 1.9%; $p < 0.05$) hours of treatment. Asiatic acid showed a significant increase in the live population of cells following 24 (normoxia 9.7 ± 2.7%, 1% hypoxia 22.1 ± 2.7%; $p < 0.001$) and a significant decrease at 48 (normoxia 21.6 ± 1.1%, 1% hypoxia 16.3 ± 0.9; $p < 0.05$) hours of treatment. A significant difference was also observed with asiatic acid in the late apoptotic population of cells following 24 (normoxia 65.7 ± 5.0%, 1% hypoxia 51.6 ± 0%; $p < 0.05$) and 48 (normoxia 37.1 ± 0.5%, 1% hypoxia 46.8 ± 4.9%; $p < 0.001$) hours of treatment. In the U87-MG cell line under 1% hypoxia, a significant decrease was observed in the live cell population of non-treated cells at 24 (normoxia 92.1 ± 1.4%, 1% hypoxia 50.8 ± 2.9%; $p < 0.001$), 48 (normoxia 95.9 ± 1.9, 1% hypoxia 43.1 ± 4.6%; $p < 0.001$) and 72 hours (normoxia 96.9 ± 0.9%, 1% hypoxia 45.6 ± 3.8; $p < 0.001$). A significant increase was also observed in the late apoptotic population of cells following 24 (normoxia 1.7 ± 0.5%, 1% hypoxia 27.1 ± 1.1%; $p < 0.001$), 48

(normoxia 0.9 ± 0.4%, 1% hypoxia 34.0 ± 3.1%; $p < 0.001$) and 72 (normoxia 0.7 ± 0.2%, 1% hypoxia 37.1 ± 2.2%; $p < 0.001$) hours of incubation. Cisplatin treatment showed a significant decrease in live cell percentage following 24 (normoxia 86.7 ± 0.5%, 1% hypoxia 52.9 ± 2.1%; $p < 0.01$), 48 (normoxia 81.0 ± 2.1%, 1% hypoxia 49.4 ± 3.7%; $p < 0.01$) and 72 (normoxia 74.3 ± 0.8%, 1% hypoxia 52.4 ± 3.2%; $p < 0.05$) hours of treatment. Asiatic acid showed a significant increase in the live (normoxia 5.8 ± 2.1%, 1% hypoxia 25.9 ± 3.3%; $p < 0.001$) and a significant decrease in the late apoptotic (normoxia 66.0 ± 7.6%, 1% hypoxia 46.7 ± 1.3%; $p < 0.001$) population of cells following 24 hours of treatment.

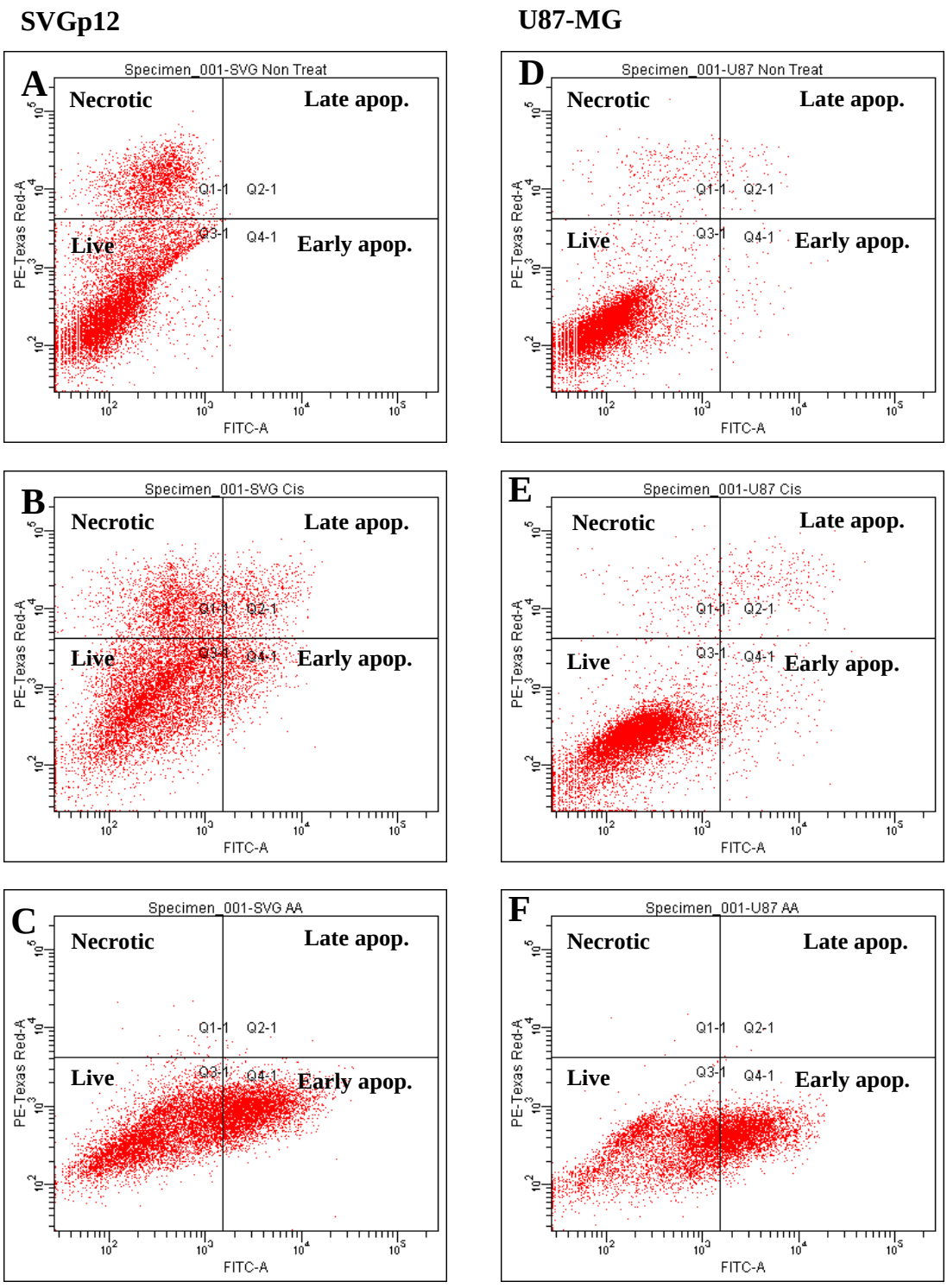

Figure 3.9: Flow cytometric plots showing cell apoptosis using Annexin V/Alexa Fluor 488® and propidium iodide on SVGp12 and U87-MG cell lines following 120 hours of incubation, under normoxia

(A, D) Non-treated cells, (B, E) cisplatin and (C, F) asiatic acid. Cisplatin and asiatic acid showed a higher number of apoptotic cells compared to control.

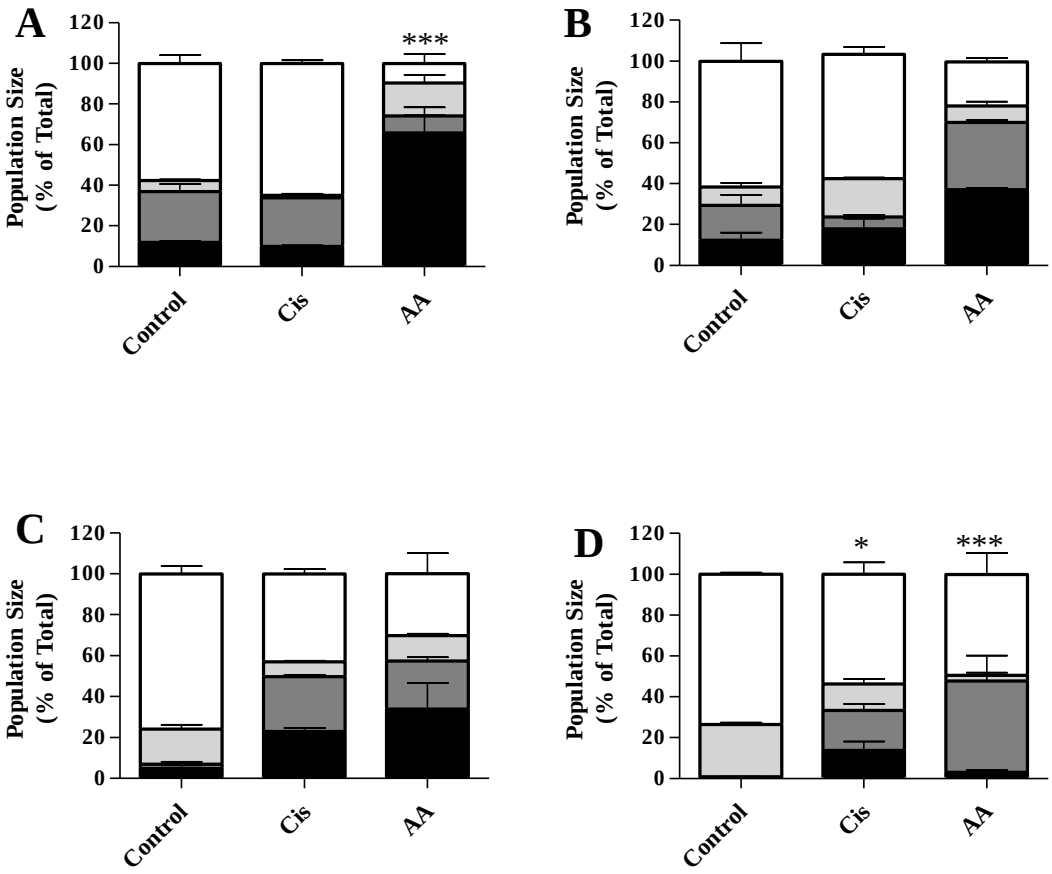

Figure 3.10: Data illustrating the effect of cisplatin and asiatic acid treatments on SVGp12 cell line using Annexin V/Aelxa Fluor 488® and propidium iodide, under normoxia

Cell apoptosis study was performed on SVGp12 cell line following 24 (A), 48 (B) and 72 (C) and 120 (D) hours of treatment. Data shows relative proportions of live (colourless), necrotic (light grey), early apoptotic (dark grey) and late apoptotic cells (black). Cisplatin did not show any differences in cell populations compared to control, however, asiatic acid showed a higher proportion of dead cells than control. Significant differences for live cell population, in comparison to control, have been displayed. Values represent mean ± S.E. for three experiments in triplicate.

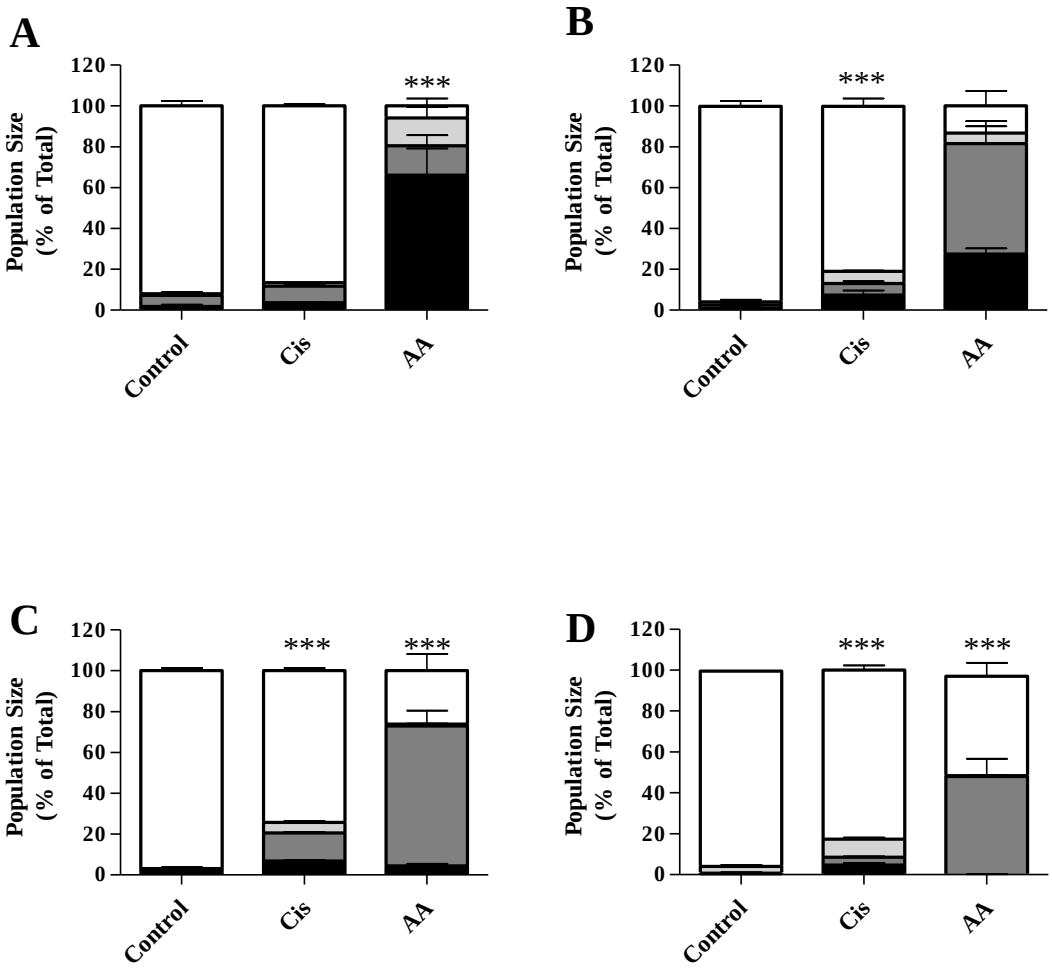

Figure 3.11: Data illustrating the effect of cisplatin and asiatic acid treatments on U87-MG cell line using Annexin V/Aelxa Fluor 488® and propidium iodide, under normoxia

Cell apoptosis study was performed on U87-MG cell line following 24 (A), 48 (B) and 72 (C) and 120 (D) hours of treatment. Data shows relative proportions of live (colourless), necrotic (light grey), early apoptotic (dark grey) and late apoptotic cells (black). Cisplatin did not show any differences in cell populations compared to control, however, asiatic acid showed a higher proportion of dead cells than control. Significant differences for live cell population, in comparison to control, have been displayed. Values represent mean ± S.E. for three experiments in triplicate.

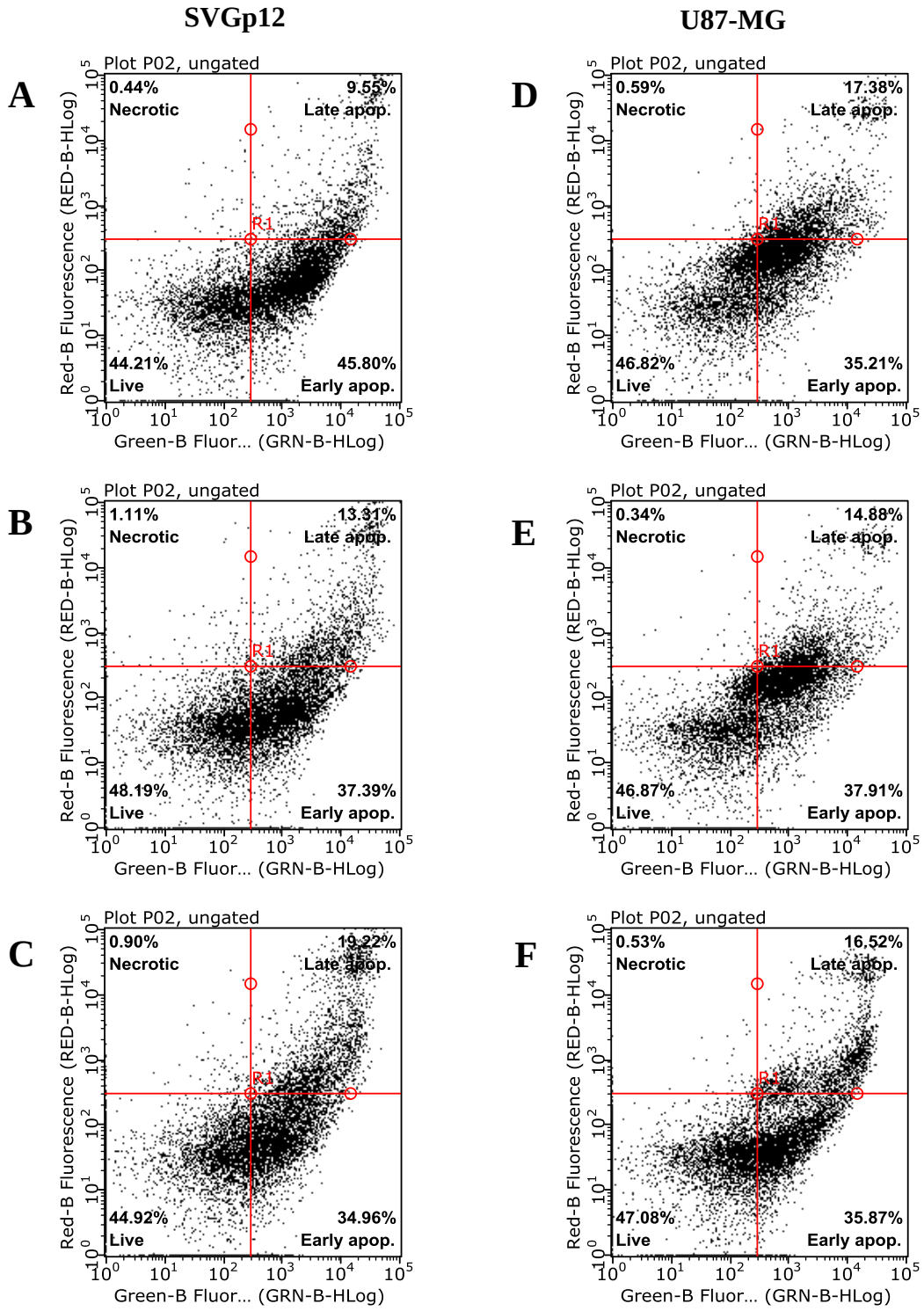

Figure 3.12: Flow cytometric plots showing cell apoptosis using Annexin V/Alexa Fluor 488® and propidium iodide on SVGp12 and U87-MG cells following 72 hours of incubation, under 5% hypoxia

Flow cytometry was performed on SVGp12 and U87-MG cell lines on non-treated (A, D), cisplatin (B, E), asiatic acid (C, F) treated cells.

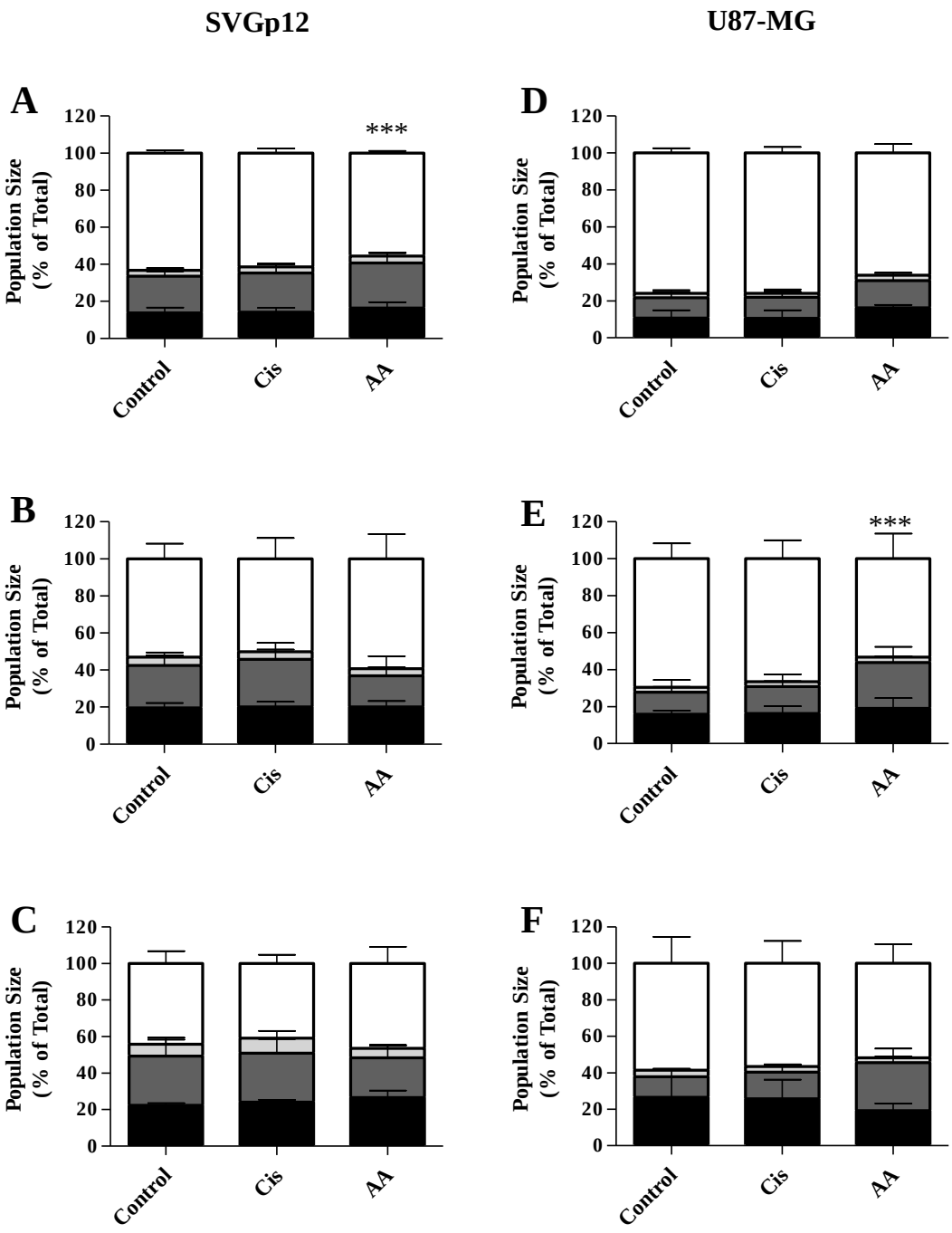

Figure 3.13: Data illustrating the effect of cisplatin and asiatic acid treatments on SVGp12 and U87-MG cell line using Annexin V/Aelxa Fluor 488® and propidium iodide, under 5% hypoxia

Cell apoptosis study was performed on SVGp12 and U87-MG cell lines following 24 (A & D), 48 (B & E) and 72 (C & F) hours of treatment. Data shows relative proportions of live (colourless), necrotic (light grey), early apoptotic (dark grey) and late apoptotic cells (black). Cisplatin did not show any differences in cell populations compared to control, however, asiatic acid showed a higher proportion of dead cells than control. Significant differences for live cell population, in comparison to control, have been displayed. Values represent mean ± S.E. for three experiments in triplicate.

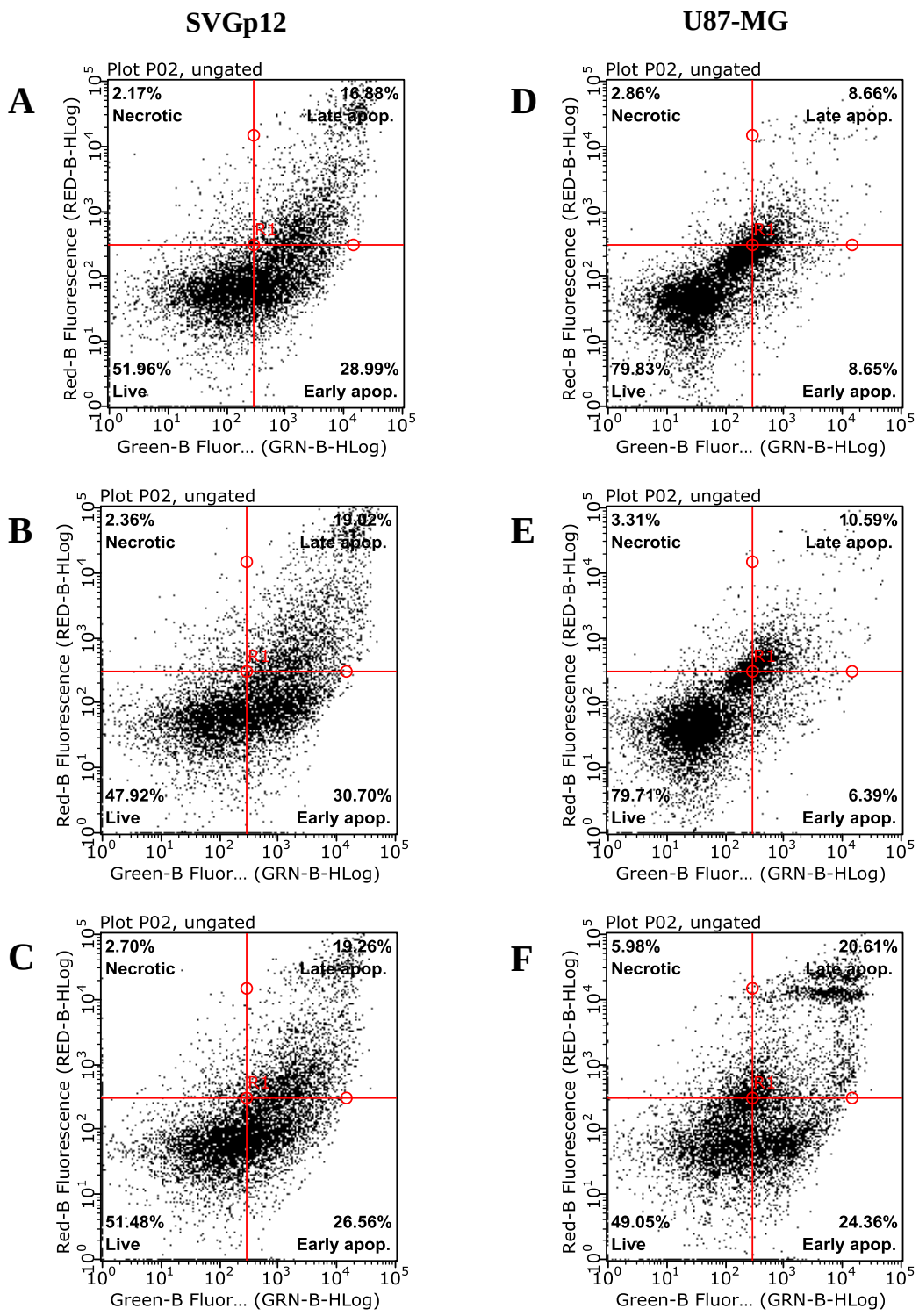

Figure 3.14: Flow cytometric plots showing cell apoptosis using Annexin V/Alexa Fluor 488® and propidium iodide on SVGp12 and U87-MG cells following 72 hours of incubation, under 1% hypoxia

Flow cytometry was performed on SVGp12 and U87-MG cell lines on non-treated (A, D), cisplatin (B, E), asiatic acid (C, F) treated cells.

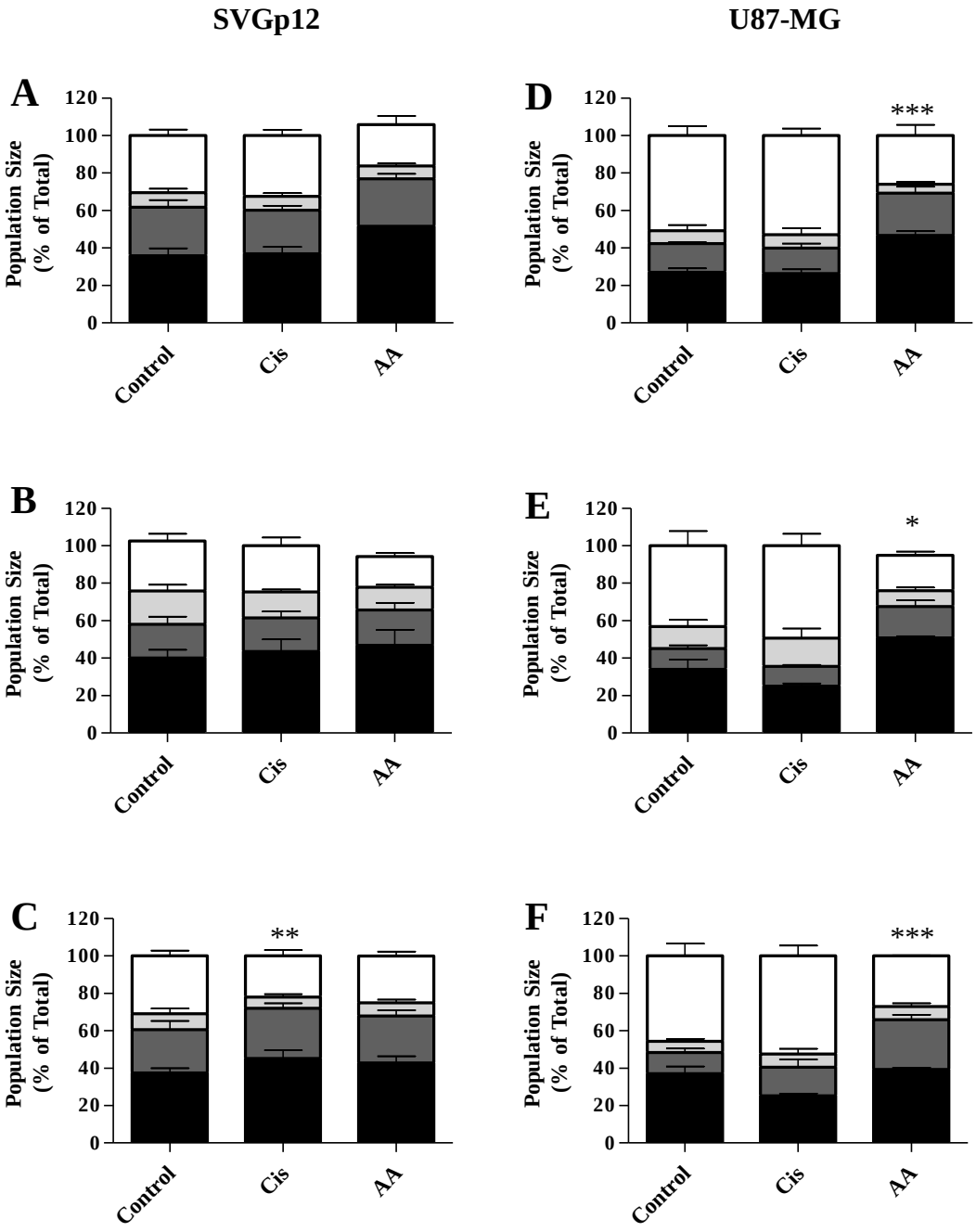

Figure 3.15: Data illustrating the effect of cisplatin and asiatic acid treatments on SVGp12 and U87-MG cell line using Annexin V/Aelxa Fluor 488® and propidium iodide under 1% hypoxia

Cell apoptosis study was performed on SVGp12 and U87-MG cell lines following 24 (A & D), 48 (B & E) and 72 (C & F) hours of treatment. Data shows relative proportions of healthy (colourless), necrotic (light grey), early apoptotic (dark grey) and late apoptotic cells (black). Significant differences for live cell population, in comparison to control, have been displayed. Values represent mean ± S.E. for three experiments in triplicate.

3.2.5 Cellular reactive oxygen species assay

ROS play an important role in cell signalling pathways and contribute towards cellular apoptosis and necrosis. To measure the amount of ROS generated in the two cell lines following treatment with cisplatin and asiatic acid, a ROS assay using the fluorescent dye DCFDA was performed.

Normoxia

Cisplatin treatments at 2, 10 and 40µM showed 136.9 ± 6.4%, 137.8 ± 6.7 and 150.7 ± 8.4% of ROS activity on the SVGp12 cell line. Asiatic acid treatments at 30, 50 and 70 µM showed 148.8 ± 5%, 153.9 ± 8.5% and 148.9 ± 6.2% activity in ROS on SVGp12 cell line (Fig. 3.16). No significant differences ($p > 0.05$) between any two groups of data, at any given time were observed.

Cisplatin treatments at 2, 10 and 40µM showed 132.4 ± 6%, 132.3 ± 8.5% and 147.9 ± 8.9% of ROS activity on the U87-MG cell line. Asiatic acid treatments at 30, 50 and 70 µM showed 135.8 ± 7.3%, 147.2 ± 4.7% and 142 ± 6.3% activity in ROS on U87-MG cell line (Fig. 3.16). No significant differences ($p > 0.05$) between any two groups of data, at any given time were observed.

1% hypoxia

The results obtained for ROS assay under 1% hypoxia were similar to the results obtained for normoxia. Cisplatin treatments at 2, 10 and 40µM showed 155.3 ± 7.4%, 166.9 ±1.4% and 133.7 ±2.4% of ROS activity on the SVGp12 cell line. Asiatic acid treatments at 30, 50 and 70 µM showed 148.5 ± 1.9%, 150.5 ± 2% and 145.4 ± 1.6% activity in ROS on SVGp12 cell line (Fig. 3.17). No significant differences ($p > 0.05$) between any two groups of data, at any given time were observed.

Cisplatin treatments at 2, 10 and 40µM showed 154.7 ± 3.2%, 148.9 ± 3.9% and 160.7 ± 4.2% of ROS activity on the U87-MG cell line. Asiatic acid treatments at 30, 50

and 70 μM showed 155.1 ± 2.1%, 151.5 ±7.7% and 160.1 ± 2.7% activity in ROS on U87-MG cell line (Fig. 3.17). No significant differences ($p > 0.05$) between any two groups of data, at any given time were observed.

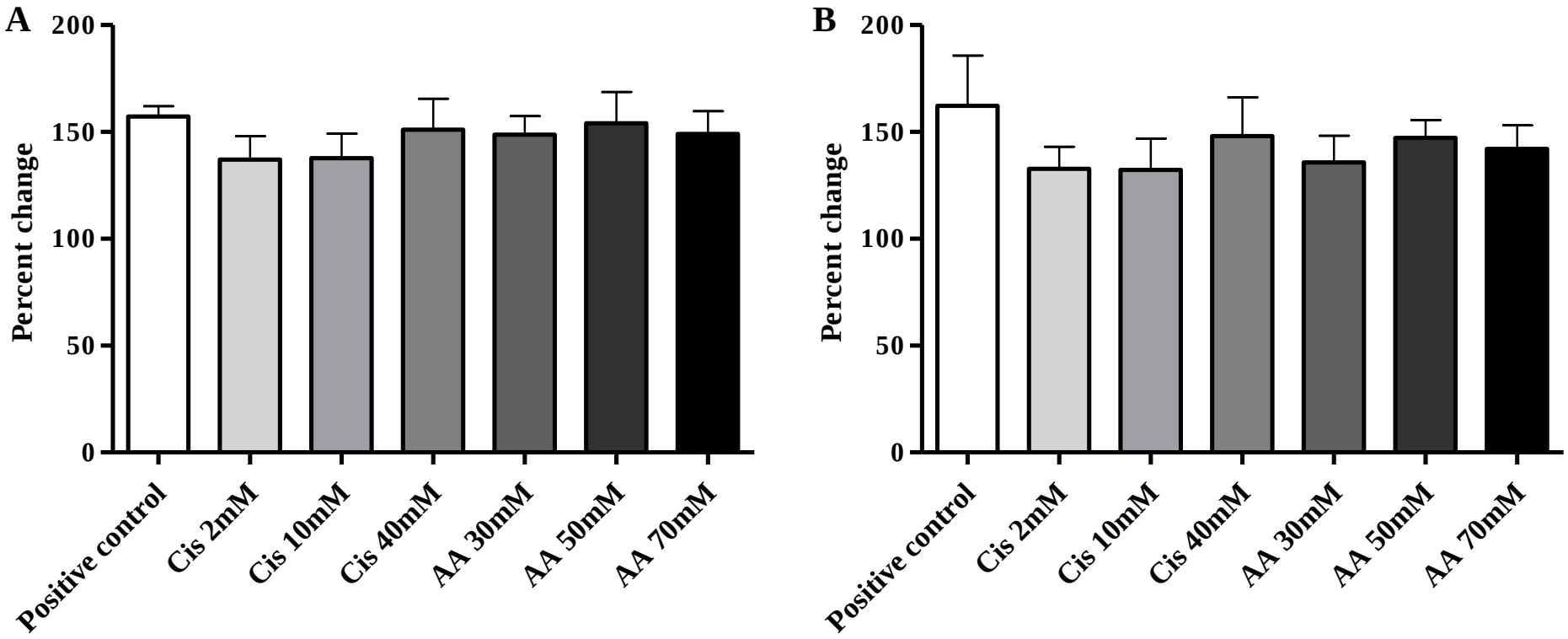

Figure 3.16: Data illustrating the effect of different concentration of cisplatin and asiatic acid treatments on SVGp12 and U87-MG cell line using DCFDA dye for intracellular ROS detection, under normoxia

Cellular ROS study was performed on SVGp12 (A) and U87-MG (B) cell lines using 2, 10 and 40µM cisplatin and 30, 50 and 70µM asiatic acid. Data shows percentage increase in ROS activity, which was similar for all three treatments. No significant differences were observed. Values represent mean ± S.E. for three experiments in triplicate.

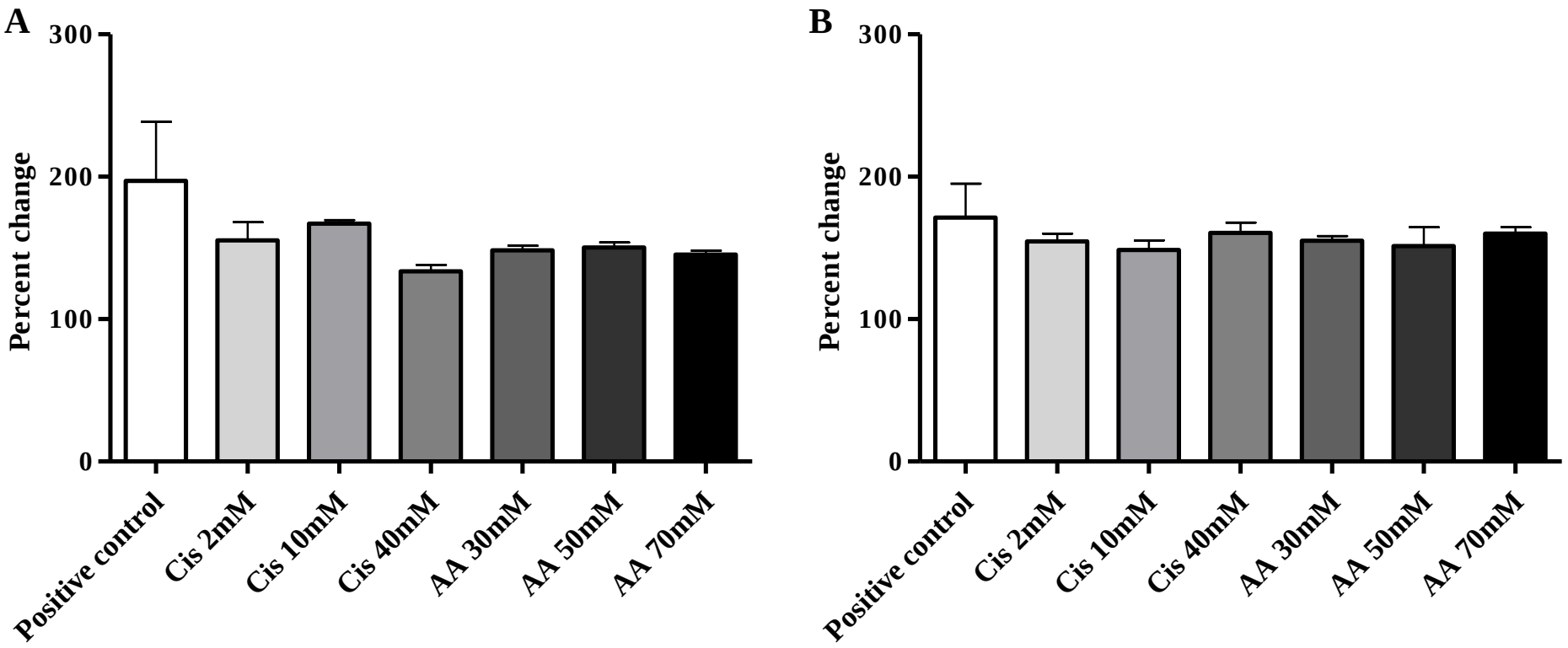

Figure 3.17: Data illustrating the effect of different concentration of cisplatin and asiatic acid treatments on SVGp12 and U87-MG cell line using DCFDA dye for intracellular ROS detection, under 1% hypoxia

Cellular ROS study was performed on SVGp12 (A) and U87-MG (B) cell lines using 2, 10 and 40µM cisplatin and 30, 50 and 70µM asiatic acid. Data shows percentage increase in ROS activity, which was similar for all three treatments. No significant differences were observed. Values represent mean ± S.E. for three experiments in triplicate.

3.3 Discussion

Growth Curves

SVGp12 is an immortalised human foetal glial cell line. It was generated in 1985 by transfecting primary foetal brain cells with a plasmid containing an origin-defective mutant of simian virus 40 (SV40) (Henriksen et al., 2014; Lou et al., 2014). The U87-MG cell line, originated in 1966, is a highly aberrant human cell line and the most commonly studied brain cancer cell line. It is classified as a grade IV (as of 2007) astrocytoma cell line (Clark et al., 2010).

Growth curve analysis of the two cell lines demonstrated U87-MG to have a higher proliferation rate compared to the SVGp12 cell line (Fig. 3.1). Arguably, the most imperative trait of a cancer cell is its sustained and chronic proliferation. The production and release of growth promoting molecules in normal cells is kept under check by various mechanisms that promote the normal maintenance of tissue architecture and function. However, cancer cells are capable of deregulating these systems, thus becoming masters of their own destiny (Hanahan and Weinberg, 2011a; Macheret and Halazonetis, 2015). Thus, a higher proliferation in the U87-MG cells was observed, compared to the SVGp12 cells.

Growth curve analysis under hypoxia showed a significantly slower growth of SVGp12 and U87-MG cell lines (Fig. 3.1). Hypoxia slows the rate of cell growth, in all cells, due to $p21^{WAF/Cip1}$ and $p27^{kip1}$, and has been explained in detail further in this chapter (Maddika et al., 2007).

PrestoBlue® Cell Linearity Assay

PrestoBlue® is a ready to use, cell permeable resazurin-based solution allowing the quantitative determination of the cell viability. PrestoBlue® reagent, when added to living cells, is modified in the reducing environment of the viable cells and changes

colour from blue to red (absorbance 570 nm), thus becoming highly fluorescent (excitation 535 nm/emission 612 nm). The amount of fluorescence can be detected using a spectrophotometer. Although PrestoBlue® can also be measured using absorbance; florescence is a more sensitive method of detection and is also recommended by the company (information from Life Technologies, UK).

PrestoBlue® linearity assay established that the fluorescence produced was directly proportional to population doubling time of the two cell lines (Fig. 3.2). Taking into consideration these results, an initial cell density of 1000 cells/well would be enough to carry out further cell viability assays following an incubation of 24 hours or more.

Assessment of Cisplatin and Asiatic acid Cytotoxicity

Cisplatin demonstrated a decrease in cell viability of the two cell lines, SVGp12 and U87-MG, in a concentration and time dependent manner (Figs. 3.3 & 3.4).

Cisplatin is a chemotherapeutic drug and shows an early effect on cell viability only at higher concentrations, such as 100µM (Figs. 3.3 & 3.4). SVGp12 cells showed a smaller proportion of dead cells with cisplatin as compared to U87-MG cells ($p < 0.05$).

Cisplatin enters the cells by passive diffusion. Upon entering, cisplatin undergoes an aquation reaction which makes it more reactive to cellular targets. Although cisplatin can induce structural changes in cells, it mainly works *via* DNA intercalation causing anomalies in cell replication, ultimately leading to apoptosis (Florea and Büsselberg, 2011; Jiang et al., 2004; Qin and Ng, 2002; Wang and Lippard, 2005). Due to these reasons, the effects of cisplatin on cell viability can only be seen after at least 48 hours of incubation with the drug.

Cisplatin showed a decrease in cell proliferation over time and cell death was mainly due to apoptosis and not necrosis (Figs. 3.9-3.11). Cisplatin causes transient cell cycle arrest in the early S phase leading to a final G2/M phase arrest and ultimately apoptosis (Sorenson et al., 1990). Hence, as the cells proliferate, an additive cytotoxic effect is seen, which in turn reduces the rate of proliferation of cisplatin treated cells (results for this have been shown further in the study). Prolonged exposure of cells to cisplatin leads to mainly apoptotic cell death, however a small proportion of cells may undergo necrosis. Apoptosis due to cisplatin occurs *via* the mitochondrial signalling pathway through activated caspase-3 (Cummings and Schnellmann, 2002; Florea and Büsselberg, 2006; Jiang et al., 2004). Some of the factors that initiate resistance in cisplatin treated cells include increased efflux and decreased influx of the drug, increased cellular glutathione and metallothionein levels, increased DNA repair, and oncogene expression (Gonzalez et al., 2001). Thus, due to the mechanism of action of cisplatin, the number of apoptotic cells increased in a time dependent manner. Also, it can be noted from the results that cisplatin is not selective for cancer cells and exerts its effects on non-cancerous cells too. This encourages the need for the investigation of drugs that are selective to cancerous cells.

Asiatic acid treatment on both cell lines showed a significant reduction in cell viability, compared to control at only the highest concentration (100µM). At 30µM, a gradual decrease in cell viability was observed over 72 hours, in both cell lines (Figs. 3.3 & 3.4). All other concentrations of asiatic acid did not show any significant differences in cell viability over time.

Asiatic acid has a reputation of being a putative anticancer agent in many cancer types. It has been reported that the carboxylic polar group at C-28 position is essential for the pharmacological activities of asiatic acid (Li et al., 2014). The molecular targets

of asiatic acid include GRP-78, calpain and cleaved caspase-3 in U87-MG tumours (Kavitha et al., 2015).

Annexin V is a calcium-dependent phospholipid binding protein with high affinity for PS, whereas PI is a DNA stain. Annexin V binding to the PS on the outer membrane of cells was observed following asiatic acid treatment (Figs. 3.9-3.11), however a small population of cells stained positive for propidium iodide too. Asiatic acid thus showed cell death mainly *via* apoptosis although a smaller fraction of cell death was *via* necrosis. Apoptosis assay using asiatic acid did not show any significant differences in the two cell lines, thus asiatic acid induced apoptosis in both cell lines.

Asiatic acid induces a loss of PS asymmetry in a concentration-dependent manner that results in the PS being exposed on the outer cell membrane and also causes DNA fragmentation (Cho et al., 2006; Hsu et al., 2004). Asiatic acid-mediated cell death is cell-type specific in the U87-MG cell line and involves caspase-9 and -3 activation (Bunpo et al., 2004; Cho et al., 2006; Kavitha et al., 2015). However, there are other mechanisms of asiatic acid-mediated cell death and this has been shown by the use of pan-caspase inhibitor, zvad-fmk. The use of this inhibitor, in a study on glioblastoma cell line by Cho et al., (2006), demonstrated that zvad-fmk did not significantly block AA-mediated cell death in the glioblastoma cell line.

Asiatic acid causes endoplasmic reticulum (ER) stress (a result of activated GRP-78) and an increase in the intracellular calcium level. It is due to this that cell death occurs; thus decreasing the mitochondrial membrane potential. Furthermore, asiatic acid treatment reduces Bcl-2 expression in cells and it has been speculated that asiatic acid mediated increase in intracellular calcium is partially *via* the inhibition of Bcl-2 expression in the ER. (Bunpo et al., 2004; Cho et al., 2006; Kavitha et al., 2014; Wang et al., 2009).

Intracellular calcium release is a mediator of chemical-induced cytotoxicity and apoptotic cell death. The two major pathways leading to increase in intracellular calcium are influx from extracellular space and release from internal source. However, with the use of calcium channel blockers, studies have confirmed that asiatic acid mediated cell death is only due to intracellular calcium release and not due to the extracellular calcium store (Hsu et al., 2004). This release in intracellular calcium triggers a biochemical cascade leading to calpain activation. Upon activation, calpain degrades cell membrane, cytoplasmic and nuclear substrates, subsequently leading to the breakdown of cellular architecture and cell death (Momeni, 2011).

Asiatic acid treatment also showed a smaller population of cells undergoing necrosis (Figs. 3.9-3.11). Necrosis is characterised by the release of the enzyme lactate dehydrogenase (LDH). A rapid release in LDH indicates traumatic cell death, i.e., necrosis, whereas a slow release indicates apoptosis (Cho et al., 2006; Scaffidi et al., 2002).

Thus, it can be speculated that asiatic acid mediates glioblastoma cell death due to caspase activation *via* intrinsic apoptosis and also necrosis. This is seen in the results obtained in this study where a small number of necrotic cell population was observed following asiatic acid treatment, however, cell death occurred mainly due to apoptosis.

Decrease in oxygen supply to the cells leads to biochemical changes that can either result in cells adaptation to hypoxia or cause cell death. HIF-1α is an important transcription factor and regulator of gene products under hypoxia. An initial moderate increase in HIF-1α is important for cells adaptation to hypoxia (Strese et al., 2013).

In this state, cancer cells respond to hypoxia *via* angiogenesis stimulation by VEGF, apoptosis inhibition *via* Bcl-2, modifying the cellular metabolism of glucose, adapting to extracellular acidic pH and up-regulation of proteins involved in metastasis

(Bogenrieder and Herlyn, 2003; Graeber et al., 1996; Vander Heiden, M. G., Cantley, L.C., Thompson, 2009; Zhou et al., 2006).

A slower rate of proliferation is observed under hypoxia, due to $p21^{WAF/Cip1}$, $p27^{kip1}$ and the increased distance of the cells from the blood vessel. These defects in cell cycle regulation, proliferation and apoptosis cause a reduction in the efficacy of anticancer/chemotherapeutic drugs (Maddika et al., 2007). From the results obtained in this study, a reduced effect of cisplatin and asiatic acid can be observed under hypoxia. Cell apoptosis assay under hypoxia has shown a higher number of live cells and smaller apoptotic population even after prolonged treatment with cisplatin and asiatic acid (Figs. 3.12-3.15).

A reduction in the activity of p53 under hypoxia causes inhibition of cell apoptosis, and cells are more likely to undergo restoration following DNA injuries. Hypoxia increases the expression of *MDR1* gene encoding membrane-resident P-gp that belongs to a family of ATP-binding cassette transporters. P-gp acts to increase chemoresistance towards a variety of drugs by acting as an efflux pump, in various types of cancers, including glioma (Comerford et al., 2002; Gottesman, 2002; Liu et al., 2008). Various studies have reported, that hypoxia increases chemo resistance (Koch et al., 2003; Rohwer et al., 2010; X. Song et al., 2006). Studies have shown that cell viability of U87-MG cells can be compromised to facilitate apoptosis in a caspase-dependent/p53 independent mechanism *via* the inhibition of HIF-1α transactivation (Dai et al., 2003). Hypoxia also reduces cell-senescence due to chemotherapeutic drugs (Sullivan et al., 2008).

Mitochondria, the ‘power house’ of the cell, play an important role in cell viability and the initiation of intrinsic apoptotic pathway (Galluzzi et al., 2008). It has been established previously that HIF can reduce mitochondrial activity of the cell,

acting once again, in a chemoresistant manner. HIF-1α suppresses the TCA cycle by inhibiting pyruvate shuttling into mitochondria *via* inactivation of PDH (pyruvate dehydrogenase), the enzyme that catalyses the transformation of pyruvate into acetyl-CoA. In this manner, HIF-1α suppresses mitochondrial activity, initiates mitophagy (mitochondrial autophagy) and also suppresses mitochondrial biogenesis. This leads to reduced cell death and increased drug resistance under hypoxia (Kim et al., 2006; Papandreou et al., 2006; Zhang et al., 2007).

Cell viability for cisplatin and asiatic acid under hypoxia showed more number of viable cells at the same drug concentrations when compared to normoxia (Figs. 3.5-3.8). Growth curve analysis of the two cell lines showed a significantly slower rate of growth of cells under hypoxia when compared to normoxia (Fig. 3.1). These results suggest that hypoxia alters cellular metabolism, cell growth is slowed and cell apoptosis is reduced. Thus, as apoptosis is suppressed, this again provides an explanation for the reduced effect of drugs that was observed under hypoxia on the two cell lines. Also, as cell growth is important for the cytotoxic effects of drugs; due to the slower growth of cells under hypoxia, the cytotoxic effect of drugs was reduced.

Results from the apoptosis assay showed a large number of apoptotic SVGp12 and U87-MG cells following 24 hours of incubation with cisplatin and asiatic acid under hypoxia (Figs. 3.12-3.15). However, this number did not change at the end of 72 hours suggesting that the apoptotic percentage of cells observed was not necessarily due to the drug treatments, but it could be due to the cells becoming acclimatised to hypoxia.

An estimated 50-60% of all tumours contain hypoxic or anoxic regions. These regions only develop as a result of an imbalance between oxygen supply and consumption in proliferating tumours. A study by Grayson et al., 2006 revealed that

hMSC cells underwent an initial acclimatisation period where they did not proliferate, thus extending their lag phase. This can be seen in Fig. 3.1 where a significantly slower growth of cells, under hypoxia, is observed and also an increase in the doubling time for both cell lines.

The hydration of carbon dioxide to carbonic acid is catalysed by carbonic anhydrase IX (CAIX), (transcription gene located on vHPL of HIF-1α). It contributes to the acidification of the extracellular tumour environment thus maintaining the normal pH in tumour cells. In this manner, CIAX allows acclimatisation of cells under hypoxia and a blockade or slow release results in cell death under hypoxia (Korkolopoulou et al., 2007; Pantuck et al., 2003; Yamagata et al., 1998).

Hypoxia creates an environment of stress and during the acclimatisation period, it can induce DNA damage, cell cycle arrest and ultimately cell death. However, as discussed previously, hypoxia also selects cells with a decreased *p53* activity, thus reducing their apoptosis and allowing them to proliferate.

It has been widely accepted that ROS play a crucial role in tumour metastasis and gene regulation in a variety of cell types (Ma et al., 2009). ROS show an increased basal level in cancer cells than in normal cells and are involved in the activation of HIF, whereby the transcription of various genes promoting tumour proliferation takes place (Section 1.8) (Kolamunne et al., 2013). Some studies have described an increase in ROS generation under hypoxia, while others have observed a decrease in ROS under hypoxia (Huang et al., 2008).

Results from in this study, a basal level of 100% ROS activity was observed. Neither cisplatin, nor asiatic acid treatments showed an increase or decrease in the ROS activity in SVGp12 or U87-MG cells, at the concentration used (Figs. 3.16 & 3.17).

Hypoxia down regulates mitochondrial activity (Kim et al., 2006; Papandreou et al., 2006; Zhang et al., 2007). Mitochondria is the main site of ROS generation due to aerobic respiration. However, in a tumour cell, anaerobic glycolysis generating lactic acid as a source of energy takes place, instead of glucose (Fig. 3.18). This shift in lactate production in cancer cells, even in the presence of oxygen, is termed as the Warburg effect (Kim and Dang, 2006; Warburg, 1956). It is due to this that a downregulation in ROS production from the mitochondria is seen in tumours.

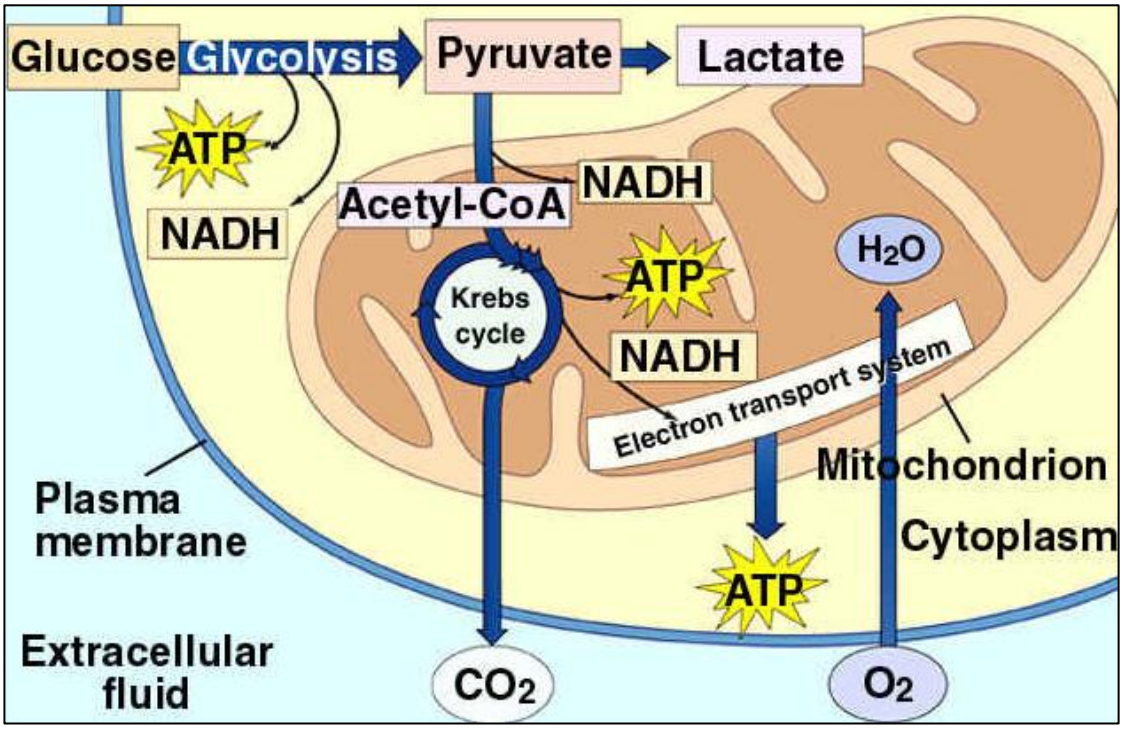

Figure 3.18: Diagrammatic representation of aerobic respiration in the mitochondria of the cell

Glycolysis is the first step in aerobic respiration. In the presence of NAD^+ and ATP, glucose is converted to pyruvate, transported into the mitochondria and converted into acetyl CoA. NADH and $FADH_2$, from the TCA/Krebs cycle, convert ADP to ATP in the inner mitochondrial membrane. Creation of H^+ concentration gradient drives the production of more ATP. A total of 38 ATP are produced *via* aerobic respiration as opposed to 2 ATP in anaerobic respiration. The end product of anaerobic respiration is either ethanol or lactic acid, and it takes place in the cell cytosol. Source: Tumour Metabolom®

ROS production not only occurs in the mitochondria; other sources of ROS production in tumour cells include chronic inflammation, increased cytokine release and activation of the c-Myc protein (Biroccio et al., 2001; Kim and Dang, 2006).

Cisplatin induces ROS generation which partially mediates apoptosis (Pelicano et al., 2004). This was shown in a study by Berndtsson et al., (2007) using ROS scavengers, that apoptosis at 24 hours was inhibited. However, massive cell death due to cisplatin induced ROS generation mainly occurs in c-Myc low-expressing cells. This is consistent with other findings that ROS are potent inducers of apoptosis. It has also been speculated that ROS production occurs only in cells unable to recover from cisplatin induced damage by c-Myc down-regulation (Biroccio et al., 2001).

Asiatic acid, on the other hand, has been shown to suppress ROS production due to UVA irradiation in human keratinocytes (Soo Lee et al., 2003). A study by Tang et al., (2009) shows that asiatic acid causes interference with the mitochondrial membrane potential, in colon cancer cells, thereby stimulating cytochrome c release and initiating caspase signalling pathways. Apoptosis and cell death in multiple cell lines is preceded by the elevation of cytochrome c (encoded by a nuclear gene) and cytochrome c oxidase subunit II (encoded by a mitochondrial gene) levels. Both of these proteins are involved in the mitochondrial respiratory chain. Transcription and up-regulation of cytochrome c results in its translocation from cytosol into mitochondria and this does not depend on mitochondrial respiration or mitochondrial protein synthesis. In contrast, mitochondrial cytochrome c release involves dynamic changes in Bcl-2 proteins, opening of permeability transition pore and loss of mitochondrial membrane potential. This overexpression of cytochrome c enhances caspase activation and apoptosis; while the downregulation of Bcl-2 promotes cell death *via* c-Myc (Chandra et al., 2002; O'Brien and Kirby, 2008). As explained earlier, asiatic acid mediated glioblastoma cell death is

mainly due to intracellular calcium release and reduction in Bcl-2 expression in cells. This suggests a mechanism for asiatic acid effects on cell apoptosis and necrosis in glioblastoma cell lines and can be investigated in the future.

In conclusion, the down regulation of mitochondrial activity occurs in hypoxia and anaerobic mode of glycolysis in tumour cells suggests a reason behind a stable level in the ROS activity observed in this study. Thus, although asiatic acid mediates cell apoptosis through ROS production, this may not necessarily be the major contributor towards cell apoptosis and other mechanisms such as Bax/Bcl-2, intracellular calcium release and caspase activation may be involved.

CHAPTER 4

Effect of Hypoxia on Cell Proliferation and Cell Cycle

4.1 Introduction

Eukaryotic cell cycle progression and proliferation are tightly regulated, irreversible and cause unidirectional changes in the state of the cell. Cell cycle is controlled by cyclin-dependent kinases and has a specific activity at every stage of the cell cycle, such as chromosome condensation, DNA replication and spindle assembly. Cell proliferation occurs due to cell cycle progression of the cell and cell cycle associated checkpoints regulate the entry into cell cycle. Thus, cells with deleterious mutations in their DNA are not allowed to progress into the cell cycle and apoptosis takes place (Crosio et al., 2002; Pinheiro and Sunkel, 2012; Rieder, 2011; Shackelford et al., 1999; Tyson et al., 2002; van den Heuvel, 2005; Vermeulen et al., 2003).

Cell proliferation is thus an important factor in the assessment of cytotoxicity of drugs. Also, tumour cells generally show increased rates of proliferation due to genetic mutations and hence the assessment of the rate of proliferation of cells is an important factor in assessing drug induced cytotoxicity (Kanu et al., 2009; Minniti et al., 2009). Cell apoptosis and cell cycle are intimately related processes, and this is evident by the presence of p53 in cell cycle progression and the induction of apoptosis (Shah and Schwartz, 2001).

In addition, the relative expression of various receptors, including EGFR expression, is modified under hypoxia and also due to drug treatments (Kanu et al., 2009; Minniti et al., 2009).

Cell migration is central to a variety of physiological processes including tissue repair and regeneration. Abnormal wound healing is a characteristic of tumour cells and an important factor determining the malignancy of tumour cells. Cell migration is regulated by EGFR expression, which is up-regulated in glioma (Gough et al., 2011;

Lalloo et al., 2006; Natarajan et al., 2006). We thus studied the effects of asiatic acid on cell migration and performed a wound healing assay over a period of 18 hours.

Biochemical synergy has been the rationale behind combination therapies. Combination therapies also help in overcoming drug resistance due to the additive and/or synergistic effects. Cisplatin is chemotherapeutic drug whereas asiatic acid is a herbal compound. By choosing chemotherapeutic drugs with different mechanisms of action, different biochemical targets were assessed (DeVita et al., 1975; Shah and Schwartz, 2001).

Objectives: Following the results obtained from apoptosis and reactive oxygen species generation of the two cell lines, we performed cell proliferation and cell cycle analysis. We also assessed the relative expression of EGFR on the two cell lines, using western blotting and performed combination studies using cisplatin and asiatic acid.

4.2 Results

4.2.1 Cell Proliferation Assay

The proliferation rates of cell lines vary following drug treatments and also due to oxygen conditions. The rate of proliferation of cells is an important factor in determining cytotoxicity of drugs. In order to assess this, cell proliferation assay using CFDA-SE was performed in SVGp12 and U87-MG cell lines, under normoxia and hypoxia (1% and 5%), following their treatments with cisplatin and asiatic acid. A reduction in CFDA-SE fluorescence indicated an increase in cell proliferation.

Normoxia

In SVGp12 cell line, reduction in fluorescence to 45 ± 2.5% at 24 hours and to 1.2 ± 0.1% at the end of 120 hours was observed. Following 24 hours of incubation, cisplatin treatment on SVGp12 cells showed a reduction to 45 ± 2.6%; this reduced to 1.6 ± 0.1% at the end of 120 hours, which means that cisplatin treated cells proliferated at a similar rate to non-treated cells (Figs. 4.1-4.3). However, cisplatin showed a significant increase in CFDA fluorescence at 48 hours (control 16.3 ± 0.2%, cisplatin 21.6 ± 1.1%; $p < 0.01$). Treatment with asiatic acid showed a reduction in fluorescence to 42.3 ± 1.0% at 24 hours and 1.5 ± 0.1% at the end of 120 hours. Asiatic acid treatment did not show any significant differences.

Similar results were obtained for U87-MG cell line. In U87-MG cell line, a reduction in fluorescence to 31.9 ± 6.0% at 24 hours and to 1 ± 0.1% at the end of 120 hours was observed. Following 24 hours of incubation, cisplatin treatment on U87-MG cells showed a reduction in fluorescence to 39.7 ± 7.6%; this reduced to 2 ± 0.5% at the end of 120 hours, which means that cisplatin treated cells proliferated at a similar rate to non-treated cells . However, cisplatin treatment showed a significant increase in CFDA fluorescence at 48 hours (and control 14.1 ± 3.5%, cisplatin 24.5 ± 5.1%, $p < 0.01$), as

observed in Figs. 4.1-4.3. Treatment with asiatic acid showed a reduction in fluorescence to 36.5 ± 6.5% at 24 hours and 1.2 ± 0.2% at the end of 120 hours. Asiatic acid treatment did not show any significant differences.

Significant differences were also observed between SVGp12 and U87-MG cell lines in the non-treated controls following 24 hours of incubation (SVGp12 39.2 ± 3.8%, U87-MG 28.5 ± 2%; $p < 0.05$). Cisplatin showed significant increase in CFDA fluorescence at 48 (SVGp12 2.4 ± 0.2%, U87-MG 3.3 ± 0.5; $p < 0.05$) and 72 hours (SVGp12 1.8 ± 0.3%, U87-MG 4.2 ± 0.8%; $p < 0.05$). Asiatic acid treatment did not show any significant differences.

5% hypoxia

In SVGp12 cell line, a reduction in fluorescence to 55.8 ± 3.0% at 24 hours and to 1.5 ± 0.3% at the end of 120 hours was observed. Following 24 hours of incubation, cisplatin treatment on SVGp12 cells showed a reduction in fluorescence to 61.9 ± 5.2%; this reduced to 15.8 ± 5.6% at the end of 120 hours (Figs. 4.4-4.6). Cisplatin treatment appeared to slow the rate of cell proliferation when compared to non-treated cells, although these differences were non-significant at any of the measured time points. Treatment with asiatic acid showed a reduction in fluorescence to 56.9 ± 4.9% at 24 hours and 1.1 ± 0.2% at the end of 120 hours. Thus, the SVGp12 cell line proliferated at a similar rate with or without any treatment. Statistical analysis of the data did not show any significant differences in the rate of proliferation of SVGp12 cells.

Similar results were obtained for U87-MG cell line. Cells proliferated to 43 ± 5.3% at 24 hours and to 2.2 ± 0.4% at the end of 120 hours. Following 24 hours of incubation, cisplatin treatment on U87-MG cells showed a reduction in fluorescence 49.3 ± 8.5%; this reduced to 15.9 ± 3.4% at the end of 120 hours (Figs. 4.4-4.6). Cisplatin showed a decreased proliferation rate in the U87-MG cell line compared to

control, although these differences were found to be non-significant upon being analysed statistically. Treatment with asiatic acid showed a fluorescence reduction to 41.4 ± 4.2% at 24 hours and 2.1 ± 0.3% at the end of 120 hours. Asiatic acid did not show any differences in the rate of proliferation of cells compared to the control. Based on these observations, the U87-MG cell line proliferated at a similar rate with or without any treatment.

No significant differences were observed between the two cell lines following incubation with any of the treatments.

1% hypoxia

In SVGp12 cell line, reduction in fluorescence by 230.8 ± 97.7% at 24 hours and to 21.8 ± 8.5% at the end of 120 hours was observed. SVGp12 cells showed a reduction in fluorescence to 251.9 ± 96.4% following 24 hours of incubation with cisplatin and this reduced to 9 ± 2.6% at the end of 120 hours (Figs. 4.7-4.9). Asiatic acid showed a fluorescence reduction to 82.3 ± 16.1% at 24 hours and 6.8 ± 1.8% at the end of 120 hours. No significant differences in the rate of proliferation of asiatic acid or cisplatin treated cells were observed (Figs. 4.7-4.9). Thus, the SVGp12 cell line proliferated at a similar rate with or without any treatment, under 1% hypoxia.

Similar results were obtained for U87-MG cell line. U87-MG cells showed a reduction in proliferation to 365.1 ± 100.8% at 24 hours and to 11.3 ± 5.3% at the end of 120 hours. Following 24 hours of incubation with cisplatin, U87-MG cells showed a fluorescence reduction to 934 ± 489.2%; this reduced to 33.4 ± 9.5% at the end of 120 hours (Figs. 4.7-4.9). Asiatic acid showed a reduction in fluorescence to 813.1 ± 424.7% at 24 hours and 22.3 ± 6.4% at the end of 120 hours. Statistical analysis of the data did not show any significant differences in the rate of proliferation of U87-MG

cells. Based on these observations, the U87-MG cell line proliferated at a similar rate with or without any treatment, under 1% hypoxia.

No significant differences were observed between the two cell lines following incubation with any of the treatments.

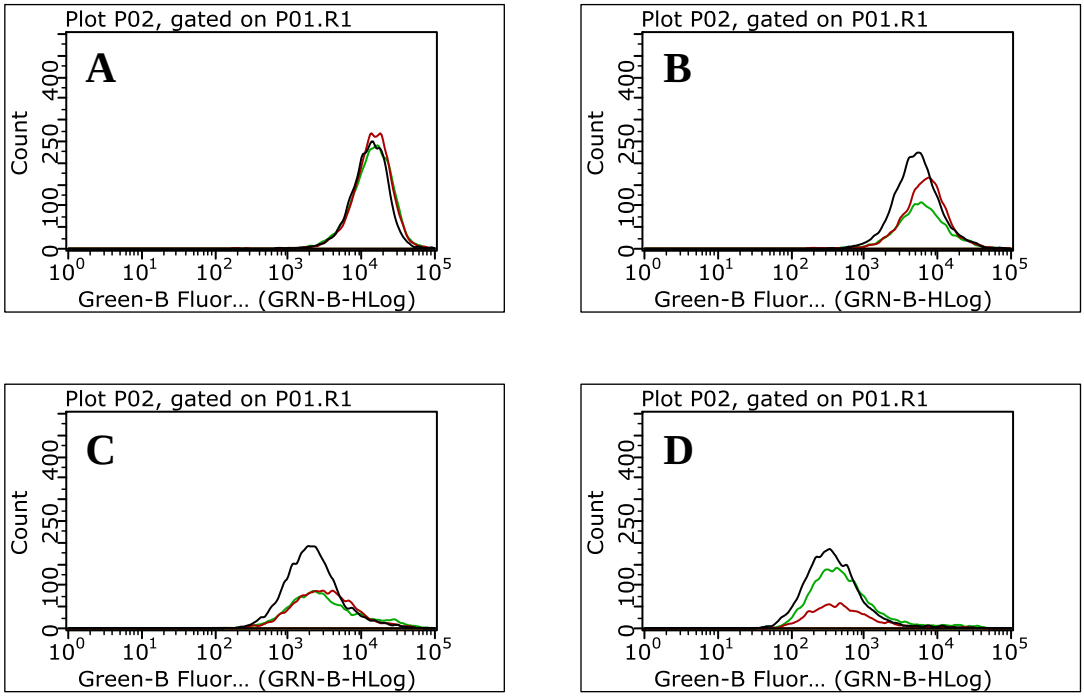

Figure 4.1: Flow cytometric plots showing cell proliferation using CFDA-SE on SVGp12 cell line under normoxia

24 hours (A), 48 hours (B), 72 hours (C), 120 hours (D). Non-treated (black), cisplatin (red), asiatic acid (green). No significant differences in the rate of proliferation of SVGp12 cell line were observed.

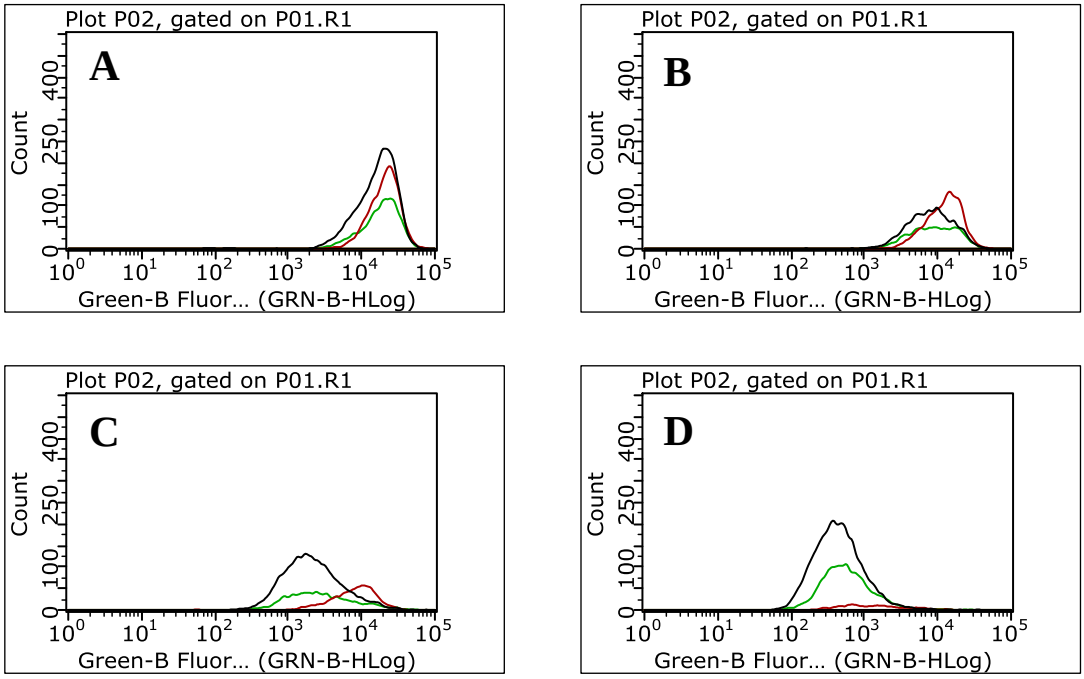

Figure 4.2: Flow cytometric plots showing cell proliferation using CFDA-SE on U87-MG cell line under normoxia

24 hours (A), 48 hours (B), 72 hours (C), 120 hours (D). Non-treated (black), cisplatin (red), asiatic acid (green). No significant differences in the rate of proliferation of U87-MG cell line were observed.

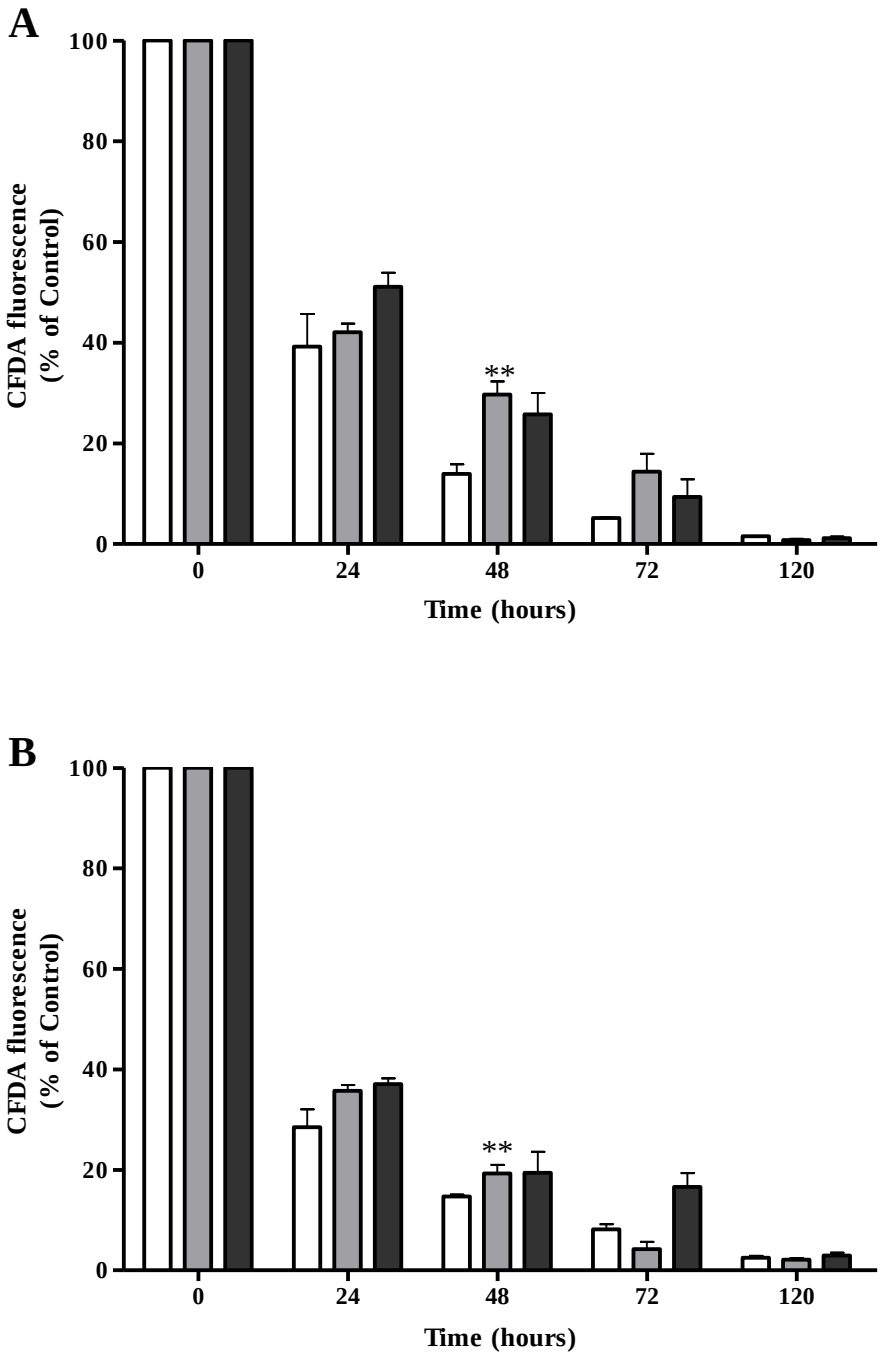

Figure 4.3: Data illustrating the effect of cisplatin and asiatic acid on SVGp12 and U87-MG cell line using CFDA-SE, under normoxia

Cell proliferation assay on SVGp12 (A) and U87-MG (B) cell lines following 24, 48, 72 and 120 hours of incubation with non-treated (clear), cisplatin (light grey) and asiatic acid (dark grey) was performed using CFDA-SE. A decrease in fluorescence indicates a higher rate of cell proliferation. Cisplatin showed a significant reduction in proliferation at 48 hours, while asiatic acid showed no significant difference; differences were compared to control. Values represent mean ± S.E. for three experiments in triplicate.

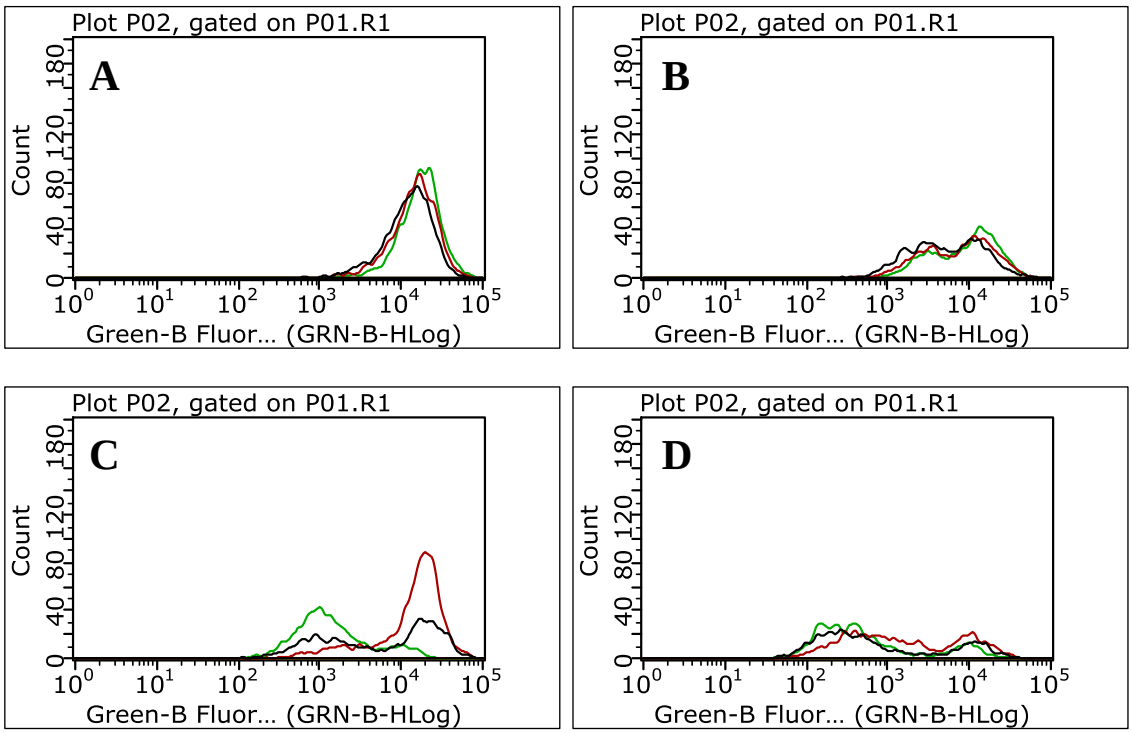

Figure 4.4: Flow cytometric plots showing cell proliferation using CFDA-SE on SVGp12 cell line under 5% hypoxia

24 hours (A), 48 hours (B), 72 hours (C), 120 hours (D). Non-treated (black), cisplatin (red), asiatic acid (green). No significant differences in the rate of proliferation of SVGp12 cell line were observed.

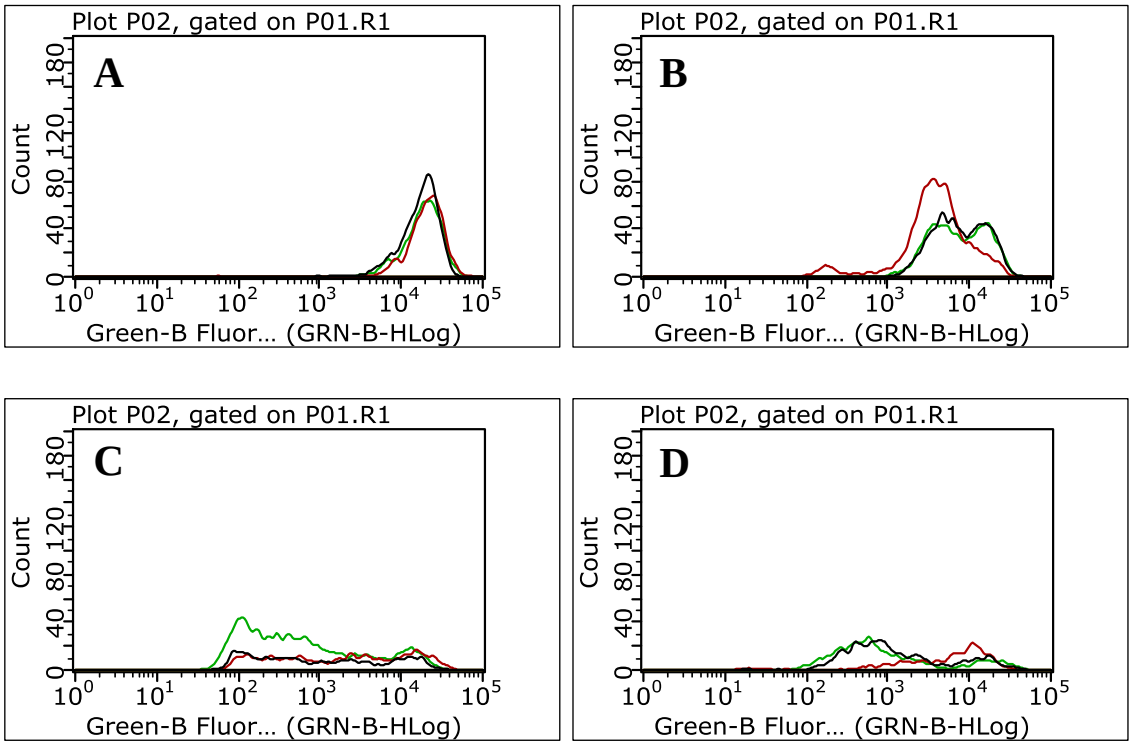

Figure 4.5: Flow cytometric plots showing cell proliferation using CFDA-SE on U87-MG cell line under 5% hypoxia

24 hours (A), 48 hours (B), 72 hours (C), 120 hours (D). Non-treated (black), cisplatin (red), asiatic acid (green). No significant differences in the rate of proliferation of U87-MG cell line were observed.

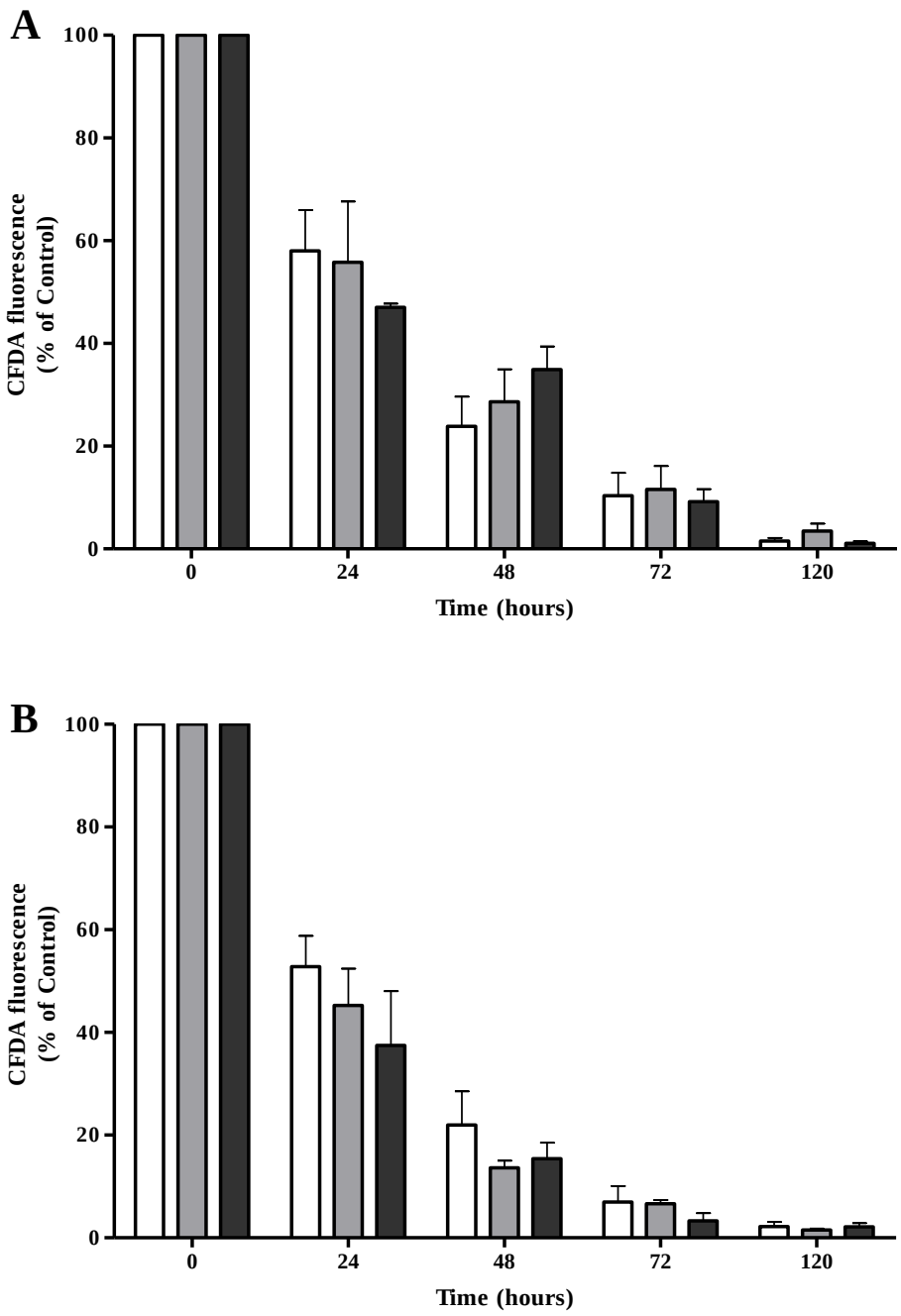

Figure 4.6: Data illustrating the effect of cisplatin and asiatic acid on SVGp12 and U87-MG cell line using CFDA-SE, under 5% hypoxia

Cell proliferation assay on SVGp12 (A) and U87-MG (B) cell lines following 24, 48, 72 and 120 hours of incubation with non-treated (clear), cisplatin (light grey) and asiatic acid (dark grey) was performed using CFDA-SE. A decrease in fluorescence indicates a higher rate of cell proliferation. No significant differences were observed in the rate of proliferation of either of the cell lines with any of the treatments. Values represent mean ± S.E. for three experiments in triplicate.

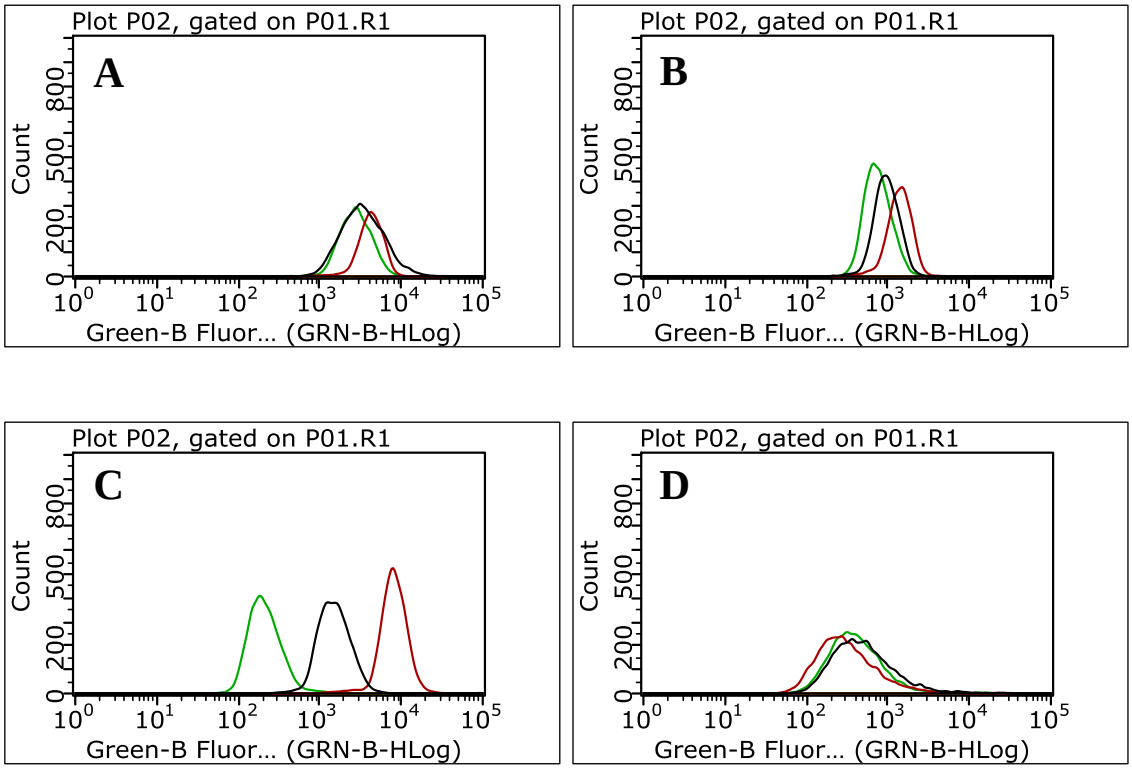

Figure 4.7: Flow cytometric plots showing cell proliferation using CFDA-SE on SVGp12 cell line, under 1% hypoxia

24 hours (A), 48 hours (B), 72 hours (C), 120 hours (D). Non-treated (black), cisplatin (red), asiatic acid (green). No significant differences in the rate of proliferation of SVGp12 cell line were observed.

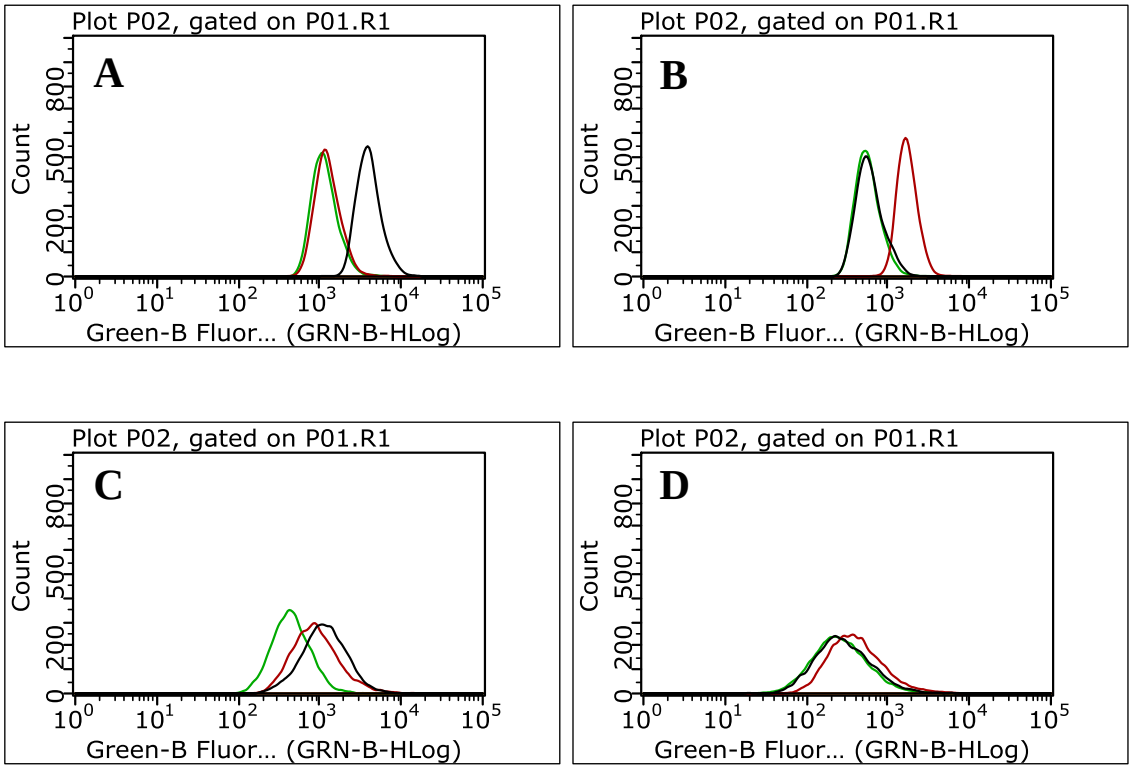

Figure 4.8: Flow cytometric plots showing cell proliferation using CFDA-SE on U87-MG cell line under 1% hypoxia

24 hours (A), 48 hours (B), 72 hours (C), 120 hours (D). Non-treated (black), cisplatin (red), asiatic acid (green). No significant differences in the rate of proliferation of U87-MG cell line were observed.

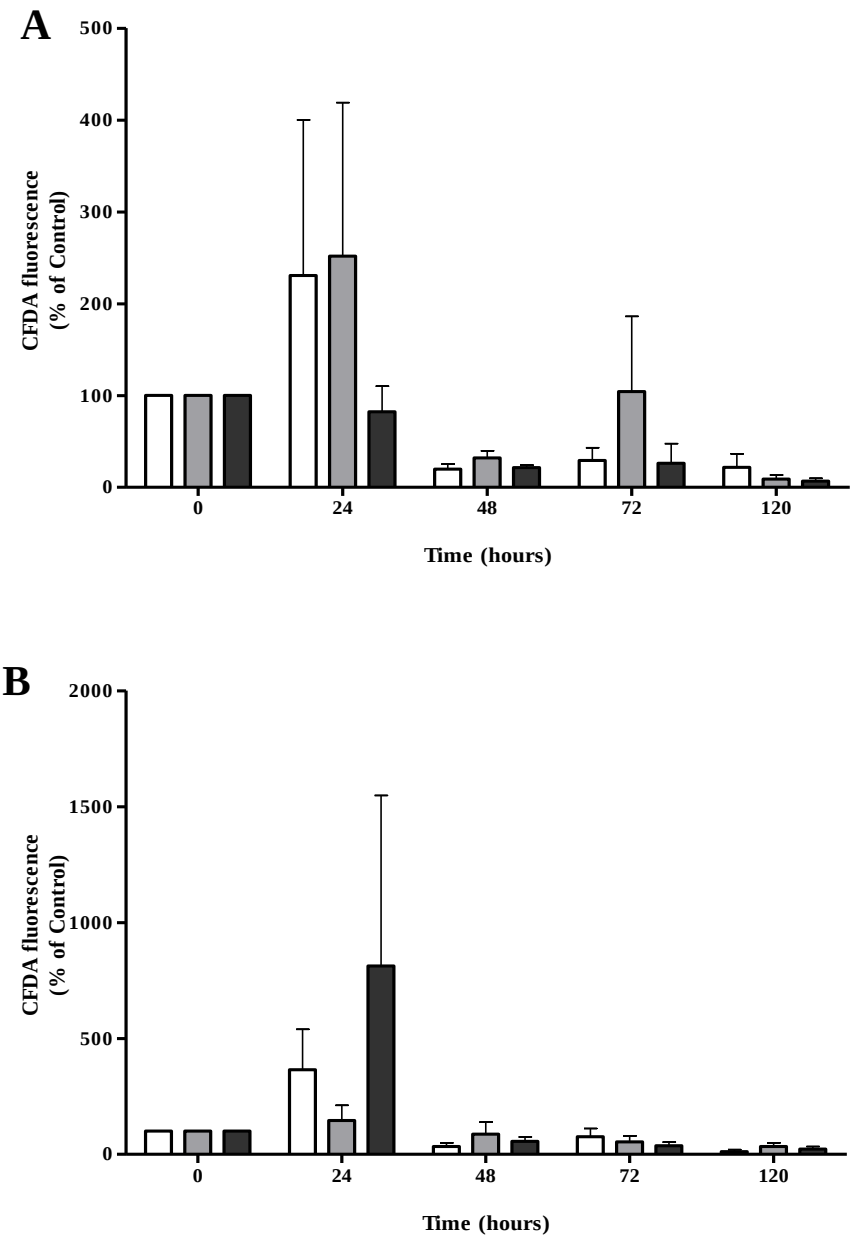

Figure 4.9: Data illustrating the effect of cisplatin and asiatic acid on SVGp12 and U87-MG cell line using CFDA-SE under 1% hypoxia

Cell proliferation assay on SVGp12 (A) and U87-MG (B) cell lines following 24, 48, 72 and 120 hours of incubation with non-treated (clear), cisplatin (light grey) and asiatic acid (dark grey) was performed using CFDA-SE. A decrease in fluorescence indicates a higher rate of cell proliferation. No significant differences were observed in the rate of proliferation of either of the cell lines with any of the treatments. Values represent mean ± S.E. for three experiments in triplicate.

4.2.2 Scratch/wound healing assay

Cell migration is an important factor in determining the malignancy of a tumorous mass. The *in vitro* scratch assay is a way of studying cell migration. When a cell monolayer is wounded or scratched, the cell monolayer responds to the cell-cell disruption by an increased amount of growth factors at the wound site and ultimately results in healing of the wound through cell proliferation and migration. We studied the effects of cisplatin and asiatic acid on the migration of SVGp12 and U87-MG cell lines.

Normoxia

The scratch assay on non-treated SVGp12 and U87-MG cell lines showed a complete closure of the wound after 18 hours (Figs. 4.10-4.12). Cisplatin showed a partial closure of the wound (from 631.07 ± 41.52μm to 333 ± 28.04 μm in SVGp12 and from 574.2 ± 28.72 μm to 233.7 ± 6.69 μm in U87-MG). Asiatic acid treated cells, too, showed a partial closure of wound (from 696.11 ± 30.89 μm to 388.04 ± 9.67 μm in SVGp12 and from 539.28 ± 38.68 μm to 199.52 ± 15.31 μm in U87-MG) following 18 hours of incubation. Statistical analysis of the data could not be performed.

1% hypoxia

The results obtained for cisplatin and asiatic acid under hypoxia were similar to the results obtained under normoxia, however, even the non-treated cells only showed a partial closure of the wound (Figs. 4.13 & 4.14). Wound healing on SVGp12 cells was recorded as 296.46 ± 86.90 μm from an initial 666.28 ± 35.66 μm for the non-treated cells, 205.45 ± 60.07 μm from an initial 676.10 ± 37.23 μm for cisplatin treatment and 454.85 ± 39.22 μm from an initial 740.27 ± 67.80 μm for asiatic acid treatment. Wound healing on U87-MG cells was recorded as 84.65 ± 48.87 μm from an initial 821.01 ± 25.82 μm for the non-treated cells, 250.06 ± 22.14 μm from an initial 742.52 ± 23.00

μm for cisplatin treatment and 483.12 ± 41.62 μm from an initial 869.58 ± 110.85 μm for asiatic acid treatment. No significant differences were observed.

No significant differences were observed between the two cell lines under 1% hypoxia.

Significant difference was observed in the non-treated control of SVGp12 cell line (normoxia 0μm, 1% hypoxia 253.94 ± 48.87 μm; $p < 0.05$).

Due to the experiment being subjective, we faced difficulties in quantifying the data.

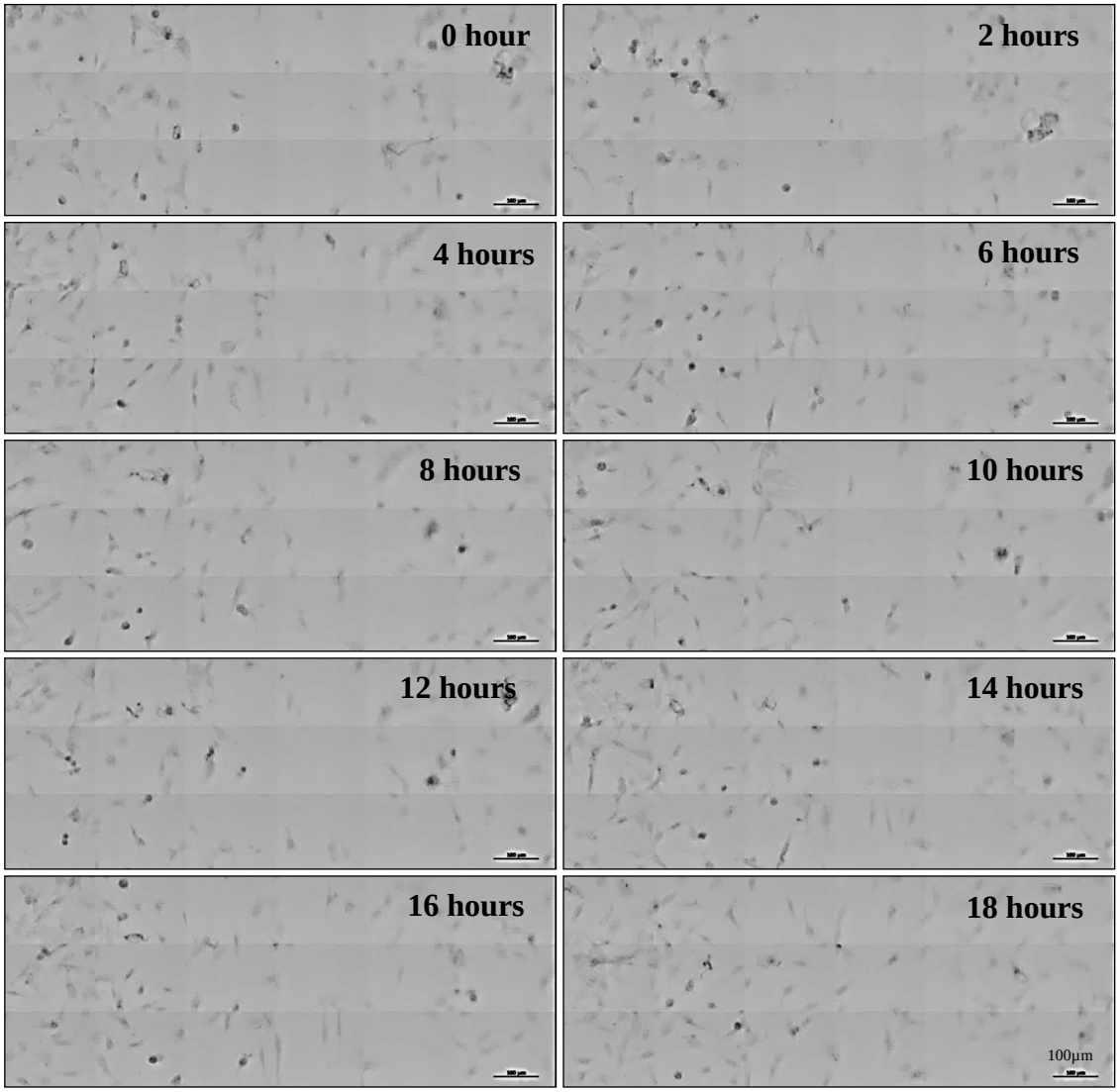

Figure 4.10: Time course imaging of U87-MG cell line showing wound healing over a period of 18 hours, under normoxia

A complete closure of the wound for non-treated U87-MG cells was observed under normoxia at 18 hours.

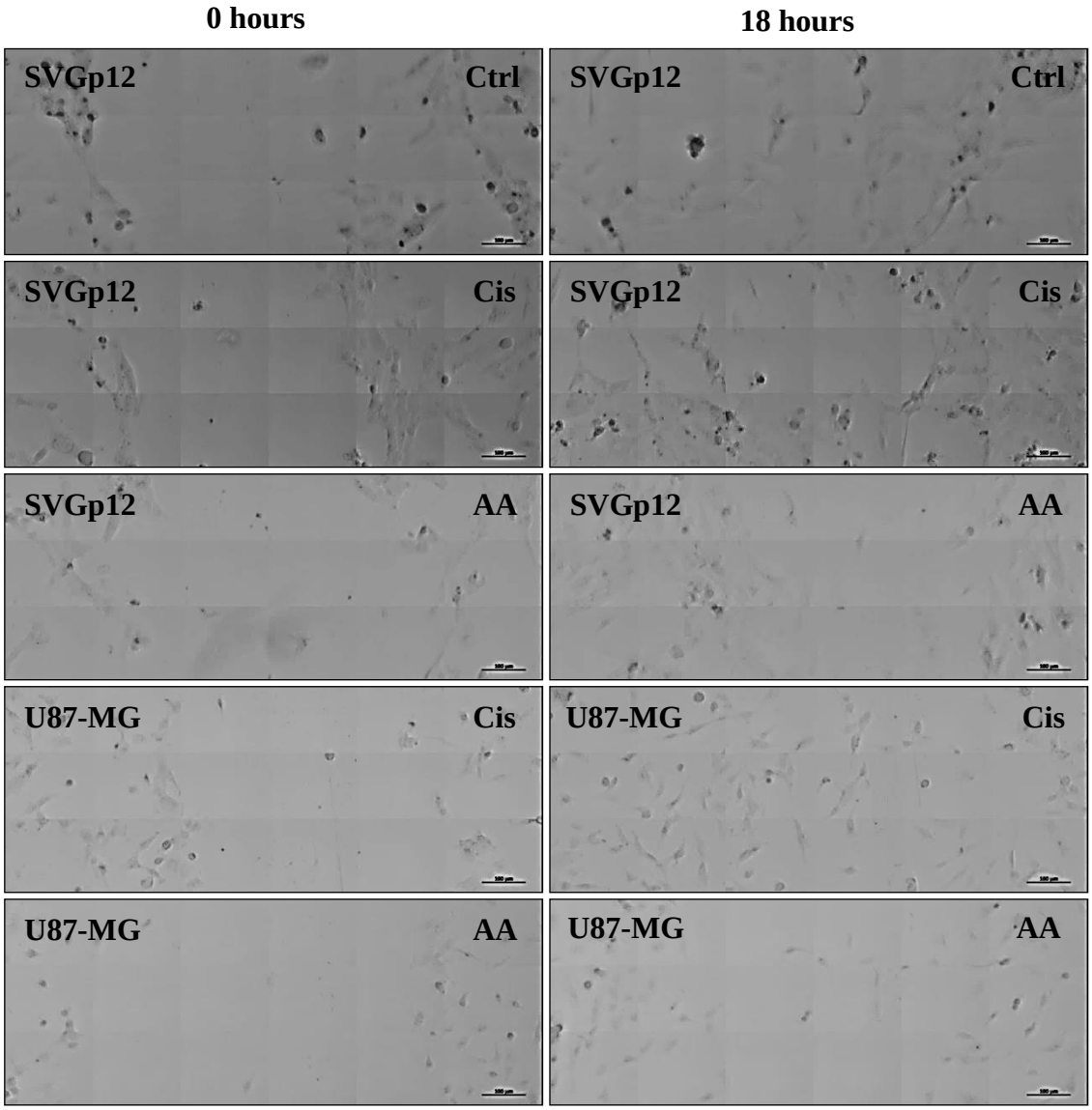

Figure 4.11: Microscopy images showing the scratch/wound healing in SVGp12 and U87-MG cell line following treatment with cisplatin and asiatic acid, under normoxia

Ctrl-control, Cis-cisplatin and AA-asiatic acid. Complete closure of the non-treated SVGp12 and U87-MG cells was observed at 18 hours. Cisplatin showed a partial closure of the wound, whereas asiatic acid did not show any wound healing at all. No significant differences with cisplatin and asiatic acid treatments were observed.

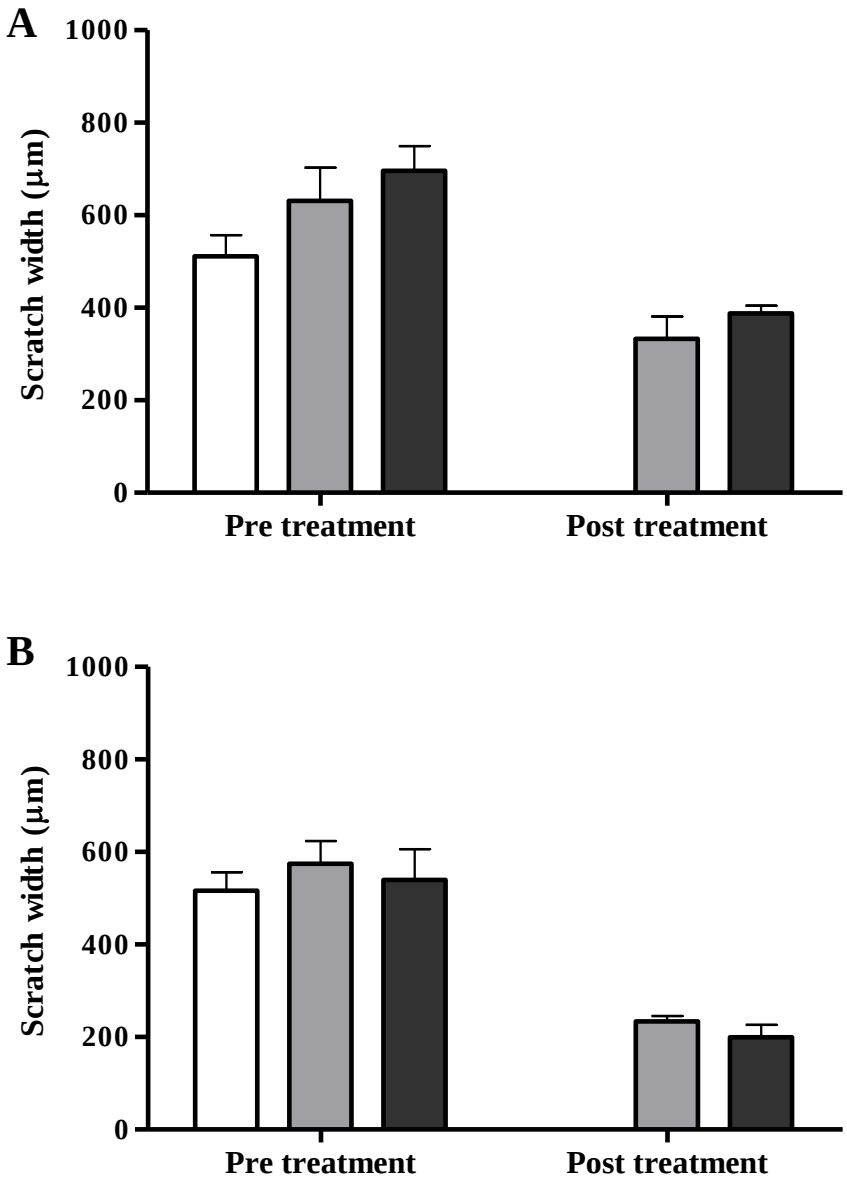

Figure 4.12: Data showing the wound distance measured in SVGp12 and U87-MG cell line following treatments with cisplatin and asiatic acid, under normoxia

Non treated (clear), cisplatin (light grey) and asiatic acid (dark grey). Data shows the wound distance before adding any treatments, followed by 18 hours of incubation with the desired drug. Complete closure of the non-treated SVGp12 (A) and U87-MG (B) cells was observed at 18 hours. Partial wound closure was observed. Statistical analysis of this data could not be performed. Values represent mean ± S.E. for three experiments in triplicate.

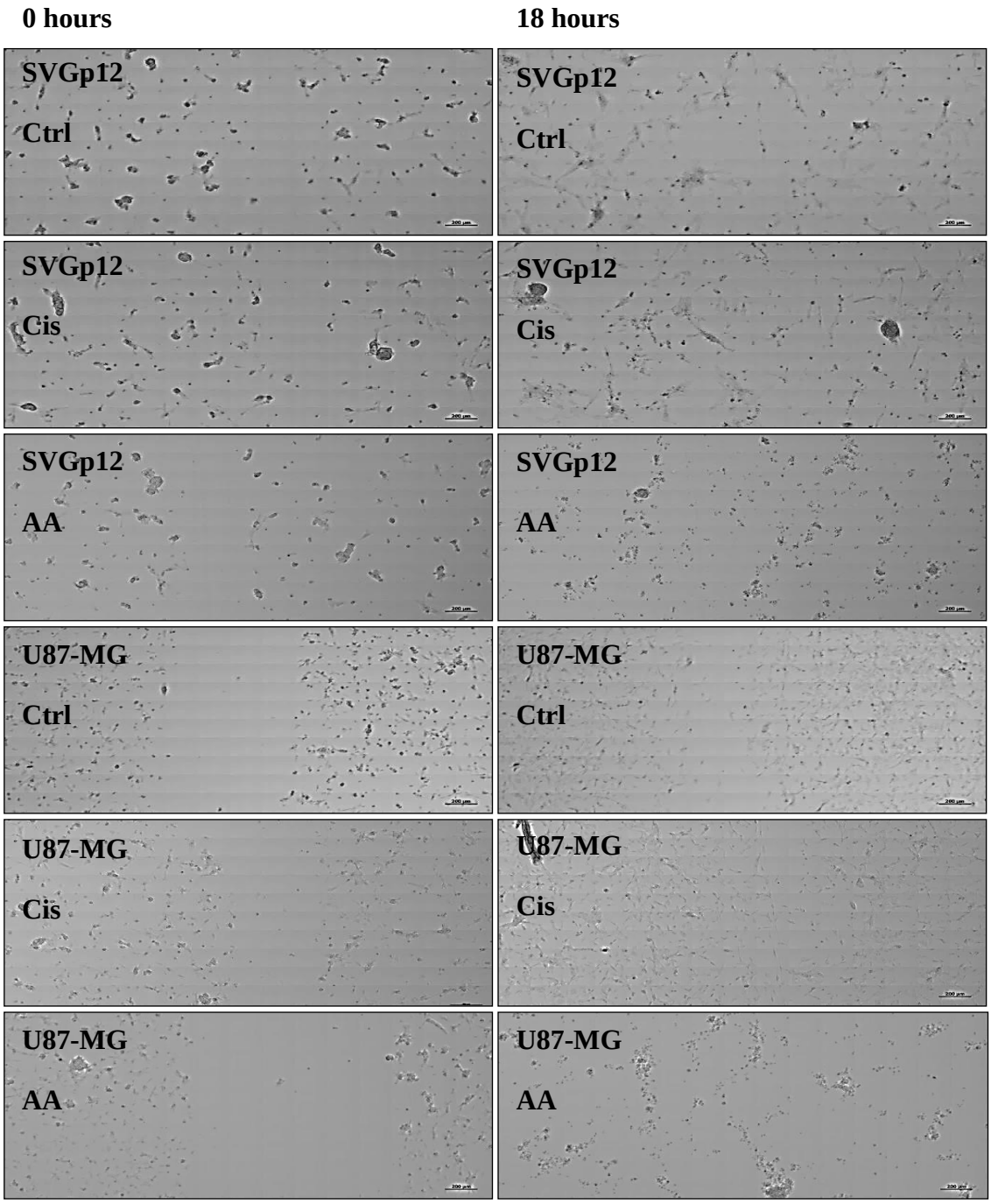

Figure 4.13: Microscopy images showing the scratch/wound healing in SVGp12 and U87-MG cell line following treatment with cisplatin and asiatic acid, under 1% hypoxia

Ctrl-control, Cis-cisplatin and AA-asiatic acid. Partial closure of the wound was observed with the non-treated and cisplatin treated cells, asiatic acid treatment did not show any wound healing at all. No significant differences with cisplatin and asiatic acid treatments were observed.

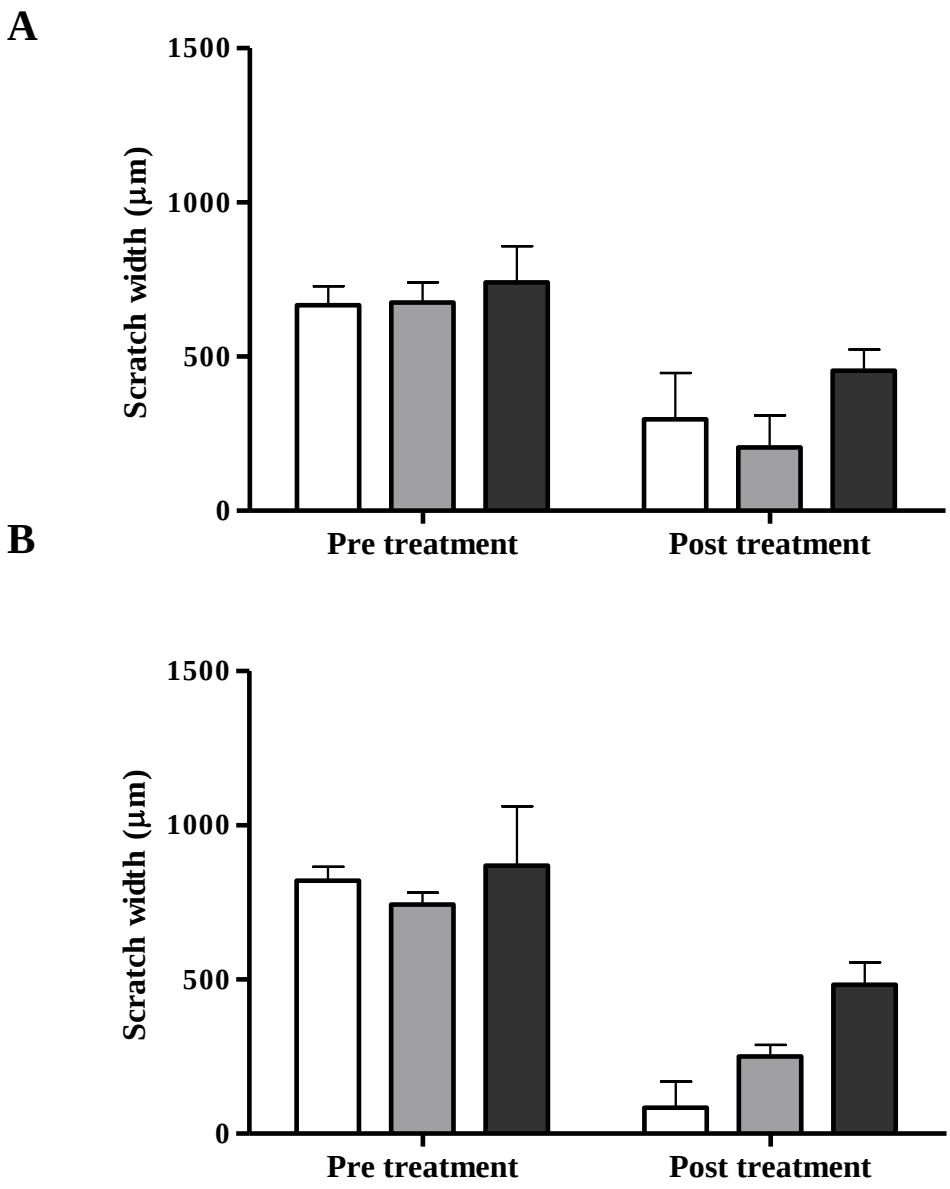

Figure 4.14: Data showing the wound distance measured in SVGp12 and U87-MG cell line following treatments with cisplatin and asiatic acid, under 1% hypoxia

Non treated (clear), cisplatin (light grey) and asiatic acid (dark grey). Data shows the wound distance at 0 hours (pre-treatment), followed by 18 hours of incubation with the desired drug (post-treatment). Partial closure of the wound was observed. No significant differences with cisplatin and asiatic acid treatments were observed. Values represent mean ± S.E. for three experiments in triplicate.

4.2.3 Immunoblotting for EGFR

Amplification of *EGFR* gene is a frequent genetic mutation associated with GBM, and results in the activation of EGFR receptor on cell surfaces. It has been confirmed by previous studies that *EGFR* amplification results in increased proliferation and invasiveness of GBM cells and is an important factor in determining patient prognosis (Montano et al., 2011). In order to assess the changes in the level of EGFR expression following drug treatments, a western blot analysis using immunoblotting was performed on SVGp12 and U87-MG cell lines.

Normoxia

EGFR expression increased in SVGp12 following cisplatin treatment (Fig. 4.15). EGFR expression in cisplatin treated SVGp12 cells was 75.77 ± 6.28% at 24 hours and 125.97 ± 7.76% at the end of 72 hours. EGFR expression for asiatic acid treated cells increased from 92.83 ± 14.84% at 24 hours to 160.58 ± 24.42% at 48 hours and reduced to 70.78 ± 20.78% at the end of 72 hours. No significant differences were observed.

In the U87-MG cell line, EGFR expression in cisplatin treated U87-MG cells was 184.57 ± 13.37% at 24 hours to 107.63 ± 14.98% at the end of 72 hours (Fig. 4.15). EGFR expression for asiatic acid treated cells increased from 62.91 ± 12.14% at 24 hours to 180.22 ± 26.03% at 72 hours. No significant differences were observed.

No significant differences were observed between the two cell lines.

1% hypoxia

EGFR expression in cisplatin treated SVGp12 cells decreased from 79.49 ± 16.07% at 24 hours to 74.33 ± 18.56% at the end of 72 hours (Fig. 4.16). EGFR expression for asiatic acid treated cells decreased from 153.39 ± 63.35% at 24 hours to 136.99 ± 3.92% at the end of 72 hours. No significant differences were observed.

Cisplatin showed a decrease in EGFR expression over time on U87-MG cell line (Fig. 4.16). EGFR activity in cisplatin treated U87-MG cells decreased from 123.76 ± 13.52% at 24 hours to 42.79 ± 7.81% at the end of 72 hours. EGFR activity for asiatic acid treated cells increased from 21.19 ± 3.04% at 24 hours to 74.28 ± 6.47% at the end of 72 hours. No significant differences were observed.

No significant differences were obtained between normoxia and hypoxia.

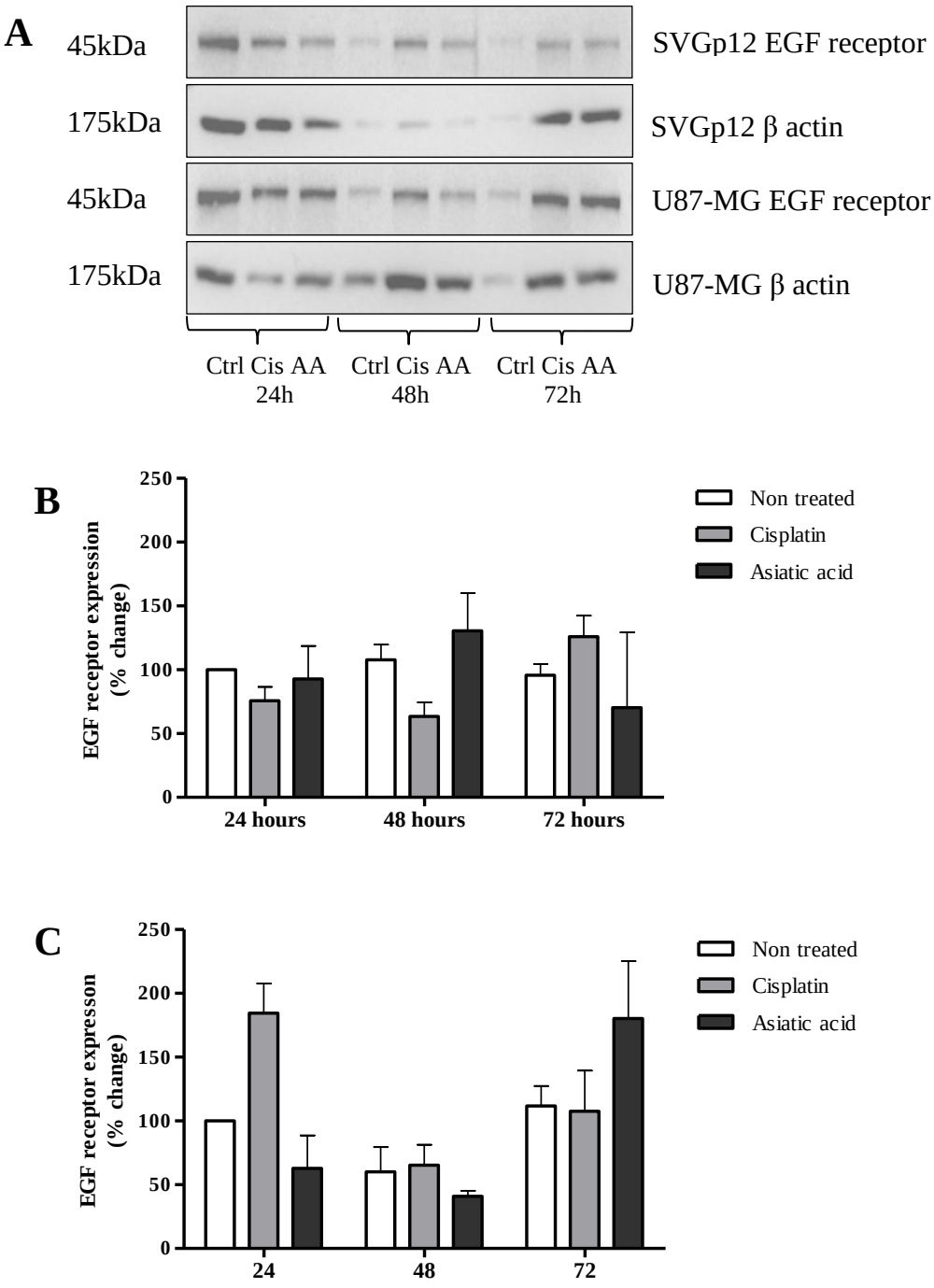

Figure 4.15: Data showing relative levels of EGF receptor expression following 24, 48 and 72 hour treatment with cisplatin and asiatic acid on SVGp12 and U87-MG cell line, under normoxia

(A) Blot images for SVGp12 and U87-MG, (B) SVGp12, (C) U87-MG.

EGF-R expression remained unchanged following cisplatin treatment in SVGp12 cell line, however, a small increase with asiatic acid was observed at 48 hours. Cisplatin showed a small decrease in EGF receptor activity over time on U87-MG cell line, however, no change was observed with asiatic acid. Values represent mean ± S.E. for three experiments in triplicate.

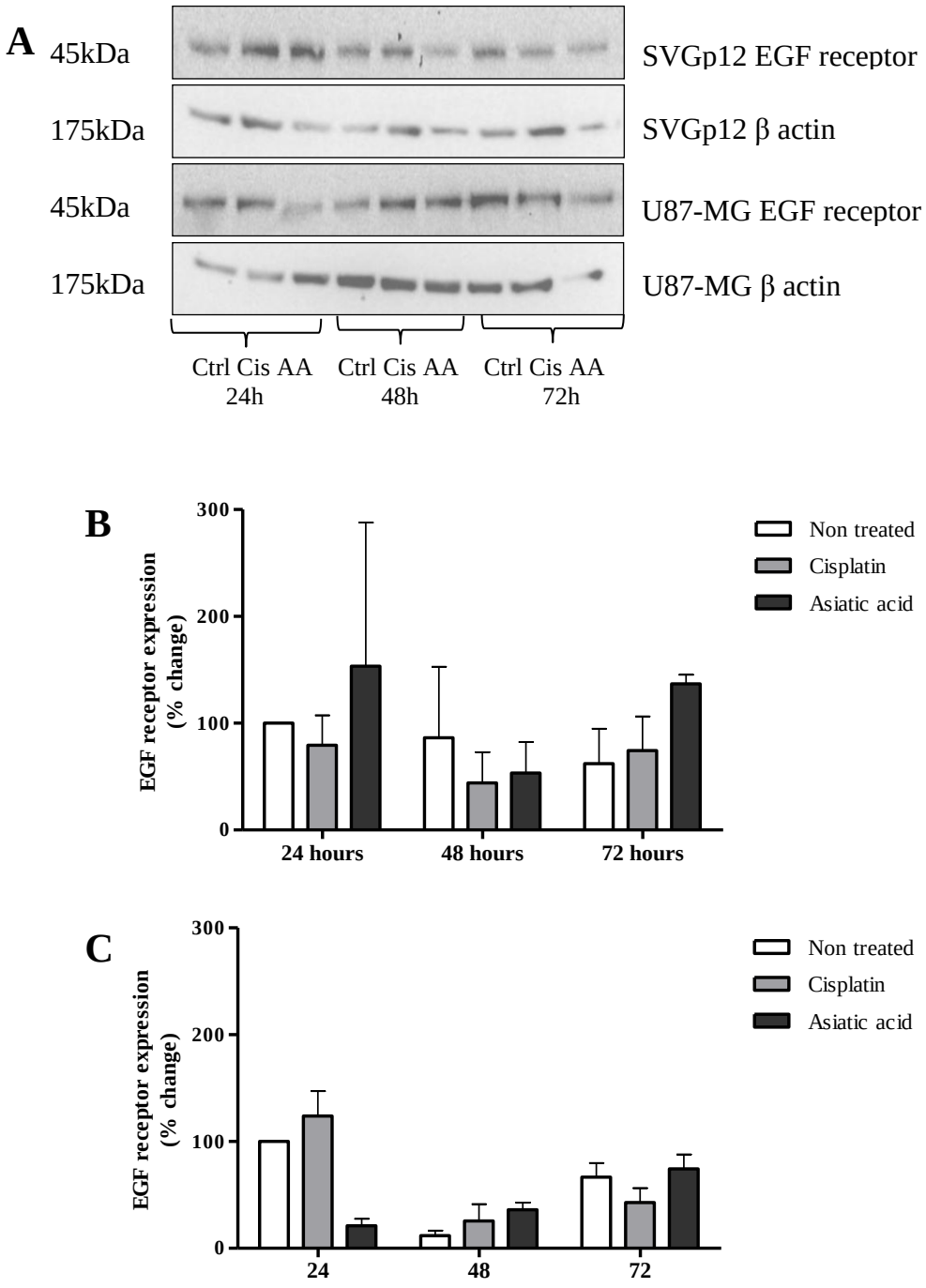

Figure 4.16: Data showing relative levels of EGF receptor expression following 24, 48 and 72 hour treatment with cisplatin and asiatic acid on SVGp12 and U87-MG cell line, under 1% hypoxia

(A) Blot images for SVGp12 and U87-MG, (B) SVGp12, (C) U87-MG.

Cisplatin and asiatic acid showed a reduction in expression of EGF receptor in SVGp12 cell line whereas asiatic acid showed an increase following 72 hours of treatment. A decrease in EGF receptor expression was observed with cisplatin, however, asiatic acid showed an increase in EGF receptor expression following 72 hour treatments in U87-MG cell line. Values represent mean ± S.E. for three experiments in triplicate.

4.2.4 Cell Cycle Analysis

Cell death due to drug treatments can take place *via* apoptosis, necrosis or due to cell cycle arrest. Cell cycle progression is a highly controlled phenomenon and various check-points in the cell cycle assure the entry of only healthy cells into the cell cycle and thus its proliferation. To investigate whether cisplatin and asiatic acid had any effects on cell cycle arrest in SVGp12 and U87-MG cell lines, a cell cycle analysis of was performed under normoxia and hypoxia (1% and 5%).

Normoxia

Cell cycle analysis of SVGp12 and U87-MG cell lines under normoxia showed differences in the cell cycle stages following drug treatments. Significant increase in G2/M population of cisplatin treated cells were observed at 24 (control 54.8 ± 1.7%, cisplatin 61.5 ± 1.4%; $p < 0.001$) and 48 (control 49.2 ± 1.1%, cisplatin 60.1 ± 2.8%; $p < 0.001$) while a significant decrease at 120 (control 49.8 ± 1.6%, cisplatin 44.1 ± 0.6%; $p < 0.001$) hours was observed (Figs. 4.17 & 4.18). Treatment with asiatic acid showed a higher percentage of cells in the S-G2/M transition of the cell cycle. Significant decrease was observed in G2/M cell population following 72 hours of asiatic acid treatment (control 48.5 ± 0.6%, asiatic acid 45.0 ± 0.6%; $p < 0.05$).

Cisplatin treatment on U87-MG cell line, when compared to control, showed a high percentage of cells in the G2/M phase of cell cycle (control 46.5 ± 2.1%, cisplatin 50.8 ± 0.7%, $p < 0.05$) following 24 hours of treatment (Fig.). Significant decrease was observed with cisplatin treatment in the G0/G1 phase of cell cycle following 24 (control 39.4 ± 2.5%, cisplatin 30 ± 1.4%; $p < 0.01$), 48 (control 46.9 ± 2.1, cisplatin 25.3 ± 5.8; $p < 0.001$), 72 hours (control 48.4 ± 0.8, cisplatin 31.8 ± 6.5; $p < 0.05$) and 120 (control 49.0 ± 1.4%, cisplatin 41.8 ± 2.2%; $p < 0.01$) hours. Following 48 hours of treatment, a significant increase was also observed in the G2/M population of cells (control 38.9 ±

1.7, cisplatin 61.1 ± 5.9%; $p < 0.001$). Treatment with asiatic acid showed a high number of cells in the G0/G1 phase and the G2/M phase of the cell cycle. Asiatic acid, at 24 hours, showed 37.7 ± 1.9% cells in the G0/G1 phase and 47.3 ± 1.0% cells in the G2/M phase. Following 120 hours of incubation with asiatic acid, the G0/G1 population increased to 50.6 ± 1.7%, whereas the G2/M population reduced to 35.4 ±1.4%. Asiatic acid did not show any significant differences.

Cisplatin also showed significant increase in the U87-MG cell line following 24 hours treatment in the G0/G1 (SVGp12 17.1 ±8%, U87-MG 30.0 ± 1.4%; $p < 0.001$) and a significant decrease in the G2/M (SVGp12 61.5 ± 1.4%, U87-MG 50.8 ± 0.7%; $p < 0.001$) population of cells (Figs. 4.13-4.15). A significant increase was also observed following 120 hours of cisplatin treatment in G0/G1 population of cells (SVGp12 25.4 ±9%, U87-MG 41.8 ± 2.2%; $p < 0.001$). Asiatic acid showed a significant increase U87-MG cells in the G0/G1 population following 24 (SVGp12 22.4 ± 0.7%, U87-MG 37.7 ±1.9%; $p < 0.001$), 48 (SVGp12 27.4 ± 0.9%, U87-MG 43.2 ± 2.3%; $p < 0.001$), 72 (SVGp12 29.1 ± 0.8%, U87-MG 47.8 ± 1.0%; $p < 0.001$) and 120 (SVGp12 25.9 ± 0.9%, U87-MG 50.6 ± 1.7; $p < 0.001$) hours of incubation. A significant decrease was observed in the G2/M population of cells with asiatic acid treatment at 24 (SVGp12 55.8 ± 1.0%, U87-MG 47.3 ± 1.0%; $p < 0.01$) and at 120 (SVGp12 45.9 ± 2.0%, U87-MG 35.4 ± 1.1; $p < 0.001$).

5% hypoxia

Cisplatin treatment on SVGp12 (Figs. 4.20 & 4.21) cells under 5% hypoxia showed a large number of cells in the S phase of the cell cycle (46.1 ± 2.6% at 24 hours). This was also the case for control (49.6 ± 2.1% at 24 hours) and asiatic acid treated cells (47.3 ± 1.3% at 24 hours). A gradual decrease in the percentage of cells in the S phase was observed by the end of 120 hours. At the end of 120 hours, control,

cisplatin and asiatic acid treated cells showed 29.8 ± 3.5%, 16.9 ± 2.3% and 29.7 ± 3.3% of the total cell population in the S phase. The decrease of the cell population in S phase was directly related to the apoptotic population of cells at the same time and increased over time from 19.8 ± 2.6% at 24 hours to 59 ± 7.3% at 120 hours for cisplatin treatment. Similar was the case for asiatic acid treated cells, 21.6 ± 0.9% at 24 hours to 33.4 ± 4.3% at 120 hours. Statistical analysis of the data did not show any significant differences ($p > 0.05$) in the cell populations of cisplatin or asiatic acid treated cells at any given time.

Cell cycle analysis of U87-MG cell line under 5% hypoxia showed a high percentage of cells in the G0/G1 and S phase of the cell cycle (Figs. 4.20 & 4.22). An increase in the population of cells in the G0/G1 phase, over time, was observed for control, cisplatin and asiatic acid treatments, which correlated directly to a decrease in the S phase population of cells. At 24 hours, non-treated, cisplatin and asiatic acid treatments showed 47 ± 3.3%, 47.6 ± 3.4% and 46.8 ±3.3% cells respectively in the G0/G1 phase. This percentage of cells increased, at the end of 120 hours, to 50.6 ± 2.7% and 55.6 ± 2.6% for control and asiatic acid respectively. Cisplatin showed a decrease in the population of cells, at 120 hours, in G0/G1 phase to 33.8 ± 6.8%; however this was due to the high number of apoptotic cells that were observed. The S phase showed 43.8 ± 3.4%, 40.8 ± 3.2% and 43.2 ± 3.1% cells for control, cisplatin and asiatic acid treatments at 24 hours, respectively. A decrease in the population of cells in the S phase was observed at the end of 120 hours. Control, cisplatin and asiatic acid showed 29.6 ± 1.7%, 26.3 ± 2.6% and 26.7 ± 1.6% of cells in the S phase at 120 hours, respectively. Statistical analysis of the data showed significant reduction in the S phase population of cisplatin treated cells 24 hours (control 43.8 ± 3.4%, cisplatin 40.8 ± 3.2%; $p < 0.05$) and also in the G0/G1 phase of cell population 120 hours (control 50.6 ± 2.7%, cisplatin 33.8 ± 6.8%; $p < 0.01$).

A significant increase in U87-MG cells was observed in the G0/G1 population of cells with cisplatin treatment following 24 (SVGp12 27.1 ± 0.6%, U87-MG 47.6 ± 3.4%; $p < 0.001$), 48 (SVGp12 22.2 ± 2.6%, U87-MG 51.9 ±1.9%; $p < 0.001$), 72 (SVGp12 23.8 ± 3.8%, U87-MG 50.6 ± 3.1%; $p < 0.001$) and 120 (SVGp12 19.0 ± 4.2%, U87-MG 33.8 ± 6.8; $p < 0.001$) hours of incubation. A significant increase was observed in the S phase population of cells following 120 hours of treatment with cisplatin (SVGp12 16.9 ± 2.3%, U87-MG 26.3 ± 2.6%; $p < 0.05$). Asiatic acid showed a significant increase in the G0/G1 population of cells following 24 (SVGp12 26.2 ± 0.7%, U87-MG 46.8 ± 3.3%; $p < 0.001$), 48 (SVGp12 31.3 ± 2.2%, U87-MG 52.7 ± 2.0%; $p < 0.001$), 72 (SVGp12 29.7 ± 2.5%, U87-MG 58.6 ± 2.3%; $p < 0.001$) and 120 (SVGp12 30.9 ± 1.3%, U87-MG 55.6 ± 2.6; $p < 0.001$) hours of incubation.

1% hypoxia

A large number of SVGp12 cells were observed in the G2/M phase of cell cycle under 1% hypoxia (Figs. 4.23 & 4.24). An increase in the cell population was observed in the G0/G1 phase from 24 to 72 hours. Control, cisplatin and asiatic acid treatments showed 31 ±.9%, 18.9 ± 1.0% and 31.8 ± 1.2% cells, respectively, in the G0/G1 phase at 24 hours which increased to 35 ± 1.0%, 34.9 ± 1.3% and 35.2 ± 1.1%, respectively, at the end of 72 hours. A decrease in the cell population from G0/G1 phase to 20.6 ± 0.6%, 26 ± 0.7% and 23.1 ± 0.2% was observed at 120 hours, for control, cisplatin and asiatic acid respectively. This decrease in the population correlated directly, to an increase in the apoptotic cell percentage at the end of 120 hours. On the other hand, cisplatin showed a decrease in the population of cells in G2/M phase from 62.3 ± 1.0% at 24 hours to 50.4 ± 0.9% at 120 hours. Control and asiatic acid treatments showed 50 ± 0.7% and 51.3 ±.6% cells, respectively, in the G2/M phase at 24 hours and 55.6 ± 1.1% and 50.4 ± 0.9% cells, respectively, at the end of 120 hours. A significant decrease was observed with cisplatin treatment in the G0/G1 phase of cell cycle following 24

(control 31.0 ± 1.9%, cisplatin 18.9 ± 1.0%; $p < 0.001$) while a significant increase was observed following 120 (control 20.6 ± 0.6%, cisplatin 26.0 ± 0.7%; $p < 0.01$) hours of incubation. A significant increase with cisplatin treatment was observed in the G2/M population of cells following 24 (control 50.0 ± 0.7%, cisplatin 62.3 ± 1.0%; $p < 0.001$) while a significant decrease was observed following 120 (control 55.6 ± 1.1%, cisplatin 49.8 ± 1.7%; $p < 0.001$) hours of incubation. Asiatic acid treatments showed no significant differences ($p > 0.05$) at any cell cycle phase at any given time.

Cell cycle analysis of U87-MG cell line showed a high number of cells in the G0/G1 and G2/M phase of cell cycle (Fig. 4.23 & 4.25). Cisplatin treatment showed an increase in the cell population of G0/G1 phase from 43.8 ± 1.6% at 24 hours to 48.2 ± 1.0% at 120 hours. However, control and asiatic acid treatments showed a decrease in the cell population from 24 hours to 120 hours in the G0/G1 phase, 57.4 ± 0.7% to 53.3 ± 1.7% for control and 54.5 ± 2.9% to 52.1 ± 0.8% for asiatic acid. This decrease in the cell population correlated to an increase in the G2/M phase of the cell population. Asiatic acid showed 30.2 ± 0.2% cells at 24 hours with an increase to 35 ± 0.1% at 120 hours in the G2/M phase. On the contrary, cisplatin showed a decrease in the cell population of G2/M from 40.4 ± 1.0% at 24 hours to 37.3 ± 0.4% at 120 hours. A significant decrease was observed following cisplatin treatment in the G0/G1 phase of cell cycle at 24 (control 57.4 ± 0.7%, cisplatin 43.8 ± 1.6; $p < 0.001$), 48 (control 57.3 ± 1.2%, cisplatin 49.1 ± 3.2%; $p < 0.01$), 72 (control 54.2 ± 0.9, cisplatin 51.9 ± 1.9; $p < 0.01$) and 120 (control 53.3 ± 1.7, cisplatin 48.2 ± 1.0%; $p < 0.001$) hours. A significant increase was observed following cisplatin treatment in the G2/M phase at 24 (control 30.9 ± 0.1%, cisplatin 40.4 ± 0.1%; $p < 0.001$), 48 (control 31.2 ± 0.8%, cisplatin 39.8 ± 2.615; $p < 0.001$), 72 (control 32.3 ± 0.8%, cisplatin 34.8 ± 1.0%; $p < 0.01$) and 120 (control 34.6 ±8%, cisplatin 37.3 ± 0.4%; $p < 0.05$) hours. Asiatic acid treatments showed no significant differences ($p > 0.05$) in any cell cycle phase at any given time.

Under 1% hypoxia, a significant increase was seen in U87-MG cell line in the G0/G1 population of cells with cisplatin treatment following 24 (SVGp12 18.9 ± 1.0%, U87-MG 43.8 ± 1.6%; $p < 0.001$), 48 (SVGp12 28.9 ± 1.3%, U87-MG 49.1 ± 3.2%; $p < 0.001$), 72 (SVGp12 34.9 ± 1.3%, U87-MG 51.5 ± 1.9%; $p < 0.001$) and 120 (SVGp12 26.0 ± 0.7%, U87-MG 48.2 ± 1.0%; $p < 0.001$) hours of incubation. A significant reduction was observed in the G2/M phase of the cell cycle with cisplatin treatment following 24 (SVGp12 62.3 ± 1.0%, U87-MG 40.4 ± 1.0%; $p < 0.001$), 48 (SVGp12 56.5 ± 1.5%, U87-MG 39.8 ± 2.6%; $p < 0.001$) and 72 (SVGp12 47.7 ± 0.7%, U87-MG 34.8 ± 1.0%; $p < 0.05$) hours of incubation. A significant increase with asiatic acid treatment in the G0/G1 phase of cell cycle was observed following 24 (SVGp12 31.8 ± 1.2%, U87-MG 54.5 ± 2.9%; $p < 0.001$), 48 (SVGp12 36.0 ± 1.7%, U87-MG 59.5 ± 0.9%; $p < 0.001$), 72 hours (SVGp12 35.2 ± 1.1%, U87-MG 55.6 ± 0.8%; $p < 0.001$) and 120 (SVGp12 23.1 ± 0.2%, U87-MG 52.1 ± 0.8%; $p < 0.001$) hours of incubation. Asiatic acid also showed significant reduction in the G2/M population of cells following 24 (SVGp12 51.3 ± 0.6%, U87-MG 30.2 ±0.2%; $p < 0.001$), 48 (SVGp12 48.1 ± 1.2, U87-MG 28.5 ± 0.7%; $p < 0.001$), 72 (SVGp12 46.8 ± 1.1%, U87-MG 31.5 ± 0.7%; $p < 0.01$) and 120 (SVGp12 50.4 ± 0.9, U87-MG 35.0 ± 0.1%; $p < 0.01$) hours of incubation.

Statistical analysis of the data at 5% hypoxia revealed significant reduction with cisplatin treatment in the G2/M population of SVGp12 cell line. These differences were observed following 24 (normoxia 61.5 ±1.4%, 5% hypoxia 7 ± 1.1%; $p < 0.001$), 48 (normoxia 60.1 ± 2.8%, 5% hypoxia 4.7 ± 0.3%; $p < 0.001$), 72 (normoxia 47.6 ± 1.2%, 5% hypoxia 5.9 ± 0.2%; $p < 0.001$) and 120 (normoxia 44.1 ± 0.6%, 5% hypoxia 5.0 ± 1.0%; $p < 0.001$) hours of incubation. A significant increase was observed in the S phase population of cisplatin treated cells following 24 (normoxia 7.1 ± 0.4%, 5% hypoxia 46.1 ± 2.6%; $p < 0.001$), 48 (normoxia 6.2 ± 0.2%, 5% hypoxia 41.2 ± 3.9%; p

< 0.001) and 72 (normoxia 7.6 ± 0.4%, 5% hypoxia 24.5 ± 1.4; $p < 0.01$) hours of incubation. Asiatic acid treatment showed significant increase in S phase population of SVGp12 cells following 24 (normoxia 6.8 ± 0.2%, 5% hypoxia 47.3 ± 1.3%; $p < 0.001$), 48 (normoxia 8.9 ± 0.9%, 5% hypoxia 28.1 ± 1.3%; $p < 0.001$), 72 (normoxia 8.8 ± 0.6%, 5% hypoxia 25.6 ± 1.8; $p < 0.001$) and 120 (normoxia 7.5 ± 0.5%, 5% hypoxia 29.7 ±3.3%; $p < 0.001$) hours of incubation. A significant decrease was observed in the G2/M population of SVGp12 cells with asiatic acid treatment following 24 (normoxia 55.8 ± 1.0%, 5% hypoxia 5.1 ± 0.2%; $p < 0.001$), 48 (normoxia 45.4 ± 0.8%, 5% hypoxia 4.7 ± 0.4%; $p < 0.001$) 72 (normoxia 45.0 ± 0.6%, 5% hypoxia 4.6 ± 0.3%; $p < 0.001$) and 120 (normoxia 45.9 ± 0.2%, 5% hypoxia 6.0 ± 0.7%; $p < 0.001$) hours of incubation. Cisplatin showed a significant increase in the S phase population of U87-MG cells following 24 (normoxia 10.8 ± 1.8%, 5% hypoxia 40.8 ± 3.2%; $p < 0.001$), 48 (normoxia 6.2 ± 0.4%, 5% hypoxia 36.5 ± 1.2%; $p < 0.001$), 72 hours (normoxia 6.8 ± 0.6%, 5% hypoxia 30.3 ± 1.2%; $p < 0.001$) and 120 hours (normoxia 6.4 ± 0.4%, 5% hypoxia 26.3 ± 2.6%; $p < 0.001$) hours of incubation. A significant decrease was observed in the G2/M population of cisplatin treated U87-MG cells following 24 (normoxia 50.8 ± 0.7%, 5% hypoxia 7.3 ± 0.5%; $p < 0.001$), 48 (normoxia 61.1 ± 5.9%, 5% hypoxia 7.4 ± 0.7%; $p < 0.001$), 72 (normoxia 51.6 ± 5.7%, 5% hypoxia 8.0 ± 0.9%; $p < 0.001$) and 120 (normoxia 37.6 ± 1.4%, 5% hypoxia 10.1 ± 0.7%; $p < 0.001$) hours of incubation. Asiatic acid showed a significant increase in the S phase population of U87-MG cells following 24 (normoxia 7.7 ± 0.7%, 5% hypoxia 43.2 ± 3.1%; $p < 0.001$), 48 (normoxia 6.4 ± 0.4%, 5% hypoxia 35.3 ± 1.4%; $p < 0.001$), 72 (normoxia 7.4 ± 0.4%, 5% hypoxia 26.1 ± 0.8%; $p < 0.001$) and 120 (normoxia 6.1 ± 0.4%, 5% hypoxia 26.7 ± 1.6%; $p < 0.001$) hours of incubation. A significant decrease was also observed in the G2/M population of asiatic acid treated U87-MG cells following 24 (normoxia 47.3 ± 1.0%, 5% hypoxia 6.8 ± 0.6%; $p < 0.001$), 48 (normoxia 42.5 ± 2.4%,

5% hypoxia 6.9 ± 0.1%; $p < 0.001$), 72 (normoxia 37.2 ± 1.3%, 5% hypoxia 5.4 ± 0.4%; $p < 0.001$) and 120 (normoxia 35.4 ± 1.1, 5% hypoxia 5.6 ± 0.6%; $p < 0.001$) hours of incubation.

Statistical analysis of the data at 1% hypoxia revealed a significant increase with cisplatin treatment in the G0/G1 population of U87-MG cell line. These differences were observed following 24 (normoxia 30.0 ± 1.4%, 1% hypoxia 43.8 ± 1.6%; $p < 0.01$), 48 (normoxia 25.3 ± 5.8%, 1% hypoxia 49.1 ± 3.2; $p < 0.001$) and 72 (normoxia 31.8 ±.5%, 1% hypoxia 51.9 ± 1.5%; $p < 0.001$) hours of incubation. Cisplatin also showed a significant decrease in the G2/M population of U87-MG cells following 48 (normoxia 61.1 ± 5.9%, 1% hypoxia 49.1 ±3.2%; $p < 0.001$) and 72 (normoxia 51.6 ± 5.7%, 1% hypoxia 34.8 ± 1.0%; $p < 0.001$) hours of incubation. Asiatic acid showed a significant increase in the G0/G1 population of U87-MG cells following 24 (normoxia 37.7 ± 1.9%, 1% hypoxia 54.5 ± 2.9%; $p < 0.001$) and 48 (normoxia 43.2 ± 2.3%, 1% hypoxia 59.5 ± 0.5%; $p < 0.001$) hours of incubation. A significant decrease with asiatic acid treatment was observed in the G2/M population of U87-MG cells following 24 (normoxia 47.3 ±1.0%, 1% hypoxia 30.2 ± 0.2%; $p < 0.001$) and 48 (normoxia 42.5 ± 2.4%, 1% hypoxia 28.5 ± 0.7%; $p < 0.01$) hours of incubation.

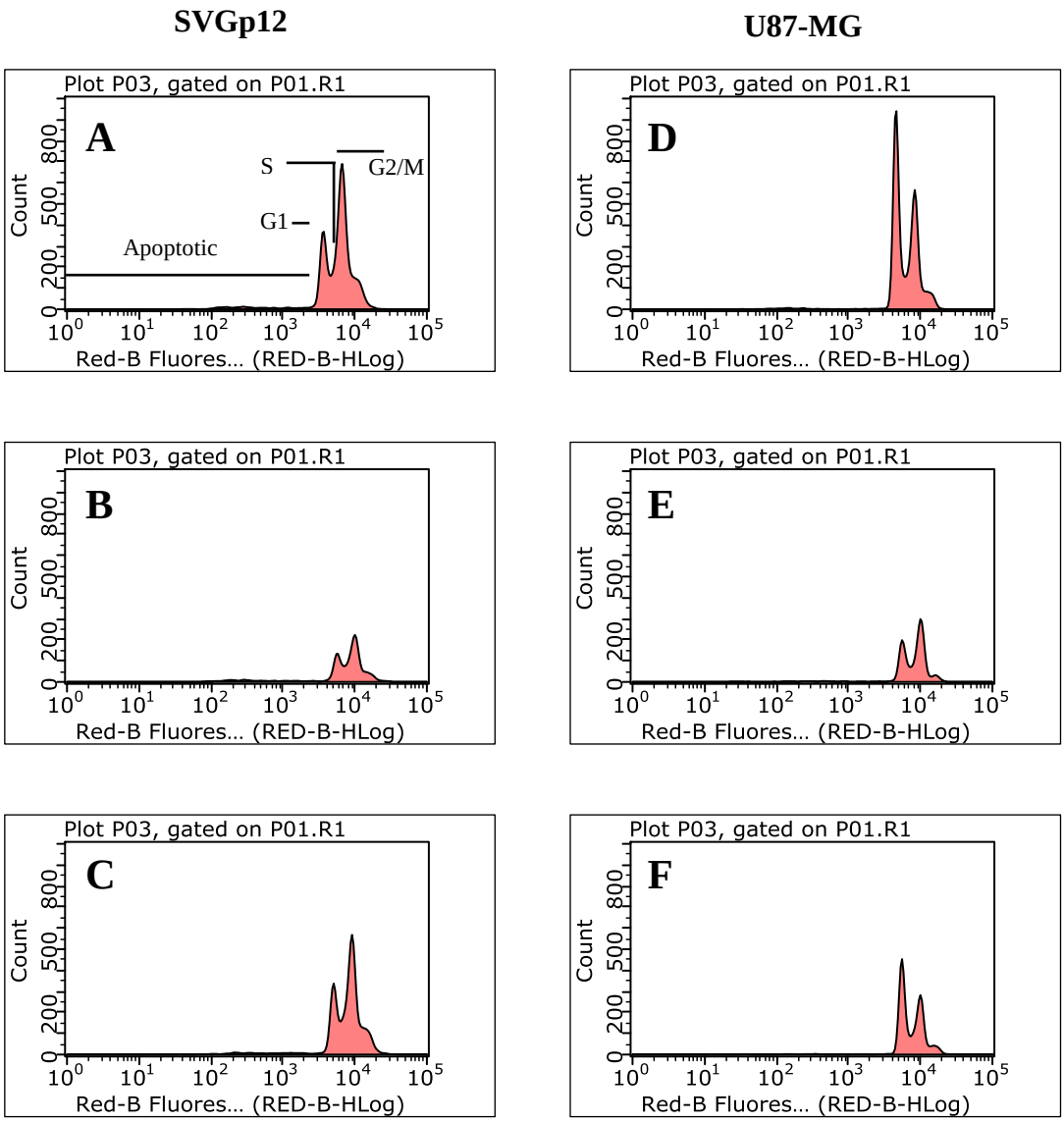

Figure 4.17: Flow cytometric plots showing cell cycle analysis using RNase and propidium iodide on SVGp12 and U87-MG cell lines following 120 hours of incubation, under normoxia

Flow cytometry analysis of SVGp12 (A-C) and U87-MG (D-F) cells on non-treated (A, D), cisplatin (B, E) and asiatic acid (C, F). Cisplatin showed G2/M phase arrest on both cell lines, asiatic acid showed S-G2/M arrest on SVGp12 and G0/G1 arrest on U87-MG cells.

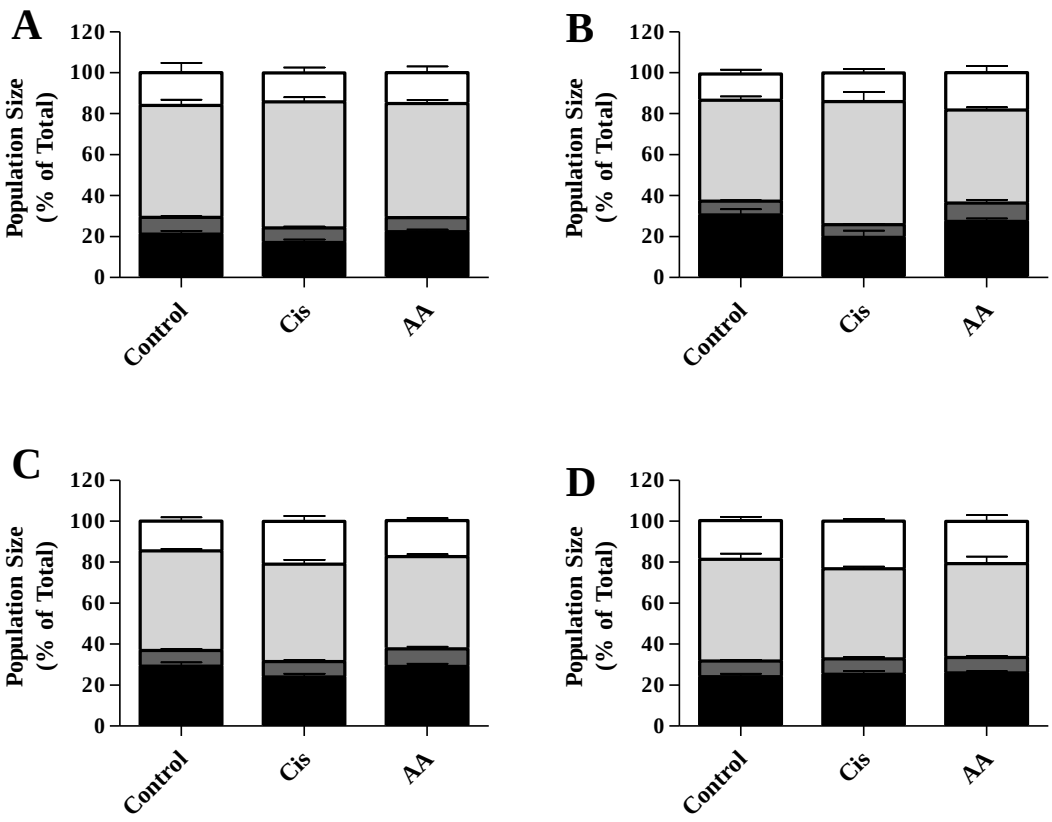

Figure 4.18: Data illustrating the effect of cisplatin and asiatic acid treatments on the cell cycle progression of SVGp12 cell line under normoxia

Cell cycle study was performed on SVGp12 cell line following 24 (A), 48 (B), 72 (C) and 120 (D) hours of treatment. Data shows relative proportions of cells in G0/G1 phase (black), S phase (dark grey), G2/M phase (light grey) and apoptotic population (colourless). Cisplatin showed G2/M phase arrest while asiatic acid showed G0/G1 arrest on SVGp12 cells. Statistical analysis did not show any differences in the G0/G1 phase of the cell cycle for any treatments. Values represent mean ± S.E. for three experiments in triplicate.

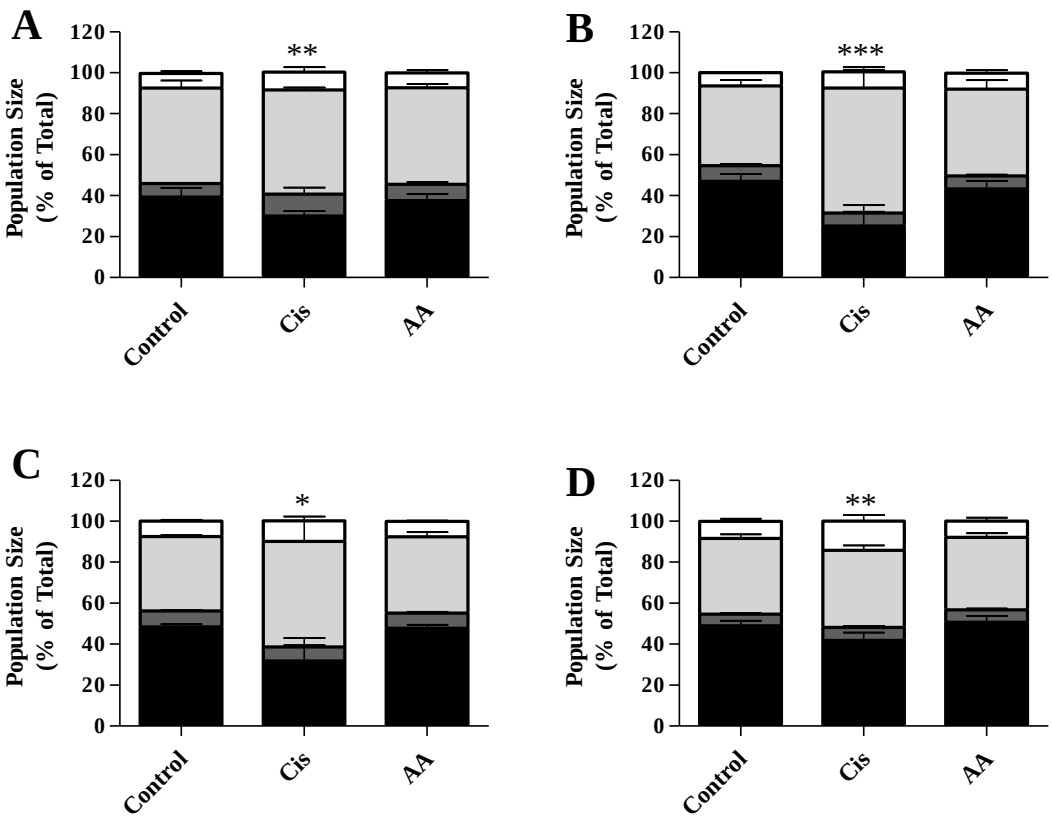

Figure 4.19: Data illustrating the effect of cisplatin and asiatic acid treatments on the cell cycle progression of U87-MG cell line under normoxia

Cell cycle study was performed on U87-MG cell line following 24 (A), 48 (B), 72 (C) and 120 (D) hours of treatment. Data shows relative proportions of cells in G0/G1 phase (black), S phase (dark grey), G2/M phase (light grey) and apoptotic population (colourless). Cisplatin showed G2/M phase arrest while asiatic acid showed S-G2/M arrest on U87-MG cells. Significant differences in the G0/G1 population of cells have been displayed. Values represent mean ± S.E. for three experiments in triplicate.

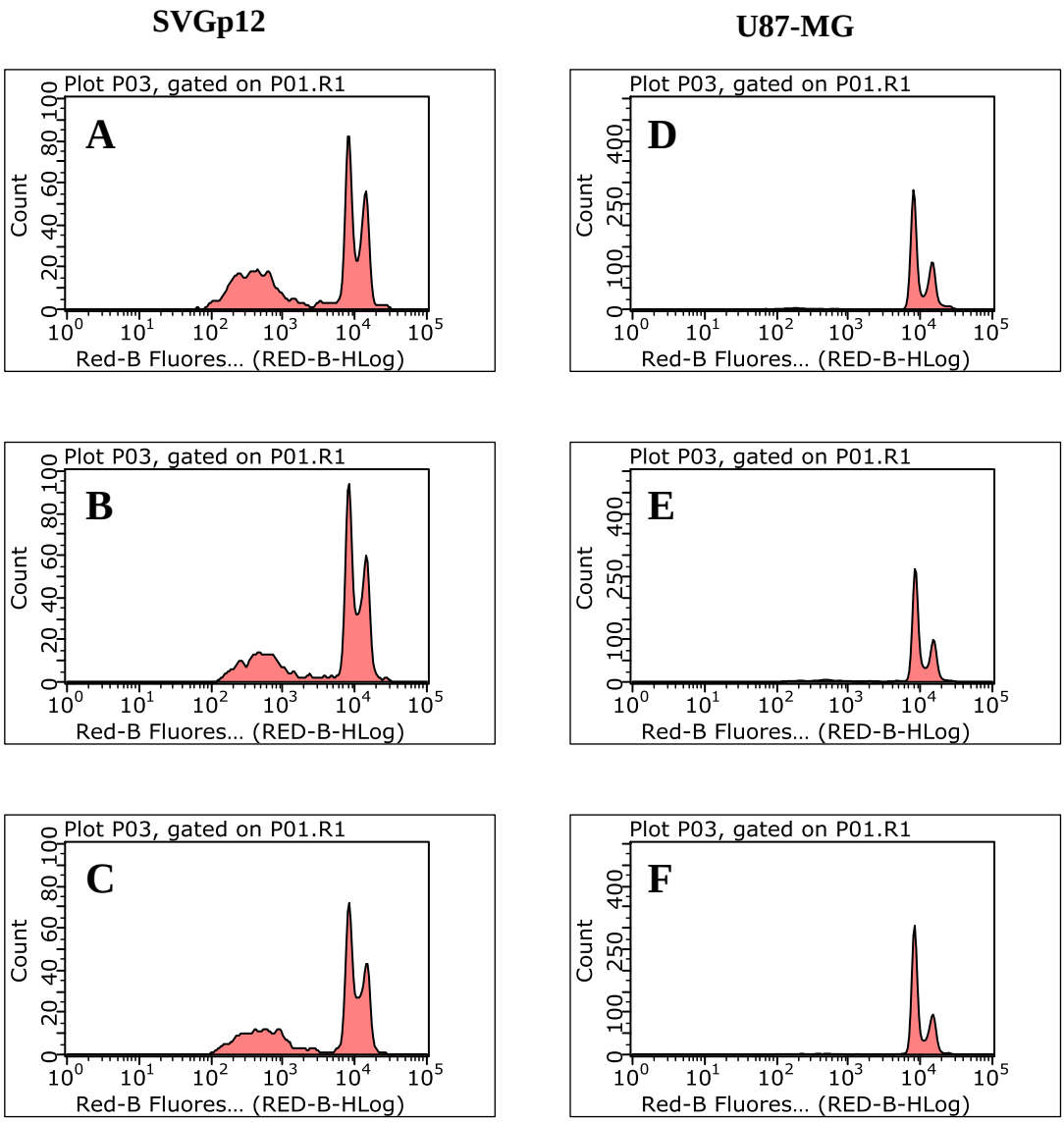

Figure 4.20: Flow cytometric plots showing cell cycle analysis using RNase and propidium iodide on SVGp12 and U87-MG cell lines following 120 hours of incubation, under 5% hypoxia

Flow cytometry analysis of SVGp12 (A-C) and U87-MG (D-F) cells on non-treated (A, D), cisplatin (B, E) and asiatic acid (C, F). A transient S phase arrest was observed for SVGp12 cell line while U87-MG cell line showed a large population of cells under G0/G1 phase.

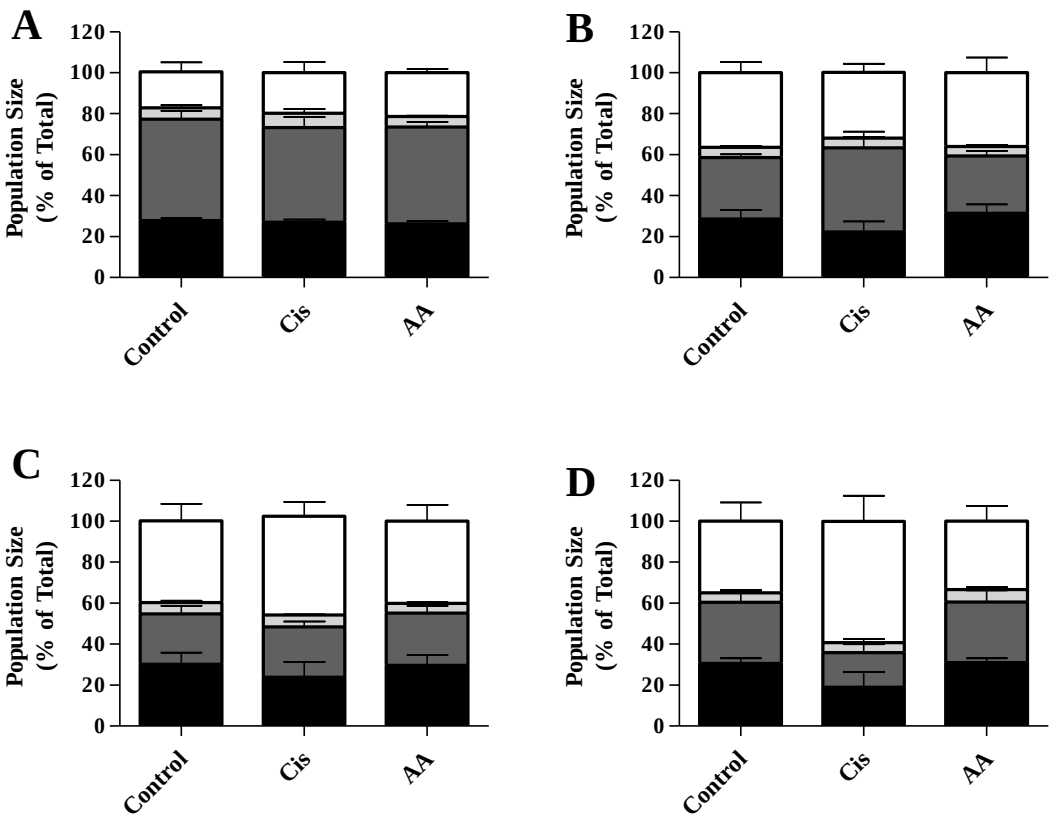

Figure 4.21: Data illustrating the effect of cisplatin and asiatic acid treatments on the cell cycle progression of SVGp12 cell line under 5% hypoxia

Cell cycle study was performed on SVGp12 cell line following 24 (A), 48 (B), 72 (C) and 120 (D) hours of treatment. Data shows relative proportions of cells in G0/G1 phase (black), S phase (dark grey), G2/M phase (light grey) and apoptotic population (colourless). A transient S phase arrest was observed for SVGp12 cell line. No significant differences were observed. Values represent mean ± S.E. for three experiments in triplicate.

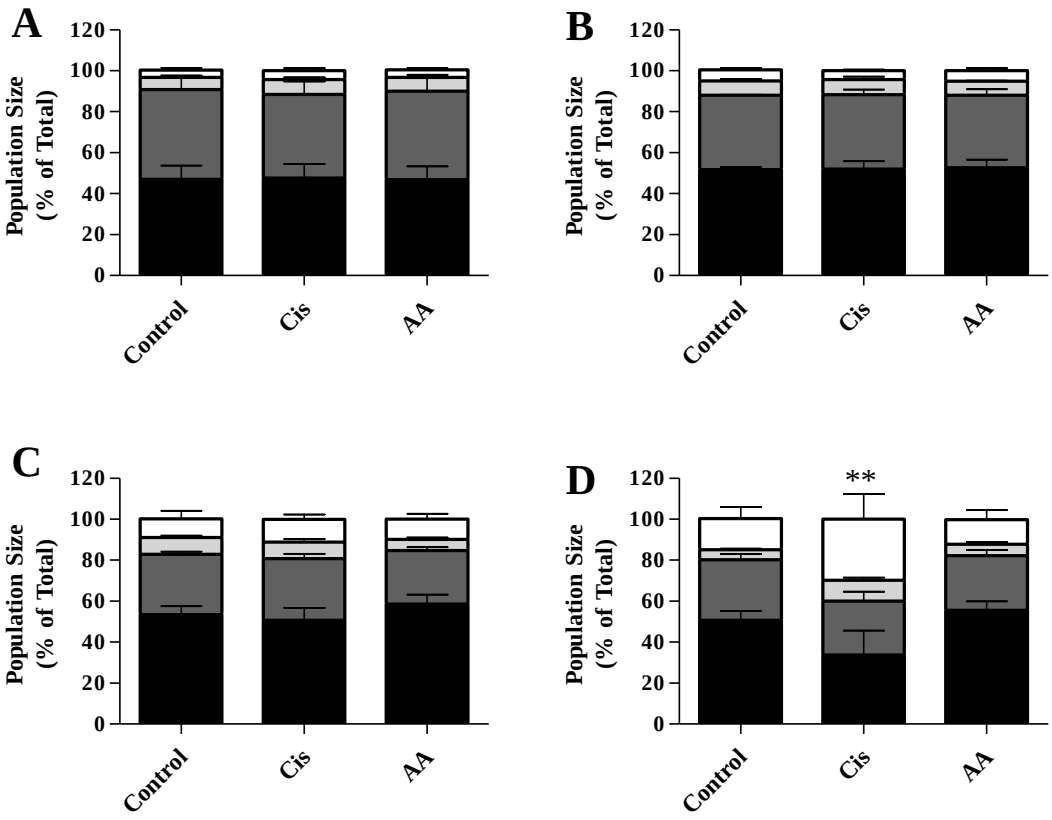

Figure 4.22: Data illustrating the effect of cisplatin and asiatic acid treatments on the cell cycle progression of U87-MG cell line under 5% hypoxia

Cell cycle study was performed on U87-MG cell line following 24 (A), 48 (B), 72 (C) and 120 (D) hours of treatment. Data shows relative proportions of cells in G0/G1 phase (black), S phase (dark grey), G2/M phase (light grey) and apoptotic population (colourless). A large population of cells was observed in the G0/G1 phase. Significant differences in the G0/G1 population of cells have been displayed. Values represent mean ± S.E. for three experiments in triplicate.

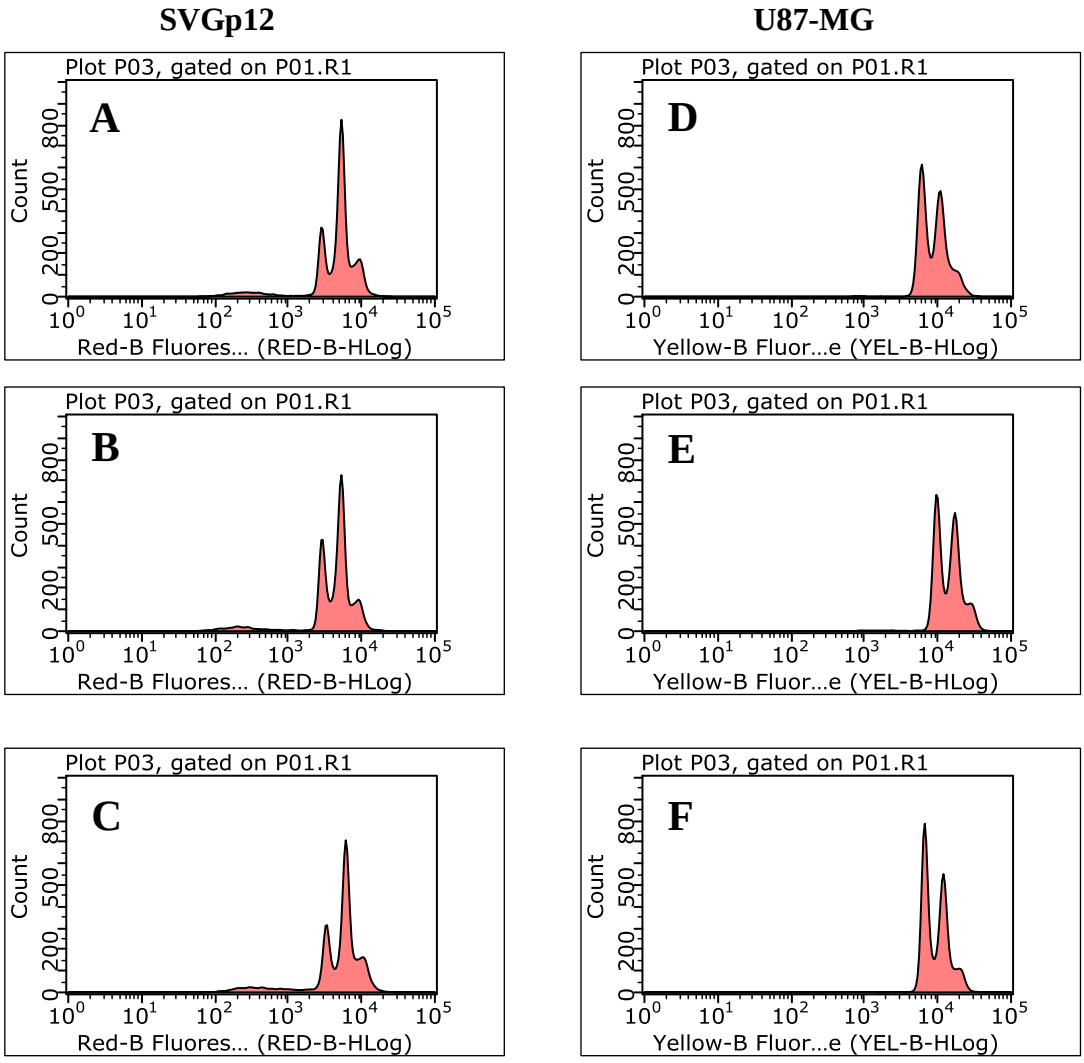

Figure 4.23: Flow cytometric plots showing cell cycle analysis using RNase and propidium iodide on SVGp12 and U87-MG cell line following 120 hours of incubation, under 1% hypoxia

Flow cytometry analysis of SVGp12 (A-C) and U87-MG (D-F) cells on non-treated (A, D), cisplatin (B, E) and asiatic acid (C, F). Cisplatin showed G2/M phase arrest on both cell lines, asiatic acid showed G0/G1 arrest on SVGp12 and S-G2/M arrest on U87-MG cells.

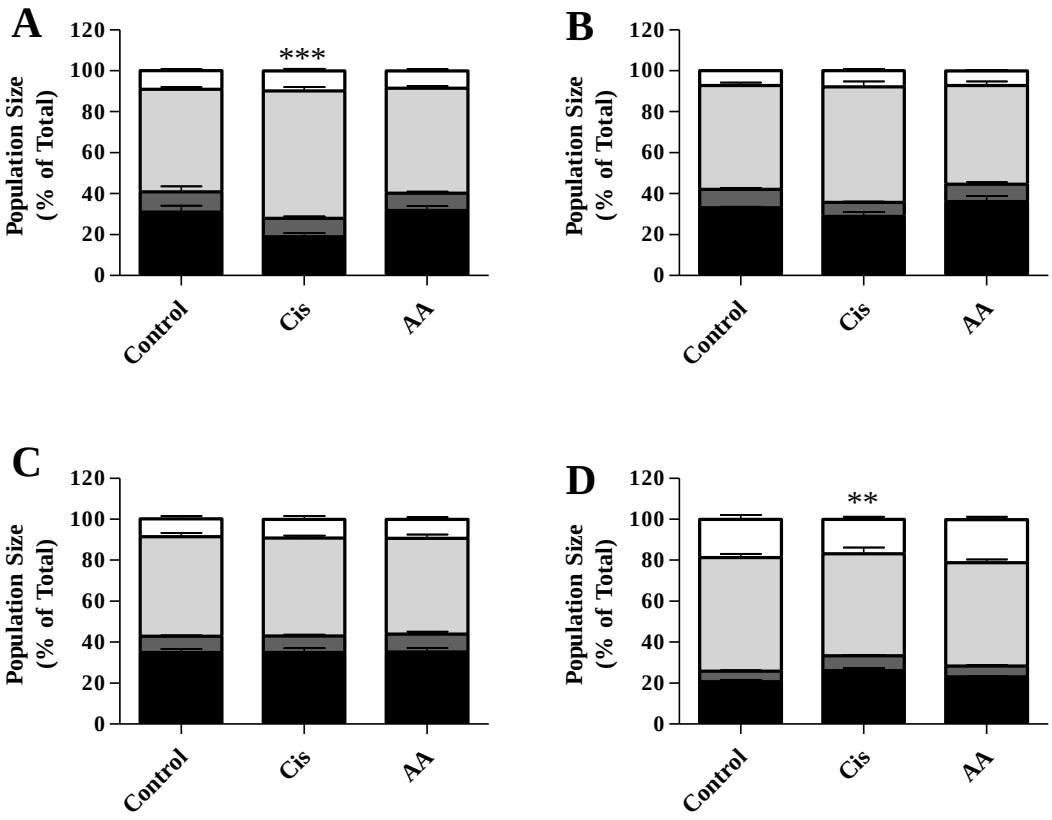

Figure 4.24: Data illustrating the effect of cisplatin and asiatic acid treatments on the cell cycle progression of SVGp12 cell line under 1% hypoxia

Cell cycle study was performed on SVGp12 cell line following 24 (A), 48 (B), 72 (C) and 120 (D) hours of treatment. Data shows relative proportions of cells in G0/G1 phase (black), S phase (dark grey), G2/M phase (light grey) and apoptotic population (colourless). Cisplatin showed G2/M phase arrest while asiatic acid showed G0/G1 arrest on SVGp12 cells. Significant differences in the G0/G1 population of cells have been displayed. Values represent mean ± S.E. for three experiments in triplicate.

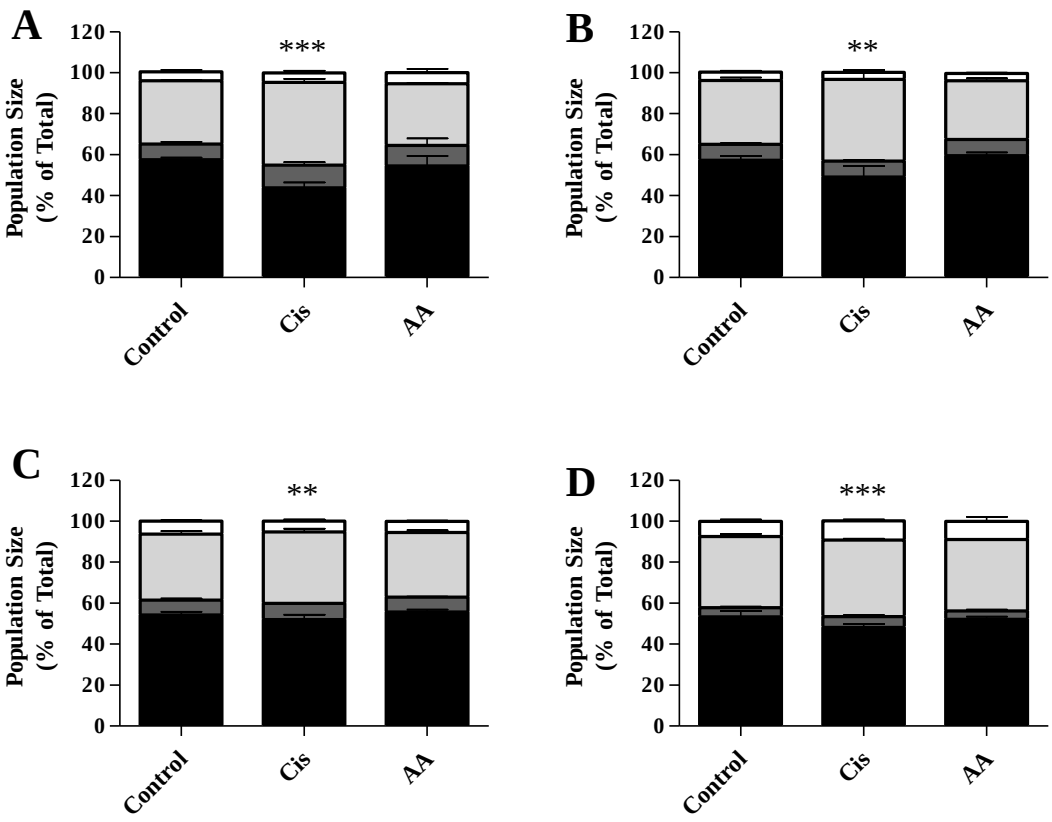

Figure 4.25: Data illustrating the effect of cisplatin and asiatic acid treatments on the cell cycle progression of U87-MG cell line under 1% hypoxia

Cell cycle study was performed on U87-MG cell line following 24 (A), 48 (B), 72 (C) and 120 (D) hours of treatment. Data shows relative proportions of cells in G0/G1 phase (black), S phase (dark grey), G2/M phase (light grey) and apoptotic population (colourless). Cisplatin showed G2/M phase arrest while asiatic acid showed S-G2/M arrest on U87-MG cells. Significant differences in the G0/G1 population of cells have been displayed. Values represent mean ± S.E. for three experiments in triplicate.

4.2.5 Combination studies

The EC_{25} values generated from earlier experiment (Section 3.2.3) was used in combination with cisplatin or asiatic acid to study any synergistic effects that may be involved following drug treatment of the two cell lines.

Cisplatin and asiatic acid showed a similar response, as described earlier, on SVGp12 and U87-MG cell lines (Section 3.2.3). The combination treatments of both, 2µM cisplatin and asiatic acid, or 30µM asiatic acid and cisplatin, did not seem to affect the viability, except at the highest concentration of the two drugs in combination with the other (Fig. 4.26).

SVGp12, cell viability decreased from 11 ± 1.76% at 24 hours to 3.33 ± 0.51% at 72 hours upon treatment with 30µM asiatic acid and 100µM cisplatin. A reduction in cell viability from 65.67 ± 0.69% at 24 hours to 25 ± 2% at 72 hours was observed upon treatment with 2µM cisplatin and 100µM asiatic acid (Fig. 4.26). Significant differences were observed only with 100µM asiatic acid treatment on cell viability at each time point against all three other treatments ($p < 0.05$).

On U87-MG, cell viability decreased from 8 ± 0.88% at 24 hours to 1.67 ± 0.19% at 72 hours upon treatment with 30µM asiatic acid and 100µM cisplatin. A reduction in cell viability from 85.33 ± 1.07% at 24 hours to 31.33 ± 0.77% at 72 hours was observed upon treatment with 2µM cisplatin and 100µM asiatic acid (Fig. 4.26). Significant differences were observed with 100µM asiatic acid treatment on cell viability ($p < 0.05$).

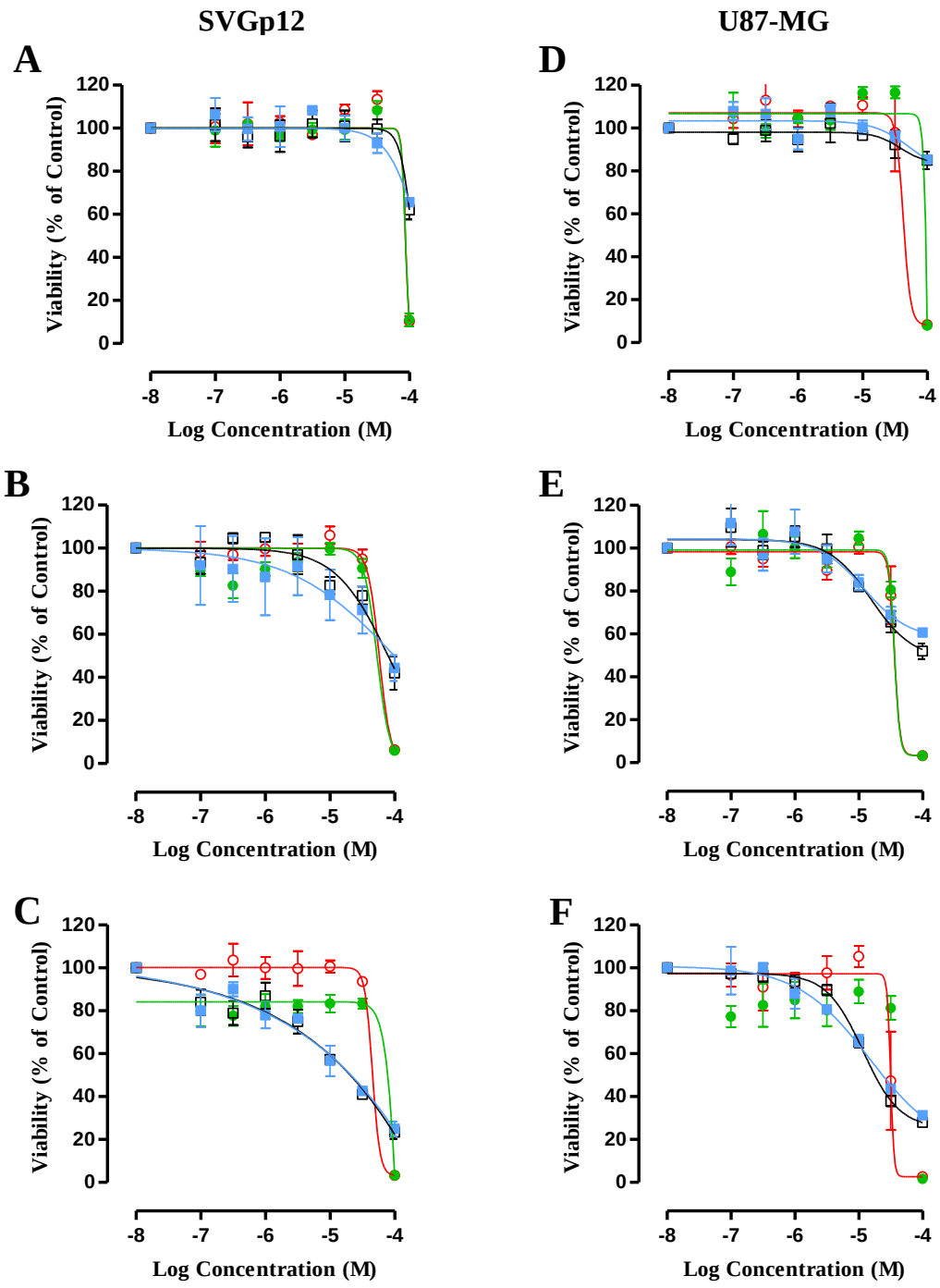

Figure 4.26: Data illustrating the effect of concentration dependent treatment of cisplatin and asiatic acid in combination on SVGp12 and U87-MG cell lines.

Cisplatin (□), asiatic acid (○), 30µM asiatic acid-cisplatin (●) and 2µM cisplatin-asiatic acid (■) on SVGp12 and U87-MG cell lines. Cell viability was measured using the PrestoBlue® reagent following 24 (A and D), 48 (B and E) and 72 (C and F) hours of incubation with respective treatments. Values represent mean ± S.E. for three experiments in triplicate.

4.3 Discussion

As explained earlier, an initial moderate increase in HIF-1α is important for cell's adaptation to hypoxia and cells respond through VEGF stimulation, apoptotic inhibition and modification of glucose metabolism (Bogenrieder and Herlyn, 2003; Graeber et al., 1996; Strese et al., 2013; Vander Heiden, Cantley, Thompson, 2009; Zhou et al., 2006).

Cell proliferation is an important factor for the anti-cancer effects of cisplatin. As explained previously (Section 3.3), cisplatin shows its anti-tumour effects through DNA intercalation. In this manner, cisplatin slows the rate of cell proliferation by binding to the DNA and causing anomalies in the cell. This effect of cisplatin on cell proliferation has been confirmed from the results obtained, where a significant effect on proliferation of SVGp12 and U87-MG was seen (Figs. 4.1-4.3).

Asiatic acid however, works through cell death which is either *via* apoptosis or necrosis (Section 3.3). It is due to the mechanism of action of asiatic acid that no significant effect on cell proliferation of SVGp12 or U87-MG cells was observed (Figs. 4.1-4.3).

Hypoxic cells are usually distant from blood vessels and are thus not adequately exposed to anti-cancer drugs. This distance from blood vessels also causes a reduction in the rate of cell proliferation (Brown and Wilson, 2004). Another reason for the slower cell proliferation is the cyclin-dependent kinase inhibitor $p27^{Kip1}$ (inhibits the activation of cyclin E-Cdk2 or cyclin D-Cdk4 complexes thus controlling cell cycle progression at G1), which is induced under hypoxic conditions (Wartenberg et al., 2003). Cellular senescence caused by DNA-damage response due to drugs results in a cell cycle arrest (Chang et al., 1999; d'Adda di Fagagna, 2008). In a study performed by Sullivan and co-workers, it was demonstrated that hypoxia can decrease cell-senescence

caused due to drug treatments, explaining another mode of chemoresistance due to hypoxia (Sullivan et al., 2008). Thus, cytotoxic effect of an anti-cancer drug is greater in rapidly proliferating cells, as opposed to slowly proliferating tumour cells under hypoxia (Figs. 4.4-4.9). Hypoxia also selects cells with low p53 expression, thus reducing or inhibiting p53-induced apoptosis in hypoxic cells. Upon exposure to hypoxia, a post-translational modification of the *p53* gene occurs, thus making it active and in turn promoting transcription of cell cycle regulating or apoptotic genes (Brown and Wilson, 2004; Graeber et al., 1996; Zhou et al., 2006). DNA injuries caused to the cells under normoxic environment are higher and more permanent than in a hypoxic environment, where cellular restoration may occur. Another cause for reduced drug cytotoxicity under hypoxia is the MDR (multi-drug resistance) gene and over expression of the gene product P-glycoprotein (P-gp), which has been identified to be involved in multidrug resistance (Wartenberg et al., 2003).

A significant reduction in cell proliferation was observed for non-treated U87-MG cells following 24 hours of incubation under hypoxia. Cisplatin, however, did not show any significant differences in the rate of cell proliferation between normoxia and hypoxia, for either of the cell lines. The growth curve data for normoxia and hypoxia of both cell lines showed a significantly slower rate of growth (Fig. 3.1). The scratch assay revealed similar results (Fig. 4.10-4.14), and a significant difference was observed in the wound healing of non-treated SVGp12 and U87-MG cells under 1% hypoxia ($p < 0.05$).

Cisplatin activity under hypoxia has been shown to be lower than under normoxic conditions. However, the anti-cancer activity of a drug under hypoxia depends largely on the cell type and may increase or decrease accordingly (Koch et al., 2003; Yao et al., 2005). Cisplatin works by forming DNA adducts in the cell. Thus, in order for cisplatin to show its effects on cells, cell proliferation is important. However,

as cell proliferation decreases under hypoxia, the efficacy of cisplatin decreases too (Figs. 4.4-4.9). Three other studies have confirmed the findings of this research wherein a reduced efficacy of cisplatin was observed under hypoxia (Koch et al., 2003; Rohwer et al., 2010; X. Song et al., 2006).

As the cells proliferate slowly under hypoxia, a failure of the wound healing was observed under microscopy, at the end of 18 hours. However, this was not the case under normoxia, where a complete closure of the wound was observed for non-treated cells and partial closure was observed for cisplatin treated cells (Figs. 4.10-4.14). These findings confirm the slower rate of growth and proliferation of the two cell lines under hypoxia. Cisplatin causes DNA interlinks and thus retards the cell migration over time. It is due to this that a partial closure of the wound was observed following cisplatin treatment. Asiatic acid, on the other hand, did not show any wound healing under hypoxia, but instead showed rounded cells, a characteristic of cell death. Thus, it suggests that asiatic acid does not affect cell proliferation but instead causes cell death only.

However, keeping this in mind, it should be noted that cell proliferation assay under 1% hypoxia did not generate very reliable results due to the fact that the cells seemed to take longer to hydrolyse CFDA-SE. A shift in the CFDA-SE fluorescence to towards the right (indicating an increase in fluorescence which correlates to increased hydrolyses of CFDA-SE) was observed following 24 hours of staining. An individual experiment to confirm this phenomenon was performed; however, the data has not been shown.

Cell cycle analysis of cisplatin treated cells under normoxia showed a G2/M phase arrest, as would be expected of cisplatin (Figs. 4.17-4.19) (O'Brien and Brown, 2006). Under hypoxia, a transient S phase arrest was seen for SVGp12 cells, however,

the U87-MG cells showed a large population under G0/G1 phase which shifted towards the apoptotic population at 120 hours (Figs. 4.20-4.25). This is due to the fact that under hypoxic conditions, cells accumulate p53 through a HIF-1α-dependent mechanism, and cause an arrest at the G0/G1 phase in the cell cycle through a non-p53-mediated pathway (Shannon et al., 2003). According to an article published by Amellem et al., (1994), hypoxia results in a slower cell cycle progression whereas extreme hypoxia (e.g. 1%) induces pre-DNA-synthetic (pre S-phase) arrest in cells, while cells in the other phases of cell cycle progress to late G1 phase before they are arrested. This transient arrest in G1 phase has been described as a possible mechanism to protect the cells from proceeding into the S phase, where they are more sensitive to hypoxia related DNA injuries (Graeber et al., 1994). This may also explain the reason for a direct increase in apoptotic population of cells with a decrease in the S phase population as the cell cycle progressed.

Under normoxia, asiatic acid treatment on SVGp12 cells showed an arrest in the S-G2/M phase of the cell cycle whereas the U87-MG cell line showed a G0/G1 phase arrest. These differences were noted to be significant between the two cell lines. S-G2/M phase arrest of the cell cycle was also observed for U87-MG cells under 1% hypoxia (Figs. 4.23 & 4.25). In a study performed by Hsu et al., (2004), S-G2/M phase arrest of the cell cycle was observed in breast cancer cell lines MCF-7 and MDA-MB-231, following asiatic acid treatment. They found that asiatic acid decreased the expression of cyclin B1 (regulates cell entry into mitosis), cyclin A (contributes to the G1/S transition, S phase progression, and G2/M transition), Cdc25c (involved in G2 phase), and Cdk2 (involved in G1/S transition), whereas it increased the amount of p21/WAF1 (Cdk inhibitor) and phosphorylation of Cdk2, as well as phospho-Cdc25c. Cdc25c is an M phase inducer and causes de-phopshorylation of cyclin B-Cdk1 complex, triggering cell's entry into mitosis. However, in a DNA damaged cell, Cdc25c

does not reach its peak hyper-phosphorylated state (Shackelford et al., 1999). This suggests that asiatic acid does not induce cell cycle arrest or cell death due to DNA damage, but other pathways may be involved and should be investigated.

In addition to this, asiatic acid also showed G0/G1 phase arrest under normoxia in U87-MG cells; under 5% hypoxia in SVGp12 and U87-MG cells; and under 1% hypoxia in SVGp12 cells. Cell cycle arrest in the G0/G1 phase is mediated by the *RB* gene. *RB* gene is a tumour suppressor gene. Cell cycle progression into S phase involves phosphorylation of Ser780 and Ser807/811, on the *Rb* gene, by Cdk4/cyclin D. Thus, a loss in the Rb-phosphorylation of these sites would result in inhibition of cell cycle progression into S phase (Bretones et al., 2014; Shukla and Gupta, 2007). From the data obtained, it is possible that asiatic acid downregulates Rb protein thus causing an arrest in the G0/G1 phase of cell cycle. Using another novel triterpenoid (25-methoxyhispidol A) in a study by Hong et al., (2008), it was shown that G1 phase arrest of the cell cycle was due to downregulation of Rb protein coupled with the cdk inhibitor $p21^{WAF1/Cip1}$. The same has also been shown in another study involving the use of another triterpene from *Aesculus hippocastanum* (horse chestnut) seed (Patlolla et al., 2006).

EGF receptor is a member of the Erb family of receptor tyrosine kinases. Its activation triggers multiple signal transduction pathways including the MAP-K and the PI3/Akt pathway, thus leading to various biological processes associated with tumour growth such as cell cycle progression, invasion, metastasis, angiogenesis, and decreased apoptosis. Thus, a down-regulation of EGF receptor activity would be considered as a potential approach to treat tumours (Pore et al., 2006; Taylor et al., 2012).

Western blot analysis of cisplatin treated SVGp12 cells under normoxia and hypoxia, showed an increase in receptor expression although these differences were non-significant. An increase in the expression was observed with asiatic acid under

normoxia and decrease under hypoxia (Figs. 4.15 & 4.16), differences were non-significant again. Cisplatin treated U87-MG cells showed a decrease in EGFR expression under normoxia and hypoxia. Asiatic acid showed an increase in EGFR expression over time on U87-MG cell line under normoxia and hypoxia both. All these differences were non-significant.

In a study by Benhar et al., (2002), it has been shown that DNA damage due to cisplatin activates a signalling pathway that culminates in the activation and expression of EGFR, although the exact mechanism is not yet known. Cisplatin mediated EGFR activation is slow, occurs once cisplatin-DNA adducts start forming and is kinase independent. It has also been suggested that EGFR activation upon cisplatin treatment occurs *via* p38 mitogen-activated kinase and leads to downstream effectors such as protein kinase B/AKT. Cisplatin induced EGFR phosphorylation could result in its nuclear translocation and lead to interaction with DNA protein kinase, thus mediating DNA repair. Thus, cisplatin mediated EGFR activation is a survival mechanism by the cell, that in turn, reduces the efficacy of cisplatin (Ahsan et al., 2010).

It could be said similarly for asiatic acid that, increase in the EGFR expression level is a mechanism of cell survival in response to the drug treatment. However, asiatic acid inhibits extracellular signal-regulated kinase (ERK) in a variety of tumour cells, which in turn prevents the cell from proliferating even with increased EGFR (Wang et al., 2013).

It is known that glioblastoma displays an increased rate of *EGFR* gene mutation and amplification (20-40%) (Franovic et al., 2007). Since U87-MG is a glioblastoma cell line, it would only be expected to see an increased expression of EGFR. On the other hand, EGFR expression is also amplified under hypoxia, in a HIF-2α dependent manner (Franovic et al., 2007). Thus, even in the absence of *EGFR* gene mutation, an

upregulation in EGFR expression can be observed under hypoxia. However, this was not the case for SVGp12 and U87-MG cell lines and the EGFR expression remained unchanged.

As explained earlier, cisplatin exerts its cytotoxic effects by interacting with the DNA. Asiatic acid, on the other hand, induces its effects by Bcl-2 inhibition, increased mitochondrial membrane potential and increase in intracellular calcium influx. The combination study with cisplatin and asiatic acid did not show significant differences in cell viability except at 100µM asiatic acid (Fig. 4.26). The EC_{50} of asiatic acid was calculated to be 50µM. 100µM is twice as concentrated as the EC_{50} of asiatic acid and thus is very potent to SVGp12 and U87-MG cell lines. It is due to this reason that a very small percentage of viable cells were observed following 100µM asiatic acid and thus the significant differences that were observed.

Asiatic acid, under normoxia, shows S-G2/M phase arrest on SVGp12 cell line and G0/G1 phase arrest on U87-MG cell line, whereas cisplatin shows G2/M phase arrest, irrespective of the cell line. Due to this reason, a decrease in cell viability that was observed with 2µM cisplatin and 100µM asiatic acid, was mainly because of asiatic acid. As most of the cells were dead at 24 hours due to asiatic acid, cisplatin could not exert its cytotoxicity as cisplatin interferes with DNA replication, which is comparatively a slow process.

Treatment with 100µM cisplatin and 30µM asiatic acid showed a gradual decrease in cell viability over time. At a very high concentration, cisplatin is capable of inducing DNA damage in a short period of time, in comparison to a low dose of cisplatin which takes longer to act. The results observed because of this treatment correlated with the results obtained for 100µM cisplatin treatment on its own. However, cisplatin treatment on its own showed a smaller percentage of viable cells ($p > 0.05$),

when compared to 100µM cisplatin and 30µM asiatic acid combination treatment. This is because, on the U87-MG cells, asiatic acid induces a G0/G1 phase arrest thus preventing the progression of cells into the G2/M phase, where cisplatin shows its effects. Thus, the combination treatments did not show any significant differences on cell viability due to the reasons explained above.

Conclusion: Hypoxia reduced the rate of cell growth as confirmed by cell proliferation and scratch assay; cisplatin and asiatic acid did not show any significant differences between hypoxia and normoxia. Cell cycle analysis revealed a G2/M phase arrest for cisplatin treated cells under normoxia and hypoxia, whereas asiatic acid showed S-G2/M arrest in SVGp12 cells and a G0/G1 phase arrest in U87-MG cells under normoxia. Cell cycle arrest due to asiatic acid under hypoxia depended on the cell type and the level of oxygen saturation.

CHAPTER 5

Nanoparticle Preparation and Characterisation

5.1 Introduction

Asiatic acid is a hydrophobic drug, solubility in water $5.98x10^{-2}$ mg/l at 25°C (data from PubChem). Problems with asiatic acid include solubility in water, thus making the delivery of asiatic acid difficult (Zhao et al., 2010). In addition, as asiatic acid is a herbal compound showing low side-effect profile, it would be an ideal candidate in the treatment of cancer. Also, previous literature has shown that asiatic acid possesses cytotoxic activity against various cancer cells and can cross the blood brain barrier (Cho et al., 2006; Hsu et al., 2004; Kavitha et al., 2011).

In order to overcome asiatic acid-solubility problem, we formulated asiatic acid-loaded PCL nanoparticles for effective drug delivery. We chose PCL for this study as it is an FDA approved polymer and can be used to formulate nanoparticles in an aqueous media containing a hydrophobic drug (Shenoy et al., 2005). PCL has been shown to be biocompatible and is applied in medical devices such as intravascular stents and external grafting material for broken bones (Sarasam, 2001).

Objectives: We prepared a drug delivery system for asiatic acid using a synthetic polymer poly-ε-caprolactone. Characterisation of the system involved size and surface charge measurements, measurement of drug loading and drug release.

5.2 Results

5.2.1 Preliminary Nanoparticle Preparation Studies

In order to establish a protocol to produce stable NPs, different experimental techniques were examined (Section 2.6.2). The ultra-sonification process generates high intensity ultra-sonic waves that help reduce the particle size. Nanoparticles obtained by this method were monodisperse, PDI 0.09 ± 0.02 to 0.11 ± 0.01 (Table 5.1) and within the range of 186.4 ± 2nm to 199 ± 2.5nm in size with a surface charge of -18 ± 0.8mV to -22 ± 1.3mV (Figs. 5.1 & 5.2). However, the NPs were not stable and aggregation was observed along with precipitation by day 7 of their preparation. Stability of the nanoparticles is a measure of the average size, surface charge and the PDI of the nanoparticles recorded over a period of time.

The homogenisation process too, like the ultra-sonification process, generated NPs with a size range of 193 ± 1.1nm to 201.7 ± 3.5nm and a surface charge of -18.4 ± 0.9mV to -23.9 ± 0.8mV (Figs. 5.1 & 5.2). Nanoparticles prepared using this protocol, however, were not monodisperse (0.09 ± 0.01 to 0.130 ± 0.01) (Table 5.1) and nanoparticle aggregation was observed along with precipitation by day 7 of their preparation.

Nanoparticles prepared by the magnetic stirring process were 196.2 ± 0.9nm to 202.8 ± 3nm with a surface charge of -19.9 ± 0.86mV to -23.3 ± 0.56mV (Figs. 5.1 & 5.2). The PDI of these NPs was less than 0.1 (0.06 ± 0.008 to 0.09 ± 0.012) all through the 10 days thus showing an improved stability ($p < 0.001$) (Table 5.1).

Nanoparticles prepared by magnetic stirring were significantly smaller in size from those prepared by ultra-sonification or homogenisation ($p < 0.001$). The average surface charge of three sets of nanoparticles was similar ($p > 0.05$) however, samples

prepared by the magnetic stirring showed a significant reduction in the PDI ($p < 0.01$). Storage time had no difference on the average size of the nanoparticles within each group in any of the above experiments ($p > 0.05$)

Thus, it was decided to take forward the magnetic stirring method of NP preparation. Further changes were carried out on this protocol to achieve an improved stability.

Table 5.1: Polydispersity comparison of blank NPs prepared by the homogenisation, ultra-sonification process and magnetic stirring processes

Day	**PDI**		
	Homogenisation	**Ultra-sonification**	**Magnetic stirring**
0	0.116 ± 0.009	0.087 ± 0.008	0.082 ± 0.007
1	0.102 ± 0.021	0.092 ± 0.016	0.058 ± 0.007
2	0.121 ± 0.012	0.089 ± 0.017	0.074 ± 0.012
3	0.085 ± 0.008	0.061 ± 0.011	0.087 ± 0.011
4	0.086 ± 0.013	0.083 ± 0.011	0.065 ± 0.009
5	0.130 ± 0.013	0.108 ± 0.008	0.058 ± 0.006
6	0.116 ± 0.005	0.096 ± 0.014	0.086 ± 0.008
7	0.111 ± 0.014	0.113 ± 0.013	0.054 ± 0.009
10	No data	No data	0.084 ± 0.005
Average PDI	**0.108 ± 0.012**	**0.09 ± 0.010**	**0.072 ± 0.008*****

NPs prepared using the magnetic stirring were more stable compared to NPs prepared by homogenisation or ultra-sonification. Nanoparticle prepared by magnetic stirring were significantly smaller in size compared to homogenisation and ultra-sonification. Values represent mean ± S.E. for three experiments in triplicate.

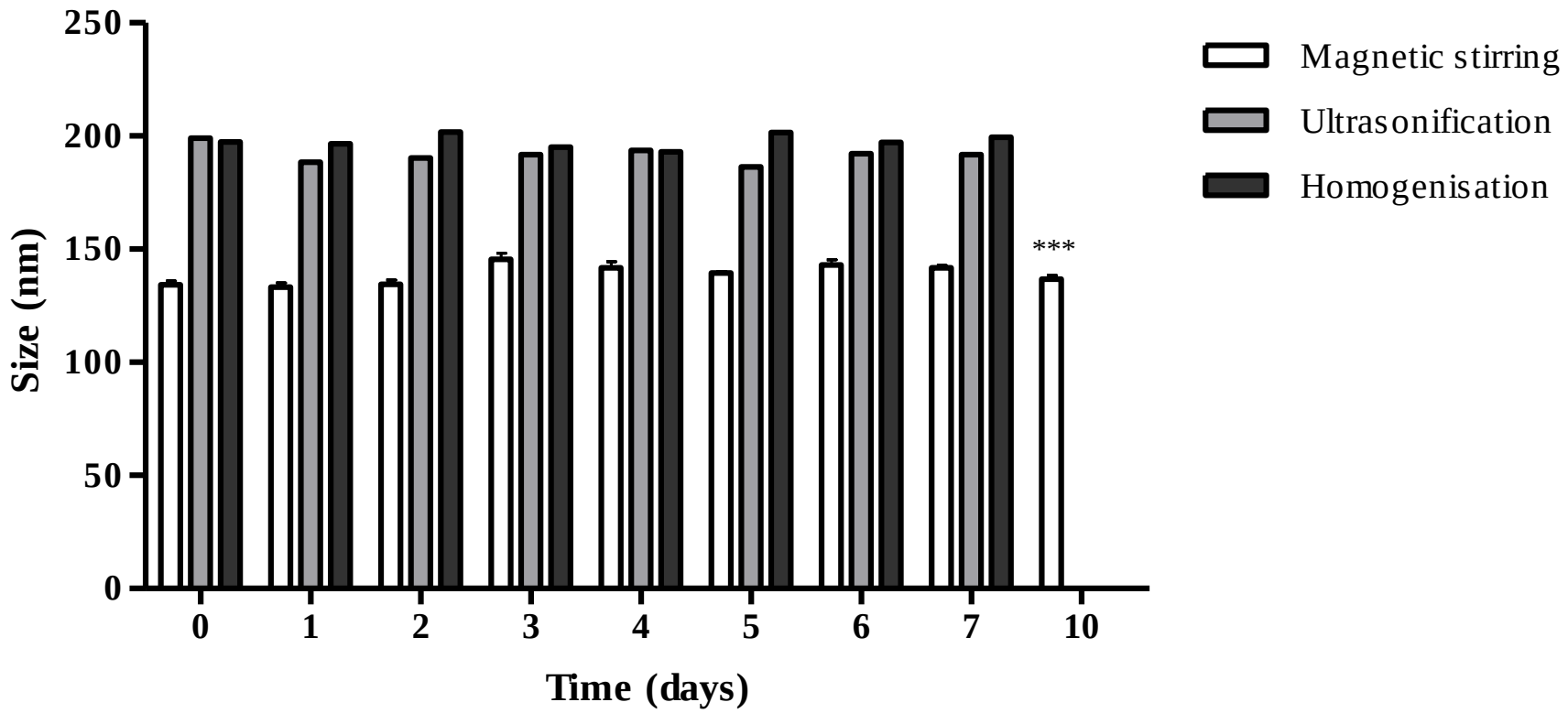

Figure 5.1: Size comparison of blank NPs prepared by the homogenisation, ultra-sonification process and magnetic stirring process

NPs prepared using the magnetic stirring were more stable compared to NPs prepared by homogenisation or ultra-sonification. Data measurement was discontinued due to precipitation in the samples. Nanoparticles prepared by magnetic were significantly different in size. Values represent mean ± S.E. for three experiments in triplicate.

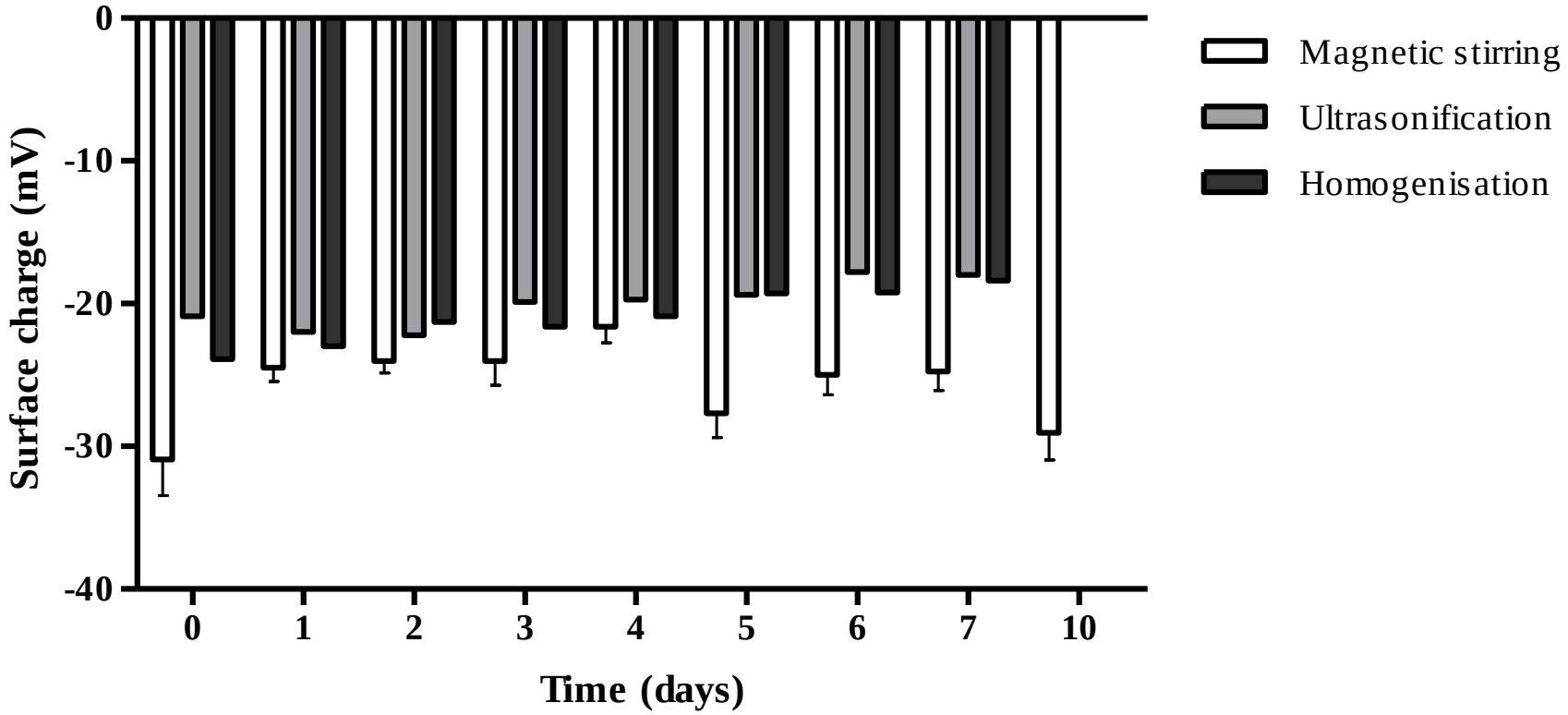

Figure 5.2: Surface charge comparison of blank NPs prepared by the homogenisation, ultra-sonification process and magnetic stirring process

NPs prepared by all three protocols had a similar average surface charge. No significant differences were observed. Values represent mean ± S.E. for three experiments in triplicate.

5.2.2 Nanoparticle Filtration Studies

Systemic delivery of nanoparticles would require their sterilisation. The type of filter used for nanoparticle filtration can affect the polymeric associations and chemical nature within the nanoparticle structure.

Blank nanoparticles were prepared (Section 2.6.1) and a volume of 5ml was filtered through three different filter types in order to establish the best-suited filter for the study. A maximum amount of 2ml from each filter disc could be filtered using the Whatman™ PES filter and the Whatman™ Nylon filters before the filter became clogged, whereas a volume of 5mL could be filtered using the Millex® MCE filters. The resulting suspension of NPs was measured for a period of 10 days and assessed for their size and surface charge. Non-filtered nanoparticles and nanoparticles filtered using Whatman™ Nylon filters precipitated out on the second day after preparation whereas nanoparticles filtered using Whatman™ PES filters and Millex® MCE filters were stable for a minimum period of 10 days (Fig. 5.3 & 5.4). Nanoparticles filtered with the Whatman™ PES filter precipitated out after day 10 of measurement whereas nanoparticles filtered using Millex® MCE filters were stable up to a minimum of 10 days following filtration. Nanoparticles filtered using Millex® MCE filters were the most stable as compared to any of the other methods of filtration ($p < 0.001$). Storage time had no significant difference on the size of NPs within each group ($p > 0.05$).

Nanoparticles filtered using Whatman™ nylon filters displayed the highest PDI whereas samples filtered by other techniques had a similar PDI (Table 5.2). Nanoparticles filtered using Millex® MCE filters showed a significant difference ($p < 0.001$) in the PDI values compared to non-filtered, Whatman™ nylon filters and Whatman™ PES filters.

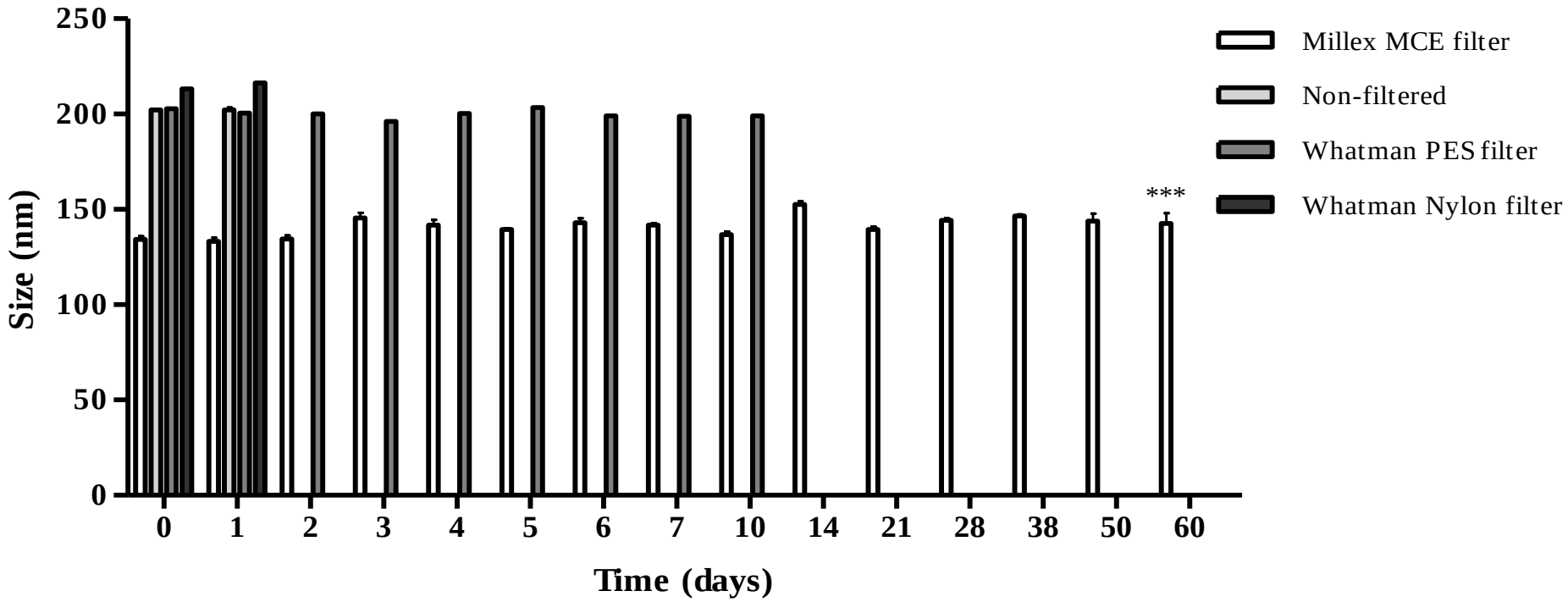

Figure 5.3: Size comparison of blank NPs filtered using various filters

Precipitation was observed in samples with no filtration, and those filtered through Whatman™ Nylon membrane circles and Whatman™ PES filters, after day 10. Nanoparticles filtered using Millex® MCE filters showed a significantly smaller size. Values represent mean ± S.E. for three experiments in triplicate.

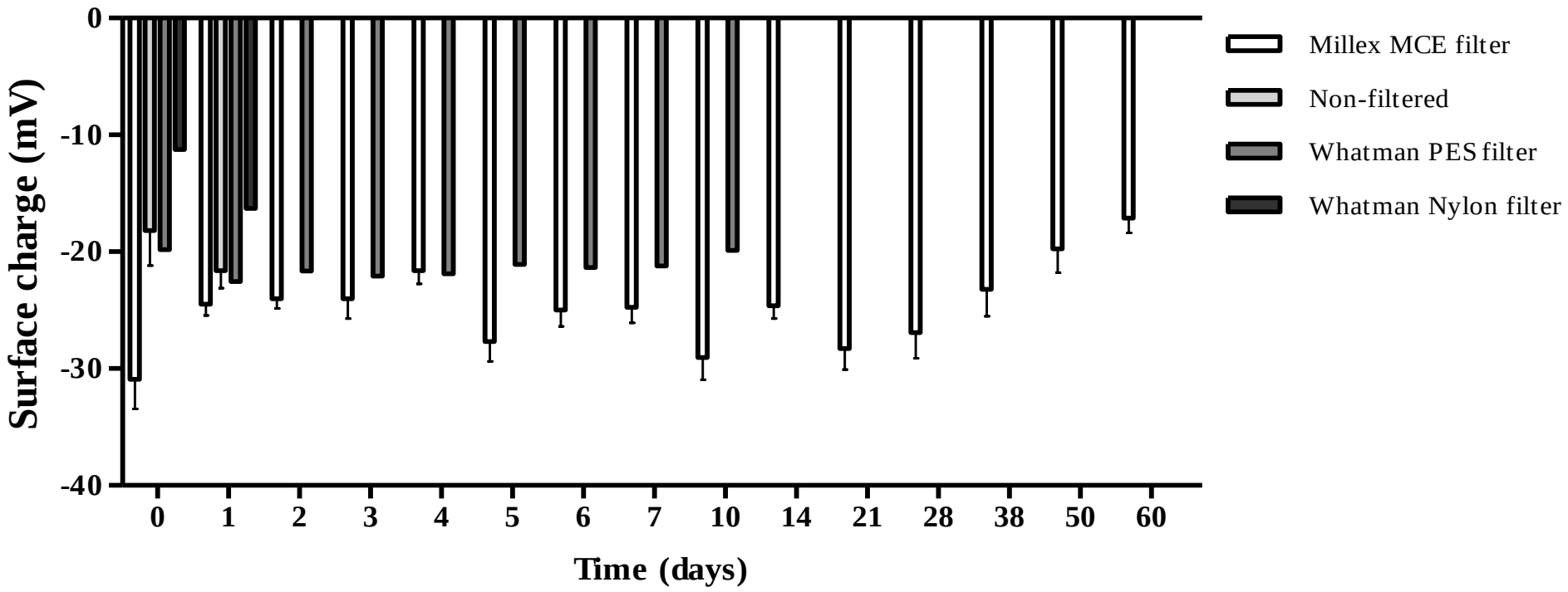

Figure 5.4: Surface charge comparison of blank NPs filtered using various filters

Precipitation was observed in samples with no filtration, and those filtered through Whatman™ Nylon membrane circles and Whatman™ PES filters, after day 10. No significant differences in surface charge were observed. Values represent mean ± S.E. for three experiments in triplicate.

Table 5.2: Polydispersity comparison of blank NPs filtered using various filters

Day	PDI			
	Millex® MCE filter	**Whatman™ PES filter**	**Whatman™ nylon filter**	**Non-filtered**
0	0.057 ± 0.016	0.092 ± 0.018	0.195± 0.059	0.087 ± 0.01
1	0.053 ± 0.005	0.048 ± 0.007	0.162 ± 0.026	0.078 ± 0.011
2	0.072 ± 0.013	0.096 ± 0.015	-	-
3	0.048 ± 0.015	0.076 ± 0.07	-	-
4	0.075 ± 0.010	0.050 ± 0.012	-	-
5	0.035 ± 0.007	0.056 ± 0.015	-	-
6	0.054 ± 0.005	0.082 ± 0.015	-	-
7	0.043 ± 0.008	0.088 ± 0.015	-	-
10	0.033 ± 0.012	0.105 ± 0.012	-	-
14	0.046 ± 0.014	-	-	-
21	0.078 ± 0.012	-	-	-
28	0.066 ± 0.008	-	-	-
38	0.067 ± 0.009	-	-	-
50	0.077 ± 0.005	-	-	-
60	0.088 ± 0.010	-	-	-
Average PDI	**0.059 ± 0.010*** **	**0.077 ± 0.013**	**0.183 ± 0.042**	**0.085 ± 0.010**

Average PDI of NPs filtered using Millex® MCE filters was lower than all other types of filters used. Nanoparticles filtered using Millex® MCE filters showed a significantly smaller PDI. Values represent mean ± S.E. for three experiments in triplicate.

5.2.3 Effect of Storage Temperature on Nanoparticle Stability

Long term storage of nanoparticles requires storage either under room temperature or in a refrigerated environment. In order to assess the effects of storage temperature on nanoparticle stability, a set of blank NPs (Section 2.6.1) was each maintained at room temperature and at 4°C and measurements for size and surface charge were performed.

Nanoparticles stored at room temperature were unstable and precipitated out on the tenth day after preparation, whereas nanoparticles stored at 4°C were stable for 60 days (Fig. 5.5) following preparation. Significant difference in the size of the NPs was observed between the two sets of NPs ($p < 0.001$). Storage time had no significant difference on NP size within each group of the two data sets ($p > 0.05$).

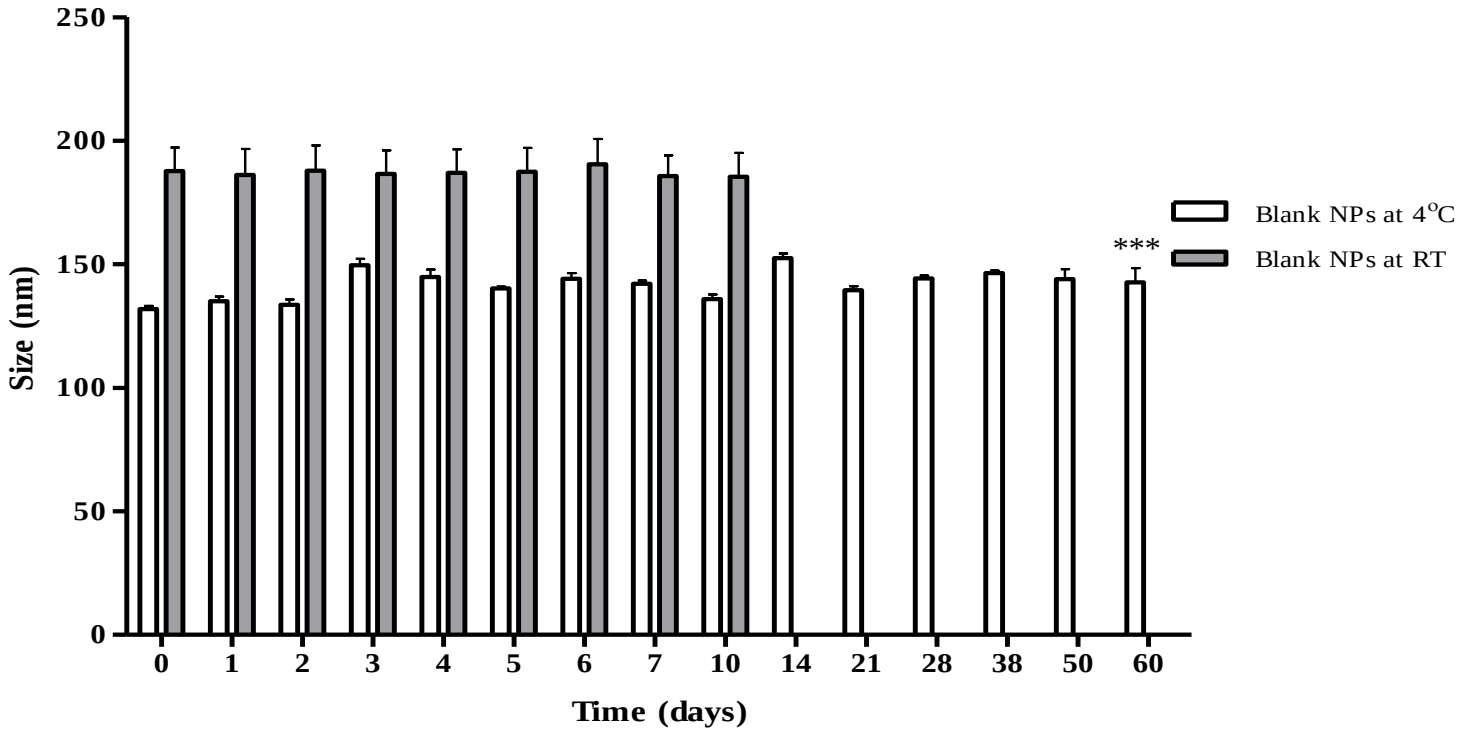

Figure 5.5: Size comparison of blank NPs at room temperature and at 4°C

NPs stored at 4°C were smaller size compared to NPs stored at room temperature. NPs stored at 4°C did not show a difference in their average size and were stable for a period of 60 days while the NPs stored at room temperature precipitated out after 10 days; hence, data measurement was discontinued for NPs stored at room temperature. Nanoparticles stored at 4°C showed a significant difference in size. Values represent mean ± S.E. for three experiments in triplicate.

5.2.4 Calibration Curves Generated using HPLC

In order to perform drug loading, drug release and to calculate the amount of PCL in the blank and asiatic acid-loaded NPs, a calibration curve for asiatic acid and PCL (Fig. 5.6) was performed. The percentage loading and the amount of drug loaded per milligram of the polymer was determined by injecting the nanoparticle suspension through the HPLC.

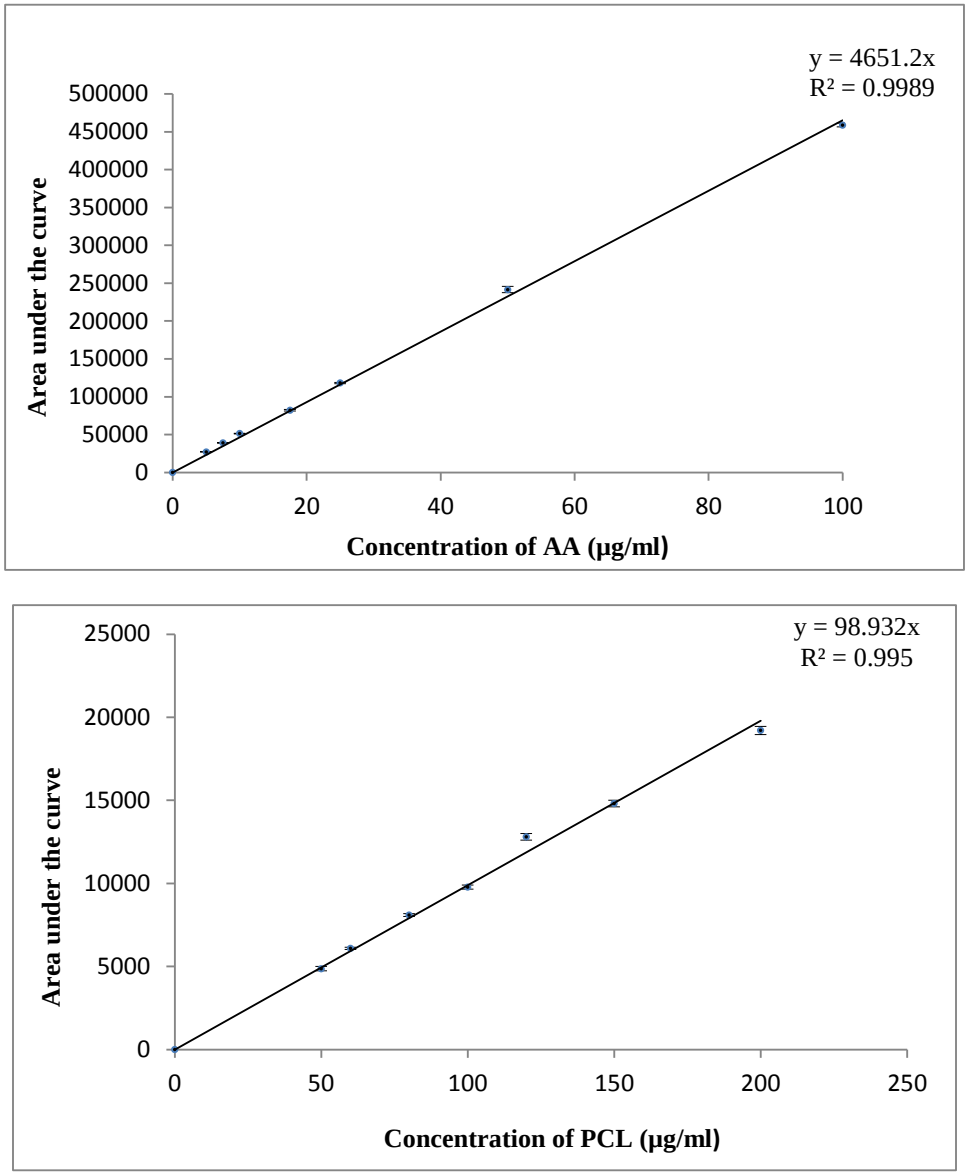

Figure 5.6: Calibration curves for asiatic acid and polycaprolactone generated using HPLC

Calibration curve generated for AA using the HPLC protocol described in Section 4.3. Values represent mean ± S.E. for three experiments in triplicate.

5.2.5 Nanoparticle Drug Loading Studies

Following the drug loading of asiatic acid into the nanoparticles, it was crucial to quantify the amount present in the nanoparticle structure. To assess the effects of concentration of asiatic acid on loading efficiency of the nanoparticles, drug loading studies were carried out using HPLC.

The percentage drug loading of the nanoparticles for all four concentrations of asiatic acid used was between 2.9 ± 1 to 3.4 ± 0.1% ($p > 0.05$) when the ratio of aqueous phase to organic phase was 1:1 (Fig. 5.7). Different amounts of asiatic acid were used to achieve the EC_{50} value of asiatic acid generated earlier (Section 3.2.3). Thus for a 20% uptake of asiatic acid into the nanoparticles, the amount of asiatic acid needed was calculated and the following range of concentrations was used. However, as the drug loading efficiency of the nanoparticles was very low, attempts were made to increase this by bringing some changes in the protocol.

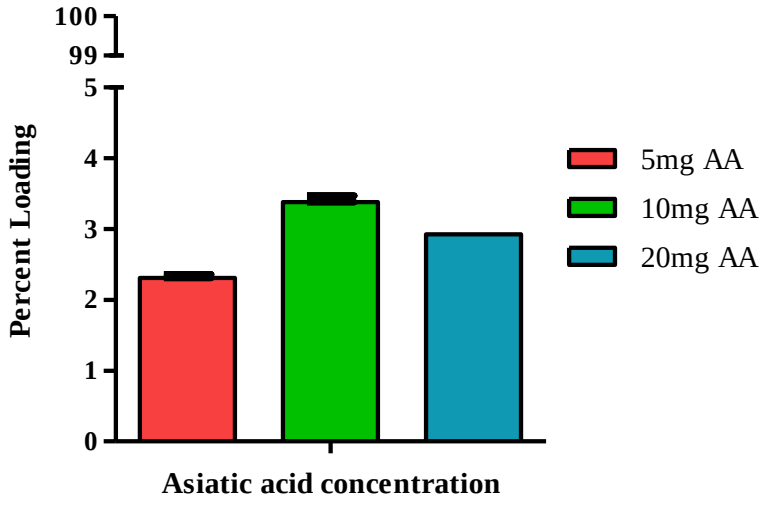

Figure 5.7: Comparison of drug loading efficiency of asiatic acid at different concentrations using 1:1 ratio of aqueous phase: organic phase

To increase the amount of drug loaded into the NPs and to determine maximum loading efficiency, the amount of AA in the formulation was varied. The percentage loading was similar for all three concentrations used. No significant differences were observed. Values represent mean ± S.E. for three experiments in triplicate.

5.2.6 Maximisation of Nanoparticle Yield

In an attempt to increase the drug loading efficiency of the nanoparticles, a number of individual parameters were modified (Section 2.7.3). An increase in the nanoparticle yield would theoretically increase the drug loading efficiency of asiatic acid. To measure nanoparticle yield, nanoparticle preparations were injected through the HPLC (Table 5.3). Nanoparticle yield (Fig. 5.8) was calculated using the calibration curve generated for PCL (Fig. 5.6).

When the ratio of aqueous phase to organic phase was changed to 2:1, the percentage loading of the drug into the nanoparticles increased (Fig. 5.9). The maximum loading efficiency obtained was 28.5 ± 1.2% when the initial amount of drug added was 20 mg ($p < 0.001$ for asiatic acid-loaded NPs prepared by using a 2:1 ratio against a 1:1 ratio of aqueous phase: organic phase). The drug-loading efficiency increased with increasing amount of drug; this correlates with the results produced by Chawla & Amiji (2002). The encapsulation efficiency of asiatic acid-loaded nanoparticles was calculated to be 72.8 ± 6.5% (Fig. 5.10), which indicates that 72.8% of the drug present in the formulation was encapsulated into the formulation whereas the remaining drug was the free drug. Encapsulation efficiency of the drug was calculated as the percentage drug in the pellet at 0 hours to the total amount of drug present in the formulation.

Please note: Drug loading efficiency refers to the total amount of drug that is encapsulated into the nanoparticles and to the amount of drug that may be adsorbed onto the surface of the nanoparticles.

Table 5.3: A table listing all the changes in the original protocol

Parameters	Original	Modifications
Aqueous: organic phase	1:1	2:1
Pluronic F-68	150mg	600mg
Acetone temperature	40°C	20°C
Stirring time	2 minutes	10 minutes
Filtration	After	Before

The above parameters were modified in order to achieve an improve nanoparticle yield

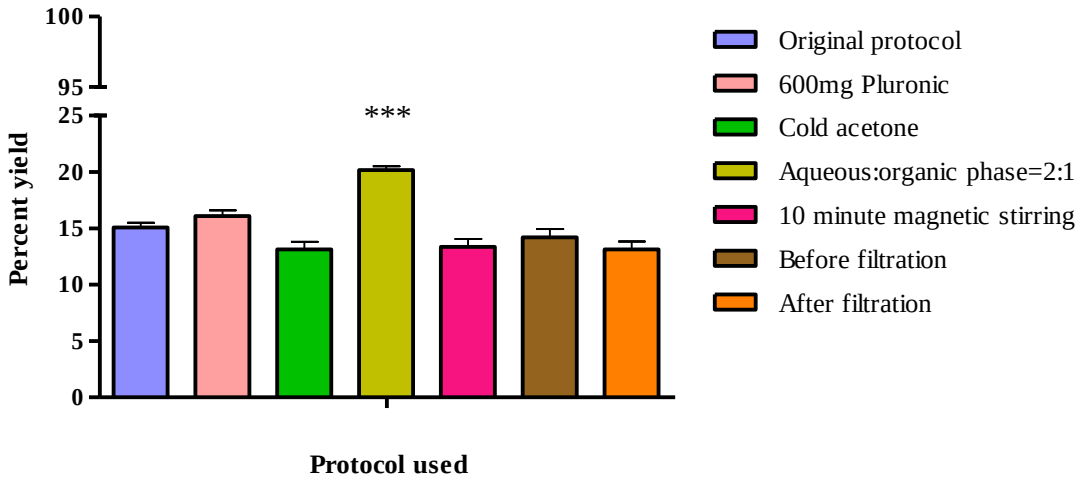

Figure 5.8: Data illustrating the comparison of PCL yield of blank NPs prepared by changing various parameters

To establish a protocol giving the highest NP yield, individual components of the preparation protocol were varied. The highest NP yield (20.2 ± 0.4%) was observed when the ratio of aqueous phase to organic phase was changed to 2:1 keeping all other variables constant. Significant difference was observed with 2:1 ratio of aqueous phase to organic phase. Values represent mean ± S.E. for three experiments.

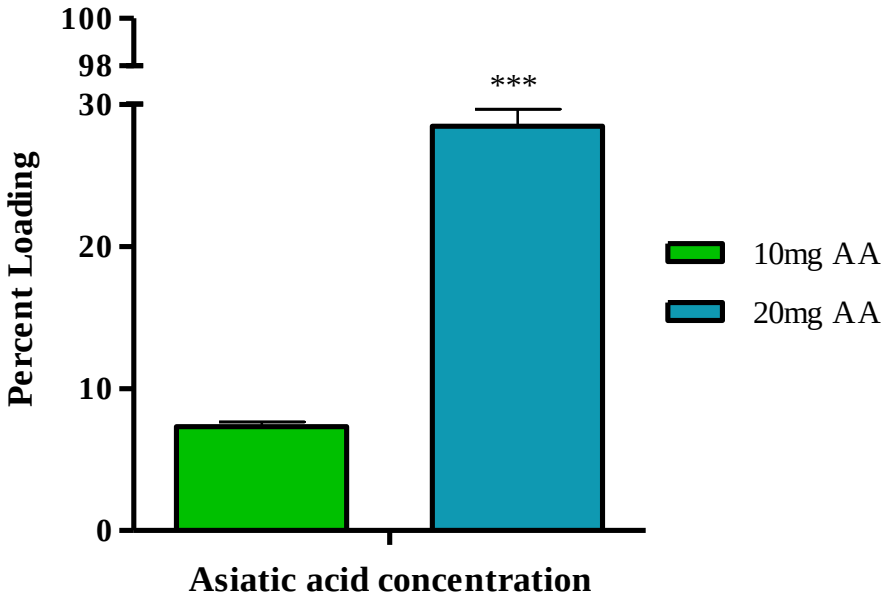

Figure 5.9: Comparison of drug loading efficiency of asiatic acid at different concentrations using 2:1 ratio of aqueous phase: organic phase

The highest NP yield was obtained when the ratio of aqueous phase to organic phase was 2:1. Thus, the maximum amount of asiatic acid that could be loaded into the NPs was re-established. As no significant differences were observed in the drug loading measurement earlier (Fig. 5.7), measurement was only performed at 10 and 20mg of asiatic acid upon making changes to the original nanoparticle preparation protocol. A significantly higher drug loading was observed at 20mg of asiatic acid. Values represent mean ± S.E. for three experiments in triplicate.

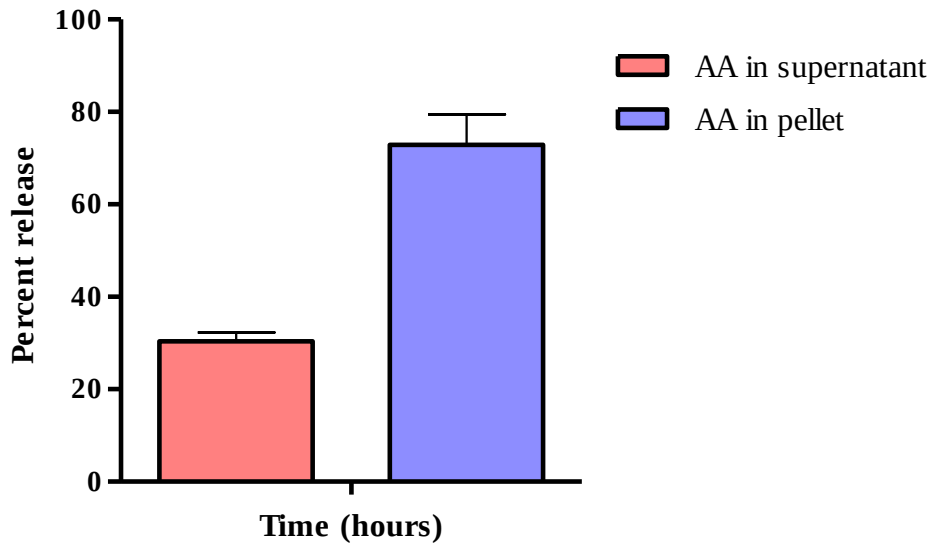

Figure 5.10: Graph showing the encapsulation efficiency of asiatic acid into the NPs

Amount of asiatic acid recorded in the pellet was the drug encapsulated within the NPs whereas amount of drug recorded in the supernatant was free drug in the formulation (i.e., un-encapsulated). Encapsulation efficiency of the NPs was 72.8 ± 6.5%, which indicates that 72.8% of the drug present in the formulation was encapsulated into the NPs, remaining drug was the free drug. Values represent mean ± S.E. for three experiments in triplicate.

5.2.7 Size, Surface Charge and Polydispersity Measurements of Blank and Asiatic acid-loaded Nanoparticles

It was important to characterise the nanoparticles prepared using the above protocol. Characterisation of nanoparticles includes measurements of size, surface charge and polydispersity (PDI). Although size and surface charge are understood by everyone, PDI is a measure of the homogeneity of the formulation. PDI < 0.1 is considered as ideal and indicates a monodisperse formulation.

Blank and asiatic acid-loaded NPs (Section 2.6.1) were characterised for their mean diameter, size distribution and surface charge. Blank and asiatic acid-loaded NPs showed a similar average diameter ranging from 133 ± 1.8nm to 152.5 ± 2.7nm and 134.4 ± 1.5nm to 150.2 ± 1.2nm respectively ($p > 0.05$), (Fig. 5.11). The diameter of asiatic acid-loaded and blank nanoparticles confirmed the encapsulation of the drug as opposed to its surface adsorption (Shah and Amiji 2006). NPs were monodispersed, PDI value not exceeding more than 0.1 (Table 5.4), thus confirming the formation of a stable suspension ($p > 0.05$ for average PDI of both sets of NPs).

Both NPs, blank and asiatic acid-loaded, showed a similar average negative surface charge ranging from -17 ± 1.3mV to -31 ± 2.5mV for blank NPs and -19.8 ± 1mV to -29.6 ± 0.7mV ($p > 0.05$) (Fig. 5.12); the negative charge is attributed to the carboxylic group present on the PCL chain (Leroueil-Le Verger et al. 1998). The high zeta potential values achieved ensure a high-energy barrier thus favouring a good stability (Benita and Levy, 1993) as it allows an ideal stabilization of nanoparticles due to prevention of aggregation by strong repulsive forces (Muller 1991).

Storage time had no significant difference on average nanoparticle size, surface charge or PDI within each of group of the two data sets ($p > 0.05$).

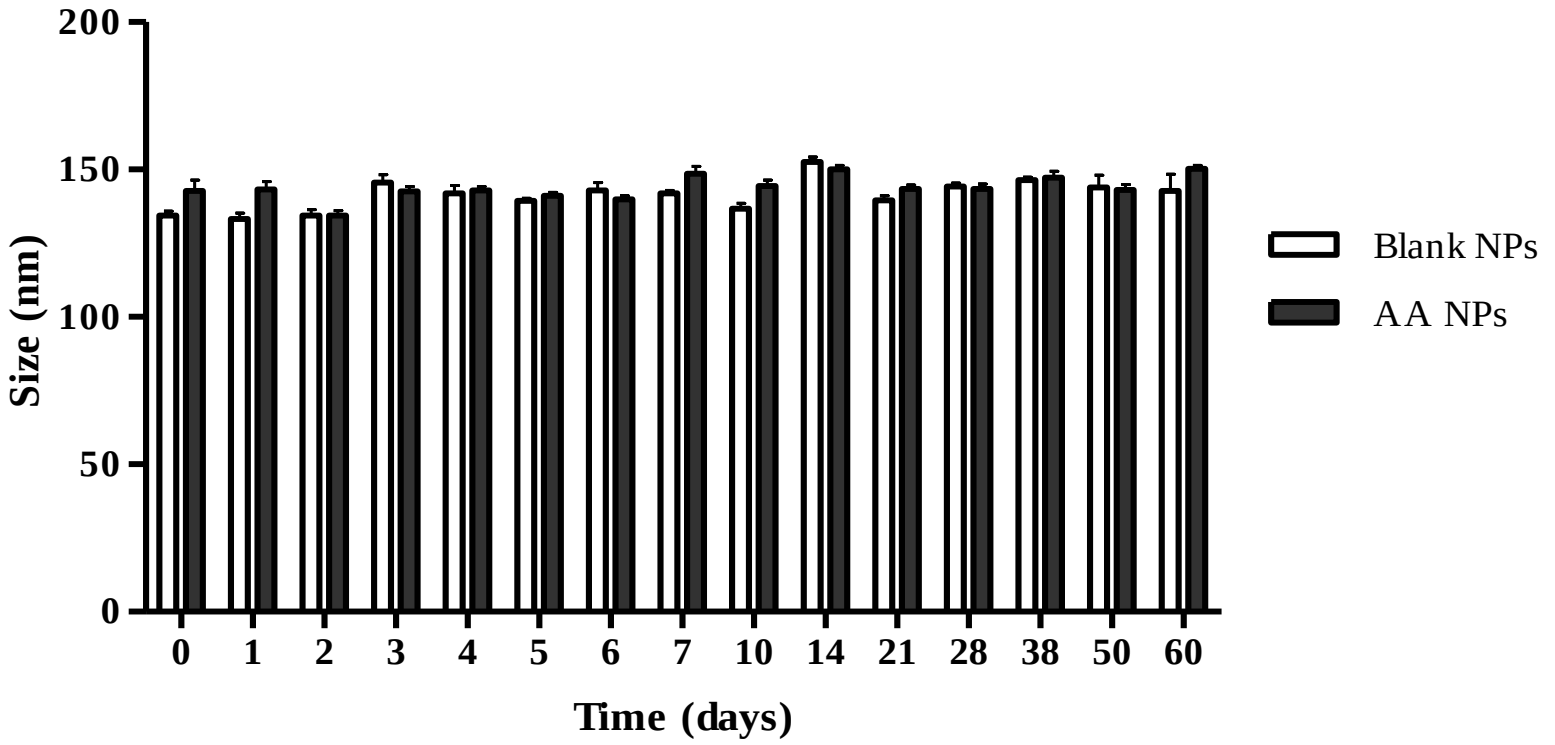

Figure 5.11: Size comparison of blank and asiatic acid-loaded NPs at 4°C.

Both, blank and asiatic acid-loaded NPs were stable at 4°C, showed a similar average diameter and did not show any significant differences in their average size over the period of 60 days. Values represent mean ± S.E. for three experiments in triplicate.

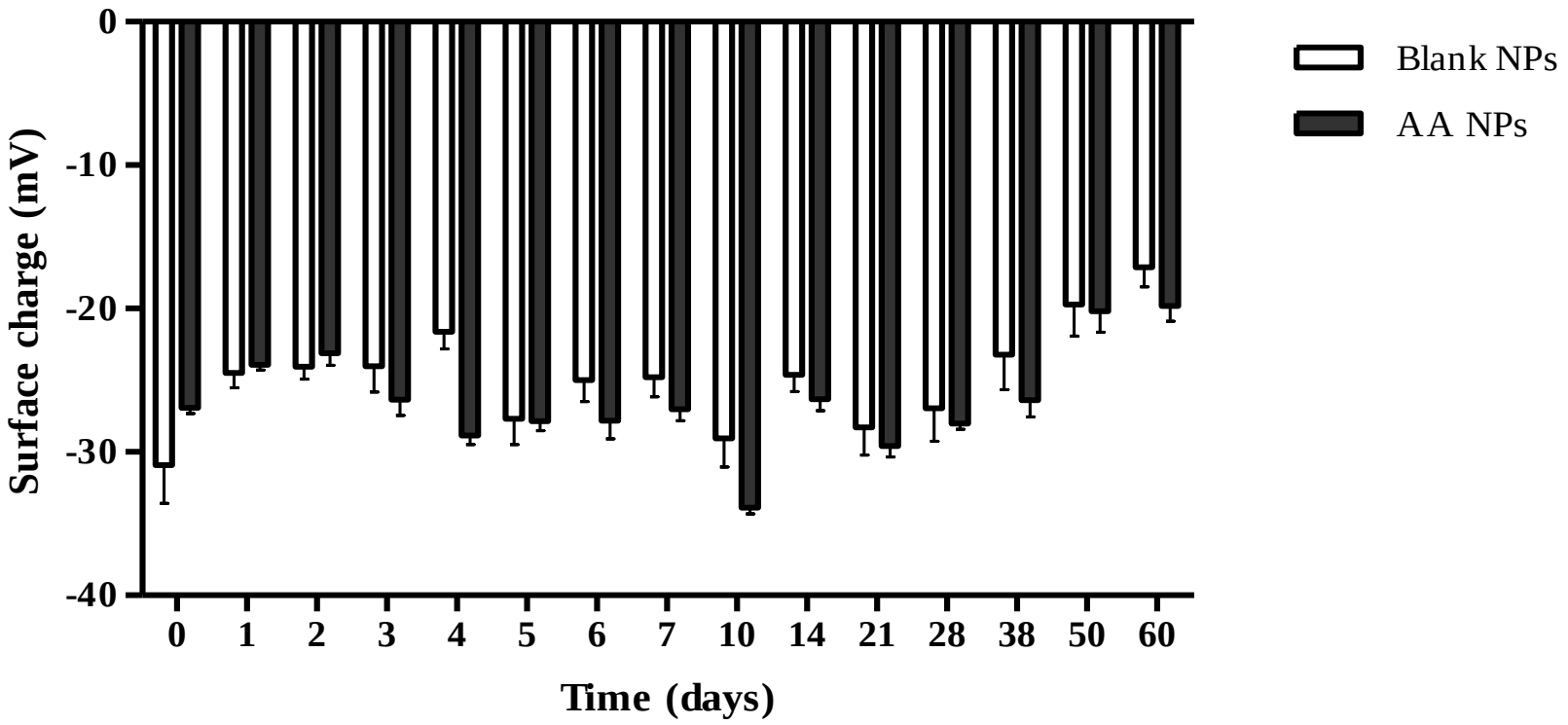

Figure 5.12: Surface charge comparison of blank and asiatic acid-loaded NPs at 4°C

Both, blank and asiatic acid-loaded NPs were stable at 4°C, showed a similar average surface charge and did not show any significant differences in their average surface charge over the period of 60 days. Values represent mean ± S.E. for three experiments in triplicate.

Table 5.4: Polydispersity comparison of blank and asiatic acid-loaded NPs at 4°C

Day	Polydispersity	
	Blank NPs	**AA NPs**
0	0.057 ± 0.016	0.068 ± 0.011
1	0.053 ± 0.005	0.055 ± 0.012
2	0.072 ± 0.013	0.065 ± 0.018
3	0.048 ± 0.015	0.060 ± 0.012
4	0.075 ± 0.010	0.067 ± 0.019
5	0.035 ± 0.007	0.068 ± 0.016
6	0.054 ± 0.005	0.035 ± 0.006
7	0.043 ± 0.008	0.063 ± 0.010
10	0.033 ± 0.012	0.070 ± 0.007
14	0.046 ± 0.014	0.063 ± 0.011
21	0.078 ± 0.012	0.061 ± 0.010
28	0.066 ± 0.008	0.050 ± 0.008
38	0.067 ± 0.009	0.048 ± 0.007
50	0.077 ± 0.005	0.060 ± 0.007
60	0.088 ± 0.010	0.071 ± 0.009
Average PDI	**0.059 ± 0.010**	**0.060 ± 0.011**

The average PDI of both sets of NPs, blank and AA-loaded, was less than 0.1 over the period of 60 days, thus indicating a monodisperse formulation.. No significant differences were observed in the PDI of blank and asiatic acid-loaded nanoparticles. Values represent mean ± S.E. for three experiments in triplicate.

5.2.8 Drug Release in PBS in the Absence and Presence of Lipase

Following the characterisation of nanoparticles for size, surface charge, PDI and drug loading, the need arose to assess the drug release profile. Also, it was important to understand the rate of drug release from asiatic acid-loaded nanoparticles to carry out further *in vitro*, cell line-based experiments.

In vitro drug release of asiatic acid-loaded nanoparticles was performed at 37°C in 1X PBS at pH 7.4, maintained on a rocker, in the absence and presence of lipase from *Pseudomonas sp.* Amount of drug released in the supernatant and the amount of drug remaining in the pellet after re-centrifugation of the nanoparticles was calculated using HPLC. For ease of understanding, concentrations were plotted as a mean percentage of the total drug present in the formulation.

The initial amount of un-encapsulated drug recorded in the absence of lipase, immediately after NP preparation, was (30 ± 1.9%) at 0 hours. Drug release plateaued after 0 hour, meaning that no additional drug was released from the nanoparticles ($p > 0.05$ for asiatic acid release over 24 hours) (Fig. 5.13). Thus, 72.8 ± 6.5% of the drug was encapsulated into the NPs and was not released even after 24 hours in 1X PBS maintained at 37°C. The total percentage of intact PCL NPs in the pellet was 74 ± 5.6% at 0 hours and 71.4 ± 5.1% at the end of 24 hours (Fig. 5.13). Hence PCL did not degrade even at the end of 24 hours ($p > 0.05$).

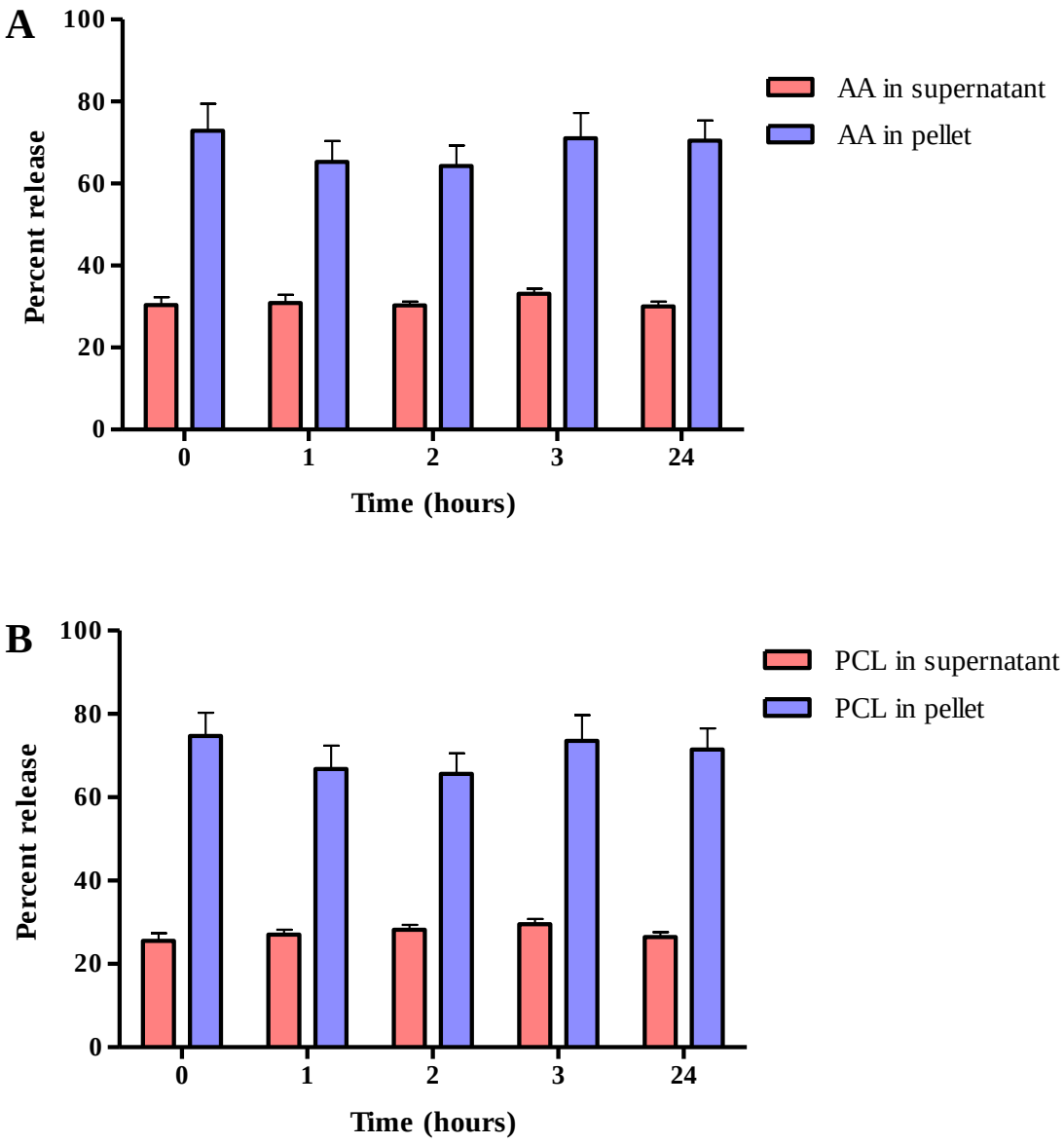

Figure 5.13: Asiatic acid release and PCL breakdown from asiatic acid-loaded NPs in PBS (pH7.4) maintained at 37°C on rocker.

The total percentage of asiatic acid release (A) and PCL breakdown (B) in the formulation was measured over a period of 24 hours. No additional drug release after the initial record of free drug was observed over 24 hours ($p > 0.05$). Majority of the PCL NPs were intact in the pellet and hence not degraded even at the end of 24 hours ($p > 0.05$). Values represent mean ± S.E. for three experiments in triplicate.

To encourage release of asiatic acid from asiatic acid-loaded NPs, 45unts/l lipase from *Pseudomonas sp*. was added to the 1X PBS. Lipase enhanced the rate of drug release from the asiatic acid-loaded nanoparticles (Fig. 5.14). Again (as previously seen in Fig. 5.13), 30 ± 4.7% of the un-encapsulated drug was measured in the supernatant at 0 hours. However, the rate of asiatic acid release from the asiatic acid-loaded nanoparticles in the presence of lipase increased steadily over a period of 24 hours. The total amount of drug released at the end of 24 hours was 65 ± 3.8% ($p < 0.001$). Results show a steady release of asiatic acid from asiatic acid-loaded nanoparticles over a period of 24 hours, in the presence of lipase. Measurement of the total percentage of the intact PCL nanoparticles in pellet showed an initial amount of 64 ± 6.9% with a steady decrease of the amount of PCL nanoparticles in the pellet (Fig. 5.14). The amount of PCL nanoparticles in the pellet at the end of 24 hours was 34 ± 4.8% ($p < 0.01$).

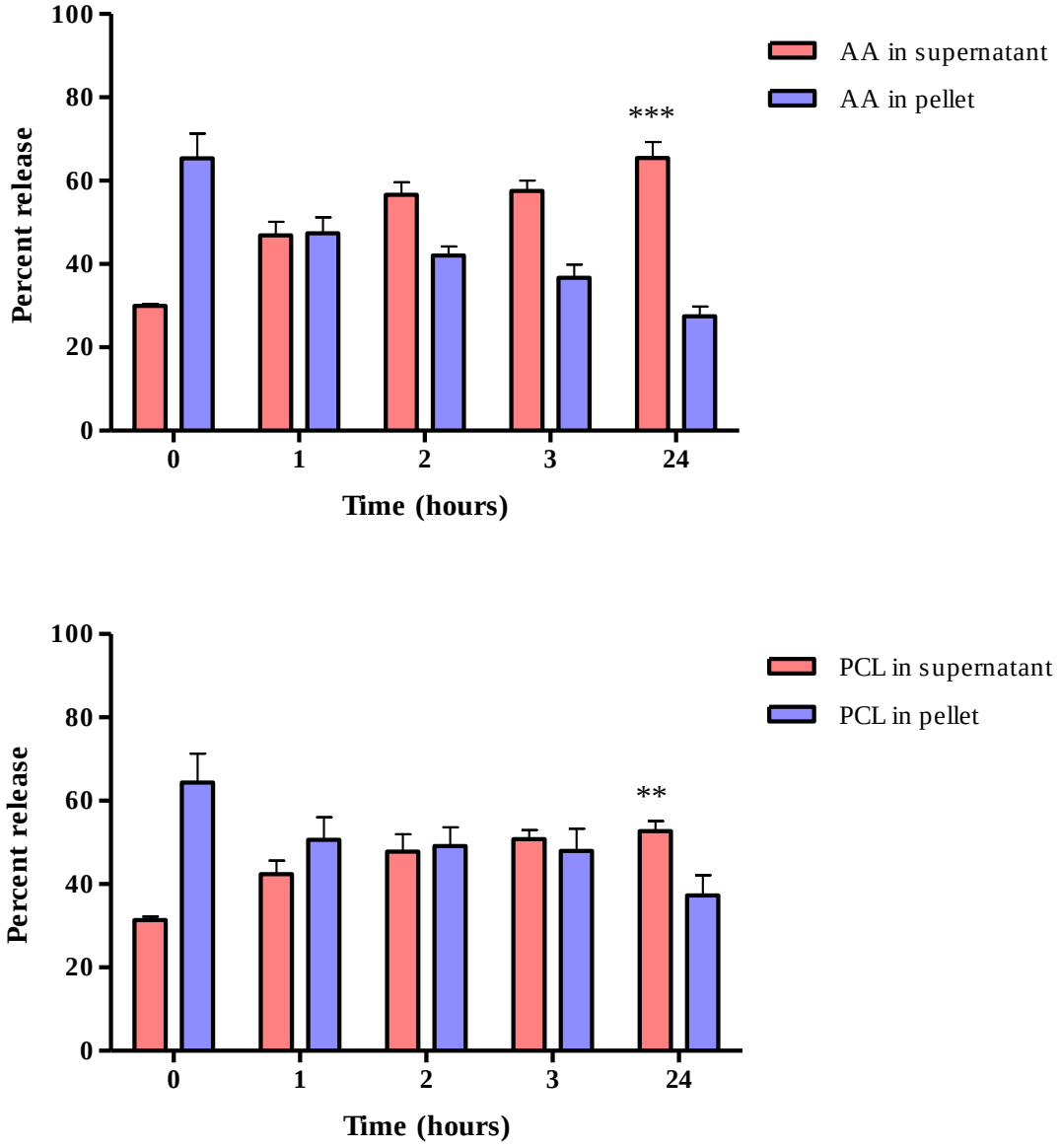

Figure 5.14: Asiatic acid release and PCL breakdown from asiatic acid-loaded NPs in PBS (pH 7.4) containing Lipase from *Pseudomonas sp.* maintained at 37°C on rocker

The total percentage of asiatic acid release (A) and PCL breakdown (B) in the formulation was measured over a period of 24 hours. A slow steady breakdown of PCL NPs along with asiatic acid release in the supernatant was observed, increasing with every hour, over a period of 24 hours. Significant differences in drug release and PCL breakdown were observed at 24 hours. Remaining drug that was not released into the supernatant was encapsulated into the PCL NPs and remained in the pellet even at the end of 24 hours. Values represent mean ± S.E. for three experiments in triplicate.

5.2.9 Drug release in Cell Culture Medium

As further experiments of nanoparticles on in vitro cell lines would require the use of cell culture medium EMEM, we assessed the rate of drug release from asiatic acid-loaded nanoparticles in EMEM.

Drug release from asiatic acid-loaded nanoparticles was very unstable ($p > 0.05$ for asiatic acid release over 24 hours) (Fig. 5.15). Although the experiment was performed three times; the inconsistency of the results can be explained by the inability of the HPLC to generate well-resolved, identifiable peaks, due to the large number of proteins present in the cell culture medium, thus generating a high background signal.

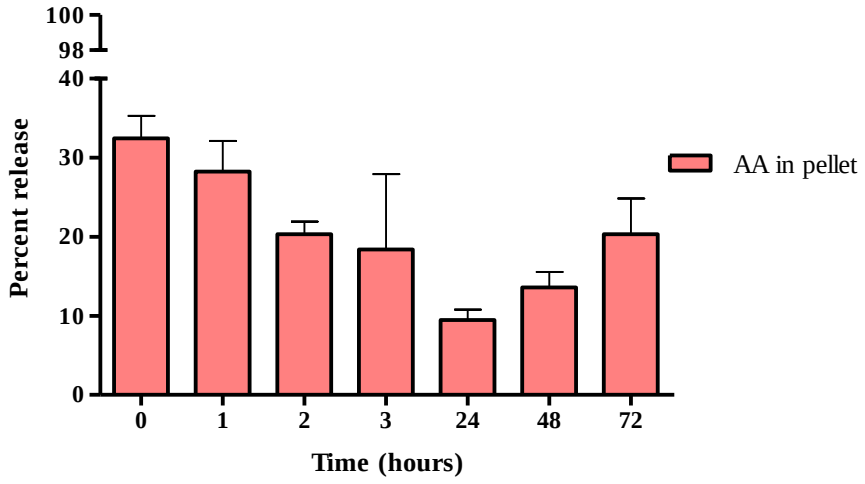

Figure 5.15: Asiatic acid release from asiatic acid-loaded NPs in cell culture media maintained at 37°C on rocker with 5% CO_2

The results of asiatic acid release from asiatic acid-loaded NPs were inconsistent due to the large background noise generated by the proteins present in the cell culture medium thus giving unresolved peaks in the HPLC. No significant differences were observed. Values represent mean ± S.E. for three experiments in triplicate.

5.2.10 Effect of pH on Drug Release from Asiatic acid-loaded Nanoparticles

As tumour cells display an acidic environment, a pH study was conducted to study the drug release characteristics from asiatic acid-loaded NPs in an acidic pH.

Drug release was performed in 1X PBS at pH5.5 maintained at 37°C. The initial amount of un-encapsulated asiatic acid, immediately after NP preparation, was 29 ± 2.8% at 0 hours (Fig. 5.16). No additional drug was released from the NPs after 24 hours ($p > 0.05$). Thus, 70 ± 7.3% of the drug was encapsulated into the NPs and was not released even after 24 hours in the 1X PBS maintained at 37°C. Data shows that the amount of PCL NPs in the supernatant increased at a very slow rate over the period of 24 hours (Fig. 5.16), and a significant difference was observed at the end of 24 hours (0 hours 78.6 ± 4.3%, 24 hours 59.1 ± 2.8%; $p < 0.01$).

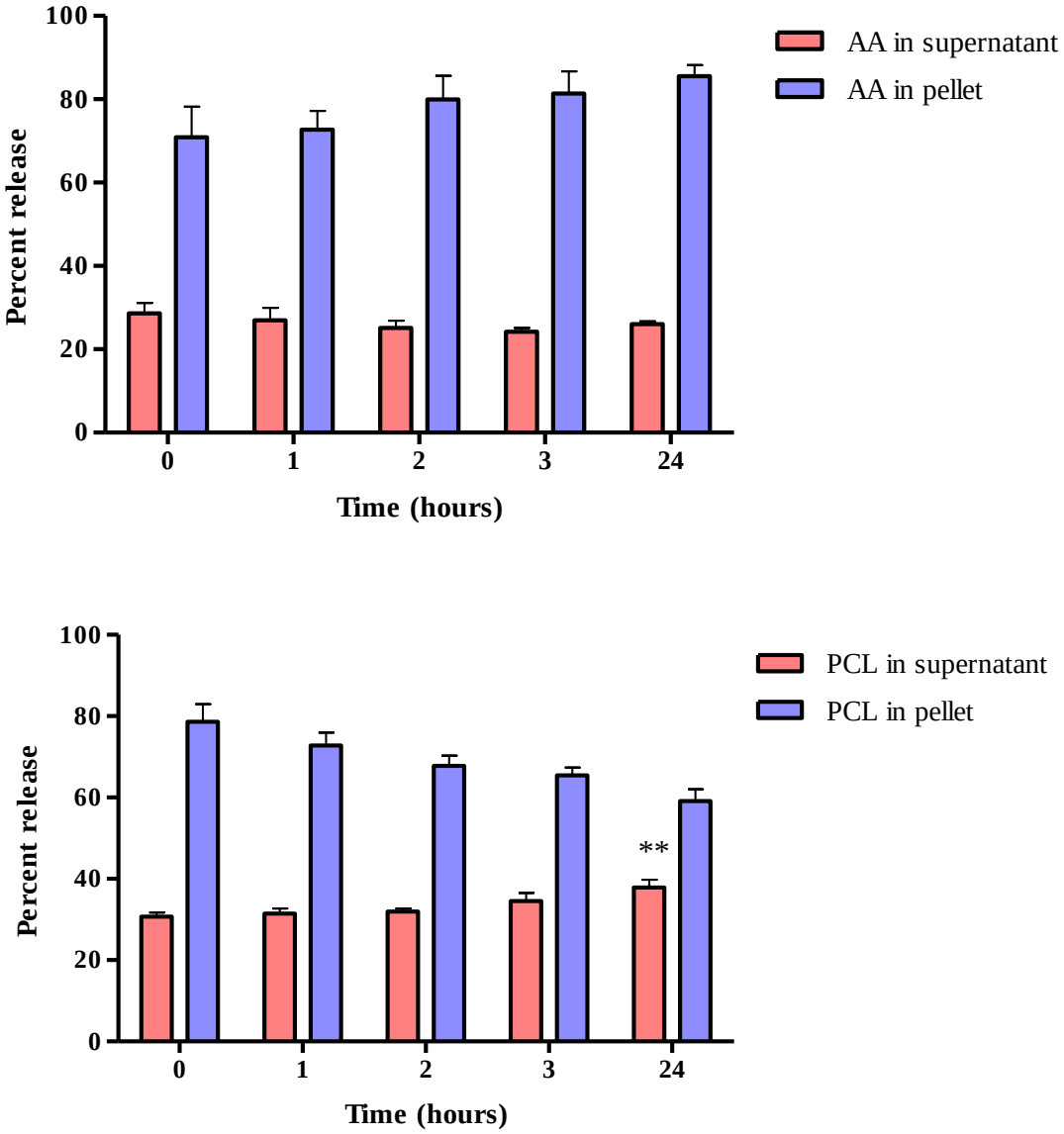

Figure 5.16: Asiatic acid release and PCL breakdown from asiatic acid-loaded NPs in PBS (pH 5.5) maintained at 37°C on rocker

The total percentage of asiatic acid release (A) and PCL breakdown (B) in the formulation was measured over a period of 24 hours. Although no additional asiatic acid was released into the supernatant after the initial record of free drug ($p > 0.05$); a significant increase in the amount of PCL was observed in the supernatant following incubation for 24 hours. The remaining drug that was not released was encapsulated into the PCL NPs in the pellet. Values represent mean ± S.E. for three experiments in triplicate.

5.2.11 Freeze Drying

Long term storage of nanoparticles can either be performed by storage in aqueous media or by freeze drying. Although not all nanoparticles are stable in aqueous media for a longer duration, freeze drying may not always be necessary. Freeze drying is method of water removal from nanoparticles which helps in increasing the shelf life.

Freeze-dried NPs were re-suspended in 5ml distilled water and analysed for their size and surface charge. Size analysis of the nanoparticles using the Malvern Zetasizer Nano-ZS showed a 10-fold increase in the size of the particles freeze-dried in the absence or presence of 1% and 10% sucrose after re-hydration in distilled water (size following re-hydration 905.1 ± 9.11nm). This increase in size is represented in the scanning electron microscopy images (Fig. 5.17) where large aggregates of nanoparticles can be seen as opposed to the presence of distinct nanoparticles. Nanoparticles were greater than 1µm in size and were not accurately measured by the zetasizer. Additionally, re-hydration of the freeze-dried particles was difficult as the particles settled at the bottom of the vial and large clumps were observed.

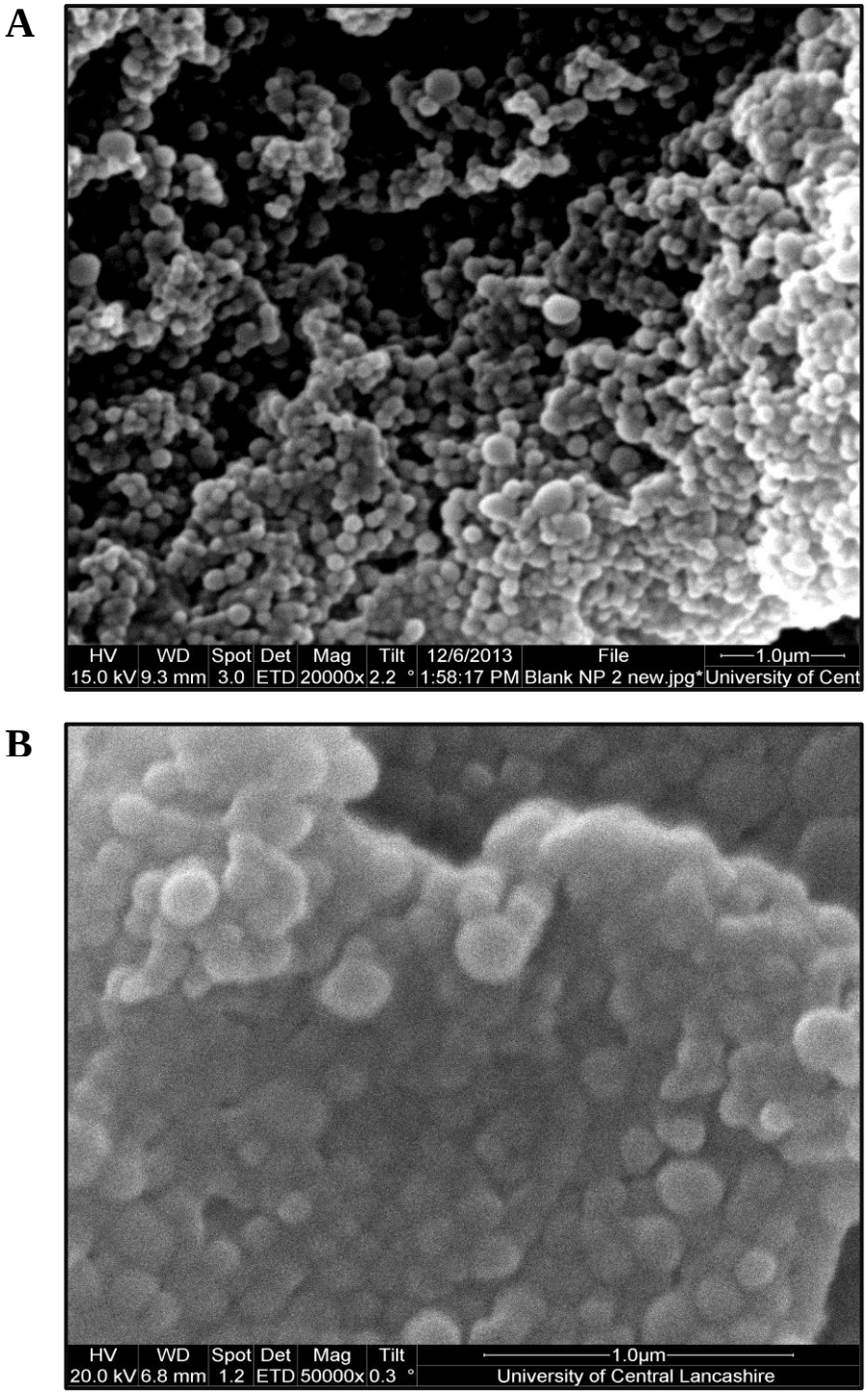

Figure 5.17: SEM image of freeze-dried blank and asiatic acid-loaded NPs in the absence of sucrose

Images show the formation of distinct spherical blank (A) and asiatic acid-loaded (B) NPs with a smooth surface and confirms the size of blank and asiatic acid-loaded NPs to be in the range of 130-150nm.

5.3 Discussion

Preliminary Nanoparticle Preparation Studies

In order to establish a protocol to produce stable nanoparticles, different experimental techniques were examined (Section 2.6). Nanoparticles produced by ultra-sonification and homogenisation processes produced NPs greater than 180nm in size (Figs. 5.1 & 5.2; Table 5.1) that were unstable and precipitated out (particle aggregation) by the tenth day after preparation. In comparison, nanoparticles prepared by magnetic stirring, although similar in size, showed an improved stability ($p < 0.001$).

One of the reasons for nanoparticle aggregation is that nanoparticle structure breakdown occurs due to the shear forces applied by the homogeniser or the ultra-sonicator (Konan et al., 2002). The high intensity ultra-sonic waves or the high pressure generated by the homogeniser helps breakdown the nanoparticle to a smaller size but also increases the temperature of the system thus inducing material degradation leading to the loss of nanoparticle stability (Konan et al., 2002; Lamprecht et al., 2000; Prombutara et al., 2012). In addition, these techniques lead to reduction in the surface charge of the nanoparticle thus making the particles more prone to aggregation due to a low electrostatic repulsion (Prombutara et al., 2012). At lower temperatures (ice cooling for ultra-sonification and homogenisation processes), the kinetic energy of the particles is reduced and the fraction of particles with kinetic energy less than the potential depth increases resulting in an increasing particle aggregation (Fiedler et al., 2007).

Another reason for nanoparticle aggregation can be explained by the DLVO (Derjaguin and Landau, Verwey and Overbeek) theory. Brownian motion between particles in a nanoparticle suspension causes particle collisions. According to the DLVO theory, exposure of particle surfaces to each other upon contact and the short-range thermodynamic interactions, such as van der Waals and electrostatic double layer

forces, may allow particle-particle attachment to occur resulting in particles over 1µm in size (Hosokawa et al. 2007; Hotze et al. 2010). As the ultra-sonification and homogenisation methods generate a lot of energy, it leads to a greater Brownian motion of the NPs thus causing homoaggregation. As the total kinetic energy of the particles is high, particles collide more often and form large dendritic aggregates, thus leading to NP aggregation as was observed in this study (Buffle and Leppard, 1995; Hotze et al., 2010).

Parenteral route of nanoparticle administration requires sterile and apyrogenic products (Goldbach et al., 1995). For the systemic delivery of NPs prepared in this study, it would be necessary to filter and create a sterile NP suspension. The type of filter used affects the long-term stability of NPs. In order to assess the best type of filter for the NPs prepared in this study, three different types of filters were used along with a set of unfiltered samples to obtain a comparison.

Non-filtered samples were not sterile and unstable, while precipitation was observed (Figs. 5.3 & 5.4, Table 5.2). Using Whatman™ nylon membranes, the filtration of nanoparticle suspension was difficult and very small amounts of sample volumes (~2ml) could be filtered before changing the membrane. Precipitation after filtration was observed in most samples except in the samples where Millex® MCE filters were used. In addition, sub 210nm particles were filtered through Millex® MCE membranes without any significant change in nanoparticle size or breakage of the nanoparticles.

The failed attempts of nanoparticle filtration techniques could be due to clogging of filtration membranes which is observed when the particle size is too close to the membrane pore size (Konan et al., 2002).

The degradation and stability of the NPs depends on their preparation method, polymer properties such as initial molecular weight and physical and chemical

parameters such as temperature and pH (Lemoine et al., 1996). To study the effects of storage temperature on PCL nanoparticles prepared using the protocol in Section 2.6.1, a set of blank nanoparticles was each stored at room temperature and at 4°C.

Nanoparticles stored at 4°C showed an improved stability over a period of 60 days with no significant changes in particle size and surface charge while at room temperature, the NPs showed rapid particle degradation and aggregation by day 10 (Fig. 5.5); similar results were also obtained by Lemoine et al., (1996). These results are also comparable to those obtained by Coffin and McGinty (1992) where only minor changes in the molecular weight of the poly(D,L-lactide) and poly(ε-caprolactone) nanoparticles was observed .

Nanoparticles, in a suspension undergo constant Brownian motion. As the temperature of the system increases, the viscosity of the base fluid in the nanoparticle suspension decreases, resulting in an increased Brownian motion of the nanoparticles. This results in the particles coming into close proximity to each other. Thus, it can be speculated that increased Brownian motion increases the size of nanoparticles due to particle attachment by short-range thermodynamic interactions (Hotze et al. 2010; Sullivan & Edmondson 2008; Jang & Choi 2004).

In addition, the third law of thermodynamics states *'The entropy of an object at absolute zero is zero, i.e. if an object is cooled down to -273°K, it would cease to have any kinetic energy within its molecules'*. Thus, at a lower temperature, kinetic energy of the particles is lost reducing their Brownian motion and particle collision (Sullivan and Edmondson, 2008). Hence, nanoparticles maintained at 4°C showed an improved stability over NPs stored at room temperature.

Nanoparticle characterisation

Effective transvascular delivery of therapeutics into malignant glioma cells remains challenging due to the presence of the BBB. However, ultra-structural studies of the BBB have shown that the size of the fenestrations and gaps in the blood tumour barrier increases to 40-90nm and 100-250nm respectively (Sarin et al., 2008). In addition, the net charge on the plasma membrane of a cell is -40 to -90mV (Purves et al. 2001). Hence, nanoparticles with a moderate negative surface charge and a size of less than 250nm should, theoretically, be able to move across the plasma membrane of the cell, unimpeded.

PCL NPs were prepared by the solvent displacement method (Section 2.6.1). The solvent displacement method is a convenient, reproducible, fast, and economic one-step manufacturing process for the preparation of monodisperse, polymeric nanoparticles in a size range of approximately 50 – 300nm (Beck-Broichsitter et al., 2010).

Nanoparticles were characterised for their mean diameter, size distribution and surface charge. No significant differences were observed in the size of blank and asiatic acid-loaded NPs (Fig. 5.11). The diameter of the drug loaded NPs confirms the encapsulation of the drug as opposed to its surface adsorption (Shah and Amiji, 2006). As the NP size has remained unchanged and drug release has been observed from asiatic acid-loaded NPs, it can be speculated that asiatic acid was incorporated into the matrix of the nanoparticles as opposed to its encapsulation in the core of the nanoparticle shell. The particles were monodisperse, the PDI value not exceeding more than 0.1, thus confirming the formation of a stable suspension (Table 5.4). Factors that are essential for the ultimate determination of particle size include polymer concentration in the organic phase, polarity of the solvents and the ratio of organic: aqueous phase (Zili et al., 2005).

Both sets of nanoparticles, blank and asiatic acid-loaded, showed a negative surface charge. The negative charge is attributed to the carboxylic group present on the PCL chain (Leroueil-Le Verger et al., 1998). Blank and asiatic acid-loaded nanoparticles had a similar surface charge, confirming again, the encapsulation of the drug as opposed to surface adsorption (Fig. 5.12) (Shah and Amiji, 2006). The negative zeta potential values achieved ensured a high-energy barrier of the nanoparticles thus favouring a good stability and prevention of aggregation by strong repulsive forces (Benita and Levy 1993; Muller 1991).

In order to increase the encapsulation efficiency of the drug into the NPs, it was first necessary to increase the yield of the nanoparticles from the polymer itself (Liu et al., 2007). Different variables were altered as previously described (Section 2.7.3).

Nanoparticle yield increased to 28.5 ± 1.2% upon altering the ratio of aqueous phase to organic phase to 2:1 (Fig. 5.8). It was thus decided to prepare nanoparticles using a 2:1 ratio of aqueous phase to organic phase for all further experiments. The increased yield of the PCL nanoparticles can be explained due to the longer hydrophobic PCL block chain that was formed as a result of an increased amount of aqueous phase (Feng et al., 2012). PCL, in the presence of PEG, forms amphiphilic PEG-PCL structures with a hydrophilic PEG block and a hydrophobic PCL block. These amphiphilic PEG-PCL blocks self-assemble in an aqueous environment to form micelles. Thus, the increased amount of the aqueous environment increased the hydrophobic property of the nanoparticles by producing longer and hydrophobic interactions between PCL microdomains in the aqueous environment. In addition, using a 2:1 ratio of aqueous phase to organic phase, the total volume of the nanoparticle suspension before centrifugation reduced to 75 ml as opposed to 100 ml while using a 1:1 ratio of aqueous phase to organic phase. This, in turn, increased the concentration of

PCL and PEG in the acetone-water environment, thus resulting in an increased number of NPs (Choi et al., 2005).

A drug loading content of the nanoparticles would increase the efficiency of the nanoparticles in its systemic administration. It is also important to be able to achieve the EC_{50} concentration of the drug inside the nanoparticles. Thus, in an attempt to increase the drug loading efficiency of the nanoparticles, the nanoparticle yield was increased (Fig. 5.8). The percentage drug loading of the nanoparticles increased upon altering the ratio of aqueous phase to organic phase to 2:1 (Fig. 5.9). The maximum loading efficiency was achieved when the initial amount of drug added was 20 mg (Fig. 5.9). The loading efficiency increased with increasing amount of drug; a finding similar to Chawla & Amiji (2002).

Encapsulation efficiency of a drug depends on the structure, length, and molecular weight of hydrophilic and hydrophobic fragments of the polymer (Wang et al., 2011). PCL is a hydrophobic polymer and thus it is insoluble in aqueous phase (Shenoy and Amiji, 2005). This insolubility of PCL in water causes it to coagulate and form a core-shell structure where the core consists of a hydrophobic PCL chain and the shell consists of a hydrophilic PEG chain (Feng et al., 2012; Wang et al., 2011). Hydrophobicity of the drug leads to hydrophobic interactions between PCL and asiatic acid, while the interaction of the water and hydrophilic PEG allows the drug to dissolve in water. This interaction is similar with other hydrophobic drugs such as curcumin used in studies by Feng et al (2012). Thus, the drug could be encapsulated into the core of the nanoparticle. As asiatic acid is a hydrophobic drug, it would be insoluble in water and thus would need a micelle-like system for its delivery. The use of PEG thus allowed PCL and asiatic acid to dissolve in water and form nanoparticles consisting of a core of the hydrophobic drug- asiatic acid.

Drug Release Studies

The *in vitro* drug release of asiatic acid-loaded nanoparticles was performed in PBS, pH 7.4, maintained at 37°C on a rocker, in the absence and presence of lipase from *Pseudomonas sp.* The amount of drug released in the supernatant and the amount of drug remaining in the pellet after re-centrifugation of the nanoparticles was determined by the HPLC. The amount of asiatic acid, in both cases, was plotted as a mean percentage of the total drug present in the formulation.

An initial amount of drug was recorded in the absence of lipase at 0 hours, with no further asiatic acid release (Fig. 5.13). Lipase enhanced the rate of drug release from the asiatic acid-loaded nanoparticles which increased steadily over 24 hours (Fig. 5.14).

PCL nanoparticles, due to their high crystallinity and hydrophobicity, have a slow degradation rate in an aqueous media. This crystallinity of PCL increases with a decrease in its molecular weight (Chawla and Amiji, 2002). PCL is available in a wide range of molecular weight. The average molar mass distribution of PCL ranges from 10,000 to 80,000. PCL used for this study has a molecular weight of 14,000 (average molar mass distribution (M_n) of 10,000). Due to these properties of PCL, no significant amount of degradation of PCL NPs was observed in PBS at pH 7.4 (Fig. 5.13). However, in the presence of lipase, the degradation of PCL nanoparticles proceeded rapidly as opposed to release in the absence of lipase, (Figs. 5.13 & 5.14). In addition, a large amount of the drug was found in the re-centrifuged pellet of the nanoparticle suspension with the remaining being present in the supernatant (Figs. 5.10 & 5.13). This phenomenon can be explained by the hydrolytic disruption of the ester bonds of polymeric nanoparticles, thus allowing drug diffusion. The ester hydrolysis and drug diffusion are also controlled by the length of the hydrophobic and hydrophilic chains present in the nanoparticle (Feng et al., 2012). Another possible explanation for the

presence of the free drug can be explained due to the surface adsorption of the drug onto the nanoparticles as opposed to their encapsulation (Shah and Amiji, 2006).

The presence of lipase enhances the degradation rate of the polymer as compared to degradation in an aqueous media (Cho et al., 2002; Shah and Amiji, 2006; Wu et al., 2000). PCL degradation begins in the amorphous region prior to degradation in the crystalline region (Cho et al., 2002). In the presence of lipase, an increased PCL degradation was observed. Gan et al., 1999 have suggested that lipase 'eats' up the nanoparticles one by one so that the rate of nanoparticle degradation is dependent on the enzyme concentration. The healthy adult serum lipase concentration is in the range of 30-190 units/l which is comparable to the *in vitro* lipase concentration used for this study (45units/l) (Chawla and Amiji, 2002). Since PCL follows surface erosion, the steady release of the drug in the presence of lipase could be due to erosion of the polymer shell and subsequent release of the drug (Mukerjee et al., 2007). Thus, it can be speculated that due to the absence of surface erosion of the polymer by the lipase, drug release from the nanoparticles was low in PBS alone.

As the future study of the nanoparticles involves the use of *in vitro* cell lines, the nanoparticles, blank or asiatic acid-loaded, would have to be suspended into the cell culture medium. To assess the stability of asiatic acid-loaded nanoparticles in the cell culture medium, we suspended the nanoparticles into EMEM. Drug release from the asiatic acid-loaded nanoparticles in the cell culture media was very unstable (Fig. 5.15). The experiment was performed three times; however, the inconsistency of the results was due to the inability of the HPLC to generate well-resolved, identifiable peaks, due to the large number of proteins present in the medium generating a high background signal. Although, no similar experiments could be found, this problem might be overcome through the use of more sophisticated machines such as gas chromatography.

The environmental acidity or pH of living cells and tissues is a major factor influencing molecular processes involved in cell cycle progression, cell proliferation, and differentiation (Song et al. 2006). Likewise, oncogenesis, malignant transformation, metastasis, and angiogenesis are greatly influenced by environmental acidity (Honasoge and Sontheimer, 2013; Song et al., 2006). It has been long proposed that the microenvironment of tumours is more acidic compared to normal tissues, with the extracellular pH being <7 (Gerweck and Seetharaman, 1996; Song et al., 2006). Tumour cells show enhanced glycolysis and preferentially convert glucose to lactic acid, thus causing a decrease in the pH of the surrounding microenvironment (Griffiths, 1991; Honasoge and Sontheimer, 2013). Hence, it was important to study the drug-release profile from asiatic acid-loaded nanoparticles in an acidic medium. PBS was used in all these experiments as PBS is isotonic and non-toxic to cells.

Figure 5.16 shows that a large amount of the drug was encapsulated into the nanoparticles and was not released even after 24 hours in the 1X PBS maintained at 37°C. The amount of PCL in the pellet decreased steadily with time, after the nanoparticle suspension was re-centrifuged and suspended in 1X PBS pH 5.5. Asiatic acid has a pKa of 4.7 and is thus acidic in nature (data from Chemicalize.org). It is due to this reason that no drug release was observed even after suspension in acidic PBS for 24 hours. Thus, the acidic pH did not significantly change the drug release profile from the NPs, however, nanoparticle degradation increased significantly, but at a slow rate in PBS pH 5.5.

Freeze Drying and Scanning Electron Microscopy

Freeze-drying is an industrial process of drying by freezing and sublimation of ice. It is used to convert solutions of labile materials into solids of sufficient stability for distribution and long-term storage (Abdelwahed et al., 2006a). Freeze drying is mainly

performed to prevent non-enzymatic polymer hydrolysis and to prevent drug leakage out of the nanoparticles. Also, long-term storage of nanoparticles in an aqueous medium can lead to particle aggregation. On the other hand, freeze-drying may generate stress that could destabilize colloidal suspension of nanoparticles, especially, the stress of freezing and dehydration (Abdelwahed et al., 2006b). Thus, in order to prevent the collapse of the nanoparticle suspension, addition of a cryoprotectant may be required. The most popular cryoprotectants encountered in the literature for freeze-drying nanoparticles are sugars: trehalose, sucrose, glucose and mannitol (Abdelwahed et al., 2006b).

The freezing step of the freeze-drying process induces dramatic changes on the frozen nanoparticle suspension. The ice crystallization leads to a phase separation and cryoconcentration of nanoparticles. Such modification induces aggregation or fusion of nanoparticles (Abdelwahed et al., 2006a). The use of a suitable cryoprotectant can prevent such damage. It has been suggested that stabilisation of liposomes and nanoparticles requires their maintenance in a vitrified state (Chasteigner et al., 1996; Crowe et al., 1994). Carbohydrates, such as sucrose, are widely used for the protection of nanoparticles and liposomes during freeze-drying as they can be easily vitrified during freezing and form a protective amorphous matrix around nanoparticles (Abdelwahed et al., 2006a).

Sucrose was chosen as the cryoprotectant in this study as it is often used for the freeze-drying of colloidal vectors. PCL nanoparticles can be freeze-dried giving an acceptable product with no macroscopic aggregation when sucrose was used (Saez et al., 2000).

In this study, freeze-drying of the nanoparticles was undertaken in the presence and absence of sucrose. However, particle size measurements of the re-hydrated freeze-

dried nanoparticles showed a 10-fold increase in size, proposing particle aggregation due to stress generated during freeze-drying (Fig. 5.17). Nanoparticles have a thin and fragile outer envelope that may not always withstand the mechanical stress of freeze-drying. Thus, the particles collapse and lead to clustering and an increase in the particle size (Abdelwahed et al., 2006a).

Based on the results of this study and the results of nanoparticle stability at 4^{o}C for 60 days, the decision was made not to freeze dry the nanoparticles but rather store them at 4°C, in distilled water, for future studies. Although nanoparticle stability was monitored following 90 days of their preparation, fungal growth was observed. Thus it was concluded that nanoparticles stable for at 4°C 60 days would be sufficient for clinical application.

SEM imaging of the nanoparticles showed the formation of distinct spherical nanoparticles, both blank and drug loaded. The particles were non-porous and had a smooth outer surface. SEM also confirmed the size of the nanoparticles to between 130-150nm (Fig. 5.17).

CHAPTER 6

Effect of Nanoparticles on Cell Viability

6.1 Introduction

Polymeric nanoparticles as vehicles of delivery of chemotherapeutic drugs have shown great potential and may revolutionize the future of cancer therapy (Ma et al., 2011). In addition, nanoparticle delivery systems may provide an improved penetration of therapeutic drugs along with a reduced risk of drug cytotoxicity in normal tissues in comparison to traditional mode of drug delivery. Factors such as reduced drug dose and increased pharmacokinetic profile can be achieved using these vectors as mode of delivery (Feng et al., 2012; Mei et al., 2009; Shenoy and Amiji, 2005). However, problems with nanoparticle delivery include biodegradation time and cellular elimination.

Objectives: We assessed the cytotoxic effects of blank and AA-loaded nanoparticles on *in vitro* cell lines using viability assay and studied differences in cell apoptosis and proliferation. Nanoparticle internalisation studies were carried out using microscopy.

6.2 Results

6.2.1 Cellular Uptake of Nanoparticles

Therapeutic effects of nanoparticles depend upon the extent of internalisation and retention by cells. Although *in vitro* experiments can provide preliminary indication to the advantages of nanoparticle formulation versus free drug, *in vivo* results may not necessarily be the same.

Nanoparticle uptake by monolayers of SVGp12 and U87-MG cell lines was examined by microscopy (Figs. 6.1-6.4). The images show fluorescence of coumarin-6 loaded PCL nanoparticles to be located in the cytoplasm, around the nucleus, thus indicating that the nanoparticles were internalised by the cells. Presence of punctate fluorescence with coumarin-6 loaded nanoparticles confirms nanoparticle uptake.

In the SVGp12 cell line, higher uptake was observed following 24 hours of incubation with 0.5% coumarin-6 loaded nanoparticles $6.0x10^8 \pm 0.15x10^8$ AU as opposed to $4.3x10^8 \pm 0.2x10^8$ AU following 18 hours of incubation.

In the U87-MG cell line, higher uptake was observed following 24 hours incubation with 0.5% coumarin-6 loaded nanoparticles $5.0x10^8 \pm 0.4x10^8$ AU as opposed to $2.9x10^8 \pm 0.1x10^8$ AU following 18 hours of incubation, $p < 0.05$.

A significant difference in the uptake of 0.05% coumarin-6 loaded nanoparticles was observed following 18 hours of incubation (SVGp12 $4.9x10^8 \pm 0.3x10^8$, U87-MG $2.3x10^8 \pm 0.1x10^8$, $p < 0.01$).

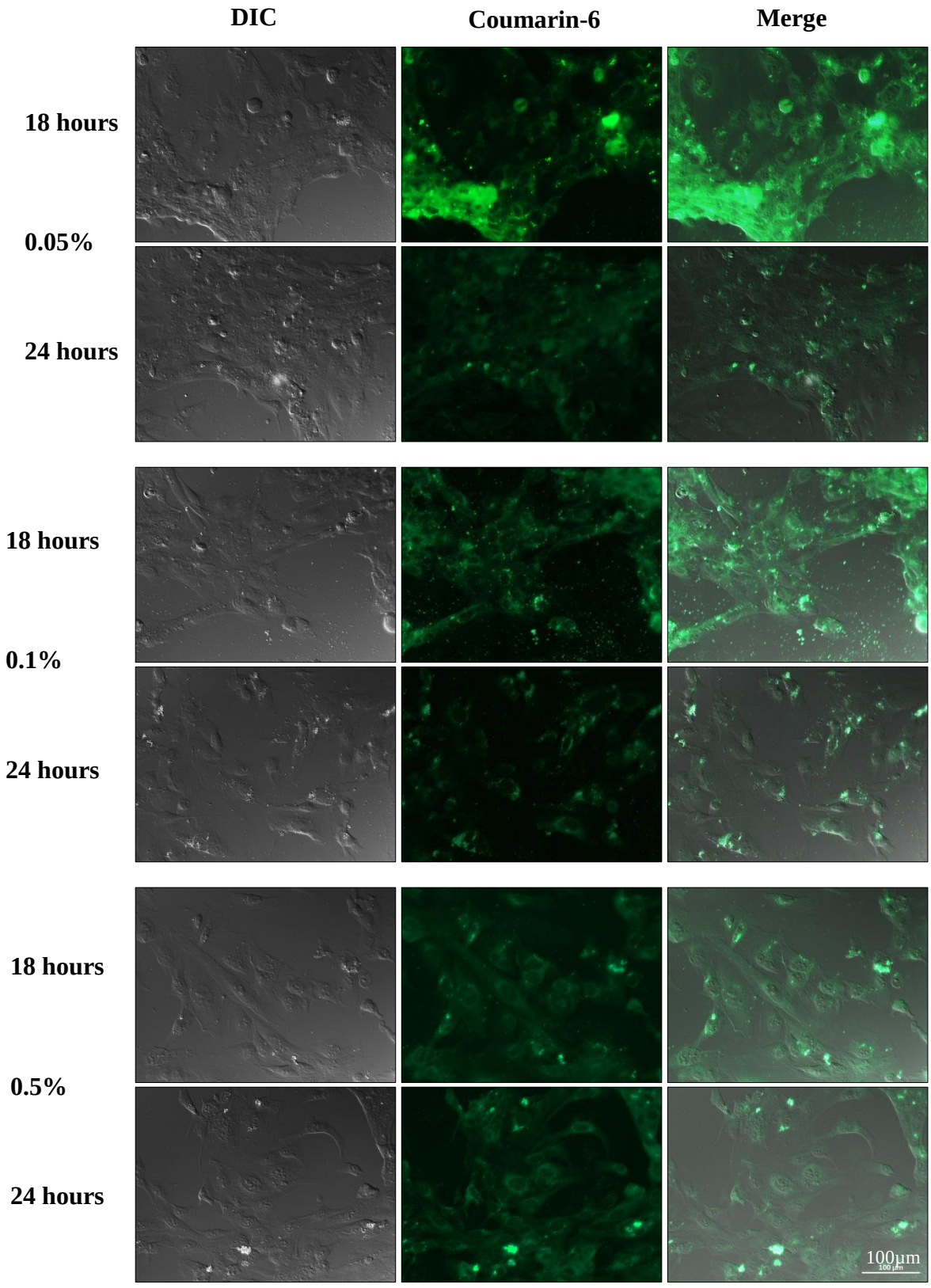

Figure 6.1: Cellular uptake of coumarin-6 loaded nanoparticles at 0.05, 0.1 and 0.5% into SVGp12 cell line following 18 and 24 hours of incubation

A higher uptake of coumarin-6 loaded nanoparticles was observed at 18 hours compared to 24 hours. Nanoparticle internalisation was confirmed due to the fluorescence observed in the cell cytoplasm.

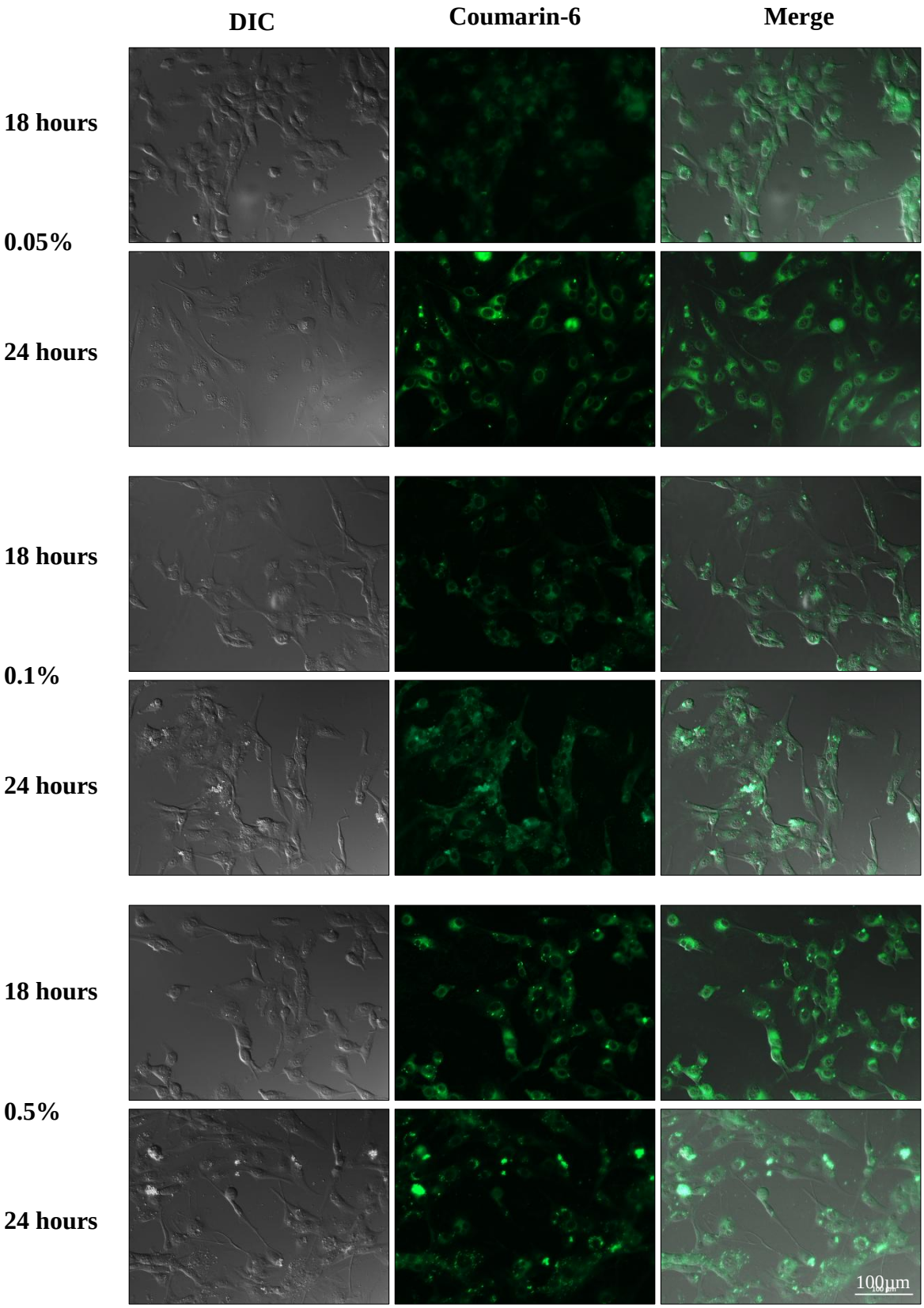

Figure 6.2: Cellular uptake of coumarin-6 loaded nanoparticles into U87-MG cell line following 18 and 24 hours of incubation

A higher uptake of coumarin-6 loaded nanoparticles was observed at 18 hours compared to 24 hours. Nanoparticle internalisation was confirmed due to the fluorescence observed in the cell cytoplasm.

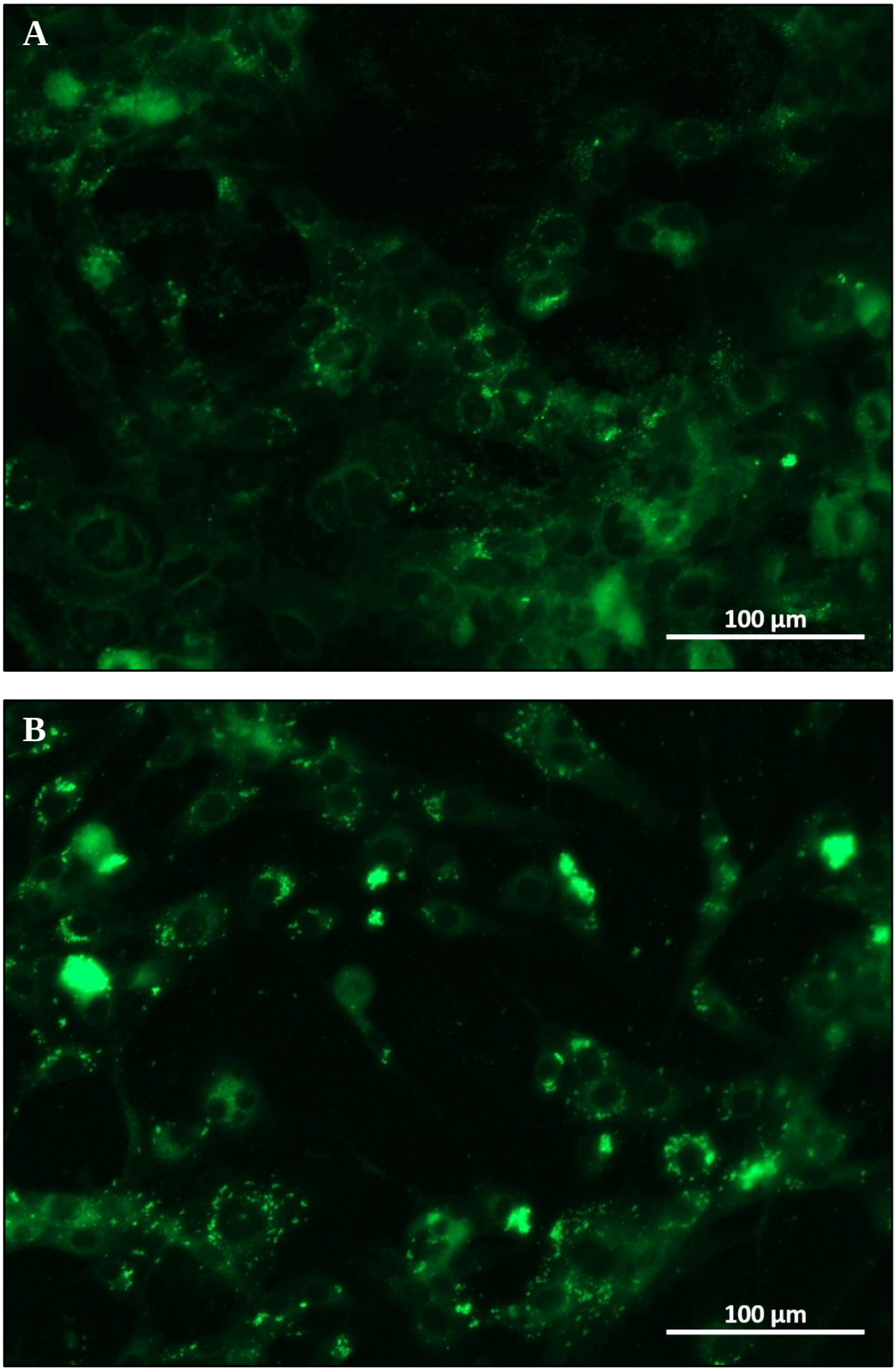

Figure 6.3: DIC images of SVGp12 and U87-MG cell line showing punctate uptake of 0.5% coumarin-6-loaded nanoparticles following 24 hours of incubation.

(A) SVGp12, (B) U87-MG. A higher nanoparticle uptake was observed following 24 hours of incubation.

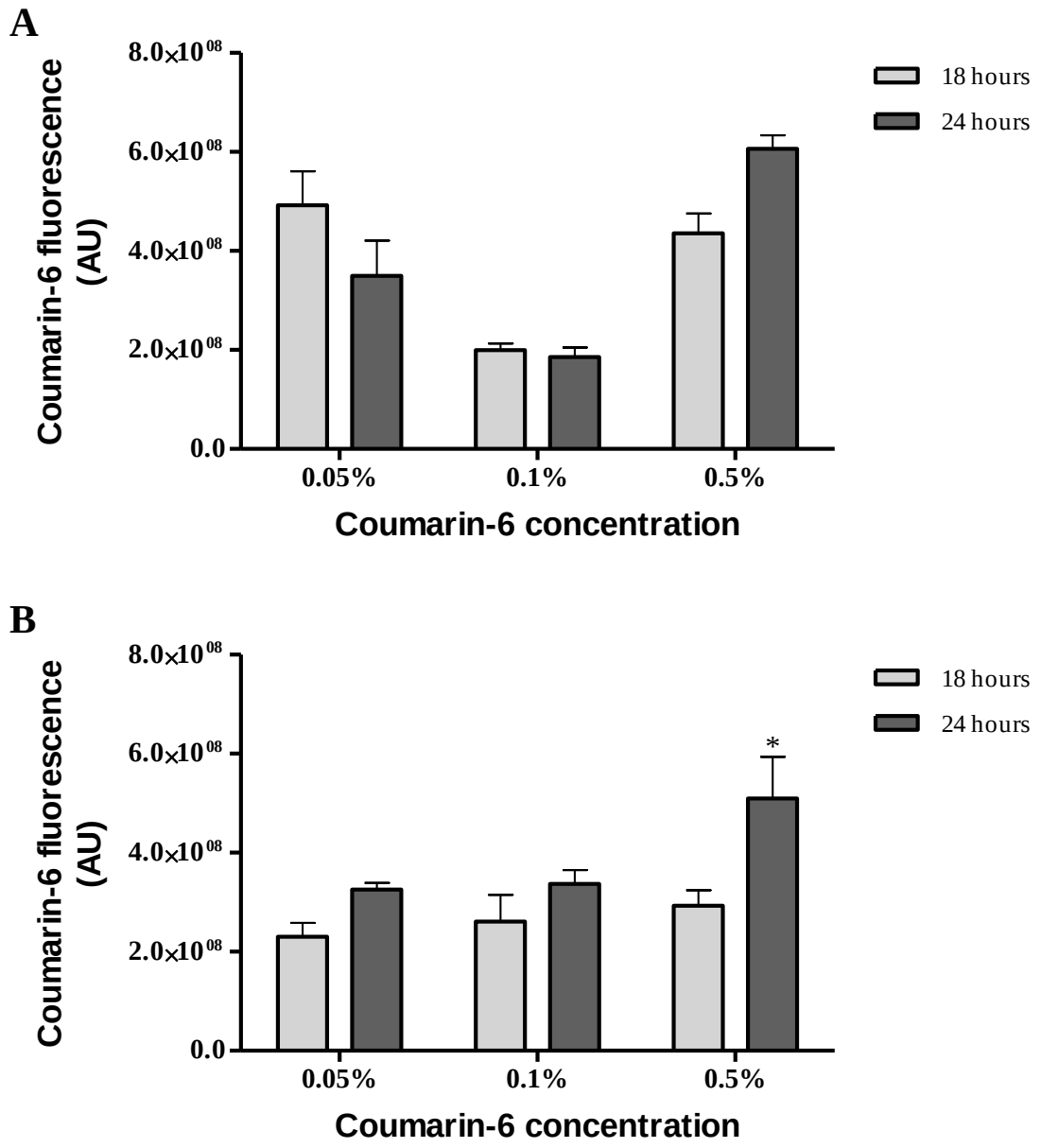

Figure 6.4: Data illustrating the uptake of coumarin-6 nanoparticles into SVGp12 and U87-MG cell lines.

The total uptake of coumarin-6 loaded nanoparticles into SVGp12 (A) and U87-MG (B) cell lines was quantified. Highest uptake was observed at 0.5% coumarin-6 loaded nanoparticles following 24 hours of incubation. Values represent mean ± S.E. for three experiments in triplicate.

6.2.2 Effect of Nanoparticle Treatment on Cell Viability

Following confirmation of uptake, the effect of nanoparticles on cell viability was examined. Blank and asiatic acid-loaded nanoparticles were prepared as described in Section 2.6.1. Cell viability in SVGp12 and U87-MG cell lines was assessed following nanoparticle treatment. Cell viability was measured using PrestoBlue® where the cells were treated for 24, 48, 72, 120 and 168 hours with increasing amounts of the blank and drug-loaded nanoparticles (Figs. 6.5 & 6.6).

Following 24 hours of 22µl blank nanoparticle treatment in SVGp12 cell line, 75.7 ±3.9% viable cells were measured. The amount of viable cells recorded at the end of 168 hours, following the same treatment was 57.3 ± 4%. The asiatic acid-loaded nanoparticles, at 22µl, showed a viability of 53.5 ±4.1% in the SVGp12 cell line, and this changed to 64.6 ± 12.3% following 168 hours of the treatment. Nanoparticle treatments did not show any significant differences.

In the U87-MG cell line, a viability of 79.8 ± 9.1% was measured at the end of 24 hour upon treatment with 22µl of blank nanoparticle treatment, and was 93.3 ± 15.9% at the end of 168 hours. Asiatic acid-loaded nanoparticles showed a similar viability of the cells, which was 74.7 ± 7% at the end of 24 hours and increased to 86.1 ± 8.2% following 168 hours of treatment. Nanoparticle treatments did not show any significant differences.

Statistical analysis of the data did not show any significant differences between the two cells following incubation with any treatment.

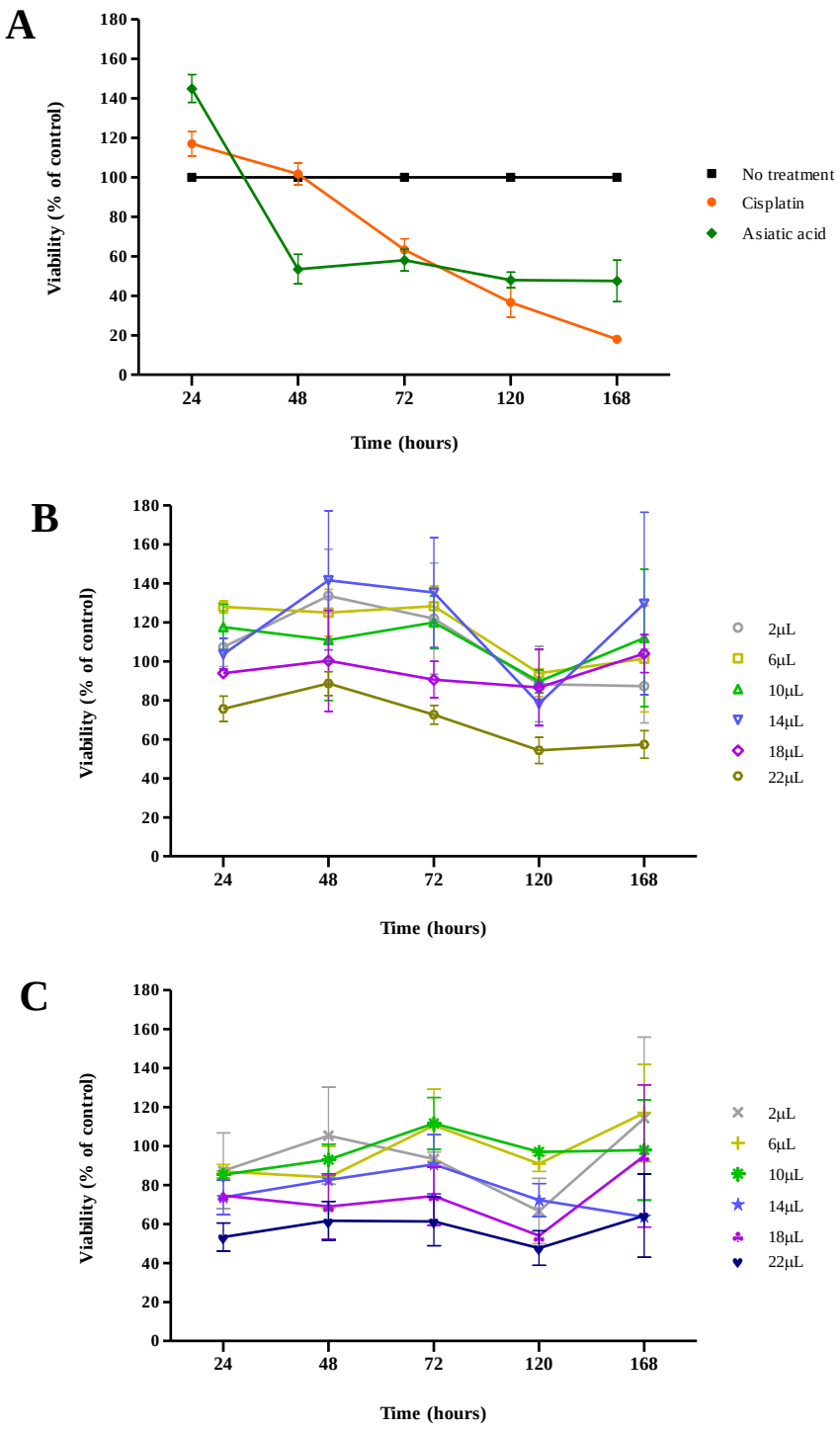

Figure 6.5: Data illustrating the effect of blank & loaded nanoparticle treatments on the viability of SVGp12 cell line

Cell viability was measured in SVGp12 cell line 24, 48, 72, 120 and 168 hours after incubation with the treatments. (A) Control treatments, (B) blank, (C) asiatic acid-loaded nanoparticle treatments. Asiatic acid and cisplatin showed a reduction in cell viability over time, however, no effect was seen with the nanoparticle treatments, blank or asiatic acid-loaded, on SVGp12 cell line. No significant differences were observed. Values represent mean ± S.E. for three experiments in triplicate.

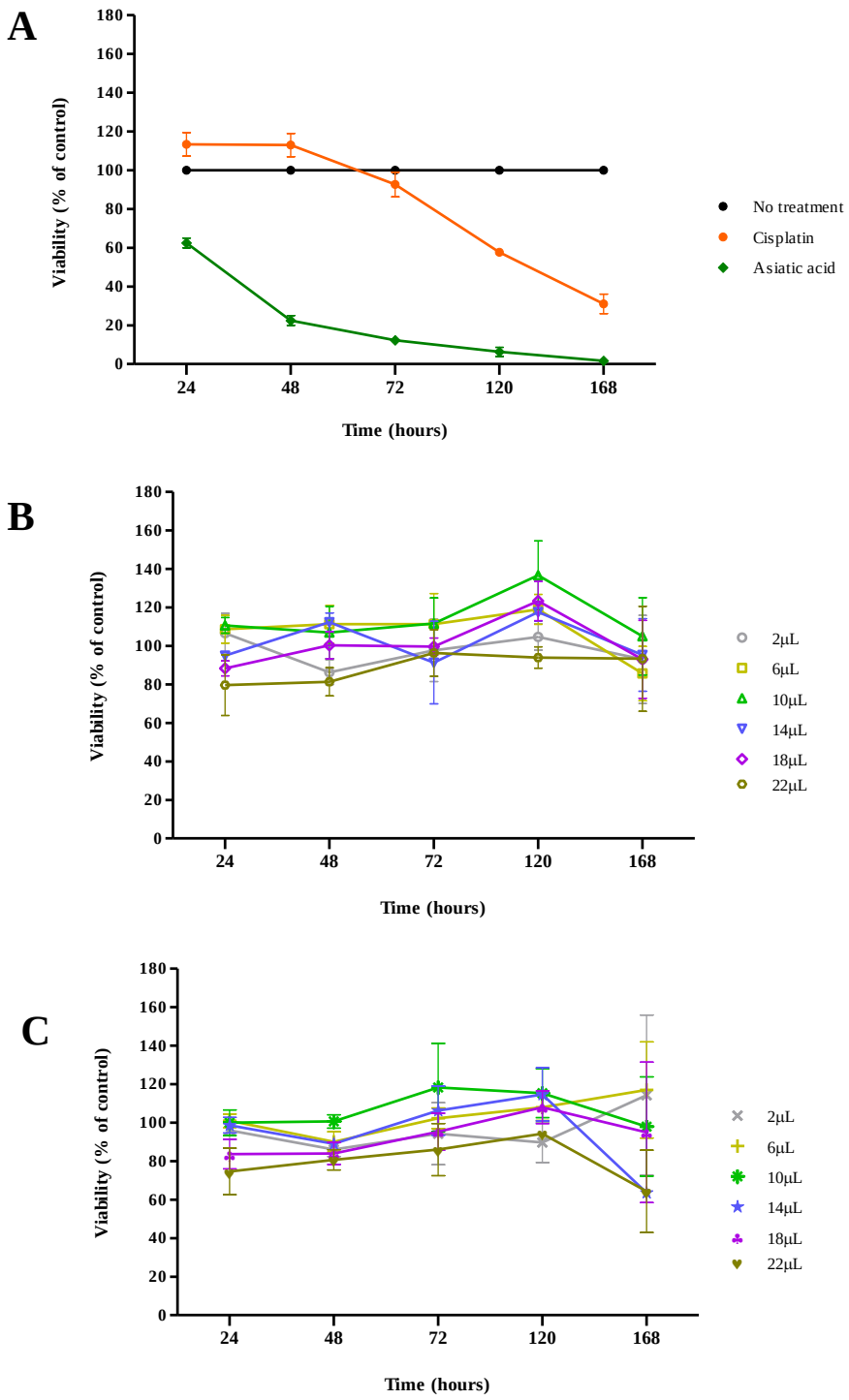

Figure 6.6: Data illustrating the effect of blank & loaded nanoparticle treatments on the viability of U87-MG cell line

Cell viability was measured in U87-MG cell line 24, 48, 72, 120 and 168 hours after incubation with the treatments. (A) Control treatments, (B) blank, (C) asiatic acid-loaded nanoparticle treatments. Asiatic acid and cisplatin showed a reduction in cell viability over time, however, no effect was seen with the nanoparticle treatments, blank or asiatic acid-loaded, on U87-MG cell line. No significant differences were observed. Values represent mean ± S.E. for three experiments in triplicates.

6.2.3 Nanoparticle Cell Proliferation Assay using CFDA-SE

To investigate the effect of nanoparticle treatments on cell proliferation, analysis using CFDA-SE as a marker was performed in SVGp12 and U87-MG cell lines. Independent treatments with 10µM cisplatin, 50µM asiatic acid and blank and asiatic acid-loaded nanoparticle treatments at 6µl and 22µl were performed.

The proliferation assay on SVGp12 cell line did not show any differences in the rate of proliferation of cells when treated blank and asiatic acid nanoparticles as it can be seen from Figs. 6.7 & 6.9. A reduction in CFDA-SE fluorescence with 22µl blank nanoparticles from 30.9 ± 1.2% at 24 hours to 1.8 ± 0% at 120 hours was observed. Asiatic acid-loaded nanoparticles at 22µl showed a reduction in CFDA-SE fluorescence from 37.1 ± 2.1% at 24 hours to 2.2 ± 0% at 120 hours. None of these differences were significant when compared to the control.

The proliferation assay on U87-MG cell line did not show any differences in the rate of proliferation of cells when treated blank and asiatic acid nanoparticles as it can be seen from Figs. 6.8 & 6.10. A reduction in CFDA-SE fluorescence with 22µl blank nanoparticles from 32.3 ± 1.1% at 24 hours to 2.6 ± 0.2% at 120 hours was observed. Asiatic acid-loaded nanoparticles at 22µl showed a reduction in CFDA-SE fluorescence from 37.2 ± 1.5% at 24 hours to 3.1 ± 0.3% at 120 hours. None of these differences were significant when compared to the control.

Statistical analysis of the data did not show any significant differences between the two cells following incubation with any treatment. Thus, cells proliferated at a similar rate in the absence and presence of nanoparticles.

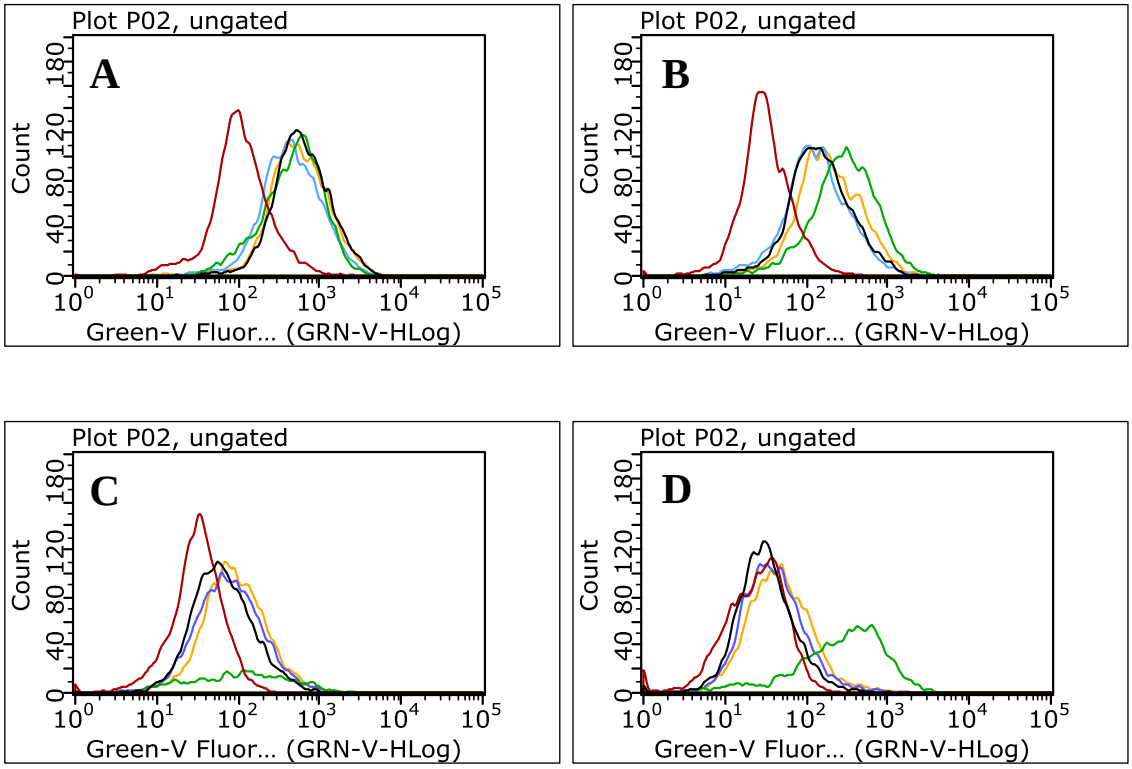

Figure 6.7: Flow cytometric plots showing cell proliferation using CFDA-SE on SVGp12 cell line following 120 hours of incubation.

24 hours (A), 48 hours (B), 72 hours (C), 120 hours (D). Non-treated (black), cisplatin (red), asiatic acid (green), 22µl blank nanoparticles (blue), 22µl asiatic acid-loaded nanoparticles (orange). Cisplatin treatment reduced the rate of proliferation of SVGp12 cells. No difference in the rate of proliferation of SVGp12 was observed with any other treatments.

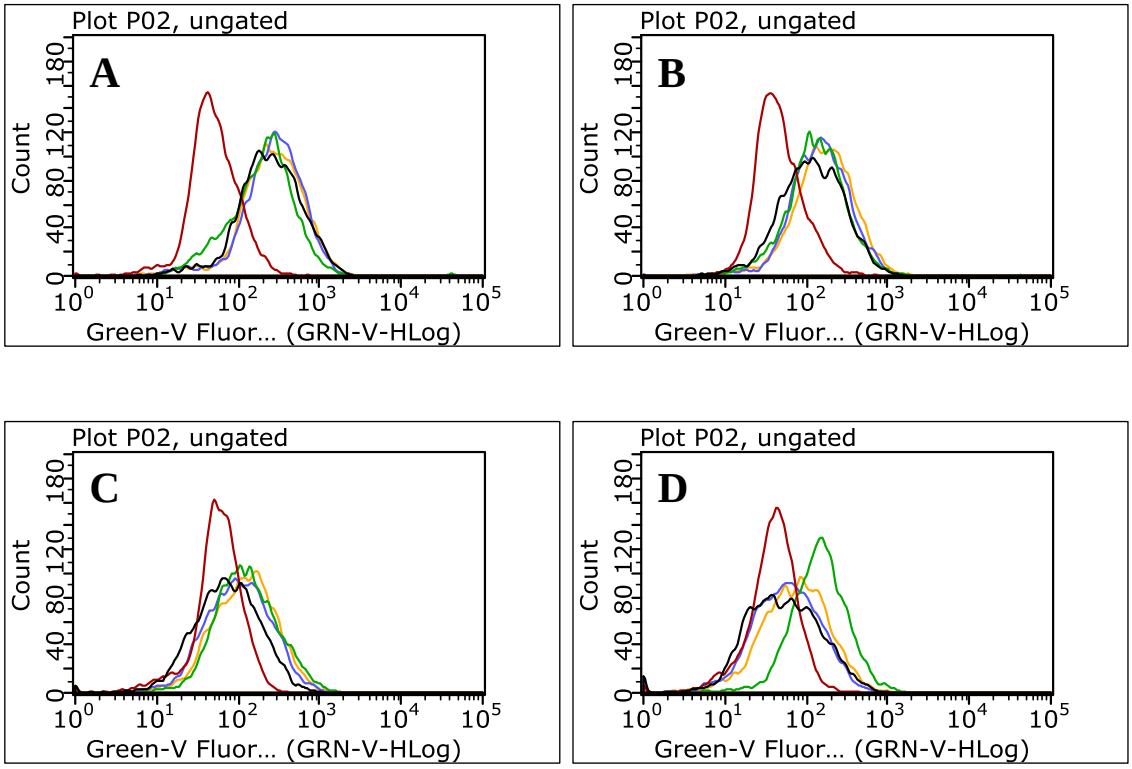

Figure 6.8: Flow cytometric plots showing cell proliferation using CFDA-SE on U87-MG cell line following 120 hours of incubation.

24 hours (A), 48 hours (B), 72 hours (C), 120 hours (D). Non-treated (black), cisplatin (red), asiatic acid (green), 22µl blank nanoparticles (blue), 22µl asiatic acid-loaded nanoparticles (orange). Cisplatin treatment reduced the rate of proliferation of U87-MG cells. No difference in the rate of proliferation of U87-MG was observed with any other treatments.

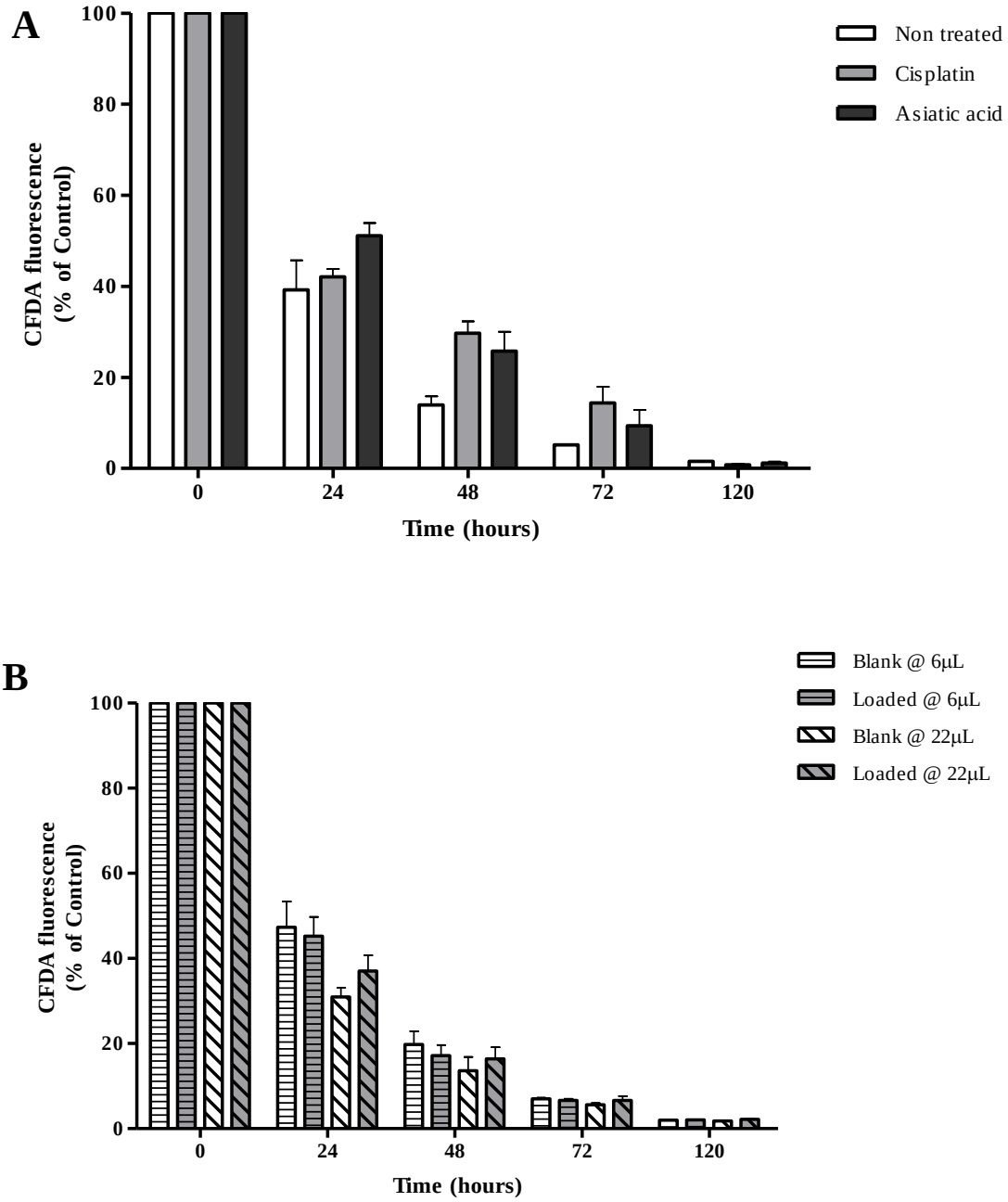

Figure 6.9: Data illustrating the effect of blank & asiatic acid-loaded nanoparticle treatments on SVGp12 cell line using CFDA-SE

Cell proliferation assay on SVGp12 cell line following 24, 48, 72 and 120 hours of incubation with the respective treatment was performed using CFDA-SE. (A) Control treatments, (B) nanoparticle treatments. A decrease in fluorescence indicates a higher rate of cell proliferation. Nanoparticle treatments, blank and asiatic acid-loaded, did not show any difference in the rate of cell proliferation of SVGp12 cells. Values represent mean ± S.E. for three experiments in triplicate.

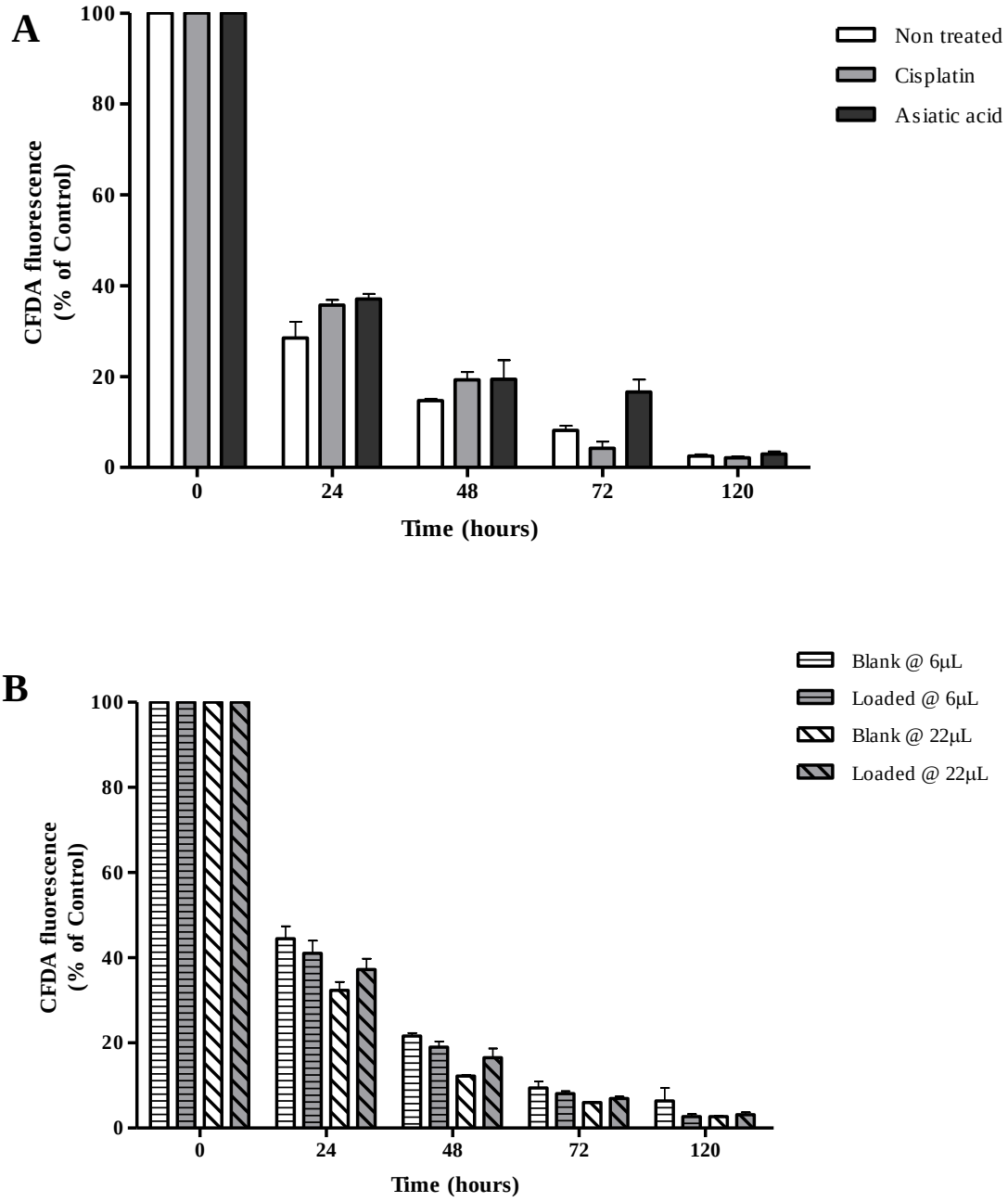

Figure 6.10: Data illustrating the effect of blank & asiatic acid-loaded nanoparticle treatments on U87-MG cell line using CFDA-SE

Cell proliferation assay on U87-MG cell line following 24, 48, 72 and 120 hours of incubation with the respective treatment was performed using CFDA-SE. (A) Control treatments, (B) nanoparticle treatments. A decrease in fluorescence indicates a higher rate of cell proliferation. Asiatic acid and the nanoparticle treatments, blank and asiatic acid-loaded, did not show any difference in the rate of cell proliferation of SVGp12 cells when compared to control, however, a reduction in proliferation was observed with cisplatin treatment. Values represent mean ± S.E. for three experiments in triplicate.

6.2.4 Nanoparticle Apoptosis Assay

The cell proliferation assay did not show any significant differences in the rate of proliferation following nanoparticle treatments. We thus decided to assess the effect of nanoparticles on cell death using flow cytometry.

The treatments with blank and asiatic acid-loaded nanoparticles at both the volumes, i.e., 6µl and 22µl did not show any significant differences on the cell lines as the proportion of cells in each stage were equivalent to the control treatment.

Again, a minimal effect of blank and asiatic acid-loaded nanoparticle treatment can be seen at both the volumes, i.e., 6µl and 22µl and the proportion of cells in each stage were equivalent to the control treatment (Figs. 6.11 & 6.13). In the SVGp12 cell line, blank nanoparticle treatment at 22µl showed 64.6 ± 1.9%, 1.1 ± 0.3%, 2.8 ± 0.9% and 31.4 ± 0.9% of live, early apoptotic, late apoptotic and necrotic cells, respectively, following 120 hours of incubation. Asiatic acid loaded nanoparticles at 22µl showed 71.2 ± 1.7%, 0.7 ± 0.3%, 1.6 ± 0.7% and 26.5 ± 0.7% of live, early apoptotic, late apoptotic and necrotic cells following 120 hours of incubation. The nanoparticle treatments did not show any significant differences in the SVGp12 cell line.

In the U87-MG cell line, blank nanoparticle treatment at 22µl showed 93.3 ± 1.2%, 1.6 ± 0.8%, 1.6 ± 0.9% and 3.4 ± 0.6% of live, early apoptotic, late apoptotic and necrotic cells, respectively, following 120 hours of incubation (Figs. 6.12 & 6.14). Asiatic acid loaded nanoparticles at 22µl showed 92.4 ± 1.4%, 7.7 ± 0.8%, 1.6 ± 0.8% and 4.2 ± 0.2% of live, early apoptotic, late apoptotic and necrotic cells following 120 hours of incubation. The nanoparticle treatments did not show any significant differences in the U87-MG cell line.

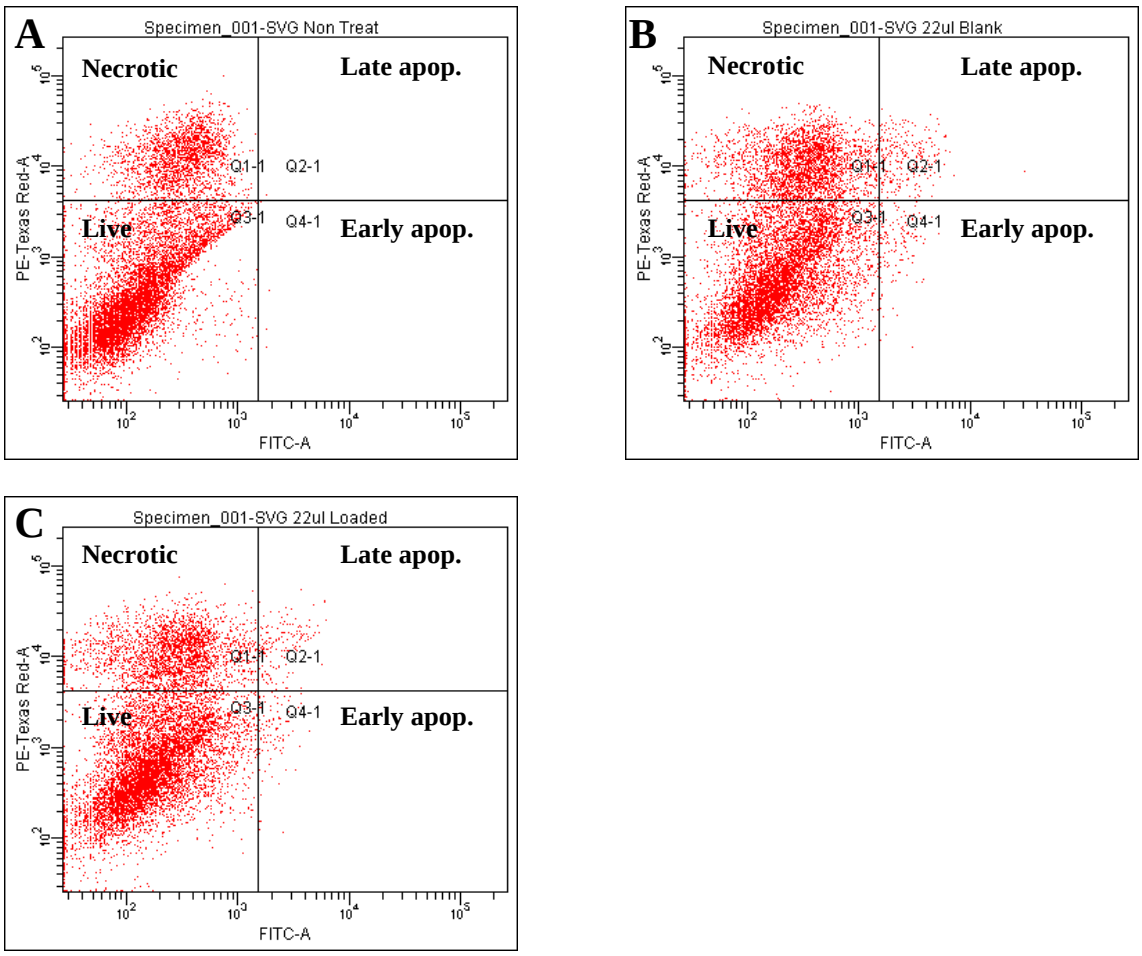

Figure 6.11: Flow cytometric plots showing cell apoptosis, following blank and loaded nanoparticle treatments, using Annexin V/Alexa Fluor 488® and propidium iodide on SVGp12 cells following 120 hours of incubation, under normoxia

(A) Non-treated cells, (B) 22 µl blank nanoparticles and (C) 22 µl asiatic acid-loaded nanoparticles. Nanoparticle treatments did not show any significant differences in the cell populations when compared to control.

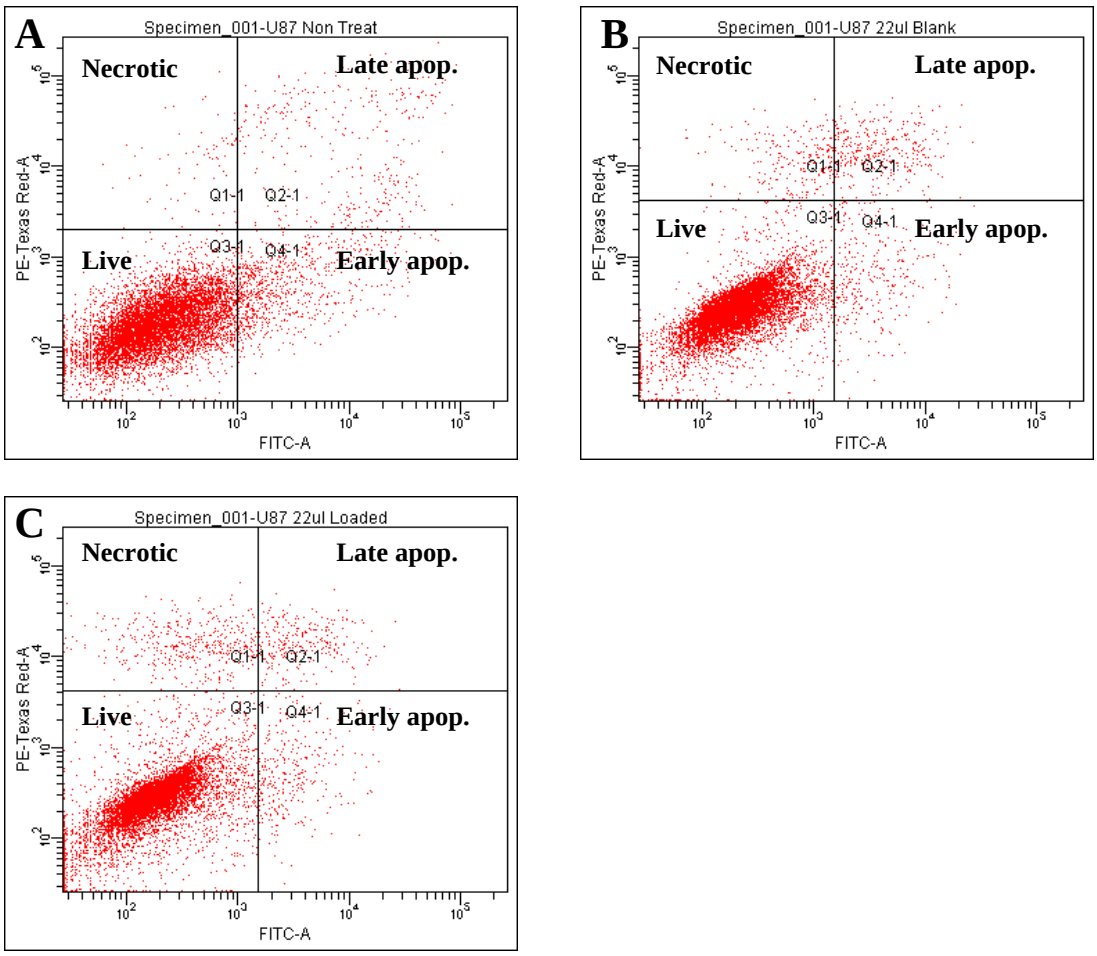

Figure 6.12: Flow cytometric data showing cell apoptosis, following blasnk and loaded nanoparticle treatments, using Annexin V/Alexa Fluor 488® and propidium iodide on U87-MG cells following 120 hours of incubation, under normoxia

(A) Non-treated cells, (B) 22 µl blank nanoparticles and (C) 22 µl asiatic acid-loaded nanoparticles. Nanoparticle treatments did not show any significant differences in the cell populations when compared to control.

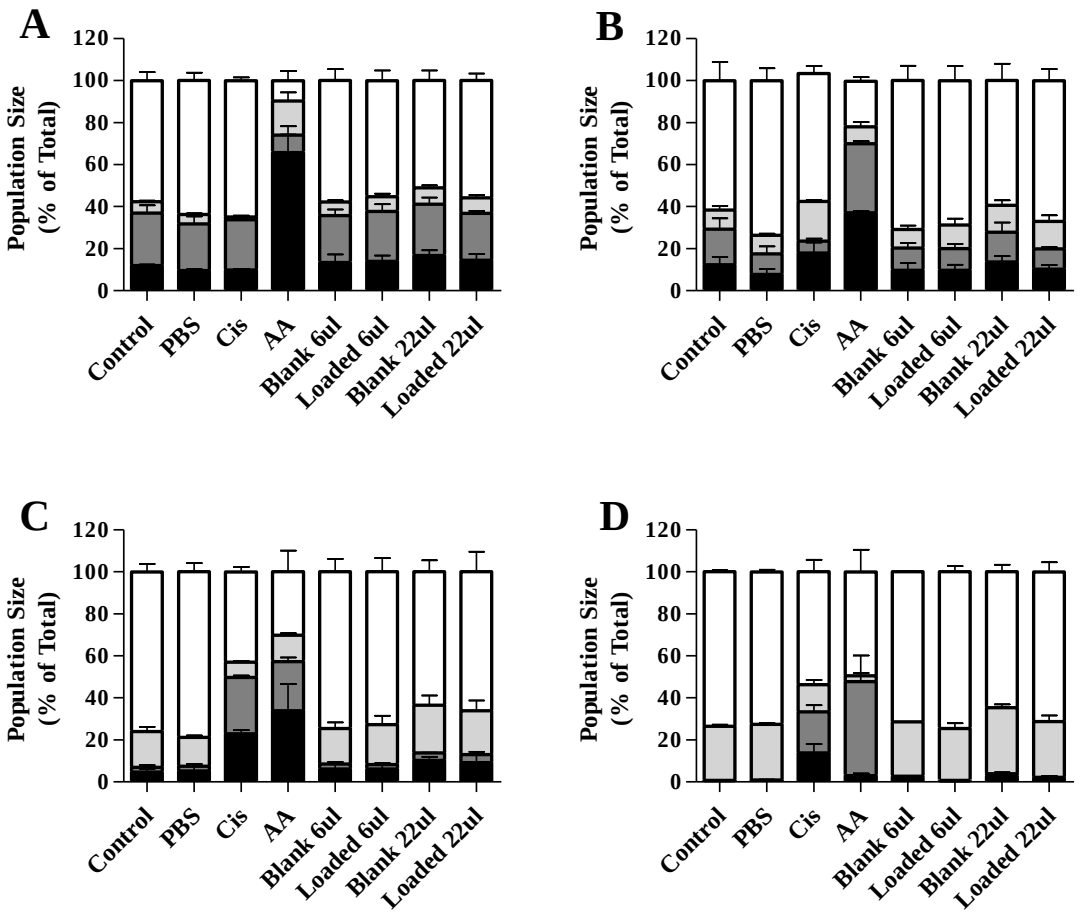

Figure 6.13: Data illustrating the effect of blank & loaded nanoparticle treatments on SVGp12 cell line using annexin V/alexa fluor 488® and propidium iodide, under normoxia

Cell apoptosis study following 24 (A), 48 (B), 72 (C) and 120 (D) hours of incubation with the respective treatment was performed on SVGp12 cell line. Data shows relative proportions of live (colourless), necrotic (light grey), early apoptotic (dark grey) and late apoptotic cells (black). Nanoparticle treatments, blank and asiatic acid-loaded, did not show any significant differences in cell populations when compared to control. Values represent mean ± S.E. for three experiments in triplicate.

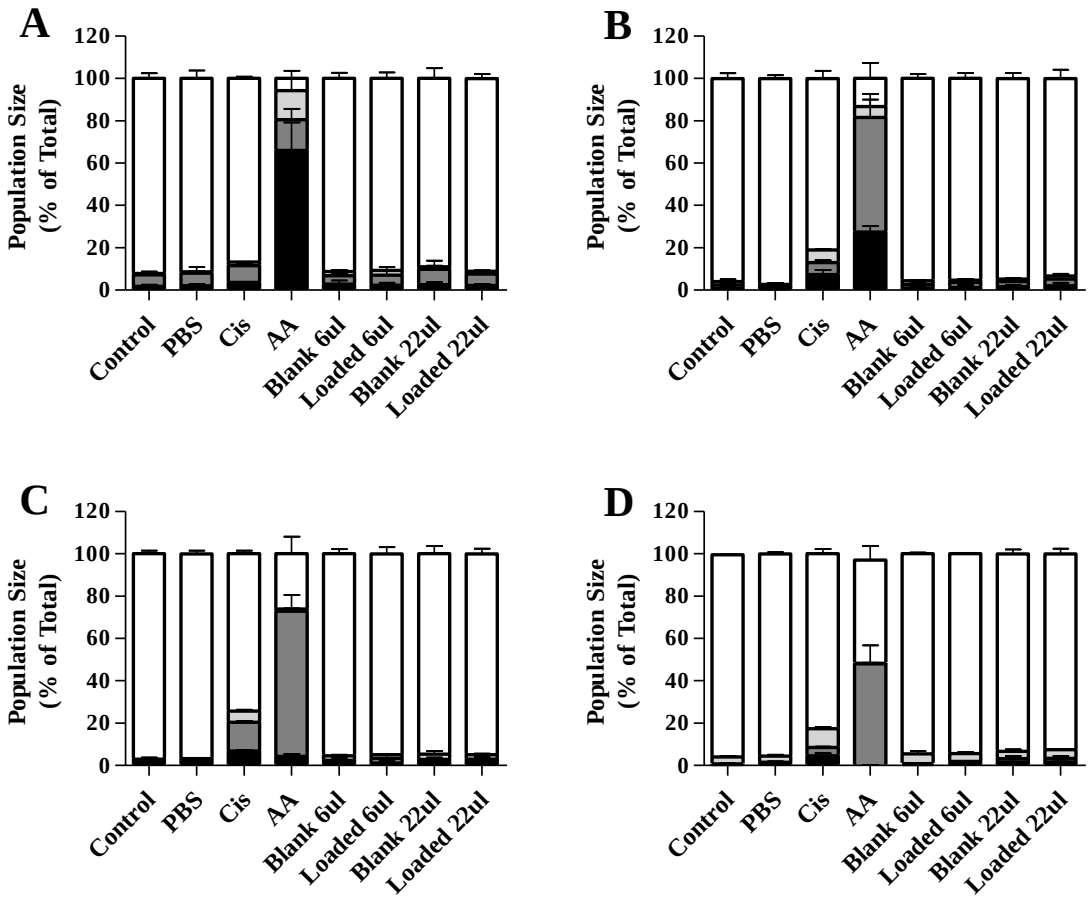

Figure 6.14: Data illustrating the effect of blank & loaded nanoparticle treatments on U87-MG cell line using Annexin V/Alexa Fluor 488® and propidium iodide, under normoxia

Cell apoptosis study following 24 (A), 48 (B), 72 (C) and 120 (D) hours of incubation with the respective treatment was performed on U87-MG cell line. Data shows relative proportions of live (colourless), necrotic (light grey), early apoptotic (dark grey) and late apoptotic cells (black). Nanoparticle treatments, blank and asiatic acid-loaded, did not show any significant differences in cell populations when compared to control. Values represent mean ± S.E. for three experiments in triplicate.

6.3 Discussion

Therapeutic effects of drug loaded nanoparticles depend on the internalisation and sustained retention of the nanoparticles by diseased cells (Ma et al., 2011). Not only nanoparticle internalisation, but also its metabolism and distribution largely depend on the size and surface charge of the nanoparticles (Gao et al., 2013).

As seen from Figs. 6.1-6.4, nanoparticle internalisation was observed upon the addition of coumarin-6-loaded nanoparticles to both cell lines. Nanoparticle internalisation was observed at 18 hours, however, it was higher following 24 hours of incubation.

Endocytosis is the main pathway for cellular uptake of nanoparticles (Gao et al., 2013). The endocytosed nanoparticles are then either confined within endo-lysosomes and are unable to reach into the cytosol, or are exported back to the exterior of the cell by exocytosis (Panyam and Labhasetwar, 2003; Verma and Stellacci, 2010). A study by Haursh-Frenkel and his associates investigated the internalisation mechanism of positively and negatively charged nanoparticles using a negative mutant of dynamin I-K44A, (a GTPase responsible for endocytosis), lacking the GTPase activity of dynamin. Their results established that the internalisation of negatively charged nanoparticles was due to pathways other than the clathrin and caveolin (Harush-Frenkel et al., 2007).

Another factor affecting nanoparticle internalisation is the negatively charged cell membrane. This results in a very low interaction and internalisation of negatively charged nanoparticles into the cell. However, some nanoparticles may be internalised through nonspecific binding and clustering of the particles on cationic sites on the plasma membrane (pinocytosis) (Agrawal et al., 2009; Kelf et al., 2010; Verma and Stellacci, 2010).

Figures 6.5 & 6.6 show the effect of blank and asiatic acid-loaded nanoparticles on cell viability of SVGp12 and U87-MG. It can be seen from the figure that neither of the nanoparticle formulations had an effect on cell viability of U87-MG.

Although PCL has been approved by the FDA for clinical use, the degradation of PCL is a very slow process, and thus only suitable for a long term drug delivery system (Shenoy and Amiji, 2005; Sinha et al., 2004). PCL degradation can be affected by its molecular weight, crystallinity, environment and temperature (Coombes et al., 2004; Passaglia et al., 2006). PCL degradation occurs by two mechanisms, the internal non-enzymatic cleavage and the enzymatic degradation. The non-enzymatic cleavage of PCL is an extremely slow process and takes 4-6 months to start. Enzymatic degradation, on the other hand, depends on the lipase concentration and takes about 3-4 weeks for the degradation to take place, depending on crystallinity (Hakkarainen and Albertsson, 2002; Sinha et al., 2004; Woodruff and Hutmacher, 2010). In a study performed by Chen et al., 2000 it was demonstrated that the degradation of PCL microspheres initiated in 3 weeks in the presence of lipase, however, it showed no signs of degradation even after 9 weeks, in the absence of lipase (Chen et al., 2000). Lipophilic drugs in a PCL based formulation are generally distributed in the matrix, while the hydrophilic drugs move towards the interface and tend to be in the adsorbed state in the formulation. PCL based formulations have been shown to release hydrophilic drugs at a much higher rate than lipophilic drugs by burst release (Chen et al., 2011; X. Wang et al., 2009). Asiatic acid is a lipophilic drug and thus only a slow release would be expected.

It has been suggested by Woodruff and Hutmacher, 2010 that PCL can only be bio-degraded by bacteria and fungi but not by humans or animals. This is due to the lack of the particular kind of lipase which is required for PCL bio-degradation. Although,

keeping this in mind, it is not to say that PCL is incompatible with humans, but rather it takes a very long time to hydrolyse. PCL can be degraded in the human body via bio-resorption; however the process may take 2-4 years to end, and depends on the molecular weight (Woodruff and Hutmacher, 2010). This rate of degradation can be readily altered by copolymerisation with other polymers or lactides and glycolides (Pulkkinen et al., 2009).

As asiatic acid is a lipophilic drug, it means that asiatic acid was dispersed in the matrix of the nanoparticles as opposed to surface adsorption. Within the limits of this project, this phenomenon has been confirmed by the *in vitro* drug release experiments that were performed on the nanoparticles (Sections 5.2.8-5.2.10). This information provides an explanation as to why the asiatic acid-loaded nanoparticles did not show an effect on cell viability (Figs. 6.5 & 6.6), cell proliferation (Figs. 6.7-6.10) or cell apoptosis (Fig. 6.11-6.14), *in vitro*.

In addition to this, even though no significant reduction in cell viability was observed with the asiatic acid-loaded nanoparticles, an increase in the viability of cells was observed following blank nanoparticle treatment (although these differences were non-significant too) (Figs. 6.5 & 6.6). The monomeric and oligomeric fragments generated by any surface erosion/non-enzymatic degradation within the cellular system *in vitro*, are taken up in the TCA cycle (Dash and Konkimalla, 2012). TCA cycle generates NADH and $FADH_2$ from acetyl CoA; NADH in turn provides cellular energy in the form of ATP, thus increasing cellular metabolism and ultimately cell growth and proliferation (Mailloux et al., 2007). This provides an explanation for the increase in cell viability that was observed with the blank nanoparticles.

CHAPTER 7

DISCUSSION

GBM is the most aggressive form of glioma and represents up to 50% of all primary brain tumours. It is caused by many genetic and epigenetic alterations in the glial cells (Kanu et al., 2009). Some of these genetic alterations involve *p53* mutation, loss of heterozygosity, *PTEN* mutation, MGMT methylation and *EGFR* amplification (Hegi et al., 2005; Hervey-Jumper and Berger, 2014; Kanu et al., 2009; Kleihues and Ohgaki, 1999). According to Cancer Research UK, the current survival rate for all types of brain tumours in England and Wales is 40% for one year post-diagnosis. Of this, only 20% of patients survive for 5 years and approximately 15% survive for 10 years (information from Cancer Research, UK. 2014). Although most GBMs develop rapidly without any clinical, radiological, or morphologic evidence, secondary GBM arises from the primary tumours such as WHO grade II and III tumours, may look histologically similar but affect different age groups (Ohgaki et al., 2004).

GBM symptoms includes headache which is not taken seriously by the patient leading to a late diagnosis of the tumour, making patient recovery difficult. Other symptoms include fits and seizures. Patients with high grade tumours show more serious symptoms such as epilepsy and high intra-cranial blood pressure (Klein et al., 2010; Preusser et al., 2011). Management of GBM involves radiation and surgery followed by chemotherapy, although most patients do not survive more than 2 years (Preusser et al., 2011; Stupp et al., 2009). Although proposed therapies vary greatly, radiotherapy with concomitant temozolomide is the preferred mode of treatment (Mandl et al., 2008). Despite this, patient prognosis remains poor and radiation along with chemotherapy reduce the overall immunity of the patient (Chamberlain et al., 1998).

Cisplatin, is also widely used for the treatment of brain tumours (Frezza et al., 2010). However, the use of cisplatin is very limited due to its toxicity on normal tissue and adverse side effects which include immunosuppression and inhibition of platelet

count in the bone marrow (Florea and Büsselberg, 2011; Momekov et al., 2006; Ramesh and Reeves, 2002; Sheleg et al., 2002).

More recently, interstitial brachytherapy with iodine and the use of permanent low-activity implants are being used as an adjuvant treatment for malignant brain tumours (Orringer et al., 2012; Pelloski and Gilbert, 2007; Schwarz et al., 2012; Zhang et al., 2012). Additionally, carmustine wafer implants following surgery are used in patients to prevent tumour resurrection, although it may delay wound healing and is associated with a higher risk of oedema (Preusser et al., 2011; Reithmeier et al., 2010; Wang et al., 2002).

A great interest has arisen in the use of herbal products with anti-cancer activity in the treatment of cancers such as glioblastoma and breast cancer. One such drug, asiatic acid, is extracted from *Centella asiatica* and shows properties such as wound healing and anti-angiogenesis demonstrating low or no side effects (Gohil et al., 2010; Hsu et al., 2004; Kavitha et al., 2011; Singh and Rastogi, 1969).

Tumours generally demonstrate a hypoxic microenvironment. Oxygen consumption in tumours is erratic due to the heterogeneity of the tumour micro-vasculature giving rise to hypoxic micro-regions (Dewhirst et al., 1994; Gnaiger, 2003; Maxwell et al., 2001). Although mammalian tissue can tolerate a wide range of oxygen tension, a drop in the partial pressure of oxygen leads to the activation of the hypoxia inducible factor. The HIF system comprises of the α and β (also known as ARNT) units. While the β unit is continually expressed, stability of the α subunit is mediated by the oxygen dependent domain (ODD) and the α subunit undergoes rapid degradation by the product of the tumour suppressor gene called the von Hippel-Lindau tumour suppressor gene (VHL). Thus, the α-subunits are undetectable when the oxygen tension is high (21%). When the oxygen tension is reduced, a stabilisation and an increase in the HIF-

1α level occurs, HIF-1α translocated into the nucleus where dimerisation with the ARNT *via* the PAS (basic helix-loop-helix DNA binding motif) domain occurs, leading to the transcription of a wide array of genes (e.g. *EGF*, *PDGF*, *VEGF* and lactate dehydrogenase) that are involved in the cell's adaptation to hypoxia (Giaccia et al., 2003; Liu and Simon, 2004; Maxwell, 2003; Semenza et al., 2000).

As the gene expression and hence cellular metabolism is altered under hypoxia, we investigated the effects of asiatic acid under hypoxia along with our control drug-cisplatin. The effects of cisplatin and asiatic acid on cell viability, proliferation, cell cycle, apoptosis and the generation of reactive oxygen species were studied.

As we already know, HIF-1α is an important regulator of transcription under hypoxia and so, an initial increase in HIF-1α is important for cell's adaptation to hypoxia (Strese et al., 2013). Cell's adaptation to hypoxia involves angiogenesis stimulation *via* VEGF, apoptosis inhibition *via* Bcl-2, modification of glucose metabolism and upregulation of proteins involved in metastasis. Thus, it is not surprising that cells under hypoxia show a slower rate of proliferation. This was demonstrated by the results obtained in this study where a reduction in the rate of cell growth and proliferation (using CFDA-SE) was observed for control treatments of both, SVGp12 and U87-MG cell lines. The wound healing assay, too, confirmed again that proliferation was slower under hypoxia as opposed to normoxia where a complete closure of the wound was observed.

We also demonstrated that cisplatin cytotoxicity was significantly reduced under hypoxia compared to normoxia. As cisplatin works by forming DNA adducts in the cell, proliferation of the cell is important. However, as a decrease in cell proliferation was observed under hypoxia, cisplatin cytotoxicity reduced. This was confirmed by the cell

apoptosis study for cisplatin that was carried out under hypoxia (Koch et al., 2003; Rohwer et al., 2010; Song et al., 2006; Yao et al., 2005).

On the other hand, asiatic acid did not show any differences in the rate of cell proliferation under normoxia or hypoxia, when compared to their respective controls. Cell apoptosis study showed, yet again, that the efficacy of asiatic acid was reduced under hypoxia as a large number of live cells were observed. Wound healing under hypoxia, using microscopy, showed rounded cells which are a characteristic of apoptosis. A partial closure of the wound for asiatic acid treatment under normoxia was observed. No significant differences were observed between any two cell lines with asiatic acid treatment.

Cell proliferation under hypoxia is inhibited by the cyclin-dependent kinase inhibitor $p27^{Kip1}$ which inhibits the activation of cyclin E-Cdk2 or cyclin D-Cdk4 complexes thus controlling cell cycle progression at G1. Also, it has been demonstrated that hypoxia can decrease cell-senescence caused due to drug treatments (Chang et al., 1999; d'Adda di Fagagna, 2008; Sullivan et al., 2008; Wartenberg et al., 2003). This leads into development of resistance towards anti-cancer drugs, under hypoxia. In addition, as cell proliferation is slower under hypoxia, drug cytotoxicity is reduced (Koch et al., 2003; Rohwer et al., 2010; Song et al., 2006). This would explain the reason behind the results obtained for cisplatin and asiatic acid under hypoxia where a reduction in cytotoxicity was observed.

Signal transduction pathways leading to various biological processes, is triggered by the EGFR and is associated with tumour growth such as cell cycle progression, invasion, metastasis, angiogenesis, and decreased apoptosis (Pore et al., 2006; Taylor et al., 2012). In order to investigate whether asiatic acid mediates its cytotoxicity *via* modulation of EGFR expression, we measured the EGFR expression in

SVGp12 and U87-MG cell lines. No significant differences in receptor expression of SVGp12 and U87-MG cell lines were observed under normoxia or hypoxia following cisplatin or asiatic acid treatments.

It has been shown previously that DNA damage due to cisplatin activates a signalling pathway culminating in the activation of EGFR, through an unknown mechanism. Cisplatin mediated EGFR activation is slow, only occurring when cisplatin-DNA adducts start forming (Benhar et al., 2002). This EGFR activation has been shown to occur *via* p38 mitogen-activated kinase and works in a SOS-type response, activating DNA protein kinase mediating DNA repair and working as a survival mechanism in response to cisplatin (Ahsan et al., 2010). Keeping this is mind, it can only be speculated that cells respond in a similar fashion to asiatic acid treatment increasing EGFR level as a survival mechanism. Although EGFR activity may be increased following asiatic acid treatment in cells, asiatic acid inhibits extracellular signal-regulated kinase (ERK) in a variety of cells, thus preventing cell proliferation despite the increase in EGFR (Wang et al., 2013). In addition to this, hypoxia also induces amplification of gene transcription and translation of EGFR. The results obtained in this study suggest that increased EGFR expression depends not only on drug treatments but also upon hypoxia and hypoxia induced amplification of *EGFR*.

Cell cycle progression is a controlled and an important biochemical process. Cell cycle regulation is crucial and only cells that do not exhibit deleterious genetic mutations progress through the cell cycle. In order to investigate the effects of cisplatin and asiatic acid on cell cycle progress, we performed a cell cycle analysis of SVGp12 and U87-MG cell line. Cell cycle analysis of cisplatin treated SVGp12 and U87-MG cells under normoxia showed G2/M phase arrest, although under hypoxia, a transient S phase arrest was seen for SVGp12 cells, however, the U87-MG cells showed a large

population of cells under G0/G1 phase which shifted towards the apoptotic population at 120 hours. Under hypoxia, cells accumulate p53 through a HIF-1α-dependent mechanism causing G0/G1 phase arrest in the cell cycle through a non-p53-mediated pathway (Shannon et al., 2003). It has been demonstrated previously that hypoxia results in a slower cell cycle progression whereas extreme hypoxia induces a pre S-phase arrest in cells. However, cells in the other phases of cell cycle continue to progress to late G1 phase before being arrested in the cell cycle progression (Amellem et al., 1994). Cells in the S phase of the cell cycle are more sensitive to DNA injuries under hypoxia. The transient G1 phase arrest is thus a possible mechanism designed to prevent DNA injuries due to hypoxia (Graeber et al., 1994).

Asiatic acid treatment in SVGp12 cell line showed S-G2/M arrest under normoxia and G0/G1 arrest under 1% and 5% hypoxia. On the U87-MG cell line, G0/G1 arrest was seen under normoxia and 5% hypoxia, whereas under 1% hypoxia, S-G2/M arrest was seen. In a study performed on breast cancer cell line, MCF-7 and MDA-MB-231, by Hsu et al., (2004), it was demonstrated that asiatic acid decreased the expression of cyclin B1, cyclin A, Cdc25c, and Cdk2, whereas it increased the expression of p21/WAF1 and phosphorylation of Cdk2, as well as phospho-Cdc25c. Cdc25c is an M phase inducer causing de-phopshorylation of cyclin B-Cdk1 complex. However, DNA damaged cells fail to express Cdc25c in its peak hyper-phosphorylated state (Shackelford et al., 1999). Thus from these studies, it can be suggested that asiatic acid does not induce cell cycle arrest due to DNA damage and other mechanisms may be involved, and thus need further investigation.

The *RB* tumour suppressor gene is involved in cell cycle progression into S phase by phosphorylation of serine residues on the *RB* gene product by Cdk4/cyclin D. A loss in the Rb-phosphorylation of these sites would result in inhibition of cell cycle

progression into S phase (Bretones et al., 2014; Shukla and Gupta, 2007). Thus, it can be speculated that asiatic acid causes cell cycle arrest due to the downregulation of Rb protein causing an arrest in the G0/G1 phase of cell cycle, although other mechanisms may be involved.

We also performed combination studies using cisplatin and asiatic acid, under normoxia only, in order to study any synergism that may be involved. The combination treatments showed a reduction in cell viability that was comparable to individual drug treatments at the same time points. It has been shown as a part of this study that asiatic acid causes S-G2/M in SVGp12 and G0/G1 arrest in U87-MG cells. The cytotoxicity observed in cells was mainly due to asiatic acid as this is a fast acting drug and induces cell cycle arrest along with apoptosis within 24 hours of treatment. Thus, as the cells are already arrested in one of the phases of cell cycle, cell proliferation slows down and cisplatin fails to create DNA adducts in the cell.

Cell death can occur due to apoptosis or necrosis. We investigated the effects of cisplatin and asiatic acid on cell apoptosis SVGp12 and U87-MG cells under normoxia and hypoxia. Cisplatin treatment under normoxia showed cell death mainly due to apoptosis, although the number of apoptotic cells under hypoxia was less compared to normoxia. Asiatic acid, too, mainly caused cell death due to apoptosis, however, a smaller fraction of cells underwent necrosis.

Cisplatin causes cell death mainly *via* the mitochondrial signalling pathway through activated caspase-3 (Cummings and Schnellmann, 2002; Florea and Büsselberg, 2006; Jiang et al., 2004). Other factors involved in cisplatin mediated cytotoxicity include increased efflux and decreased influx of the drug, increased cellular glutathione and metallothionein levels, increased DNA repair, and oncogene expression (Gonzalez et al., 2001).

Asiatic acid-mediated cell death is cell-type specific in the U87-MG cell line and involves caspase -9 and -3 activation (Bunpo et al., 2004; Cho et al., 2006; Kavitha et al., 2015). However, there are other mechanisms involved in cell death due to asiatic acid and these include reduction in mitochondrial membrane potential due to endoplasmic reticulum stress, inhibition of Bcl-2 expression in cells and intracellular calcium release. Asiatic acid also causes a loss in the phophatidylserine (PS) asymmetry in cells leading to exposure of PS on the outer membrane of the cell. In addition, asiatic acid also leads to DNA fragmentation in some cells (Bunpo et al., 2004; Cho et al., 2006; Hsu et al., 2004; Kavitha et al., 2015). Asiatic acid mediated necrotic cell death is mainly due to the release of the enzyme lactate dehydrogenase, where a rapid release causes traumatic cell death (Cho et al., 2006; Scaffidi et al., 2002).

We observed that apoptotic activity under hypoxia was significantly less compared to normoxia, following treatments with both, cisplatin and asiatic acid. Hypoxia has a tendency to select cells with a low p53 expression, where a post-translational modification of the *p53* gene occurs, making it active and promoting transcription of cell cycle regulating or apoptotic genes, thus reducing cell apoptosis (Brown and Wilson, 2004; Graeber et al., 1996; Zhou et al., 2006). Also, under hypoxia, cellular restoration following DNA injuries is common as opposed to normoxia, where these injuries are more permanent.

In addition, an increase in the expression of *MDR1* gene is observed under hypoxia. The *MDR1* gene encodes membrane-resident P-gp protein where P-gp acts as an efflux pump in various types of cancers including glioma, thus causing resistance towards various drugs (Comerford et al., 2002; Gottesman, 2002; Liu et al., 2008). Hypoxia also reduces cell-senescence due to chemotherapeutic drugs, as mentioned earlier.

Hypoxia can also modulate mitochondrial activity in a cell *via* the suppression of the TCA cycle following the inhibition of pyruvate shuttling into mitochondria. The resultant deactivation of pyruvate dehydrogenase initiates mitochondrial autophagy by suppressing mitochondrial biogenesis. This ultimately causes a reduction in cell death and increased drug resistance (Galluzzi et al., 2008; Kim et al., 2006; Papandreou et al., 2006; Zhang et al., 2007). It can thus be speculated that the absence of a huge population of apoptotic cells under hypoxia was due to hypoxia-related biochemical changes in the cell that have been explained above.

We also observed that apoptosis due to cisplatin under hypoxia showed a percentage of apoptotic cells that did not change over time. Hypoxia creates an environment of stress. An approximate of 50% of all tumours contains hypoxic or anoxic regions. It has been demonstrated that following the introduction of a hypoxic environment, cells undergo an initial acclimatisation period (Grayson et al., 2006). Under hypoxia, the hydration of carbon dioxide is catalysed by carbonic anhydrase IX (CAIX), which acts to maintain the extracellular pH environment in tumour cells. Thus, CAIX allows the adaptation of tumour cells to hypoxia and a slow release of the enzyme leads to cell death under hypoxia. In this manner, due to the acclimatisation of cells, a small number of apoptotic cells were observed, however, as hypoxia also downregulates p53 promoting cell proliferation and inhibiting apoptosis, no further increase in the apoptotic percentage of cells was observed (Korkolopoulou et al., 2007; Pantuck et al., 2003; Yamagata et al., 1998).

It is known that reactive oxygen species (ROS) play an important role in tumour metastasis and ROS generation can mediate cell apoptosis (Ma et al., 2009). Cancer cells show an increased basal level of ROS activity and are also involved in the activation of HIF (Huang et al., 2008; Kolamunne et al., 2013).

In order to understand the relationship between cell survival and ROS, we examined the ROS activity in cells following cisplatin and asiatic acid treatments. Results did not show any significant differences in the ROS activity in SVGp12 and U87-MG cell lines following drug treatments.

ROS are mainly generated in the mitochondria due to aerobic respiration. In tumour cells, anaerobic respiration takes place, producing lactate instead of glucose as a source of energy. Also, HIF is a negative regulator of mitochondrial activity (Kim and Dang, 2006; Kim et al., 2006; Papandreou et al., 2006; Zhang et al., 2007). This could be a possible reason why we did not observe a change in ROS production in this study.

Although cisplatin has been shown to mediate cell apoptosis due to ROS, cisplatin induced ROS generation mainly occurs in c-Myc low-expressing cells (Berndtsson et al., 2007; Biroccio et al., 2001; Pelicano et al., 2004). While cisplatin has been shown to increase ROS activity, asiatic acid has been shown to suppress ROS production. This is because, asiatic acid interference with the mitochondrial membrane potential stimulates cytochrome c release which initiates caspase signalling pathways (Lee et al., 2002; Tang et al., 2009). Transcription, upregulation and translocation of cytochrome c, into cell cytosol from the mitochondria, results in dynamic changes including downregulation Bcl-2 proteins, opening of permeability transition pore and loss of mitochondrial membrane potential, ultimately causing cell death (Chandra et al., 2002; O'Brien and Kirby, 2008). Thus, we speculate that asiatic acid causes cell death via downregulation of ROS.

Keeping in mind the results generated above, problems with asiatic acid administration involve reduced solubility due to its hydrophobicity thus potentially decreasing its bioavailability (Cho et al., 2006; Lee et al., 2002; Zhao et al., 2010). In order to overcome this problem, we formulated asiatic acid-loaded nanoparticles using

the synthetic polymer poly-ε-caprolactone. PCL is a non-toxic polymer approved by the FDA for clinical use and the applications include suture coating and surgical stent supports (Cho et al., 2002; Sarasam, 2001; Shenoy and Amiji, 2005; Tarafder et al., 2013).

Blood brain barrier is the biggest challenge to the delivery of chemotherapeutic drugs into the brain. We speculated that the preparation of nanoparticles smaller than the pore size of the BBB fenestrations would theoretically allow the free movement of nanoparticles into the brain microenvironment.

We prepared monodisperse, negatively charged asiatic acid-loaded nanoparticles with a smooth spherical surface. These particles were stable at 4°C for a minimum of 60 days and were characterised for drug loading and drug release. We demonstrated a steady drug release in PBS containing lipase due to the enzymatic PCL degradation; no drug release was observed in the absence of lipase. As PCL is hydrophobic, it degrades slowly in an aqueous medium, in the absence of lipase. The presence of lipase causes disruption of ester bonds, thus degrading the polymer and leading to drug release. It is also known that cancer cells have an acidic microenvironment; thus we also investigated drug release in PBS pH 5.5. Although we observed PCL degradation at pH 5.5, drug release into the supernatant did not occur. This can be attributed to the 4.7 pKa value of asiatic acid which can cause repulsive forces in the acidic medium, thus preventing drug release from the nanoparticles.

Although we demonstrated that the nanoparticles were stable for a minimum of 60 days in aqueous medium at 4°C, an even longer storage of nanoparticles involves freeze drying. Freeze drying of blank and asiatic acid-loaded nanoparticles showed a 10-fold increase in size and re-hydration was difficult as the particles settled at the bottom of the vial and large clumps were observed. We thus decided to not freeze dry

the formulation for any further experiments but continue long term storage in distilled water.

Following nanoparticle characterisation, we investigated the effects of nanoparticles on *in vitro* cell lines, SVGp12 and U87-MG. As the cytotoxic effects of nanoparticles would depend upon nanoparticle internalisation into the cells, we investigated this using microscopy. Nanoparticle internalisation into SVGp12 and U87-MG cells was observed at 18 hours and was higher at 24 hours. Cell membranes carry a negative charge on the outside. This leads to a low interaction between the cell membrane and the negatively charged nanoparticles and thus nanoparticle internalisation is reduced. However, some nanoparticles may be internalised through nonspecific binding and clustering of the particles on cationic sites on the plasma membrane (pinocytosis) (Agrawal et al., 2009; Kelf et al., 2010; Verma and Stellacci, 2010).

Following nanoparticle internalisation studies, we investigated the effects of nanoparticle formulations on cell viability. Neither of the nanoparticle formulations, blank or asiatic acid-loaded, had an effect on cell viability of SVGp12 and U87-MG. This can be explained due to the fact that PCL degradation, due to hydrolysis, is a slow process and depends on the molecular weight and the crystallinity of the compound (Coombes et al., 2004; Passaglia et al., 2008). PCL hydrolysis is an extremely slow process and takes 4-6 months to start (Hakkarainen and Albertsson, 2002; Sinha et al., 2004; Woodruff and Hutmacher, 2010). In addition, it was brought to our attention by Woodruff and Hutmacher, (2010) that PCL can only be bio-degraded by bacteria and fungi but not by humans or animals and this is due to the lack of the particular kind of lipase required for PCL bio-degradation. Although PCL can undergo degradation due to hydrolysis, this is a very slow process and take can up to 4 years in the human body

(Woodruff and Hutmacher, 2010). As asiatic acid is a hydrophobic drug, it was mainly encapsulated due to dispersion in the nanoparticle matrix and as a result of no/low degradation of PCL by *in vitro* cells, drug could not be released into the medium. Thus, asiatic acid-loaded nanoparticles did not show an effect on cell viability, cell proliferation or cell apoptosis *in vitro.*

8 CONCLUSION

Asiatic acid has demonstrated cytotoxic activity in the glioblastoma cell line, *in vitro*. An increased apoptosis under hypoxia, in comparison to cisplatin was observed. Although asiatic acid did not show any effects on cell proliferation, cell cycle arrest was observed. Results of this study have also shown that asiatic acid possess a higher cytotoxicity compared to cisplatin under hypoxia. In addition, as asiatic acid is a herbal compound with low side-effects, it could possibly replace the use of chemotherapeutic drugs in the market, and the results from study have demonstrated the anti-cancer effects.

Results of this study have also demonstrated that PCL nanoparticles cannot be used a short term delivery mode in humans due to the lack of degradation following uptake into cells.

9 FUTURE WORK

In an attempt of cell survival as result of hypoxia, various gene expressions are modulated due to oxygen stress. Keeping in mind the time scale of this project, we did not have the opportunity to acclimatise cells to hypoxia prior to performing drug treatments. In order to study the effects of hypoxia on cellular response to drug treatments, it is important to acclimatize cells to hypoxia in order to optimise energy metabolism and protein expression due to mitochondrial alteration, and reduce oxidative stress (Levett et al., 2012; Watson et al., 2009). Future studies could involve acclimatisation of cells to hypoxia for a minimum period of 8-10 weeks. Cells can be introduced to hypoxia from normoxia and the oxygen tension can be gradually decreased over a period of 10 weeks in order to reduce the effect of oxygen stress on the cells. Protein measurements including caspases, p53, P-gp and cyclins levels can be checked at each stage to give an idea of the change in cellular metabolism resulting due to oxygen stress. This would help obtain a better understanding of the effects of asiatic acid under hypoxia.

In addition, it has been estimated that tumour areas are exposed to cycling hypoxia that can range from 12-43%. This has direct consequences on tumour behaviour and promotes spontaneous metastasis. In this manner, the effectiveness of anti-cancer therapies is affected and the cells are more chemo- and radio-resistant (Cairns et al., 2001; Olbryt et al., 2014; Rofstad et al., 2007). Also, oxygen level in tumours is found to be heterogeneous. Thus it would be beneficial to expose cells to cycling hypoxia and measure the levels of different proteins that are affected by hypoxia. This would expand the knowledge towards understanding the behaviour of cells under hypoxia and help in designing strategies to overcome this.

As cellular metabolism is altered under hypoxia, it would be useful to study the differences in cellular metabolism of non-treated and asiatic acid treated cells under

normoxia and hypoxia. This would be beneficial in understanding the mechanism of increased tumour cell survival and decreased cytotoxicity of drugs under hypoxia and can be performed using the Seahorse Biosciences. Cells can be examined for mitochondrial stress by measuring mitochondrial respiration and glycolysis; this would help assess cellular metabolism and characterise the metabolic phenotypes by enabling real time measurement of intact cells (Parks et al., 2013; Verduzco et al., 2015).

Although physiologically relevant information on cellular behaviour due to various treatments is generated through 3D live animal studies, this can sometimes be too far-fetched an idea. An alternative approach to this can be applied using *ex vivo* 3D cellular models in the form of cell culture spheroids, as opposed to 2D monolayers. Due to the formation of large cellular aggregates, the mutual contacts can be re-established thus generating specific micro-environments allowing them to express a tissue-like phenotype. In addition, 3D cell cultures provide a deeper insight into cell adhesion and migration (Antoni et al., 2015; De Witt Hamer et al., 2008; Pampaloni et al., 2007). Due to the different levels of cell depth in a spheroid, the amount of oxygen reaching each cell differs thus altering hypoxia conditions within the spheroid. Spheroids mimic the *in vivo* tumour masses closely and can thus provide more accurate results towards the behaviour of these cells in response to drug treatments.

The results of this study have demonstrated the anti-cancer effects of asiatic acid under normoxia and under hypoxia. Although it has been mentioned in the literature that apoptosis due to asiatic acid is *via* caspase activation, ER stress and an increase in intracellular calcium, however, these studies have only been carried out under normoxic conditions. Therefore, it would be interesting to study the mechanism of action of asiatic acid under hypoxia. This could involve the use of caspase inhibitors,

measurement of mitochondrial membrane potential and measurement of intracellular calcium release.

Immunoblotting for caspases can be carried out and relative levels can be quantified. However, this would require the use of high-quality antibodies that react with specific individual caspases. An increase in caspase level following asiatic acid treatment would indicate the activation of caspases for apoptosis. Caspase activation can also be investigated by flow cytometric analysis using anti-CD95 (Bantel et al., 2001). Another method of caspase detection is *via* measurement of cleavage of synthetic substrates upon their incubation with lysates of apoptotic cells. Specific substrates for caspases are commercially available in the market and are tagged with fluorescent compounds thus making measurement easy. Caspase activity can also be measured using caspase inhibitors. Commercially available caspase inhibitors work by reversible or irreversible binding to caspases, forming adducts in the cysteine residues of the caspases. A few examples of caspase inhibitors include zvad-fmk, YV(biotin)KD-aomk, biotin-YVAD-aomk, DEVD-amc and z-EK(biotin)D-aomk (Borutaite and Brown, 2001; Cho et al., 2006; Köhler et al., 2002; Pennington and Thornberry, 2015).

Mitochondrial membrane potential can be measured using fluorescent dyes such as tetramethylrhodamine methyl and ethyl ester, rhodamine 123, 3,3′-dihexyloxacarbocyanine iodide and 5,5′,6,6’-tetrachloro-1,1’,3,3′-tetraethylbenzimidazolylcarbocyanineiodide. Mitochondrial accumulation of these dyes can be visualised by microscopy or quantified using flow cytometry and fluorescent plate reader. As these dyes are cationic, the amount of mitochondrial accumulation of these dyes will provide an inverse proportion to the measure of the mitochondrial membrane potential (Ly et al., 2003; Nicholls and Ward, 2000; Perry et al., 2011).

Apoptosis due to calcium release can be using TMB-8, dantrolene, Fura-2 and EGTA, all of which are calcium channel blockers. TMB-8, Fura-2 and dantrolene are intracellular calcium channel blockers, whereas EGTA is an extracellular calcium channel blocker. The use of specific blockers would answer if apoptosis due to asiatic acid is *via* intracellular or extracellular calcium release or neither (Hsu et al., 2004; Wertz and Dixit, 2000). In addition, immunoblotting can also be used.

The results of this study have been unable to clearly identify cell cycle arrest mechanisms. It would be beneficial to study the effects of asiatic acid on cell proliferation and cell cycle arrest mechanisms, under normoxia and hypoxia. The results of this study have shown that asiatic acid does not affect cell proliferation. Also, cell cycle arrest due to asiatic acid is cell type specific and may depend on oxygen level, as has been observed in the results obtained. Cell cycle arrest due to asiatic acid can be confirmed by using high quality cyclin-specific antibodies for immunoblotting. Measurements of cyclin A, B and E, p21/WAF1,p38 kinase, MAPK, p53, Cdc2 and Cdc25c could provide a further insight into the arrest mechanisms.

It would also be beneficial to study the downregulation of apoptosis due to hypoxia in asiatic acid treated cells. DNA breaks due to asiatic acid can be studied through southern blotting and would provide an insight into the direct effects of asiatic acid on cellular DNA.

Although we did not see any degradation of PCL nanoparticles in the absence of lipase, alternative approaches can be applied. Conversion of PCL nanoparticles prepared in this study into a hydrogel formulation could be a useful tool in the post-operative care of brain tumours. As PCL can take up to 4 years to degrade, the slow drug release from the resultant hydrogel degradation over time would be helpful in preventing relapse following tumour removal (Woodruff and Hutmacher, 2010). In addition, modification

of the preparation technique to allow a higher drug loading might be extremely beneficial in long term hydrogel implantation into the tumour site.

Modification of PCL nanoparticles, for rapid degradation, using natural polymers can also be investigated. Few examples of natural polymers include chitosan, alginate, hyaluronan, albumin and dextran (Almond et al., 2003; Augst et al., 2006; Cai et al., 2010; Gurski et al., 2010; Souza et al., 2010; Susa et al., 2009; Ta et al., 2008; van Dijk-Wolthuis et al., 1995). On the other hand, asiatic acid loaded nanoparticles using only natural polymers can be investigated.

The transport of asiatic acid-loaded nanoparticles across the blood brain barrier and its effects in a flow-based 3D cell culture apparatus can be studied using the Flocel Dynamic *in vitro* Blood Brain Barrier (DIV-BBB) model (FlocelInc, Ohio, USA). The Flocel apparatus mimics the blood brain barrier *in vitro*, and can be a helpful tool in assessment of asiatic acid toxicity. Other models of in vitro drug transport evaluation include using filter inserts allowing the growth of endothelial cells on one surface and astrocytes on the other. Although the formation of tight junctions is observed, this is a static model lacking the presence of dynamic pulsatile flow and also the capillary endothelial monolayer is 150 times more permeable than BBB *in vivo*. The lack of pulsatile flow leads to an inability to produce active transport mechanisms and metabolic transformations. This is a major drawback in assessing drug transport across the BBB as the bioavailability of the drug is reduced (Cecchelli et al., 1999; Deli et al., 2005; Naik and Cucullo, 2012; Pardridge et al., 1990).

The advantage of using the Flocel DIV-BBB model over any other BBB model is that it replicates the physiological levels of shear stress experienced by *in situ* endothelial cells. It also allows the formation of physiological trans-endothelial

resistance, and formation of gap junctions. Thus, this BBB model resembles closely to the *in vivo* BBB, both functionally and anatomically (Naik and Cucullo, 2012).

PCL nanoparticles that were prepared in this study can be injected through the BBB system to investigate the transport of these particles across the barrier. The dynamic flow of the system and the resultant movement of nanoparticles may lead to a mechanical stress causing some breakdown of the nanoparticles allowing drug release.

10 REFERENCES

Abbott, N.J., 2002. Astrocyte-endothelial interactions and blood-brain barrier permeability. J. Anat. 200, 629–38.

Abbott, N.J., Patabendige, A. a K., Dolman, D.E.M., Yusof, S.R., Begley, D.J., 2010. Structure and function of the blood-brain barrier. Neurobiol. Dis. 37, 13–25.

Abbott, N.J., Romero, I. a, 1996. Transporting therapeutics across the blood-brain barrier. Mol. Med. Today 2, 106–13.

Abbott, N.J., Rönnbäck, L., Hansson, E., 2006. Astrocyte-endothelial interactions at the blood-brain barrier. Nat. Rev. Neurosci. 7, 41–53.

Abdelwahed, W., Degobert, G., Fessi, H., 2006a. A pilot study of freeze drying of poly(epsilon-caprolactone) nanocapsules stabilized by poly(vinyl alcohol): formulation and process optimization. Int. J. Pharm. 309, 178–88.

Abdelwahed, W., Degobert, G., Stainmesse, S., Fessi, H., 2006b. Freeze-drying of nanoparticles: formulation, process and storage considerations. Adv. Drug Deliv. Rev. 58, 1688–713.

Agrawal, A., Min, D., Singh, N., Zhu, H., Birjiniuk, A., Maltzahn, G. Von, Harris, T.J., Xing, D., Woolfenden, S.D., Sharp, P.A., Charest, A., Bhatia, S., 2009. Functional Delivery of siRNA in Mice Using Dendriworms. ACS Nano 3, 2495–2504.

Ahsan, A., Hiniker, S.M., Ramanand, S.G., Nyati, S., Hegde, A., Helman, A., Menawat, R., Bhojani, M.S., Lawrence, T.S., Nyati, M.K., 2010. Role of epidermal growth factor receptor degradation in cisplatin-induced cytotoxicity in head and neck cancer. Cancer Res. 70, 2862–2869.

Almond, B. a, Hadba, A.R., Freeman, S.T., Cuevas, B.J., York, A.M., Detrisac, C.J., Goldberg, E.P., 2003. Efficacy of mitoxantrone-loaded albumin microspheres for intratumoral chemotherapy of breast cancer. J. Control. Release 91, 147–55.

Amellem, O., Löffler, M., Pettersen, E.O., 1994. Regulation of cell proliferation under extreme and moderate hypoxia: the role of pyrimidine (deoxy)nucleotides. Br. J. Cancer 70, 857–866.

Andoniou, C.E., Sutton, V.R., Wikstrom, M.E., Fleming, P., Thia, K.Y.T., Matthews, A.Y., Kaiserman, D., Schuster, I.S., Coudert, J.D., Eldi, P., Chaudhri, G., Karupiah, G., Bird, P.I., Trapani, J. a., Degli-Esposti, M. a., 2014. A Natural Genetic Variant of Granzyme B Confers Lethality to a Common Viral Infection. PLoS Pathog. 10, e1004526.

Antoni, D., Burckel, H., Josset, E., Noel, G., 2015. Three-Dimensional Cell Culture: A Breakthrough in Vivo. Int. J. Mol. Sci. 16, 5517–5527.

Augst, A.D., Kong, H.J., Mooney, D.J., 2006. Alginate hydrogels as biomaterials. Macromol. Biosci. 6, 623–33.

Ballabh, P., Braun, A., Nedergaard, M., 2004. The blood-brain barrier: an overview: structure, regulation, and clinical implications. Neurobiol. Dis. 16, 1–13.

Bantel, H., Lügering, a, Poremba, C., Lügering, N., Held, J., Domschke, W., Schulze-Osthoff, K., 2001. Caspase activation correlates with the degree of inflammatory liver injury in chronic hepatitis C virus infection. Hepatology 34, 758–767.

Bart, J., Groen, H.J.M., Hendrikse, N.H., Graaf, W.T.A. Van Der, Vaalburg, W., Vries, E.G.E. De, 2000. The blood-brain barrier and oncology : new insights into function and modulation. Tumour Biol. 26, 449–462.

Baruah, H., Rector, C.L., Monnier, S.M., Bierbach, U., 2002. Mechanism of action of non-cisplatin type DNA-targeted platinum anticancer agents: DNA interactions of novel acridinylthioureas and their platinum conjugates. Biochem. Pharmacol. 64, 191–200.

Bashan, N., Kovsan, J., Kachko, I., 2009. Positive and negative regulation of insulin signaling by reactive oxygen and nitrogen species. Physiol. … 27–71.

Bassermann, F., Eichner, R., Pagano, M., 2014. The ubiquitin proteasome system - implications for cell cycle control and the targeted treatment of cancer. Biochim. Biophys. Acta 1843, 150–62.

Bauer, G., Zarkovic, N., 2015. Revealing mechanisms of selective, concentration-dependent potentials of 4-hydroxy-2-nonenal to induce apoptosis in cancer cells through inactivation of membrane-associated catalase. Free Radic. Biol. Med. 81, 128–144.

Beck-Broichsitter, M., Rytting, E., Lebhardt, T., Wang, X., Kissel, T., 2010. Preparation of nanoparticles by solvent displacement for drug delivery: a shift in the "ouzo region" upon drug loading. Eur. J. Pharm. Sci. 41, 244–53.

Begley, D.J., 2004. Delivery of therapeutic agents to the central nervous system: the problems and the possibilities. Pharmacol. Ther. 104, 29–45.

Benhar, M., Engelberg, D., Levitzki, A., 2002. Cisplatin-induced activation of the EGF receptor. Oncogene 21, 8723–8731.

Berndtsson, M., Hägg, M., Panaretakis, T., Havelka, A.M., Shoshan, M.C., Linder, S., 2007. Acute apoptosis by cisplatin requires induction of reactive oxygen species but is not associated with damage to nuclear DNA. Int. J. Cancer 120, 175–180.

Berthet, C., Aleem, E., Coppola, V., Tessarollo, L., Kaldis, P., 2003. Cdk2 Knockout Mice Are Viable. Curr. Biol. 13, 1775–1785.

Biroccio, a, Benassi, B., Amodei, S., Gabellini, C., Del Bufalo, D., Zupi, G., 2001. c-Myc down-regulation increases susceptibility to cisplatin through reactive oxygen species-mediated apoptosis in M14 human melanoma cells. Mol. Pharmacol. 60, 174–182.

Bobustuc, G.C., Baker, C.H., Limaye, A., Jenkins, W.D., Pearl, G., Avgeropoulos, N.G., Konduri, S.D., 2010. Levetiracetam enhances p53-mediated MGMT inhibition and sensitizes glioblastoma cells to temozolomide. Neuro. Oncol. 12,

917–927.

Bogenrieder, T., Herlyn, M., 2003. Axis of evil: molecular mechanisms of cancer metastasis. Oncogene 22, 6524–6536.

Borutaite, V., Brown, G.C., 2001. Caspases are reversibly inactivated by hydrogen peroxide. FEBS Lett. 500, 114–118.

Brendler, T., Wyble, C., Hamid, M., Nathan, J., Potter, J.C., Rodgers, K., Phayre, A.M., 2000. PDR for Herbal Medicines. Montvale.

Bretones, G., Delgado, M.D., León, J., 2014. Myc and cell cycle control. Biochim Biophys Acta 1849, 506–516.

Brinkhaus, B., Lindner, M., Schuppan, D., Hahn, E.G., 2000. Chemical, pharmacological and clinical profile of the East Asian medical plant Centella aslatica. Phytomedicine 7, 427–448.

Brinkhaus, B., Lindner, M., Schuppan, D., Hahn, E.G., 2000. Chemical, pharmacological and clinical profile of the East Asian medical plant Centella asiatica. Phytomedicine 7, 427–448.

Brown, J.M., Wilson, W.R., 2004. Exploiting tumour hypoxia in cancer treatment. Nat. Rev. Cancer 4, 437–447.

Bruick, R.K., McKnight, S.L., 2001. A conserved family of prolyl-4-hydroxylases that modify HIF. Science (80-.). 294, 1337–1340.

Brunner, T., 2003. Fas (CD95/Apo-1) ligand regulation in T cell homeostasis, cell-mediated cytotoxicity and immune pathology. Semin. Immunol. 15, 167–176.

Buffle, J., Leppard, G.G., 1995. Characterization of Aquatic Colloids and Macromolecules. 1. Structure and Behavior of Colloidal Material. Environ. Sci. Technol. 29, 2169–2175.

Bunpo, P., Kataoka, K., Arimochi, H., Nakayama, H., Kuwahara, T., Bando, Y., Izumi, K., Vinitketkumnuen, U., Ohnishi, Y., 2004. Inhibitory effects of Centella asiatica on azoxymethane-induced aberrant crypt focus formation and carcinogenesis in the intestines of F344 rats. Food Chem. Toxicol. 42, 1987–97.

Bunpo, P., Kataoka, K., Arimochi, H., Nakayama, H., Kuwahara, T., Vinitketkumnuen, U., Ohnishi, Y., 2005. Inhibitory effects of asiatic acid and CPT-11 on growth of HT-29 cells. J. Med. Investig. 52, 65–73.

Cai, S., Thati, S., Bagby, T.R., Diab, H., Davies, N.M., Cohen, M.S., Forrest, M.L., 2010. Localizd doxorubicin chemotherapy with a biopolymeric nanocarrier improves survival and reduces toxicity in xenografts of human breast cancer. J. Control. release 146, 212–218.

Cairns, R. a., Kalliomaki, T., Hill, R.P., 2001. Acute (cyclic) hypoxia enhances spontaneous metastasis of KHT murine tumors. Cancer Res. 61, 8903–8908.

Cecchelli, R., Dehouck, B., Descamps, L., Fenart, L., Buée-Scherrer, V., Duhem, C., Lundquist, S., Rentfel, M., Torpier, G., Dehouck, M., 1999. In vitro model for evaluating drug transport across the blood-brain barrier. Adv. Drug Deliv. Rev. 36, 165–178.

Cerqueira, A., Martín, A., Symonds, C.E., Odajima, J., Dubus, P., Barbacid, M., Santamaría, D., 2014. Genetic characterization of the role of the Cip/Kip family of proteins as cyclin-dependent kinase inhibitors and assembly factors. Mol Cell Biol 34, 1452–9.

Chalmers, A.J., 2011. Glioma. Glasgow.

Chamberlain, M.C., Kormanik, P.A., Diego, S., 1998. Practical Guidelines for the Treatment of Malignant Gliomas. WJM 168, 114–120.

Chandra, D., Liu, J.-W., Tang, D.G., 2002. Early mitochondrial activation and cytochrome c up-regulation during apoptosis. J. Biol. Chem. 277, 50842–54.

Chang, B.D., Broude, E. V., Dokmanovic, M., Zhu, H., Ruth, A., Xuan, Y., Kandel, E.S., Lausch, E., Christov, K., Roninson, I.B., 1999. A senescence-like phenotype distinguishes tumor cells that undergo terminal proliferation arrest after exposure to anticancer agents. Cancer Res. 59, 3761–3767.

Chapple, I.L., 1997. Reactive oxygen species and antioxidants in inflammatory diseases. J. Clin. Periodontol. 24, 287–296.

Chasteigner, S. De, Cave, G., Fessi, H., Devissaguet, J., Puisieux, F., 1996. Freeze- D ry i ng of It raconazole-Loaded Nanosphere Suspensions : A Feasibility Study. Drug Dev. Res. 124, 116–124.

Chawla, J.S., Amiji, M.M., 2002. Biodegradable poly (ε-caprolactone) nanoparticles for tumor- targeted deli v ery of tamoxifen. Int. J. Pharm. 249, 127–138.

Chen, C., Cai, G., Zhang, H., Jiang, H., Wang, L., 2011. Chitosan-poly(ε-caprolactone)-poly(ethylene glycol) graft copolymers: Synthesis, self-assembly, and drug release behavior. J. Biomed. Mater. Res. - Part A 96, 116–124.

Chen, D.R., Bei, J.Z., Wang, S.G., 2000. Polycaprolactone microparticles and their biodegradation 67, 455–459.

Chen, S., Li, X., Lu, D., Xu, Y., Mou, W., Wang, L., Chen, Y., Liu, Y., Li, X., Li, L.Y., Liu, L., Stupack, D., Reisfeld, R. a., Xiang, R., Li, N., 2014. SOX2 regulates apoptosis through MAP4K4-Survivin signaling pathway in human lung cancer cells. Carcinogenesis 35, 613–623.

Chen, X., Qian, Y., Wu, S., 2015. The Warburg effect: Evolving interpretations of an established concept. Free Radic. Biol. Med. 79, 253–263.

Cheung, H.-H., Liu, X., Rennert, O.M., 2012. Apoptosis: Reprogramming and the Fate of Mature Cells. ISRN Cell Biol. 2012, 1–8.

Chiang, Y.-T., Yen, Y.-W., Lo, C.-L., 2015. Reactive oxygen species and glutathione dual redox-responsive micelles for selective cytotoxicity of cancer. Biomaterials 61, 150–161.

Chicheportiche, Y., Bourdon, P.R., Xu, H., Hsu, Y.M., Scott, H., Hession, C., Garcia, I., Browning, J.L., 1997. TWEAK, a new secreted ligand in the tumor necrosis factor family that weakly induces apoptosis. J. Biol. Chem. 272, 32401–32410.

Cho, C.W., Choi, D.S., Cardone, M.H., Kim, C.W., Sinskey, a J., Rha, C., 2006. Glioblastoma cell death induced by asiatic acid. Cell Biol. Toxicol. 22, 393–408.

Cho, K., Lee, J., Xing, P., 2002. Enzymatic Degradation of Blends of Poly (-caprolactone) and Poly (styrene-co-acrylonitrile) by Pseudomonas Lipase. J. Appl. Polym. Sci. 868–879.

Choi, C., Chae, S.Y., Kim, T., Jang, M., Cho, C.S., Nah, J., 2005. Preparation and Characterizations of Poly(ethylene glycol)-Poly(ε-caprolactone) Block Copolymer Nanoparticles. Bull. Korean Chem. Soc. 26, 523–528.

Cioffi, C.L., Liu, X.Q., Kosinski, P. a., Garay, M., Bowen, B.R., 2003. Differential regulation of HIF-1?? prolyl-4-hydroxylase genes by hypoxia in human cardiovascular cells. Biochem. Biophys. Res. Commun. 303, 947–953.

Clark, M.J., Homer, N., O'Connor, B.D., Chen, Z., Eskin, A., Lee, H., Merriman, B., Nelson, S.F., 2010. U87MG decoded: The genomic sequence of a cytogenetically aberrant human cancer cell line. PLoS Genet. 6.

Clerici, W.J., DiMartino, D.L., Prasad, M.R., 1995. Direct effects of reactive oxygen species on cochlear outer hair cell shape in vitro. Hear. Res. 84, 30–40.

Cockman, M.E., Masson, N., Mole, D.R., Jaakkola, P., Chang, G.W., Clifford, S.C., Maher, E.R., Pugh, C.W., Ratcliffe, P.J., Maxwell, P.H., 2000. Hypoxia inducible factor-alpha binding and ubiquitylation by the von Hippel-Lindau tumor suppressor protein. J. Biol. Chem. 275, 25733–41.

Colgan, O.C., Ferguson, G., Collins, N.T., Murphy, R.P., Meade, G., Cahill, P.A., Cummins, P.M., Oc, C., Ferguson, G., Nt, C., Rp, M., Meade, G., 2007. Regulation of bovine brain microvascular endothelial tight junction assembly and barrier function by laminar shear stress. Am. J. Physiol. 3190–3197.

Comerford, K.M., Wallace, T.J., Karhausen, J., Louis, N.A., Montalto, M.C., Colgan, S.P., 2002. Hypoxia-inducible Factor-1-dependent Regulation of the Multidrug Resistance (MDR1) Gene. Cancer Res. 62, 3387–3394.

Cooke, M.S., Evans, M.D., Dizdaroglu, M., Lunec, J., 2003. Oxidative DNA damage: mechanisms, mutation, and disease. FASEB J. 17, 1195–1214.

Coombes, A.G.., Rizzi, S.C., Williamson, M., Barralet, J.E., Downes, S., Wallace, W.A., 2004. Precipitation casting of polycaprolactone for applications in tissue engineering and drug delivery. Biomaterials 25, 315–325.

Crosio, C., Fimia, G.M., Loury, R., Kimura, M., Okano, Y., Zhou, H., Sen, S., Allis, C.D., Sassone-corsi, P., 2002. Mitotic Phosphorylation of Histone H3 : Spatio-Temporal Regulation by Mammalian Aurora Kinases. Mol. Cell. Biol. 22, 874–885.

Crowe, J.H., Leslie, S.B., Crowe, L.M., 1994. Is vitrification sufficient to preserve liposomes during freeze drying.pdf. Cryobiology 31, 355–366.

Cummings, B.S., Schnellmann, R.G., 2002. Cisplatin-Induced Renal Cell Apoptosis : Caspase 3-Dependent and -Independent Pathways. J. Pharmacol. Exp. Ther. 302, 8–17.

d'Adda di Fagagna, F., 2008. Living on a break: cellular senescence as a DNA-damage response. Nat. Rev. Cancer 8, 512–522.

Dai, S., Huang, M.L., Hsu, C.Y., Chao, K.S.C., 2003. Inhibition of hypoxia inducible factor 1?? causes oxygen-independent cytotoxicity and induces p53 independent apoptosis in glioblastoma cells. Int. J. Radiat. Oncol. Biol. Phys. 55, 1027–1036.

Dallas, S., Miller, D.S., Bendayan, R., 2006. Multidrug Resistance-Associated Proteins : Expression and Function in the Central Nervous System. Pharmacol. Rev. 58, 140–161.

Dash, T.K., Konkimalla, V.B., 2012. Poly-ϵ-caprolactone based formulations for drug delivery and tissue engineering: A review. J. Control. release 158, 15–33.

Dauchy, S., Dutheil, F., Weaver, R.J., Chassoux, F., Daumas-Duport, C., Couraud, P.-O., Scherrmann, J.-M., De Waziers, I., Declèves, X., 2008. ABC transporters, cytochromes P450 and their main transcription factors: expression at the human blood-brain barrier. J. Neurochem. 107, 1518–28.

Davies, D.C., 2002. Blood-brain barrier breakdown in septic encephalopathy and brain tumours. J. Anat. 200, 639–646.

De Witt Hamer, P.C., Van Tilborg, a a G., Eijk, P.P., Sminia, P., Troost, D., Van Noorden, C.J.F., Ylstra, B., Leenstra, S., 2008. The genomic profile of human malignant glioma is altered early in primary cell culture and preserved in spheroids. Oncogene 27, 2091–2096.

Dean, M., Hamon, Y., Chimini, G., 2001. The human ATP-binding cassette (ABC) transporter superfamily. J. Lipid Res. 42, 1007–17.

Deaton, A.M., Webb, S., Kerr, A.R.W., Illingworth, R.S., Guy, J., Andrews, R., Bird, A., 2011. Cell type-specific DNA methylation at intragenic CpG islands in the immune system. Genome Res. 21, 1074–86.

Deeken, J.F., Löscher, W., 2007. The blood-brain barrier and cancer: transporters, treatment, and Trojan horses. Clin. Cancer Res. 13, 1663–74.

Deli, M. a., Ábrahám, C.S., Kataoka, Y., Niwa, M., 2005. Permeability studies on in vitro blood-brain barrier models: Physiology, pathology, and pharmacology. Cell.

Mol. Neurobiol. 25, 59–127.

Demeule, M., Poirier, J., Jodoin, J., Bertrand, Y., Desrosiers, R.R., Dagenais, C., Nguyen, T., Lanthier, J., Gabathuler, R., Kennard, M., Jefferies, W. a, Karkan, D., Tsai, S., Fenart, L., Cecchelli, R., Béliveau, R., 2002. High transcytosis of melanotransferrin (P97) across the blood-brain barrier. J. Neurochem. 83, 924–33.

Denecker, G., Vercammen, D., Declercq, W., Vandenabeele, P., 2001. Cellular and Molecular Life Sciences Apoptotic and necrotic cell death induced by death domain receptors 58, 356–370.

Desoize, B., Madoulet, C., 2002. Particular aspects of platinum compounds used at present in cancer treatment. Crit. Rev. Oncol. Hematol. 42, 317–325.

DeVita, V.T., Young, R.C., Canellos, G.P., 1975. Combination versus single agent chemotherapy: a review of the basis for selection of drug treatment of cancer. Cancer 35, 98–110.

Dewhirst, M.W., Secomb, T.W., Ong, E.T., Hsu, R., Gross, J.F., 1994. Advances in Brief Determination of Local Oxygen Consumption Rates in Tumors ' 3333–3336.

Dizdaroglu, M., Jaruga, P., Birincioglu, M., Rodriguez, H., 2002. Free radical-induced damage to DNA: Mechanisms and measurement. Free Radic. Biol. Med. 32, 1102–1115.

Elmore, S., 2007. Apoptosis: a review of programmed cell death. Toxicol. Pathol. 35, 495–516.

Epstein, A.C.R., Gleadle, J.M., Mcneill, L.A., Hewitson, K.S., Rourke, J.O., Mole, D.R., Mukherji, M., Metzen, E., Wilson, M.I., Dhanda, A., Tian, Y., Masson, N., Hamilton, D.L., Jaakkola, P., Barstead, R., Hodgkin, J., Maxwell, P.H., Pugh, C.W., Schofield, C.J., Ratcliffe, P.J., Drive, R., Ox, O., 2001. Cell 44 of HIF and molecular oxygen, and suggested a role for Critical Function of a VHL Homolog in the Regulation of. Cell 107, 43–54.

Esteban, M. a, Maxwell, P.H., 2005. Manipulation of oxygen tensions for in vitro cell culture using a hypoxic workstation. Expert Rev. Proteomics 2, 307–314.

Fan, Z., Beresford, P.J., Oh, D.Y., Zhang, D., Lieberman, J., 2003. Tumor Suppressor NM23-H1 Is a Granzyme A-Activated DNase during CTL-Mediated Apoptosis, and the Nucleosome Assembly Protein SET Is Its Inhibitor. Cell 112, 659–672.

Feng, R., Song, Z., Zhai, G., 2012. Preparation and in vivo pharmacokinetics of curcumin-loaded PCL-PEG-PCL triblock copolymeric nanoparticles. Int. J. Nanomedicine 7, 4089–98.

Fiedler, S.L., Izvekov, S., Violi, A., 2007. The effect of temperature on nanoparticle clustering. Carbon N. Y. 45, 1786–1794.

Florea, A.-M., Büsselberg, D., 2006. Occurrence, use and potential toxic effects of metals and metal compounds. Biometals 19, 419–427.

Florea, A.-M., Büsselberg, D., 2011. Cisplatin as an anti-tumor drug: cellular mechanisms of activity, drug resistance and induced side effects. Cancers (Basel). 3, 1351–71.

Franovic, A., Gunaratnam, L., Smith, K., Robert, I., Patten, D., Lee, S., 2007. Translational up-regulation of the EGFR by tumor hypoxia provides a nonmutational explanation for its overexpression in human cancer. Proc. Natl. Acad. Sci. U. S. A. 104, 13092–13097.

Frezza, M., Hindo, S., Chen, D., Davenport, A., Schmitt, S., Tomco, D., Ping Dou, Q., 2010. Novel Metals and Metal Complexes as Platforms for Cancer Therapy. Curr. Pharm. Des. 16, 1813–1825.

Fulda, S., Gorman, A.M., Hori, O., Samali, A., 2010. Cellular stress responses: cell survival and cell death. Int. J. Cell Biol. 2010, 214074.

Furnari, F.B., Fenton, T., Bachoo, R.M., Mukasa, A., Stommel, J.M., Stegh, A., Hahn, W.C., Ligon, K.L., Louis, D.N., Brennan, C., Chin, L., DePinho, R. a., Cavenee, W.K., 2007. Malignant astrocytic glioma: Genetics, biology, and paths to treatment. Genes Dev. 21, 2683–2710.

Furuya, T., Kamada, T., Murakami, T., Kurose, A., Sasaki, K., 1997. Laser scanning cytometry allows detection of cell death with morphological features of apoptosis in cells stained with PI. Cytometry 29, 173–177.

Galluzzi, L., Joza, N., Tasdemir, E., Maiuri, M.C., Hengartner, M., Tavernarakis, N., Penninger, J., Madeo, F., Kroemer, G., 2008. No death without a life: vital functions of apoptotic effectors. Cell 15, 1113–1123.

Gan, Z., Yu, D., Zhong, Z., Liang, Q., Jing, X., 1999. Enzymatic degradation of poly (□ -caprolactone)/ poly (dl -lactide) blends in phosphate buffer solution. Polymer (Guildf). 40, 2859–2862.

Gao, H., Yang, Z., Zhang, S., Cao, S., Shen, S., Pang, Z., Jiang, X., 2013. Ligand modified nanoparticles increases cell uptake, alters endocytosis and elevates glioma distribution and internalization. Sci. Rep. 3, 2534.

Garrido, C., Galluzzi, L., Brunet, M., Puig, P.E., Didelot, C., Kroemer, G., 2006. Mechanisms of cytochrome c release from mitochondria. Cell Death Differ. 13, 1423–33.

Gerweck, L.E., Seetharaman, K., 1996. Cellular pH Gradient in Tumor versus Normal Tissue : Potential Exploitation for the Treatment of Cancer. Cancer Res. 56, 1194–1198.

Giaccia, A., Siim, B.G., Johnson, R.S., 2003. HIF-1 as a target for drug development. Nat. Rev. Drug Discov. 2, 803–11.

Gingrich, M.B., Junge, C.E., Lyuboslavsky, P., Traynelis, S.F., 2000. Potentiation of NMDA receptor function by the serine protease thrombin. J. Neurosci. 20, 4582–

95.

Gingrich, M.B., Traynelis, S.F., 2000. Serine proteases and brain damage – is there a link? Trends Neurosci. 23, 399–407.

Gnaiger, E., 2003. OXYGEN CONFORMANCE OF CELLULAR RESPIRATION A perspective of mitochondrial physiology. In: Hypoxia: Through the Lifecycle. pp. 39–55.

Gohil, K.J., Patel, J. a, Gajjar, A.K., 2010. Pharmacological Review on Centella asiatica: A Potential Herbal Cure-all. Indian J. Pharm. Sci. 72, 546–56.

Goldbach, P., Brochart, H., Wehrle, P., Stamm, A., 1995. Sterile filtration of liposomes : retention of encapsulated carboxyfluorescein. Int. J. Pharm. 117, 225–230.

Gonzalez, V.M., Fuertes, M. a, Alonso, C., Perez, J.M., 2001. Is cisplatin-induced cell death always produced by apoptosis? Mol. Pharmacol. 59, 657–663.

Gordan, J.D., Bertovrt, J.A., Hu, C., Diehl, J.A., Celeste, M., 2007. HIF-2 α promotes hypoxic cell proliferation by enhancing c-Myc transcriptional activity. Cancer Cell 11, 335–347.

Gottesman, M.M., 2002. MECHANISMS OF CANCER DRUG RESISTANCE. Annu. Rev. Med. 53, 615–27.

Gough, W., Hulkower, K.I., Lynch, R., McGlynn, P., Uhlik, M., Yan, L., Lee, J. a, 2011. A quantitative, facile, and high-throughput image-based cell migration method is a robust alternative to the scratch assay. J. Biomol. Screen. Off. J. Soc. Biomol. Screen. 16, 155–163.

Graeber, T.G., Osmanian, C., Jacks, T., Housman, D.E., Kock, C.J., Lowe, S.W., Giaccia, A.J., 1996. Hypoxia-mediated selection of cells with diminished apoptotic potential in solid tumours.pdf. Nature 379, 88–91.

Graeber, T.G., Peterson, J.F., Tsai, M., Monica, K., Fornace, a J., Giaccia, a J., 1994. Hypoxia induces accumulation of p53 protein, but activation of a G1-phase checkpoint by low-oxygen conditions is independent of p53 status. Mol. Cell. Biol. 14, 6264–6277.

Grayson, W.L., Zhao, F., Izadpanah, R., Bunnell, B., Ma, T., 2006. Effects of Hypoxia on Human Mesenchymal Stem Cell Expansion and Plasticity in 3D Constructs. J. Cell. Physiol. 207, 331–339.

Griffiths, J.R., 1991. Are cancer cells acidic? Br. J. Cancer 64, 425–7.

Guicciardi, M.E., Werneburg, N.W., Bronk, S.F., Franke, A., Yagita, H., Thomas, G., Gores, G.J., 2014. Cellular Inhibitor of Apoptosis (cIAP)-mediated ubiquitination of Phosphofurin Acidic Cluster Sorting protein 2 (PACS-2) negatively regulates Tumor necrosis factor-Related Apoptosis-Inducing Ligand (TRAIL) cytotoxicity. PLoS One 9.

Gurski, L.A., Jha, A.K., Zhang, C., Jia, X., Farach-, M.C., 2010. NIH Public Access 30, 6076–6085.

Hagrman, D., Goodisman, J., Dabrowiak, J.C., Souid, A.-K., 2003. Kinetic Study of the Reaction of Cisplatin With Metallothionein. Drug Metab. Depos. 31, 916–923.

Hakkarainen, M., Albertsson, A.C., 2002. Heterogeneous biodegradation of polycaprolactone - Low molecular weight products and surface changes. Macromol. Chem. Phys. 203, 1357–1363.

Haley, B., Frenkel, E., 2008. Nanoparticles for drug delivery in cancer treatment. Urol. Oncol. Semin. Orig. Inmvestigations 26, 57–64.

Hanahan, D., Weinberg, R. a, 2011a. Hallmarks of cancer: the next generation. Cell 144, 646–74.

Hanahan, D., Weinberg, R. a., 2011b. Hallmarks of cancer: The next generation. Cell 144, 646–674.

Harush-Frenkel, O., Debotton, N., Benita, S., Altschuler, Y., 2007. Targeting of nanoparticles to the clathrin-mediated endocytic pathway. Biochem. Biophys. Res. Commun. 353, 26–32.

Hawkins, B.T., Davis, T.P., 2005. The Blood-Brain Barrier / Neurovascular Unit in Health and Disease. Pharmacol. Rev. 57, 173–185.

Hegi, M.E., Diserens, A.-C., Gorlia, T., Hamou, M.-F., de Tribolet, N., Weller, M., Kros, J.M., Hainfellner, J. a, Mason, W., Mariani, L., Bromberg, J.E.C., Hau, P., Mirimanoff, R.O., Cairncross, J.G., Janzer, R.C., Stupp, R., 2005. MGMT gene silencing and benefit from temozolomide in glioblastoma. N. Engl. J. Med. 352, 997–1003.

Hengartner, M.O., 2001. Apoptosis : Corralling the Corpses Minireview. Cell 104, 325–328.

Henriksen, S., Tylden, G.D., Dumoulin, A., Sharma, B.N., Hirsch, H.H., Rinaldo, C.H., 2014. The human fetal glial cell line SVG p12 contains infectious BK polyomavirus (BKPyV). J. Virol. 88, 7556–7568.

Hervey-Jumper, S.L., Berger, M.S., 2014. Role of surgical resection in low- and high-grade gliomas. Curr. Treat. Options Neurol. 16, 284.

Holmquist-Mengelbier, L., Fredlund, E., Löfstedt, T., Noguera, R., Navarro, S., Nilsson, H., Pietras, A., Vallon-Christersson, J., Borg, A., Gradin, K., Poellinger, L., Påhlman, S., 2006. Recruitment of HIF-1alpha and HIF-2alpha to common target genes is differentially regulated in neuroblastoma: HIF-2alpha promotes an aggressive phenotype. Cancer Cell 10, 413–23.

Holzer, A.K., Samimi, G., Katano, K., Naerdemann, W., Lin, X., Safaei, R., Howell, S.B., 2004. The copper influx transporter human copper transport protein 1 regulates the uptake of cisplatin in human ovarian carcinoma cells. Mol.

Pharmacol. 66, 817–823.

Honasoge, A., Sontheimer, H., 2013. Involvement of tumor acidification in brain cancer pathophysiology. Front. Physiol. 4, 316.

Hong, J.Y., Min, H.Y., Guang, H.X., Lee, J.G., Lee, S.H., Young, S.K., Sam, S.K., Sang, K.L., 2008. Growth inhibition and G1 cell cycle arrest mediated by 25-methoxyhispidol A, a novel triterpenoid, isolated from the fruit of Poncirus trifoliata in human hepatocellular carcinoma cells. Planta Med. 74, 151–155.

Hotze, E.M., Phenrat, T., Lowry, G. V., 2010. Nanoparticle Aggregation: Challenges to Understanding Transport and Reactivity in the Environment. J. Environ. Qual. 39, 1909–1924.

Hsu, Y., Kuo, P., Lin, L., Lin, C., 2004. Asiatic acid, a triterpene, induces apoptosis and cell cycle arrest through activation of extracellular signal-regulated kinase and p38 mitogen-activated protein kinase pathways in human breast cancer cells. J. Pharmacol. Exp. Ther. 313, 333–344.

Huang, E.L., Gu, J., Maureen, S., Bunn, F., 1998. Regulation of hypoxia-inducible factor 1α is mediated by an O 2 -dependent degradation domain via the ubiquitin-proteasome pathway. Biochemistry 95, 7987–7992.

Huang, S.-S., Chiu, C.-S., Chen, H.-J., Hou, W.-C., Sheu, M.-J., Lin, Y.-C., Shie, P.-H., Huang, G.-J., 2011. Antinociceptive activities and the mechanisms of anti-inflammation of asiatic Acid in mice. Evid. Based. Complement. Alternat. Med.

Huang, X.Z., Wang, J., Huang, C., Chen, Y.Y., Shi, G.Y., Hu, Q.S., Yi, J., 2008. Emodin enhances cytotoxicity of chemotherapeutic drugs in prostate cancer cells: The mechanisms involve ROS-mediated suppression of multidrug resistance and hypoxia inducible factor-1. Cancer Biol. Ther. 7, 468–475.

Hubbi, M.E., Semenza, G.L., 2015. An essential role for chaperone-mediated autophagy in cell cycle progression. Autophagy 11, 850–851.

Igney, F.H., Krammer, P.H., 2002. Death and anti-death: tumour resistance to apoptosis. Nat. Rev. Cancer 2, 277–88.

Ishida, S., Lee, J., Thiele, D.J., Herskowitz, I., 2002. Uptake of the anticancer drug cisplatin mediated by the copper transporter Ctr1 in yeast and mammals. Proc. Natl. Acad. Sci. U. S. A. 99, 14298–14302.

Jamil, S.S., Nizami, Q., Salam, M., Urban, L., 2007. Centella asiatica (Linn .) Urban óA Review. Nat. Prod. Radiance 6, 158–170.

Jang, S.H., Wientjes, M.G., Lu, D., Au, J.L.S., 2003. Drug delivery and transport to solid tumors. Pharm. Res. 20, 1337–50.

Jang, S.P., Choi, S.U.S., 2004. Role of Brownian motion in the enhanced thermal conductivity of nanofluids. Appl. Phys. Lett. 84, 4316–4318.

Jia, Z., Geng, D., Xie, T., Zhang, J., Liu, Y., 2012. Quantitative analysis of neovascular permeability in glioma by dynamic contrast-enhanced MR imaging. J. Clin. Neurosci. 19, 820–3.

Jiang, M., Yi, X., Hsu, S., Wang, C.-Y., Dong, Z., 2004. Role of p53 in cisplatin-induced tubular cell apoptosis: dependence on p53 transcriptional activity. Am. J. Physiol. Renal Physiol. 287, F1140–F1147.

Johnson, V.L., Ko, S.C.W., Holmstrom, T.H., Eriksson, J.E., Chow, S.C., 2000. Effector caspases are dispensable for the early nuclear morphological changes during chemical-induced apoptosis. J. Cell Sci. 113, 2941–2953.

Kamura, T., Sato, S., Iwai, K., Czyzyk-krzeska, M., Conaway, R.C., Weliky, J., 2000. Activation of HIF1α ubiquitination by a reconstituted von Hippel-Lindau (VHL) tumor suppressor complex. PNAS 97, 10430–10435.

Kanu, O.O., Hughes, B., Di, C., Lin, N., Fu, J., Bigner, D.D., Yan, H., Adamson, C., 2009. Glioblastoma Multiforme Oncogenomics and Signaling Pathways. Clin. Med. Oncol. 3, 39–52.

Kavitha, C. V, Agarwal, C., Agarwal, R., Deep, G., 2011. Asiatic Acid inhibits pro-angiogenic effects of VEGF and human gliomas in endothelial cell culture models. PLoS One 6, e22745.

Kavitha, C. V., Jain, A.K., Agarwal, C., Pierce, A., Keating, A., Huber, K.M., Serkova, N.J., Wempe, M.F., Agarwal, R., Deep, G., 2015. Asiatic acid induces endoplasmic reticulum stress and apoptotic death in glioblastoma multiforme cells both in vitro and in vivo. Mol. Carcinog. 54, 1417–29.

Kelf, T.A., Sreenivasan, V.K.A., Sun, J., Kim, E.J., Goldys, E.M., Zvyagin, A. V, 2010. Non-specific cellular uptake of surface-functionalized quantum dots. Nanotechnology 21, 1–14.

Kelso, T.W.R., Baumgart, K., Eickhoff, J., Albert, T., Antrecht, C., Lemcke, S., Klebl, B., Meisterernst, M., 2014. CDK7 controls mRNA synthesis by affecting stability of preinitiation complexes, leading to altered gene expression, cell cycle progression and survival of tumor cells. Mol. Cell. Biol. MCB.00595–14.

Kerr, J.F.R., Wyllie, A.H., Currie, A.R., 1972. APOPTOSIS : A BASIC BIOLOGICAL PHENOMENON WITH WIDE-RANGING IMPLICATIONS IN TISSUE KINETICS. Br. J. Cancer 26, 239–257.

Kikusato, M., Yoshida, H., Furukawa, K., Toyomizu, M., 2015. Effect of heat stress-induced production of mitochondrial reactive oxygen species on NADPH oxidase and heme oxygenase-1 mRNA levels in avian muscle cells. J. Therm. Biol. 52, 8–13.

Kim, J.W., Dang, C. V., 2006. Cancer's molecular sweet tooth and the warburg effect. Cancer Res. 66, 8927–8930.

Kim, J.W., Tchernyshyov, I., Semenza, G.L., Dang, C. V., 2006. HIF-1-mediated expression of pyruvate dehydrogenase kinase: A metabolic switch required for cellular adaptation to hypoxia. Cell Metab. 3, 177–185.

Kleihues, P., Ohgaki, H., 1999. Primary and secondary glioblastomas: from concept to clinical diagnosis. Neuro. Oncol. 1, 44–51.

Klein, M., Reijneveld, J.C., Taphoorn, M.J.B., S, D.N.E.M., Health, O., 2010. phase of high-grade glioma patients. Neuro. Oncol. 12, 1162–1166.

Koch, S., Mayer, F., Honecker, F., Schittenhelm, M., Bokemeyer, C., 2003. Efficacy of cytotoxic agents used in the treatment of testicular germ cell tumours under normoxic and hypoxic conditions in vitro. Br. J. Cancer 89, 2133–2139.

Köhler, C., Orrenius, S., Zhivotovsky, B., 2002. Evaluation of caspase activity in apoptotic cells. J. Immunol. Methods 265, 97–110.

Kolamunne, R.T., Dias, I.H.K., Vernallis, A.B., Grant, M.M., Griffiths, H.R., 2013. Nrf2 activation supports cell survival during hypoxia and hypoxia/reoxygenation in cardiomyoblasts; the roles of reactive oxygen and nitrogen species. Redox Biol. 1, 418–426.

Komatsu, M., Sumizawa, T., Mutoh, M., Chen, Z.S., Terada, K., Furukawa, T., Yang, X.L., Gao, H., Miura, N., Sugiyama, T., Akiyama, S.I., 2000. Copper-transporting P-type adenosine triphosphatase (ATP7B) is associated with cisplatin resistance. Cancer Res. 60, 1312–1316.

Konan, Y.N., Gurny, R., Allémann, E., 2002. Preparation and characterization of sterile and freeze-dried sub-200 nm nanoparticles. Int. J. Pharm. 233, 239–52.

Korkolopoulou, P., Perdiki, M., Thymara, I., Boviatsis, E., Agrogiannis, G., Kotsiakis, X., Angelidakis, D., Rologis, D., Diamantopoulou, K., Thomas-Tsagli, E., Kaklamanis, L., Gatter, K., Patsouris, E., 2007. Expression of hypoxia-related tissue factors in astrocytic gliomas. A multivariate survival study with emphasis upon carbonic anhydrase IX. Hum. Pathol. 38, 629–638.

Krishnamurthy, R.G., Senut, M., Zemke, D., Min, J., Frenkel, B., Greenberg, E.J., Yu, S., Ahn, N., Goudreau, J., Kassab, M., Panickar, K.S., Majid, A., 2009. Asiatic acid, a Pentacyclic Triterpene From Centella Asiatica, Is Neuroprotective in a Mouse Model of Focal Cerebral Ischemia. J. Neurosci. Res. 87, 2541–2550.

Kroemer, G., Galluzzi, L., Brenner, C., 2007. Mitochondrial membrane permeabilization in cell death. Physiol. Rev. 87, 99–163.

Kroemer, G., Galluzzi, L., Vandenabeele, P., Abrams, J., Alnemri, E.S., Baehrecke, E.H., Blagosklonny, M. V, El-Deiry, W.S., Golstein, P., Green, D.R., Hengartner, M., Knight, R. a, Kumar, S., Lipton, S. a, Malorni, W., Nuñez, G., Peter, M.E., Tschopp, J., Yuan, J., Piacentini, M., Zhivotovsky, B., Melino, G., 2009. Classification of cell death: recommendations of the Nomenclature Committee on Cell Death 2009. Cell Death Differ. 16, 3–11.

Kryston, T.B., Georgiev, A.B., Pissis, P., Georgakilas, A.G., 2011. Role of oxidative stress and DNA damage in human carcinogenesis. Mutat. Res. 711, 193–201.

Kumari, A., Yadav, S.K., Yadav, S.C., 2010. Biodegradable polymeric nanoparticles based drug delivery systems. Colloids Surf. B. Biointerfaces 75, 1–18.

Kurosaka, K., Takahashi, M., Watanabe, N., Kobayashi, Y., 2003. Silent Cleanup of Very Early Apoptotic Cells by Macrophages. J. Immunol. 171, 4672–4679.

LaCasse, E.C., Mahoney, D.J., Cheung, H.H., Plenchette, S., Baird, S., Korneluk, R.G., 2008. IAP-targeted therapies for cancer. Oncogene 27, 6252–75.

Lalloo, A., Chao, P., Hu, P., Stein, S., Sinko, P.J., 2006. Pharmacokinetic and pharmacodynamic evaluation of a novel in situ forming poly(ethylene glycol)-based hydrogel for the controlled delivery of the camptothecins. J. Control. Release 112, 333–42.

Lamprecht, a, Ubrich, N., Hombreiro Pérez, M., Lehr, C., Hoffman, M., Maincent, P., 2000. Influences of process parameters on nanoparticle preparation performed by a double emulsion pressure homogenization technique. Int. J. Pharm. 196, 177–82.

Lando, D., Peet, D.J., Whelan, D. a, Gorman, J.J., Whitelaw, M.L., 2002. Asparagine hydroxylation of the HIF transactivation domain a hypoxic switch. Science 295, 858–861.

Lanjwani, S.N., Zhu, R., Khuhawar, M.Y., Ding, Z., 2006. High performance liquid chromatographic determination of platinum in blood and urine samples of cancer patients after administration of cisplatin drug using solvent extraction and N,N???-bis(salicylidene)-1,2-propanediamine as complexation reagent. J. Pharm. Biomed. Anal. 40, 833–839.

Lebwohl, D., Canetta, R., 1998. Clinical Oncology Update Clinical Development of Platinum Complexes in Cancer Therapy : an Historical Perspective and an Update. Eur. J. Cancer 34, 1522–1534.

Lee, K.Y., Bae, O., Serfozo, K., Hejabian, S., Moussa, A., Reeves, M., Rumbeiha, W., Fitzgerald, S.D., Stein, G., Baek, S., Goudreau, J., Kassab, M., Majid, A., 2012. Asiatic Acid Attenuates Infarct Volume , Mitochondrial Dysfunction , and Matrix Metalloproteinase-9 Induction After Focal Cerebral Ischemia. Stroke 43, 1632–1638.

Lee, K.Y., Bae, O., Weinstock, S., Kassab, M., Majid, A., 2014a. Neuroprotective Effect of Asiatic Acid in Rat Model of Focal Embolic Stroke. Biological 37, 1397–1401.

Lee, K.Y., Bae, O., Weinstock, S., Kassab, M., Majid, A., 2014b. Neuroprotective Effect of Asiatic Acid in Rat Model of Focal Embolic Stroke 37, 1397–1401.

Lee, N., MacDonald, H., Reinhard, C., Halenbeck, R., Roulston, a, Shi, T., Williams, L.T., 1997. Activation of hPAK65 by caspase cleavage induces some of the

morphological and biochemical changes of apoptosis. Proc. Natl. Acad. Sci. U. S. A. 94, 13642–13647.

Lee, Y.S., Jin, D.-Q., Kwon, E.J., Park, S.H., Lee, E.-S., Jeong, T.C., Nam, D.H., Huh, K., Kim, J.-A., 2002. Asiatic acid, a triterpene, induces apoptosis through intracellular Ca2+ release and enhanced expression of p53 in HepG2 human hepatoma cells. Cancer Lett. 186, 83–91.

Lemoine, D., Francois, C., Kedzierewicz, F., Preat, V., Hoffman, M., Maincent, P., 1996. Stability study of nanoparticles of and poly (D , L-lactide-co-glycolide). Biomaterials 17, 2191–2197.

Leroueil-Le Verger, M., Fluckiger, L., Kim, Y.I., Hoffman, M., Maincent, P., 1998. Preparation and characterization of nanoparticles containing an antihypertensive agent. Eur. J. Pharm. Biopharm. 46, 137–43.

Levene, P.A., Meyer, G.M., 1912a. On the action of leucocytes on glucose. J. Biol. Chem. 12, 265–273.

Levene, P.A., Meyer, G.M., 1912b. Action of Leucocytes on Glucose. J. Biol. Chem. 11, 361–370.

Levett, D., Radford, E., Menassa, D., Graber, E., Morash, A., Hoppeler, H., Clarke, K., Martin, D., Ferguson-Smith, A., Montgomery, H., Grocott, M., Murray, A., Group, C.X.E.R., 2012. Acclimatization of skeletal muscle mitochondria to high-altitude hypoxia during an ascent of Everest. 1431–1441.

Levin, S., Bucci, T.J., Cohen, S.M., Fix, A.S., Hardisty, J.F., Legrand, E.K., Maronpot, R.R., Trump, B.F., 1999. The Nomenclature of Cell Death : Recommendations of an ad hoc Committee of the Society of Toxicologic Pathologists *. Toxicol. Pathol. 27, 484–490.

Li, J.-F., Huang, R.-Z., Yao, G.-Y., Ye, M.-Y., Wang, H.-S., Pan, Y.-M., Xiao, J.-T., 2014. Synthesis and biological evaluation of novel aniline-derived asiatic acid derivatives as potential anticancer agents. Eur. J. Med. Chem. 86, 175–188.

Li, P., Nijhawan, D., Budihardjo, I., Srinivasula, S.M., Ahmad, M., Alnemri, E.S., Wang, X., 1997. Cytochrome c and dATP-dependent formation of Apaf-1/caspase-9 complex initiates an apoptotic protease cascade. Cell 91, 479–489.

Liebner, S., Fischmann, a, Rascher, G., Duffner, F., Grote, E.H., Kalbacher, H., Wolburg, H., 2000. Claudin-1 and claudin-5 expression and tight junction morphology are altered in blood vessels of human glioblastoma multiforme. Acta Neuropathol. 100, 323–331.

Liu, L., Ning, X., Sun, L., Zhang, H., Shi, Y., Guo, C., Han, S., Liu, J., Sun, S., Han, Z., Wu, K., Fan, D., 2008. Hypoxia-inducible factor-1?? contributes to hypoxia-induced chemoresistance in gastric cancer. Cancer Sci. 99, 121–128.

Liu, L., Simon, M.C., 2004. Regulation of Transcription and Translation by Hypoxia.

Cancer Biol. Ther. 3, 492–497.

Liu, X., Tu, M., Kelly, R.S., Chen, C., Smith, B.J., 2004. Development of a Computational Approach to Predict Blood Brain Barrier Permiability. Drug Metab. Depos. 32, 132–139.

Liu, Z., Jiao, Y., Liu, F., Zhang, Z., 2007. Heparin / chitosan nanoparticle carriers prepared by polyelectrolyte complexation. J. Biomed. Mater. Res. Part A.

Loboda, A., Jozkowicz, A., Dulak, J., 2010. HIF-1 and HIF-2 transcription factors--similar but not identical. Mol. Cells 29, 435–42.

Locksley, R.M., Killeen, N., Lenardo, M.J., 2001. The TNF and TNF Receptor Superfamilies : Integrating Mammalian Biology. Cell 104, 487–501.

Loeb, L. a., 2001. A mutator phenotype in cancer. Cancer Res. 61, 3230–3239.

Lou, Y.-W., Wang, P.-Y., Yeh, S.-C., Chuang, P.-K., Li, S.-T., Wu, C.-Y., Khoo, K.-H., Hsiao, M., Hsu, T.-L., Wong, C.-H., 2014. Stage-specific embryonic antigen-4 as a potential therapeutic target in glioblastoma multiforme and other cancers. Proc. Natl. Acad. Sci. U. S. A. 111, 2482–7.

Lowe, S.W., Lin, A.W., 2000. Apoptosis in cancer. Carcinogenesis 21, 485–495.

Lu, T.-H., Su, C.-C., Tang, F.-C., Chen, C.-H., Yen, C.-C., Fang, K.-M., Lee, kuan-I., Hung, D.-Z., Chen, Y.-W., 2015. Chloroacetic acid triggers apoptosis in neuronal cells via a reactive oxygen species-induced endoplasmic reticulum stress signaling pathway. Chem. Biol. Interact. 225, 1–12.

Ly, J.D., Grubb, D.R., Lawen, a., 2003. The mitochondrial membrane potential (δψm) in apoptosis; an update. Apoptosis 8, 115–128.

Ma, K., Zhang, Y., Zhu, D., Lou, Y., 2009. Protective effects of asiatic acid against D-galactosamine/lipopolysaccharide-induced hepatotoxicity in hepatocytes and kupffer cells co-cultured system via redox-regulated leukotriene C4 synthase expression pathway. Eur. J. Pharmacol. 603, 98–107.

Ma, Y., Zheng, Y., Zeng, X., Jiang, L., Chen, H., Liu, R., Huang, L., Mei, L., 2011. Novel docetaxel-loaded nanoparticles based on PCL-Tween 80 copolymer for cancer treatment. Int. J. Nanomedicine 6, 2679–88.

Macheret, M., Halazonetis, T.D., 2015. DNA Replication Stress as a Hallmark of Cancer.

Maddika, S., Ande, S.R., Panigrahi, S., Paranjothy, T., Weglarczyk, K., Zuse, A., Eshraghi, M., Manda, K.D., Wiechec, E., Los, M., 2007. Cell survival, cell death and cell cycle pathways are interconnected: Implications for cancer therapy. Drug Resist. Updat. 10, 13–29.

Maeda, H., 2001. The enhanced permeability and retention (EPR) effect in tumor vasculature: the key role of tumor-selective macromolecular drug targeting. Adv.

Enzyme Regul. 41, 189–207.

Maher, E. a, Furnari, F.B., Bachoo, R.M., Rowitch, D.H., Louis, D.N., Cavenee, W.K., DePinho, R. a, 2001. Malignant glioma: genetics and biology of a grave matter. Genes Dev. 15, 1311–33.

Mailloux, R.J., Bériault, R., Lemire, J., Singh, R., Chénier, D.R., Hamel, R.D., Appanna, V.D., 2007. The tricarboxylic acid cycle, an ancient metabolic network with a novel twist. PLoS One 2, e690.

Mamenta, E.L., Poma, E.E., Kaufmann, W.K., Poina, E.E., Kaufmann, K., Delmastro, D. a, Grady, L., Chane, S.G., 1994. Enhanced Replicative Bypass of Platinum-DNA Adducts in Cisplatin-resistant Human Ovarian Carcinoma Cell Lines Enhanced Replicative Bypass of Platinum-DNA Adducts in Cisplatin-resistant Human Ovarian Carcinoma Cell Lines1. Cancer Res. 54, 3500–3505.

Mandl, E.S., Dirven, C.M.F., Buis, D.R., Postma, T.J., Vandertop, W.P., 2008. Repeated surgery for glioblastoma multiforme: only in combination with other salvage therapy. Surg. Neurol. 69, 506–509.

Martinvalet, D., Zhu, P., Lieberman, J., 2005. Granzyme A induces caspase-independent mitochondrial damage, a required first step for apoptosis. Immunity 22, 355–70.

Matés, J.M., Pérez-Gómez, C., Núñez de Castro, I., 1999. Antioxidant enzymes and human diseases. Clin. Biochem. 32, 595–603.

Matés, J.M., Sánchez-Jiménez, F.M., 2000. Role of reactive oxygen species in apoptosis: implications for cancer therapy. Int. J. Biochem. Cell Biol. 32, 157–170.

Matsumura, Y., Maeda, H., 1986. A New Concept for Macromolecular Therapeutics in Cancer Chemotherapy : Mechanism of Tumoritropic Accumulation of Proteins and the Antitumor Agent Smancs A New Concept for Macromolecular Therapeutics in Cancer Chemotherapy : Mechanism of Tumoritropic Accum. Cancer Res. 46, 6387–6392.

Maxwell, P., 2003. HIF-1: An Oxygen Response System with Special Relevance to the Kidney. J. Am. Soc. Nephrol. 14, 2712–2722.

Maxwell, P.H., Pugh, C.W., Ratcliffe, P.J., 2001. Activation of the HIF pathway in cancer 293–299.

McCord, J.M., Fridovich, I., 1969. An Enzymic Function for Erythrocuprein (Hemocuprein)*. J. Biol. Chem. 244, 6049–6055.

McDermott, M.W., Sneed, P.K., Gutin, P.H., 1998. Interstitial Brachytherapy for Malignant. Semin. Surg. Biol. 14, 79–87.

Mei, L., Zhang, Y., Zheng, Y., Tian, G., Song, C., Yang, D., Chen, H., Sun, H., Tian, Y., Liu, K., Li, Z., Huang, L., 2009. A novel docetaxel-loaded poly (e-caprolactone)/Pluronic F68 nanoparticle overcoming multidrug resistance for

breast cancer treatment. Nanoscale Res. Lett. 4, 1530–1539.

Melillo, G., 2004. HIF-1: A Target for cancer, Ischemia and Inflammation. Cell Cycle 3, 154–155.

Mineo, J.-F., Bordron, A., Baroncini, M., Ramirez, C., Maurage, C., Blond, S., Dam-Hieu, P., 2007. Prognosis factors of survival time in patients with glioblastoma multiforme: a multivariate analysis of 340 patients. Acta Neurochir. (Wien). 149, 245–52.

Minniti, G., Muni, R., Lanzetta, G., Marchetti, P., Enrici, R.M., 2009. Chemotherapy for glioblastoma: current treatment and future perspectives for cytotoxic and targeted agents. Anticancer Res. 29, 5171–84.

Miyashita, H., Nitta, Y., Mori, S., Kanzaki, A., Nakayama, K., Terada, K., Sugiyama, T., Kawamura, H., Sato, A., Morikawa, H., Motegi, K., Takebayashi, Y., 2003. Expression of copper-transporting P-type adenosine triphosphatase (ATP7B) as a chemoresistance marker in human oral squamous cell carcinoma treated with cisplatin. Oral Oncol. 39, 157–162.

Momekov, G., Ferdinandov, D., Bakalova, A., Zaharieva, M., Konstantinov, S., Karaivanova, M., 2006. In vitro toxicological evaluation of a dinuclear platinum(II) complex with acetate ligands. Arch. Toxicol. 80, 555–560.

Momeni, H.R., 2011. Role of calpain in apoptosis. Cell J. 13, 65–72.

Montano, N., Cenci, T., Martini, M., D'Alessandris, Q.G., Pelacchi, F., Ricci-Vitiani, L., Maira, G., De Maria, R., Larocca, L.M., Pallini, R., 2011. Expression of EGFRvIII in glioblastoma: prognostic significance revisited. Neoplasia 13, 1113–21.

Mori, S., Kunieda, K., Sugiyama, Y., Saji, S., 2003. Prediction of 5-fluorouracil and cisplatin synergism for advanced gastrointestinal cancers using a collagen gel droplet embedded culture. Surg. Today 33, 577–583.

Mukerjee, A., Sinha, V.R., Pruthi, V., 2007. Preparation and Characterization of Poly- ε -caprolactone Particles for Controlled Insulin Delivery. J. Biomed. Pharm. Eng. 1, 40–44.

Nagata, S., 2000. Apoptotic DNA fragmentation. Exp. Cell Res. 256, 12–8.

Naik, P., Cucullo, L., 2012. In vitro blood-brain barrier models: Current and perspective technologies. J. Pharm. Sci. 101, 1337–1354.

Nakayama, K., Kanzaki, A., Ogawa, K., Miyazaki, K., Neamati, N., Takebayashi, Y., 2002. Copper-transporting P-type adenosine triphosphatase (ATP7B) as a cisplatin based chemoresistance marker in ovarian carcinoma: Comparative analysis with expression of MDR1, MRP1, MRP2, LRP and BCRP. Int. J. Cancer 101, 488–495.

Natarajan, M., Stewart, J.E., Golemis, E. a, Pugacheva, E.N., Alexandropoulos, K., Cox, B.D., Wang, W., Grammer, J.R., Gladson, C.L., 2006. HEF1 is a necessary

and specific downstream effector of FAK that promotes the migration of glioblastoma cells. Oncogene 25, 1721–1732.

Nevins, J.R., 2001. The Rb/E2F pathway and cancer. Hum. Mol. Genet. 10, 699–703.

Nicholls, D.G., Ward, M.W., 2000. Mitochondrial membrane potential and neuronal glutamate excitotoxicity: Mortality and millivolts. Trends Neurosci. 23, 166–174.

Nishimoto, T., Furuta, M., Kataoka, M., Kishida, M., 2015. Important Role of Catalase in the Cellular Response of the Budding Yeast Saccharomyces cerevisiae Exposed to Ionizing Radiation. Curr. Microbiol. 70, 404–407.

Normanno, N., De Luca, A., Bianco, C., Strizzi, L., Mancino, M., Maiello, M.R., Carotenuto, A., De Feo, G., Caponigro, F., Salomon, D.S., 2006. Epidermal growth factor receptor (EGFR) signaling in cancer. Gene 366, 2–16.

O'Brien, M. a., Kirby, R., 2008. Apoptosis: A review of pro-apoptotic and anti-apoptotic pathways and dysregulation in disease. J. Vet. Emerg. Crit. Care 18, 572–585.

O'Brien, V., Brown, R., 2006. Signalling cell cycle arrest and cell death through the MMR System. Carcinogenesis 27, 682–692.

Ohgaki, H., Dessen, P., Jourde, B., Horstmann, S., Nishikawa, T., Di Patre, P.-L., Burkhard, C., Schüler, D., Probst-Hensch, N.M., Maiorka, P.C., Baeza, N., Pisani, P., Yonekawa, Y., Yasargil, M.G., Lütolf, U.M., Kleihues, P., 2004. Genetic pathways to glioblastoma: a population-based study. Cancer Res. 64, 6892–9.

Ohgaki, H., Kleihues, P., 2013. The definition of primary and secondary glioblastoma. Clin. Cancer Res. 19, 764–772.

Ohh, M., Park, C.W., Ivan, M., Hoffman, M.A., Kim, T., Huang, L.E., Chau, V., Kaelin, W.G., Hughes, H., 2000. Ubiquitination of hypoxia-inducible factor requires direct binding to the β -domain of the von Hippel – Lindau protein. Nat. Cell Biol. 2, 423–427.

Olbryt, M., Habryka, a, Student, S., Jarzab, M., Tyszkiewicz, T., Lisowska, K.M., 2014. Global Gene Expression Profiling in Three Tumor Cell Lines Subjected to Experimental Cycling and Chronic Hypoxia. PLoS One 9.

Orringer, D., Lau, D., Khatri, S., Zamora-Berridi, G.J., Zhang, K., Wu, C., Chaudhary, N., Sagher, O., 2012. Extent of resection in patients with glioblastoma: limiting factors, perception of resectability, and effect on survival. J. Neurosurg. 117, 851–9.

Pampaloni, F., Reynaud, E.G., Stelzer, E.H.K., 2007. The third dimension bridges the gap between cell culture and live tissue. Nat. Rev. Mol. Cell Biol. 8, 839–845.

Pantuck, A.J., Zeng, G., Belldegrun, A.S., Figlin, R. a, 2003. Pathobiology , Prognosis , and Targeted Therapy for Renal Cell Carcinoma : Exploiting the Hypoxia-Induced Pathway Pathobiology , Prognosis , and Targeted Therapy for Renal Cell

Carcinoma : Exploiting the Hypoxia-Induced Pathway 9, 4641–4652.

Panyam, J., Labhasetwar, V., 2003. Biodegradable nanoparticles for drug and gene delivery to cells and tissue. Adv. Drug Deliv. Rev. 55, 329–347.

Papandreou, I., Cairns, R. a., Fontana, L., Lim, A.L., Denko, N.C., 2006. HIF-1 mediates adaptation to hypoxia by actively downregulating mitochondrial oxygen consumption. Cell Metab. 3, 187–197.

Pardo, J., Bosque, A., Brehm, R., Wallich, R., Naval, J., Müllbacher, A., Anel, A., Simon, M.M., 2004. Apoptotic pathways are selectively activated by granzyme A and/or granzyme B in CTL-mediated target cell lysis. J. Cell Biol. 167, 457–68.

Pardridge, W.M., Triguero, D., Yang, J., Cancilla, P., 1990. Comparison of in vitro and in vivo models of drug transcytosis through the blood-brain barrier . J Pharmacol Exp Ther 253 : 884-891 Comparison of in Vitro and in Vivo Models of Drug Transcytosis Through the Blood-Brain Barrier ’. J. Pharmacol. Exp. Ther. 253, 884–891.

Parks, S.K., Mazure, N.M., Counillon, L., Pouysségur, J., 2013. Hypoxia promotes tumor cell survival in acidic conditions by preserving ATP levels. J. Cell. Physiol. 228, 1854–1862.

Passaglia, E., Bertoldo, M., Coiai, S., Augier, S., Savi, S., Ciardelli, F., 2006. Nanostructured polyolefins / clay composites : role of the molecular interaction at the interface. Polym. Adv. Technol. 17, 474–478.

Patlolla, J.M.R., Raju, J., Swamy, M. V, Rao, C. V, 2006. Beta-escin inhibits colonic aberrant crypt foci formation in rats and regulates the cell cycle growth by inducing p21(waf1/cip1) in colon cancer cells. Mol. Cancer Ther. 5, 1459–1466.

Pelicano, H., Carney, D., Huang, P., 2004. ROS stress in cancer cells and therapeutic implications. Drug Resist. Updat. 7, 97–110.

Pelloski, C.E., Gilbert, M.R., 2007. Current Treatment Options in Adult Glioblastoma, Neurological cancer.

Pennington, M.W., Thornberry, N. a, 2015. Synthesis of a fluorogenic interleukin-1 beta converting enzyme substrate based on resonance energy transfer. Pept. Res. 7, 72–76.

Perry, S.W., Norman, J.P., Barbieri, J., Brown, E.B., Gelbard, H. a., 2011. Mitochondrial membrane potential probes and the proton gradient: A practical usage guide. Biotechniques 50, 98–115.

Pinheiro, D., Sunkel, C., 2012. Mechanisms of cell cycle control. Canal bq 4–17.

Pore, N., Jiang, Z., Gupta, A., Cerniglia, G., Kao, G.D., Maity, A., 2006. EGFR tyrosine kinase inhibitors decrease VEGF expression by both hypoxia-inducible factor (HIF)-1-independent and HIF-1-dependent mechanisms. Cancer Res. 66, 3197–3204.

Preusser, M., de Ribaupierre, S., Wöhrer, A., Erridge, S.C., Hegi, M., Weller, M., Stupp, R., 2011. Current concepts and management of glioblastoma. Ann. Neurol. 70, 9–21.

Prombutara, P., Kulwatthanasal, Y., Supaka, N., Sramala, I., Chareonpornwattana, S., 2012. Production of nisin-loaded solid lipid nanoparticles for sustained antimicrobial activity. Food Control 24, 184–190.

Pulkkinen, M., Malin, M., Böhm, J., Tarvainen, T., Wirth, T., Seppälä, J., Järvinen, K., 2009. In vivo implantation of 2,2′-bis(oxazoline)-linked poly-ε-caprolactone: Proof for enzyme sensitive surface erosion and biocompatibility. Eur. J. Pharm. Sci. 36, 310–319.

Qin, L.F., Ng, I.O.L., 2002. Induction of apoptosis by cisplatin and its effect on cell cycle-related proteins and cell cycle changes in hepatoma cells. Cancer Lett. 175, 27–38.

Rahman, Z.S.M., Shao, W.-H., Khan, T.N., Zhen, Y., Cohen, P.L., 2010. Impaired apoptotic cell clearance in the germinal center by Mer-deficient tingible body macrophages leads to enhanced antibody-forming cell and germinal center responses. J. Immunol. 185, 5859–5868.

Raizer, J.J., Abrey, L.E., Lassman, A.B., Chang, S.M., Lamborn, R., Kuhn, J.G., Yung, W.K.A., Gilbert, M.R., Aldape, K.A., Wen, P.Y., Fine, H.A., Mehta, M., Deangelis, L.M., Lieberman, F., Cloughesy, T.F., Robins, H.I., Dancey, J., Prados, M.D., 2010. A phase II trial of erlotinib in patients with recurrent malignant gliomas and nonprogressive glioblastoma multiforme postradiation therapy. Neuro. Oncol. 12, 95–103.

Ramesh, G., Brian Reeves, W., 2002. TNF-α mediates chemokine and cytokine expression and renal injury in cisplatin nephrotoxicity. J. Clin. Invest. 110, 835–842.

Reithmeier, T., Graf, E., Piroth, T., Trippel, M., Pinsker, M.O., Nikkhah, G., 2010. BCNU for recurrent glioblastoma multiforme: efficacy, toxicity and prognostic factors. BMC Cancer 10, 30.

Rich, J.N., Reardon, D. a, Peery, T., Dowell, J.M., Quinn, J. a, Penne, K.L., Wikstrand, C.J., Van Duyn, L.B., Dancey, J.E., McLendon, R.E., Kao, J.C., Stenzel, T.T., Ahmed Rasheed, B.K., Tourt-Uhlig, S.E., Herndon, J.E., Vredenburgh, J.J., Sampson, J.H., Friedman, A.H., Bigner, D.D., Friedman, H.S., 2004. Phase II trial of gefitinib in recurrent glioblastoma. J. Clin. Oncol. 22, 133–42.

Rieder, C.L., 2011. Mitosis in vertebrates: the G2/M and M/A transitions and their associated checkpoints. Chromosome Res. 19, 291–306.

Risau, W., Wolburg, H., 1990. Development of the blood-brain barrier. Trends Neurosci. 13, 174–8.

Rofstad, E.K., Galappathi, K., Mathiesen, B., Ruud, E.B.M., 2007. Fluctuating and

diffusion-limited hypoxia in hypoxia-induced metastasis. Clin. Cancer Res. 13, 1971–1978.

Rohwer, N., Dame, C., Haugstetter, A., Wiedenmann, B., Detjen, K., Schmitt, C. a., Cramer, T., 2010. Hypoxia-inducible factor 1α determines gastric cancer chemosensitivity via modulation of p53 and Nf-κB. PLoS One 5, 17–20.

Roschitzki-Voser, H., Schroeder, T., Lenherr, E.D., Frölich, F., Schweizer, A., Donepudi, M., Ganesan, R., Mittl, P.R.E., Baici, A., Grütter, M.G., 2012. Human caspases in vitro: Expression, purification and kinetic characterization. Protein Expr. Purif. 84, 236–246.

Rosenberger, C., 2002. Expression of Hypoxia-Inducible Factor-1 and -2 in Hypoxic and Ischemic Rat Kidneys. J. Am. Soc. Nephrol. 13, 1721–1732.

Saelens, X., Festjens, N., Vande Walle, L., van Gurp, M., van Loo, G., Vandenabeele, P., 2004. Toxic proteins released from mitochondria in cell death. Oncogene 23, 2861–74.

Saez, a, Guzmán, M., Molpeceres, J., Aberturas, M.R., 2000. Freeze-drying of polycaprolactone and poly(D,L-lactic-glycolic) nanoparticles induce minor particle size changes affecting the oral pharmacokinetics of loaded drugs. Eur. J. Pharm. Biopharm. 50, 379–87.

Sarasam, A., 2001. Chitosan-Polycaprolactone mixtures as biomaterials-Influence of surface morphology on cellular activity. Jawaharlal Nehru Technological University.

Saraste, A., Pulkki, K., 2000. Morphologic and biochemical hallmarks of apoptosis. Cardiovasc. Res. 45, 528–537.

Sarin, H., Kanevsky, A.S., Wu, H., Brimacombe, K.R., Fung, S.H., Sousa, A. a, Auh, S., Wilson, C.M., Sharma, K., Aronova, M. a, Leapman, R.D., Griffiths, G.L., Hall, M.D., 2008. Effective transvascular delivery of nanoparticles across the blood-brain tumor barrier into malignant glioma cells. J. Transl. Med. 6, 80.

Scaffidi, P., Misteli, T., Bianchi, M.E., 2002. Release of chromatin protein HMGB1 by necrotic cells triggers inflammation. Nature 418, 191–195.

Schneider, P., Tschopp, J., 2000. Apoptosis induced by death receptors. Pharm. Acta Helv. 74, 281–286.

Schwarz, S.B., Thon, N., Nikolajek, K., Niyazi, M., Tonn, J.-C., Belka, C., Kreth, F.-W., 2012. Iodine-125 brachytherapy for brain tumours--a review. Radiat. Oncol. 7, 30.

Semenza, G.L., Botting, K.J., Mcmillen, I.C., Forbes, H., Nyengaard, J.R., Janna, L., Coudyzer, P., Lemoine, P., Jordan, B.F., Gallez, B., Galant, C., Nisolle, M., Courtoy, P.J., Henriet, P., Marbaix, E., Rathburn, C.K., Sharp, N.J., Ryan, J.C., Neely, M.G., Cook, M., Chapman, W., Burnett, L.E., Burnett, K.G., 2000. HIF-1:

mediator of physiological and pathophysiological responses to hypoxia. J. Appl. Physiol. 88, 1474–1480.

Shackelford, R.E., Kaufmann, W.K., Paules, R.S., 1999. Cell Cycle Control , Checkpoint Mechanisms , and Genotoxic Stress. Environ. Health Perspect. 107, 5–24.

Shah, L.K., Amiji, M.M., 2006. Intracellular delivery of saquinavir in biodegradable polymeric nanoparticles for HIV/AIDS. Pharm. Res. 23, 2638–45.

Shah, M. a, Schwartz, G.K., 2001. Cell Cycle-mediated Drug Resistance : An Emerging Concept in Cancer Therapy Cell Cycle-mediated Drug Resistance : An Emerging Concept in 7, 2168–2181.

Shannon, A.M., Bouchier-Hayes, D.J., Condron, C.M., Toomey, D., 2003. Tumour hypoxia, chemotherapeutic resistance and hypoxia-related therapies. Cancer Treat. Rev. 29, 297–307.

Sheleg, S. V, Korotkevich, E. a, Zhavrid, E. a, Muravskaya, G. V, Smeyanovich, A.F., Shanko, Y.G., Yurkshtovich, T.L., Bychkovsky, P.B., Belyaev, S. a, 2002. Local chemotherapy with cisplatin-depot for glioblastoma multiforme. J. Neurooncol. 60, 53–9.

Shen, H., Shi, C., Shen, Y., 1996. Detection of elevated reactive oxygen species level in cultured rat hepatocytes treated with aflatoxin B1. Free Radic. Biol. Med. 21, 139–146.

Shenoy, D., Little, S., Langer, R., Amiji, M.M., 2005. Poly(Ethylene Oxide)-Modified Poly(β-Amino Ester) Nanoparticles as a pH-Sensitive System for Tumor-Targeted Delivery of Hydrophobic Drugs: Part 2. In Vivo Distribution and Tumor Localization Studies. Pharm. Res. 22, 2107–2114.

Shenoy, D.B., Amiji, M.M., 2005. Poly(ethylene oxide)-modified poly(epsilon-caprolactone) nanoparticles for targeted delivery of tamoxifen in breast cancer. Int. J. Pharm. 293, 261–70.

Shukla, S., Gupta, S., 2007. Apigenin-induced cell cycle arrest is mediated by modulation of MAPK, PI3K-Akt, and loss of cyclin D1 associated retinoblastoma dephosphorylation in human prostate cancer cells. Cell Cycle 6, 1102–1114.

Siddik, Z.H., 2003. Cisplatin: mode of cytotoxic action and molecular basis of resistance. Oncogene 22, 7265–79.

Simon, H., Haj-Yehia, A., Levi-Schaffer, F., 2000. Role of reactive oxygen species (ROS) in apoptosis induction. Apoptosis 5, 415–418.

Singh, B., Rastogi, R.P., 1969. A Reinvestigation of the Triterpenes of Centella asiatica*. Phytochemistry 8, 917–921.

Sinha, V.R., Bansal, K., Kaushik, R., Kumria, R., Trehan, a, 2004. Poly-epsilon-caprolactone microspheres and nanospheres: an overview. Int. J. Pharm. 278, 1–23.

Skog, J., Würdinger, T., van Rijn, S., Meijer, D.H., Gainche, L., Sena-Esteves, M., Curry, W.T., Carter, B.S., Krichevsky, A.M., Breakefield, X.O., 2008. Glioblastoma microvesicles transport RNA and proteins that promote tumour growth and provide diagnostic biomarkers. Nat. Cell Biol. 10, 1470–6.

Song, C.W., Griffin, R., Park, H.J., 2006. Influence of Tumor pH on Therapeutic Response. In: Cancer Drug Discovery and Development: Cancer Drug Resistance. pp. 21–43.

Song, M., Chen, Y., Gong, G., Murphy, E., Rabinovitch, P.S., Dorn, G.W., 2014. Super-suppression of mitochondrial reactive oxygen species signaling impairs compensatory autophagy in primary mitophagic cardiomyopathy. Circ. Res. 115, 348–353.

Song, X., Liu, X., Chi, W., Liu, Y., Wei, L., Wang, X., Yu, J., 2006. Hypoxia-induced resistance to cisplatin and doxorubicin in non-small cell lung cancer is inhibited by silencing of HIF-1?? gene. Cancer Chemother. Pharmacol. 58, 776–784.

Soo Lee, Y., Jin, D.Q., Beak, S.M., Lee, E.S., Kim, J. a., 2003. Inhibition of ultraviolet-A-modulated signaling pathways by asiatic acid and ursolic acid in HaCaT human keratinocytes. Eur. J. Pharmacol. 476, 173–178.

Sorenson, C.M., Barry, M. a, Eastman, a, 1990. Analysis of events associated with cell cycle arrest at G2 phase and cell death induced by cisplatin. J. Natl. Cancer Inst. 82, 749–755.

Souza, R. De, Zahedi, P., Allen, C.J., Piquette-miller, M., De Souza, R., 2010. Polymeric drug delivery systems for localized cancer chemotherapy. Drug Deliv. 17, 365–75.

Strese, S., Fryknäs, M., Larsson, R., Gullbo, J., 2013. Effects of hypoxia on human cancer cell line chemosensitivity. BMC Cancer 13, 331.

Stupp, R., Hegi, M.E., Mason, W.P., van den Bent, M.J., Taphoorn, M.J.B., Janzer, R.C., Ludwin, S.K., Allgeier, A., Fisher, B., Belanger, K., Hau, P., Brandes, A. a, Gijtenbeek, J., Marosi, C., Vecht, C.J., Mokhtari, K., Wesseling, P., Villa, S., Eisenhauer, E., Gorlia, T., Weller, M., Lacombe, D., Cairncross, J.G., Mirimanoff, R.-O., 2009. Effects of radiotherapy with concomitant and adjuvant temozolomide versus radiotherapy alone on survival in glioblastoma in a randomised phase III study: 5-year analysis of the EORTC-NCIC trial. Lancet Oncol. 10, 459–66.

Stupp, R., Mason, W., van den Bent, M., Weller, M., Fisher, B., Taphoorn, M.J.B., Belanger, K., Brandes, A.A., Marosi, C., Bogdahn, U., Curschmann, J., Janzer, R.C., Ludwin, S.K., Gorlia, T., Allgieger, A., Lacombe, D., Cairncross, J.G., Eisenhauer, E., Mirimanoff, R.O., 2005. Radiotherapy plus concomitant and adjuvant temozolomide for glioblastoma. N. Engl. J. Med. 352, 987–996.

Suliman, a, Lam, a, Datta, R., Srivastava, R.K., 2001. Intracellular mechanisms of TRAIL: apoptosis through mitochondrial-dependent and -independent pathways.

Oncogene 20, 2122–2133.

Sullivan, G., Edmondson, C., 2008. Heat and temperature. Contin. Educ. Anaesthesia, Crit. Care Pain 8, 104–107.

Sullivan, R., Paré, G.C., Frederiksen, L.J., Semenza, G.L., Graham, C.H., 2008. Hypoxia-induced resistance to anticancer drugs is associated with decreased senescence and requires hypoxia-inducible factor-1 activity. Mol. Cancer Ther. 7, 1961–1973.

Susa, M., Iyer, A.K., Ryu, K., Hornicek, F.J., Mankin, H., Amiji, M.M., Duan, Z., 2009. Doxorubicin loaded Polymeric Nanoparticulate Delivery System to overcome drug resistance in osteosarcoma. BMC Cancer 9, 399–410.

Ta, H.T., Dass, C.R., Dunstan, D.E., 2008. Injectable chitosan hydrogels for localised cancer therapy. J. Control. Release 126, 205–16.

Taal, W., Brandsma, D., de Bruin, H.G., Bromberg, J.E., Swaak-Kragten, A.T., Smitt, P. a E.S., van Es, C. a, van den Bent, M.J., 2008. Incidence of early pseudo-progression in a cohort of malignant glioma patients treated with chemoirradiation with temozolomide. Cancer 113, 405–410.

Tang, X.-L., Yang, X.-Y., Jung, H.-J., Kim, S.-Y., Jung, S.-Y., Choi, D.-Y., Park, W.-C., Park, H., 2009. Asiatic acid induces colon cancer cell growth inhibition and apoptosis through mitochondrial death cascade. Biol. Pharm. Bull. 32, 1399–1405.

Tanimoto, K., Makino, Y., 2000. Mechanism of regulation of the hypoxia-inducible factor-1 a by the von Hippel-Lindau tumor suppressor protein 19.

Tarafder, S., Nansen, K., Bose, S., 2013. Lovastatin release from polycaprolactone coated β-tricalcium phosphate: effects of pH, concentration and drug-polymer interactions. Mater. Sci. Eng. C. Mater. Biol. Appl. 33, 3121–8.

Taylor, T.E., Furnari, F.B., Cavenee, W.K., 2012. Targeting EGFR for Treatment of Glioblastoma: Molecular Basis to Overcome Resistance. Curr. Cancer Drug Targets 12, 197–209.

Tezcan, S., Özdemir, F., Turhal, S., Vehbi, F., 2013. High performance liquid chromatographic determination of free cisplatin in different cancer types. Der Pharma Chem. 5, 169–174.

Tong, L., Chuang, C.-C., Wu, S., Zuo, L., 2015. Reactive oxygen species in redox cancer therapy. Cancer Lett.

Toyooka, M., Kimura, H., Uematsu, H., Kawamura, Y., Takeuchi, H., Itoh, H., 2008. Tissue characterization of glioma by proton magnetic resonance spectroscopy and perfusion-weighted magnetic resonance imaging: glioma grading and histological correlation. Clin. Imaging 32, 251–8.

Trapani, J. a, Smyth, M.J., 2002. Functional significance of the perforin/granzyme cell death pathway. Nat. Rev. Immunol. 2, 735–47.

Tyson, J.J., Csikasz-Nagy, A., Novak, B., 2002. The dynamics of cell cycle regulation. Bioessays 24, 1095–109.

Vafa, O., Wade, M., Kern, S., Beeche, M., Pandita, T.K., Hampton, G.M., Wahl, G.M., 2002. c-Myc can induce DNA damage, increase reactive oxygen species, and mitigate p53 function: A mechanism for oncogene-induced genetic instability. Mol. Cell 9, 1031–1044.

Valko, M., Rhodes, C.J., Moncol, J., Izakovic, M., Mazur, M., 2006. Free radicals, metals and antioxidants in oxidative stress-induced cancer. Chem. Biol. Interact. 160, 1–40.

van den Bent, M.J., Brandes, A. a, Rampling, R., Kouwenhoven, M.C.M., Kros, J.M., Carpentier, A.F., Clement, P.M., Frenay, M., Campone, M., Baurain, J.-F., Armand, J.-P., Taphoorn, M.J.B., Tosoni, A., Kletzl, H., Klughammer, B., Lacombe, D., Gorlia, T., 2009. Randomized phase II trial of erlotinib versus temozolomide or carmustine in recurrent glioblastoma: EORTC brain tumor group study 26034. J. Clin. Oncol. 27, 1268–74.

van den Heuvel, S., 2005. Cell-cycle regulation. In: Cell-Cycle Regulation. pp. 1–16.

van Dijk-Wolthuis, W.N.E., Franssen, O., Talsma, H., van Steenbergen, M.J., Kettenes-van den Bosch, J.J., Hennink, W.E., 1995. Synthesis, Characterization, and Polymerization of Glycidyl Methacrylate Derivatized Dextran. Macromolecules 28, 6317–6322.

Vander Heiden, M. G., Cantley, L.C., Thompson, C.B., 2009. Understanding the Warburg Effect: the metabolic requirements of cells proliferation. Science (80-.). 324, 1029–1033.

Vanlangenakker, N., Berghe, T., Krysko, D., Festjens, N., Vandenabeele, P., 2008. Molecular Mechanisms and Pathophysiology of Necrotic Cell Death. Curr. Mol. Med. 8, 207–220.

Verduzco, D., Lloyd, M., Xu, L., Ibrahim-Hashim, A., Balagurunathan, Y., Gatenby, R. a., Gillies, R.J., 2015. Intermittent Hypoxia Selects for Genotypes and Phenotypes That Increase Survival, Invasion, and Therapy Resistance. PLoS One 10, e0120958.

Verhoeff, J.J.C., van Tellingen, O., Claes, A., Stalpers, L.J. a, van Linde, M.E., Richel, D.J., Leenders, W.P.J., van Furth, W.R., 2009. Concerns about anti-angiogenic treatment in patients with glioblastoma multiforme. BMC Cancer 9, 444.

Verma, A., Stellacci, F., 2010. Effect of surface properties on nanoparticle-cell interactions. Small 6, 12–21.

Vermeulen, K., Van Bockstaele, D.R., Berneman, Z.N., 2003. The cell cycle: a review of regulation, deregulation and therapeutic targets in cancer. Cell Prolif. 36, 131–149.

Wajant, H., 2002. The Fas signaling pathway: more than a paradigm. Science 296, 1635–6.

Walmsley, S.R., Print, C., Farahi, N., Peyssonnaux, C., Johnson, R.S., Cramer, T., Sobolewski, A., Condliffe, A.M., Cowburn, A.S., Johnson, N., Chilvers, E.R., 2005. Hypoxia-induced neutrophil survival is mediated by HIF-1alpha-dependent NF-kappaB activity. J. Exp. Med. 201, 105–15.

Wang, D., Lippard, S.J., 2005. Cellular processing of platinum anticancer drugs. Nat. Rev. Drug Discov. 4, 307–320.

Wang, L., Xu, J., Zhao, C., Zhao, L., Feng, B., 2013. Antiproliferative, cell-cycle dysregulation effects of novel asiatic acid derivatives on human non-small cell lung cancer cells. Chem. Pharm. Bull. (Tokyo). 61, 1015–23.

Wang, M., Wey, S., Zhang, Y., Ye, R., Lee, A.S., 2009. Role of the unfolded protein response regulator GRP78/BiP in development, cancer, and neurological disorders. Antioxid. Redox Signal. 11, 2307–2316.

Wang, P.P., Frazier, J., Brem, H., 2002. Local drug delivery to the brain. Adv. Drug Deliv. Rev. 54, 987–1013.

Wang, T., Li, M., Gao, H., Wu, Y., 2011. Nanoparticle carriers based on copolymers of poly(ε-caprolactone) and hyperbranched polymers for drug delivery. J. Colloid Interface Sci. 353, 107–15.

Wang, X., Wang, Y., Wei, K., Zhao, N., Zhang, S., Chen, J., 2009. Drug distribution within poly(ε-caprolactone) microspheres and in vitro release. J. Mater. Process. Technol. 209, 348–354.

Wang, Z., Fan, M., Candas, D., Zhang, T.Q., Qin, L., Eldridge, A., Wachsmann-Hogiu, S., Ahmed, K.M., Chromy, B. a., Nantajit, D., Duru, N., He, F., Chen, M., Finkel, T., Weinstein, L.S., Li, J.J., 2014. Cyclin B1/Cdk1 coordinates mitochondrial respiration for Cell-Cycle G2/M progression. Dev. Cell 29, 217–232.

Warburg, O., 1956. On the Origin of Cancer Cells. Science (80-.). 123, 309–314.

Wartenberg, M., Ling, F.C., Klein, F., Acker, H., Petrat, K., Sauer, H., 2003. Regulation of the multidrug resistance transporter P- glycoprotein in multicellular tumor spheroids by hypoxia- inducible factor-1 and reactive oxygen species. Fasebj 17, 503–5.

Watson, J. a., Watson, C.J., McCrohan, A.M., Woodfine, K., Tosetto, M., McDaid, J., Gallagher, E., Betts, D., Baugh, J., O'Sullivan, J., Murrell, A., Watson, R.W.G., McCann, A., 2009. Generation of an epigenetic signature by chronic hypoxia in prostate cells. Hum. Mol. Genet. 18, 3594–3604.

Weidinger, A., Kozlov, A., 2015. Biological Activities of Reactive Oxygen and Nitrogen Species: Oxidative Stress versus Signal Transduction. Biomolecules 5, 472–484.

Weller, M., Cloughesy, T., Perry, J.R., Wick, W., 2013. Standards of care for treatment of recurrent. Neuro. Oncol. 15, 4–27.

Wertz, I.E., Dixit, V.M., 2000. Characterization of calcium release-activated apoptosis of LNCaP prostate cancer cells. J. Biol. Chem. 275, 11470–11477.

Westphal, M., Hilt, D.C., Bortey, E., Delavault, P., Olivares, R., Warnke, P.C., Whittle, I.R., Jääskeläinen, J., Ram, Z., 2003. A phase 3 trial of local chemotherapy with biodegradable carmustine (BCNU) wafers (Gliadel wafers) in patients with primary malignant glioma. Neuro. Oncol. 5, 79–88.

Wiseman, H., Halliwell, B., 1996. Damage to DNA by reactive oxygen and nitrogen species: role in inflammatory disease and progression to cancer. Biochem. J. 313, 17–29.

Wohlbold, L., Larochelle, S., Liao, J.C.F., Livshits, G., Singer, J., Shokat, K.M., Fisher, R.P., 2006. The cyclin-dependent kinase (CDK) family member PNQALRE/CCRK supports cell proliferation but has no intrinsic CDK-activating kinase (CAK) activity. Cell Cycle 5, 546–554.

Wolburg, H., Lippoldt, A., 2002. Tight junctions of the blood-brain barrier: development, composition and regulation. Vascul. Pharmacol. 38, 323–37.

Wong, R.S.Y., 2011. Apoptosis in cancer: from pathogenesis to treatment. J. Exp. Clin. Cancer Res. 30, 87.

Woodruff, M.A., Hutmacher, D.W., 2010. The return of a forgotten polymer - Polycaprolactone in the 21st century. Prog. Polym. Sci. 35, 1217–1256.

Wu, C., Jim, T.F., Gan, Z., Zhao, Y., Wang, S., 2000. A heterogeneous catalytic kinetics for enzymatic biodegradation of poly (ε -caprolactone) nanoparticles in aqueous solution. Polymer (Guildf). 41, 3593–3597.

Yamagata, M., Hasuda, K., Stamato, T., Tannock, I.F., 1998. The contribution of lactic acid to acidification of tumours: studies of variant cells lacking lactate dehydrogenase. Br. J. Cancer 77, 1726–1731.

Yang, R., Morosetti, R., Koeffler, H.P., Koeffler, H.P., 1997. Characterization of a Second Human Cyclin A That Is Highly Expressed in Testis and in Several Leukemic Cell Lines Characterization of a Second Human Cyclin A That Is Highly Expressed in Testis and in Several Leukemic Cell Lines ’ 913–920.

Yang, X., Chang, H.Y., Baltimore, D., 1998. Autoproteolytic Activation of Pro-Caspases by Oligomerization. Mol. Cell 1, 319–325.

Yao, K., Gietema, J. a, Shida, S., Selvakumaran, M., Fonrose, X., Haas, N.B., Testa, J., O’Dwyer, P.J., 2005. In vitro hypoxia-conditioned colon cancer cell lines derived from HCT116 and HT29 exhibit altered apoptosis susceptibility and a more angiogenic profile in vivo. Br. J. Cancer 93, 1356–1363.

Yordanov, G., 2012. Poly (alkyl cyanoacrylate) nanoparticles as drug carriers : 33 years

later. Bulg. J. Chem. 1, 61–73.

Yu, Y., Song, J., Guo, X., Wang, S., Yang, X., Chen, L., Wei, J., 2014. Characterization and structural analysis of human selenium-dependent glutathione peroxidase 4 mutant expressed in Escherichia coli. Free Radic. Biol. Med. 71, 332–8.

Zhang, E.Y., Knipp, G.T., Ekins, S., Swaan, P.W., 2002. Structural biology and function of solute transporters: implications for identifying and designing substrates. Drug Metab. Rev. 34, 709–50.

Zhang, H., Gao, P., Fukuda, R., Kumar, G., Krishnamachary, B., Zeller, K.I., Dang, C.V., Semenza, G.L., 2007. HIF-1 Inhibits Mitochondrial Biogenesis and Cellular Respiration in VHL-Deficient Renal Cell Carcinoma by Repression of C-MYC Activity. Cancer Cell 11, 407–420.

Zhang, X., Zhang, W., Cao, W.-D., Cheng, G., Zhang, Y.-Q., 2012. Glioblastoma multiforme: Molecular characterization and current treatment strategy (Review). Exp. Ther. Med. 3, 9–14.

Zhao, Y., Wei, H. a I., Zheng, H., Guo, Z., Wei, Y.-S., Zhang, D.-H., Zhang, J., 2010. Enhancing Water-Solubility of Poorly Soluble Drug , Asiatic Acid With Hydroxypropyl-B-Cyclodextrin. Dig. J. Nanomater. Biostructures 5, 419–425.

Zhou, J., Schmid, T., Schnitzer, S., Brüne, B., 2006. Tumor hypoxia and cancer progression. Cancer Lett. 237, 10–21.

Ziegler, U., Groscurth, P., 2004. Morphological Features of Cell Death. News Physiol. Sci. 19, 124–128.

Zili, Z., Sfar, S., Fessi, H., 2005. Preparation and characterization of poly-epsilon-caprolactone nanoparticles containing griseofulvin. Int. J. Pharm. 294, 261–7.

Zong, W., Ditsworth, D., Bauer, D.E., Wang, Z., Thompson, C.B., 2004. Alkylating DNA damage stimulates a regulated form of necrotic cell death. Genes Dev. 18, 1272–1282.

Zorov, D.B., Juhaszova, M., Sollott, S.J., 2014. Mitochondrial Reactive Oxygen Species (ROS) and ROS-Induced ROS Release. Physiol. Rev. 94, 909–950.